DESIGN, SYNTHESIS AND CHARACTERIZATION OF CHEMOSENSORS FOR DETERMINATION OF HEAVY METAL IONS

Thesis

Submitted in partial fulfilment of the requirements for the degree of

DOCTOR OF PHILOSOPHY

by

VENKATADRI TEKURI

DEPARTMENT OF CHEMISTRY

NATIONAL INSTITUTE OF TECHNOLOGY KARNATAKA,

SURATHKAL, MANGALORE -575025

February, 2020

DEDICATED TO

MY PARENTS AND FAMILY MEMBERS

DECLARATION

by the Ph.D. Research Scholar

I hereby declare that the Research Thesis entitled "**Design, synthesis and characterization of chemosensors for determination of heavy metal ions**" which is being submitted to the National Institute of Technology Karnataka, Surathkal in partial fulfilment of the requirements for the award of the Degree of Doctor of Philosophy in Chemistry is a *bonafide report of the research work carried out by me*. The material contained in this Research Thesis has not been submitted to any University or Institution for the award of any degree.

Venkatadri Tekuri
Reg. No. 155077CY15F06
Department of Chemistry

Place: NITK - Surathkal
Date:

CERTIFICATE

This is to *certify* that the Research Thesis entitled "**Design, synthesis and characterization of chemosensors for determination of heavy metal ions**" submitted by **Mr. Venkatadri Tekuri (Register Number: 155077CY15F06)** as the record of the research work carried out by him, is *accepted as the Research Thesis submission* in partial fulfilment of the requirements for the award of degree of Doctor of Philosophy.

Research Guide
Name: Dr. Darshak R. Trivedi
(Signature with Date and Seal)

Chairman - DRPC
(Signature with Date and Seal)

ACKNOWLEDGEMENT

My heartfelt acknowledgement to the National Institute of Technology Karnataka (NITK), Surathkal, for providing me a wonderful research environment and research facilities. I am obliged to NITK to provide a research fellowship throughout my research work. I would like to extend my sincere thanks to Dr. Darshak R. Trivedi, a Research guide for his support and encouragement during my research work. It wouldn't be possible without his support and timely guidance. I am sure that the experience I gained from NITK Surathkal will boost my life and career in a positive direction. I take this opportunity to thank all my friends and colleagues who supported me directly/indirectly throughout my research work.

I am thankful to Prof. Arun M Isloor, Head, Department of Chemistry and Chairman-DRPC. I thank RPAC members Prof. Ampar Chitharanjan Hegde, Department of Chemistry and Dr. Kartick Tarafder, Department of Physics for their support, guidance and valuable suggestions during my research progress. Their timely suggestions and inputs were highly noticeable during my research work. I thank all the faculty members of the department of chemistry for their encouragement, timely help, and support. I thank Dr. Keyur Raval from the department of Chemical Engineering, NITK Surathkal, for his support. I extend my gratitude to the Department of Science and Technology (DST), Govt. of India, for providing the SC-XRD facility to the Department of Chemistry, NITK Surathkal, under the FIST program.

I am extending my gratitude to Dr. Suban K Sahoo from the Department of Applied Chemistry, S.V. NIT-Surat, for the DFT support. I thank Mr. Venkatesh Pilli, Dr. S. Bala Konda Reddy and Mr. S. Ramanjaneyule for their timely supports for the characterization during my research work.

I extend my appreciation to all the non-teaching staff of the Chemistry Department, namely, Mrs. Shamila Nandini, Mr. Prashant, Mrs. Sharmila, Mr. Pradeep, Mr. Harish Mis. Vikhitha and Mrs. Deepa for their support in the department.

I extend my sincere thanks to my friends and colleagues, namely, Mr. Gogineni Rajesh, Mr. P Srinivasulu and G. Bala Narasimha, for their timely help and support. I thank Mrs. Trithila Shetty from the Chemical engineering department, NITK Surathkal, for her timely help.

I extend my sincere thanks to all the research colleagues from the chemistry department. My special thanks to Mr. Bharath Kumar, Dr. Sunil Kumar N, Dr. Srikala P, Mis. Archana, Mr. Aranganathan V, Mr. Nagaraju, Mis. Rajalakshmi K and Dr. Vinaya Kumara DR for their help and support throughout my research.

Finally, I extend my sincere thanks to my parents Mrs. Ramalakshumamma Tekuri and Late. Mr. Venkata Subbaiah Tekuri, brothers (Venkateswarlu Tekuri, Seshadri Tekuri, Srikanth Tekuri, Sivakoti Narayana Tekuri, and Dr. Chandra Sekhar Tekuri), brother-in-law Mr. Srinivasulu Ramisetty, sister-in-law, Venkata Rathnamma Tekuri, wife Mrs. Sandhya Gundlapalli and all my Tekuri family members for their continuous support for my research activities and also for making me what I am today. My sincere thanks to my teachers Dr. B V Ramana and Dr. Rambabu G, for their help and support throughout my research. I dedicate my thesis work to my parents and brothers for their hard work and support to achieve my Ph. D. degree.

Venkatadri Tekuri

ABSTRACT

Heavy metals such as Hg^{2+}, Cd^{2+}, Pb^{2+}, As^{3+}/As^{5+} are highly toxic because of clinical and environmental reasons. Here we have been designed and synthesized five new series of chemosensors for the colorimetric detection of heavy metal ions (Cu^{2+}, Hg^{2+}, Cd^{2+}, Pb^{2+}, As^{3+}/As^{5+}) and utilized for versatile applications of environmental concern. All the chemosensors have been characterized using different standard spectroscopic techniques like FT-IR, ^{1}H-NMR, ^{13}C-NMR and LC-Mass (ESI-MS). The selected chemosensors have been considered for three-dimensional structural elucidation using Single Crystal X-Ray diffraction (SCXRD) studies.

The qualitative and quantitative, binding properties and detection limits for the developed chemosensors have been carried out using UV–Vis spectroscopic studies. The binding mechanism has been proposed based on UV–Vis titration and the same has been confirmed by FT-IR, ^{1}H-NMR, LC-Mass and DFT studies. Among the synthesized chemosensors, the S4R1 showed a lower detection limit of 2, 11, 2, 7 ppb for Cu^{2+}, Hg^{2+}, Cd^{2+}, Pb^{2+} ions, respectively. The S5R1 showed 8 ppb detection limit for As^{3+} ions, which is much lower than the WHO, US–EPA stated limit of 10 ppb.

From the experimental and theoretical DFT results, it has been concluded that the simple organic molecules could act as very good colorimetric chemosensors for heavy metal ions such as Cu^{2+}, Hg^{2+}, Cd^{2+}, Pb^{2+} and arsenate/arsenite ions. The S2R1 S3R3 and S3R4 showed brilliant analytical and environmental significant applications for the quantitative analysis of Cu^{2+}, Cd^{2+}, Hg^{2+} ion present in river, tap, and drinking water samples. The analytical method results of S3R3 and S3R4 for the determination of Cu^{2+} and Cd^{2+} indicates acceptable precision, linearity and accuracy of the developed method. Further, a good agreement found between proposed and well-established methods (AAS). The chemosensors S4R1–S4R3 and S5R1–S5R3 displayed colorimetric responses towards detection of heavy metal ions. S4R3 and S5R1 showed good naked eye response for the As^{3+}/ As^{5+} ions. The S4R3 showed detection limit of 213 ppb for As^{3+} and the S5R1 displayed detection limit of 8 ppb/13 ppb for As^{3+}/ As^{5+} ions. Further, successfully demonstrated the test strips applications.

Keywords: Colorimetric chemosensor, UV–Vis titration, Analytical method validation, B-H plot, Binding constant, Schiff's base, Heavy metal ions.

NOMENCLATURE

ABBREVIATIONS

API	:	Active Pharmaceutical Ingredient
CSD	:	Cambridge Structural Database
CCDC	:	Cambridge Crystallographic Data Centre
FT–IR	:	Fourier Transform Infrared
NMR	:	Nuclear Magnetic Resonance
SC–XRD	:	Single Crystal X-ray Diffraction
UV–Vis	:	Ultraviolet-Visible
DFT	:	Density Functional Theory
DMSO-d_6	:	Dimethyl Sulfoxide-deuterated
$CDCl_3$	:	Chloroform-deuterated
MP	:	Melting point
WHO	:	World health organization
USP	:	United states pharmacopeia
ICH	:	International conference on harmonisation
US–EPA	:	United states environmental protection agency
AAS	:	Atomic absorption spectroscopy
ICP-MS	:	Inductively coupled plasma mass spectrometry
ICP–OES	:	Inductively coupled plasma optical emission spectrometry
LC–MS	:	Liquid chromatography–mass spectrometry
ESI	:	Electro spray ionization
DL	:	Detection limit
QL	:	Quantification limit
DMF	:	Dimethylformamide
EtOH	:	Ethanol
equiv.	:	Equivalence
Fig.	:	Figure
HPLC	:	High-performance liquid chromatography
ACN	:	Acetonitrile

AcOH	:	Acetic acid
ICT	:	Intramolecular charge transfer
HOMO	:	Highest occupied molecular orbitals
LUMO	:	Lowest unoccupied molecular orbitals
TMS	:	Tetramethylsilane
TLC	:	Thin-layer chromatography
RT	:	Room temperature
ORTEP	:	Oak ridge thermal ellipsoidal plot

SYMBOLS AND UNITS

α	:	Alpha
cm	:	Centimeter
Nm	:	Nanometer
°	:	Degree
Å	:	Angstrom
°C	:	Degree Celsius
∠	:	Angle
G	:	Gram
Mg	:	Milligram
Mg	:	Microgram
>	:	Greater than
Hz	:	Hertz
$^{-1}$	:	Inverse
λ	:	Lamda
<	:	Less than
L	:	Liter
mL	:	Milliliter
µL	:	Microlitter
M	:	Molar/Mole
mM	:	Millimol
µM	:	Micromol
ppm	:	Parts per million
Ppb	:	Parts per billion
MHz	:	Megahertz
µ	:	Mu
Σ	:	Sigma
Π	:	Pai
θ	:	Theta
V	:	Volume
kJ	:	Kilojoule

N	:	Normal/Normality
min	:	Minute
H/h	:	Hour

CONTENTS

CHAPTER-1.....1

1. INTRODUCTION.....1

1.1. Supramolecular chemistry.....1

1.2. Overview of heavy metal ions.....4

1.3. Chemistry, principles and design of chemosensors 6

1.3.1. Overview of cation sensing chemosensors and principle of molecular recognition 6

1.3.2. Design of chemosensor 7

1.3.3. Fluorescent cation sensors.....8

1.4. Conventional methods for the estimation of cations and application of chemosensors 9

1.5. Challenges in cation receptor chemistry 10

1.6. Literature review 11

1.7. Scope of work.....18

1.8. Objectives.....19

CHAPTER–2 21

2. MULTI-SIGNALING THIOCARBOHYDRAZIDE BASED COLORIMETRIC SENSORS FOR THE SELECTIVE RECOGNITION OF HEAVY METAL IONS IN AN AQUEOUS MEDIUM 21

2.1. Introduction 21

2.2. Experimental section 22

2.2.1. Colorimetric and UV–Vis studies 23

2.2.2. Synthesis of chemosensors S1R1–S1R3.....23

2.2.3. Characterization spectra of chemosensor S1R1-S1R3.....25

2.3. Results and discussion.....30

2.3.1. Colorimetric Studies.....30

2.3.2. UV–Visible absorption studies.....31

2.3.3. Selectivity of chemosensor S1R1–S1R3 towards metal ions 33

2.3.4. Binding constant and detection limit determination 36

2.4. Conclusions 40

CHAPTER-3.....41

3. Hg^{2+} INDUCED HYDROLYSIS OF THIAZOLE AMINE BASED SCHIFF BASE: COLORIMETRIC AND FLUOROGENIC CHEMODOSIMETER FOR Hg^{2+} IONS IN AN AQUEOUS MEDIUM.....41

3.1. Introduction 41

3.2. Experimental details.....43

3.2.1. General information 43

3.2.2. Colorimetric, UV–Vis and fluorescence experiments.....43

3.2.3. Synthesis of chemosensors S2R1–S2R3 and characterization.....44

3.2.4. Characterization spectra of chemosensors S2R1– S2R3.....46

3.3. Results and discussion.....52

3.3.1. Colorimetric detection of cations 52

3.3.2. UV–Vis and fluorescence recognition of cations.....52

3.3.3. Determination of detection limit (DL) and quantization limit (QL) 54

3.3.4. Density functional theory (DFT).....55

3.3.5. Binding mechanism of S2R1 with mercury metal ion 56

3.3.6. Real life application 60

3.4. Conclusions 62

CHAPTER-4.....63

4. A NEW COLORIMETRIC CHEMOSENSORS FOR Cu^{2+} AND Cd^{2+} IONS DETECTION: APPLICATION IN ENVIRONMENTAL WATER SAMPLES AND ANALYTICAL METHOD VALIDATION.....63

4.1. Introduction 63

4.2. Experimental section 65

4.2.1. Materials and methods 65

4.2.2. Colorimetric and UV–Vis studies 65

4.2.3. General synthesis procedure for chemosensor S3R1–S3R4 66

4.2.4. Characterization 67

4.2.5. Characterization spectra of chemosensors S3R1–S3R4.....69

4.3. Results and discussion.....75

4.3.1. Colorimetric study.....75

4.3.2. UV–Vis absorption spectroscopy studies.....76

4.3.3. Benesi-Hildebrand Plot, determination of association constant (K) 79

4.3.4. Method validation for determination of Cu^{2+} and Cd^{2+} ions.....80

4.3.5. Application to different environmental water samples 84

4.3.6. Binding mechanism 85
4.3.7. Comparison with other Cu^{2+} and Cd^{2+} sensing chemosensors 88
4.3.8. Crystallographic data of chemosensor S3R1–S3R3 91
4.4. Conclusion 94
CHAPTER 5 95
5. SMART COLORIMETRIC RESPONSE FOR HEAVY METAL DETECTION: SYNTHESIS, SPECTRAL RESPONSE AND DFT STUDIES ..95
5.1. Introduction 95
5.2. Experimental section 97
5.2.1. Synthesis of chemosensor S4R1-S4R3 97
5.2.2. Characterization data of chemosensors S4R1–S4R3 99
5.3. Results and discussion 104
5.3.1. Colorimetric sensing experiments 104
5.3.2. UV–Visible sensing studies 105
5.3.3. Binding properties and determination of detection limit (DL) 111
5.3.4. DFT Study of S4R1-S4R3 114
5.3.5. Proposed binding interaction between metal ions and chemosensors 121
5.3.6. Test strip application 129
5.4. Conclusions 130
CHAPTER-6 131
6. SIMPLE COLORIMETRIC RESPONSE FOR ARSENATE, ARSENITE, Cu^{2+} AND Hg^{2+} IONS: SYNTHESIS, SPECTRAL RESPONSE AND TEST STRIPS APPLICATION 131
6.1. Introduction 131
6.2. Experimental section 133
6.2.1. Materials and methods 133
6.2.2. Analytical solutions preparation 134
6.2.3. Synthesis of chemosensor S5R1–S5R4 134
6.2.4. Characterization data for S5R1-S5R3 136
6.3. Results and discussion 141
6.3.1 Naked-eye detection studies 141
6.3.2 Recognition of ions by UV–Visible studies 142
6.3.3 UV–Visible titration experiments 143
6.3.4 Investigation of binding properties and detection limit (DL) 146

6.3.5 Investigation of binding interaction by FT-IR and Mass analysis 148
6.3.6 Test strip application 155
6.4. Conclusions 155
CHAPTER-7.....157
7. SUMMARY AND CONCLUSIONS 157
7.1. Summary of the present work 157
7.2. Conclusions 162
7.3. Future work 166
7.3.1. Heavy metal ions detection and application.....166
REFERENCES.....167
LIST OF PUBLICATIONS 185

CHAPTER-1

INTRODUCTION

CHAPTER-1

1. INTRODUCTION

Abstract

A brief introduction of supramolecular chemistry, cation recognition, and cation binding chemistry for the chemosensors were discussed. Further, challenges in cation detection, the scope of the work, and objectives are discussed in this chapter.

1.1. Supramolecular chemistry

Jean-Marie Lehn introduced the term supramolecular chemistry (SP) in the year 1978. He won the Nobel Prize for his work in the year 1987; he has defined the supramolecular chemistry as '*chemistry of molecular assemblies and of the intermolecular bond*' broadly; it can be demonstrated as '*chemistry beyond the molecule*'. In another way, it can be said as '*the chemistry of the non-covalent bond and non-molecular chemistry*'. Originally, SP was defined in terms of the non-covalent interaction between a '*host*' and a '*guest*' molecule (Steed, J. W., and Atwood 2010). **Fig. 1.1**, represents the connection between the molecular chemistry and SP through the structures and function (Manandhar and Wallace 2012; You et al. 2015b).

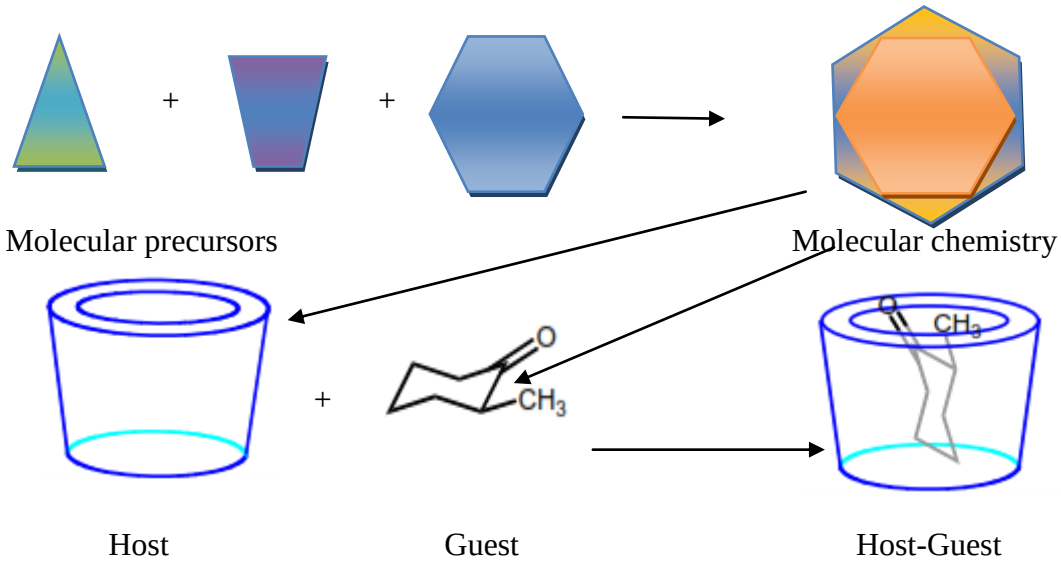

Fig. 1.1: The representation of Host-Guest Chemistry

In broad-spectrum, SP concern only the 'non-covenant' interactions, such as ion-ion, dipole-dipole, cation–π, anion–π, π–π interactions, hydrogen bonding, and van der waals forces. Many concepts can be explained based on supramolecular chemistry interactions. Some of the important concepts of SP are molecular self-assembly (**Fig. 1.2a**), folding (**Fig. 1.2b**), molecular recognition host-guest chemistry **(Fig. 1.2(c))**, mechanically-interlocked molecular architectures (**Fig. 1.2d**), etc. In the literature, Yoon and co-workers have synthesized a bis-pyrene derivative bearing two pyridine groups in binding with Ag^{+} ions (Wang et al. 2011b). The ^{1}H NMR and density functional theory (DFT) confirms the host-guest interaction(Wang et al. 2011b). The importance of molecular recognition and its applications in the analytical chemistry for the detection of single, multi-analytes.(Manandhar and Wallace 2012; You et al. 2015b)

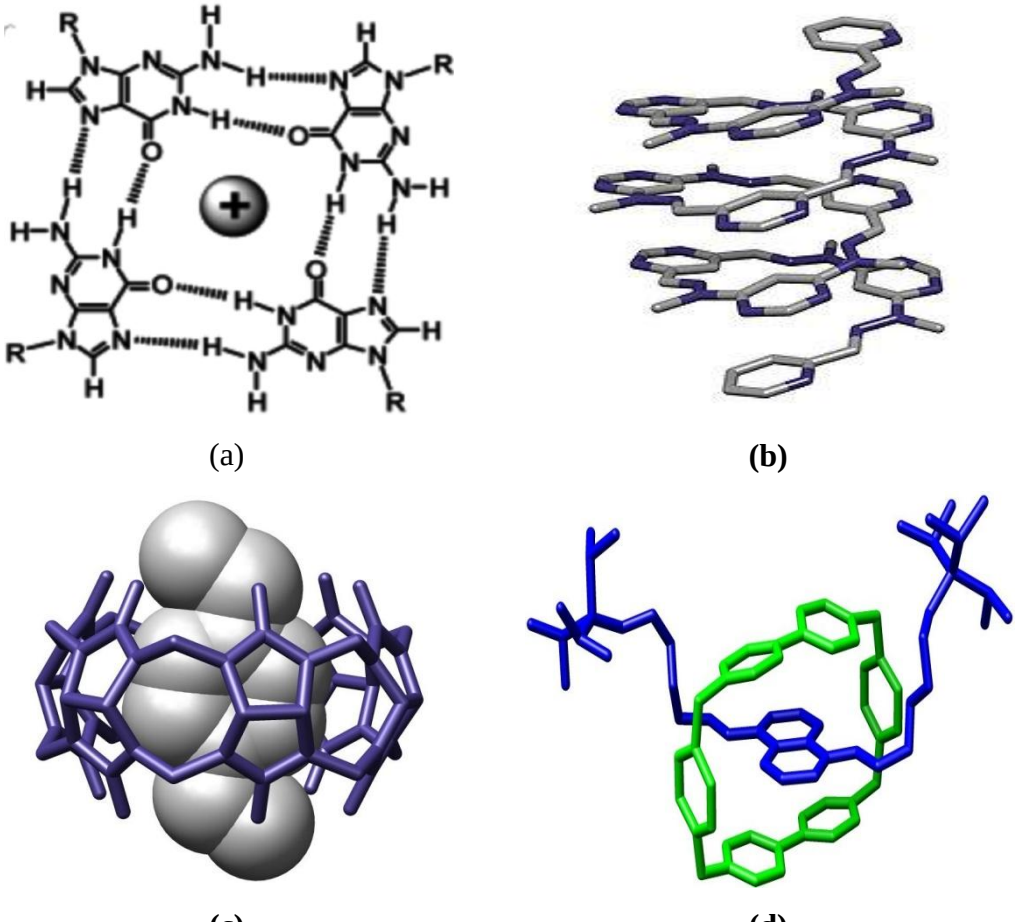

(a) **(b)**

(c) **(d)**

Fig. 1.2: Different type of molecular assemblies in SP

In 1873, Johannes Diderik vander waals explained the forces of intermolecular interactions. However, the theory of supramolecular chemistry was started in 1894, when Emil Fischer proposed the lock and key (**Fig. 1.3**) model for the binding of receptor substrates to the enzymes. In 1920, Latimer and Rodebush defined the "*hydrogen bonding*." The observable facts led to understand the non-covalent interactions of the molecules in detail, and the scientific population might apply these non-covalent interactions to the artificial systems.

Lock and key model

Induced fit concept

Conformational isomerism

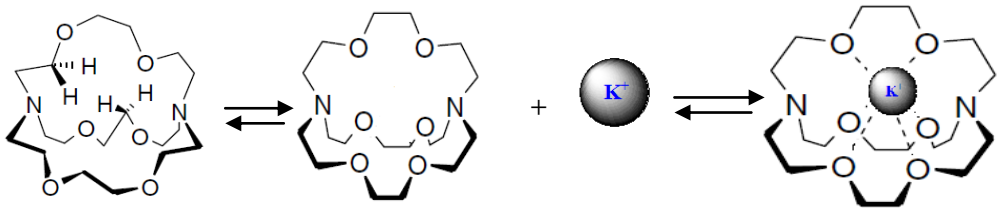

Conformational selection

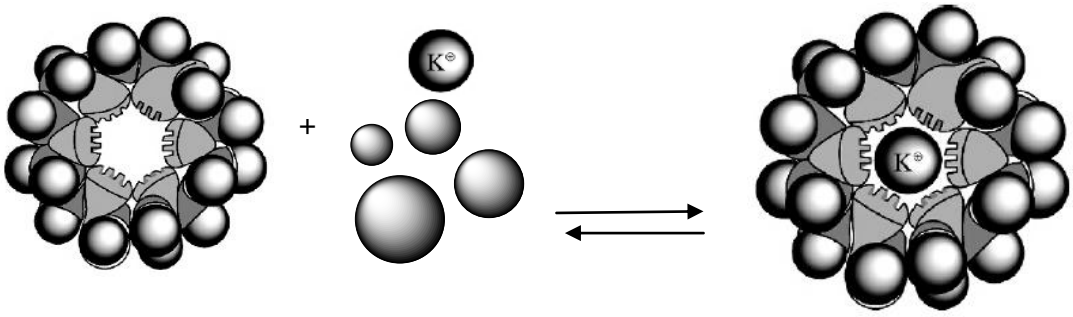

Fig. 1.3: Various concepts for binding mechanisms

In the mid-to-late 1960s, the development of macrocyclic chemistry led further development of SP, especially by the concept of reporting process of macrocyclic ligands for metal cations. A group of scientists (Curtis, Busch, Jäger, and Pedersen) introduced a four-base macrocyclic compound (among them three are imines by Schiff base reaction of an aldehyde with an amine) (**Fig. 1.4**) (Steed, J. W., and Atwood 2010).

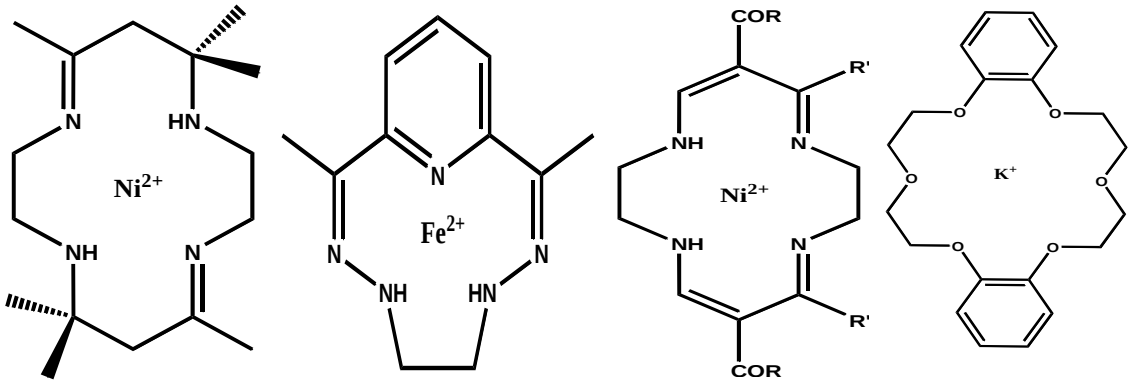

1 **2** **3** **4**

Fig. 1.4: Macrocyclic compounds, 1)**.** Curtis-1961, 2). Busch-1964, 3). Jager-1964, 4). Pedersen-1967

In recent decades, supramolecular chemistry spread over the new fields such as crystal engineering, synthetic organic chemistry, inorganic chemistry, solid-state chemistry, biochemistry, biology, computational molecular modeling, and nanotechnology, etc., (Manandhar and Wallace 2012; You et al. 2015b).

1.2. Overview of heavy metal ions

Heavy metals are metals with a density of more than 5 g/cm^3, such as lead, cadmium, arsenic, copper, and mercury. These heavy metals could be extremely harmful to human health. The early detection of cations is a difficult task for the analytical chemists, due to the lower minimal detection limit given by standard guidelines/agencies. The metal ions Pb^{2+}, Hg^{2+}, $As^{3+,}$ and Cd^{2+}, are more toxic and produce adverse effects in flora and fauna (**Fig. 1.5**), so recognition in the environment is necessary. The toxicity and maximum permeable limits of Pb^{2+}, Hg^{2+}, Cu^{2+}, As^{3+}, and Cd^{2+} ions are given below in **table 1.1**.

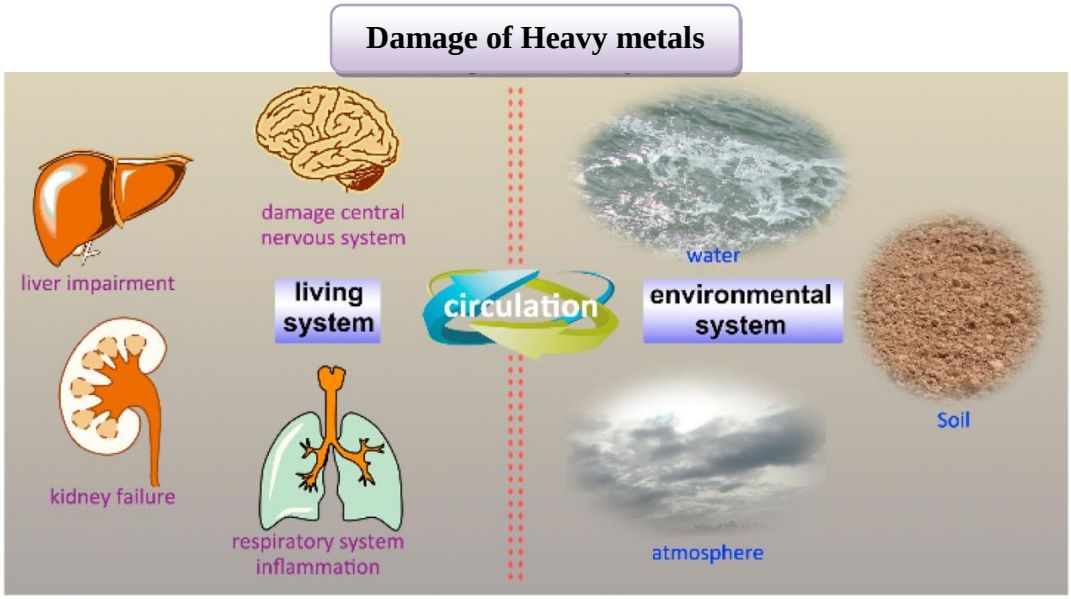

Fig. 1.5: Damage of Heavy metals

Table 1.1: The toxicity and maximum permeable limits of Pb^{2+}, Hg^{2+}, Cu^{2+}, $As^{3+,}$ and Cd^{2+} ions.

Metal	**Limits set by (EPA/WHO/ USP/ICH)**	**Adverse effects/Toxicity**	**Reference**
Copper (Cu^{2+})	1.3 mg/L	Metal fume fever, Vomiting, acute hemolytic anemia, liver damage, and aching muscles	(He et al. 2005; Hughes et al. 2011; Karlsson et al. 2014; Sarkar 2002; Tchounwou et al. 2012)
Lead (Pb^{2+})	0.015 mg/L	Hypertension decreased IQ level children, cardiovascular, reproductive, neurological, and developmental disorders.	
Cadmium (Cd^{2+})	0.005 mg/L	Damage to liver and kidney, carcinogenic, and cardiovascular diseases.	
Mercury (Hg^{2+})	0.002 mg/L	Myocardial infarction, Minamata, neurodevelopmental disorder, damage to endocrine, central nervous system, kidneys, and brain.	
Arsenic (As^{3+})	0.01 mg/L	Carcinogenicity and mutagenicity	

1.3. Chemistry, principles, and design of chemosensors

A chemosensor is an organic molecule that can sense the presence of an analyte by some physical or optical changes via definite, non-covalent binding interaction of a guest molecule with an organic host moiety. The molecular detection originates from the development of macrocyclic species, for the elective recognition of simple alkali earth metal ions in the field SC. The molecular recognition is more important for monitoring heavy metal cations, and this has effectively given birth to the field of molecular detection. The selective recognition of cations has various applications in chemistry, biology, and the environment. Hence, the selective recognition of cations is one of the emerging fields in current research.

1.3.1. Overview of cation sensing chemosensors and principle of molecular recognition

Molecular sensors play a vital role in environmental chemistry as well as in analytical / bio-medicinal science. These molecular sensors have advantages in terms of cost, sensitivity, and selectivity for the determination of toxic heavy metal ions. The development of chemosensors for the selective cation detection in the field of excessive research significance in SC and biological chemistry as well, because a range of cations plays imperative roles in biological, chemical, environmental and industrial processes.

One of the important principles involving molecular detection is explained by the hard and soft bases theory (HSAB) (Pearson 1963). Thus, soft acids, like Cu^{+}, Ag^{+}, Cd^{2+}, $Hg^{2+,}$ and Pb^{2+} ions, preferably bind to sensor molecules having a soft base like sulfur. The borderline acids like Cu^{2+}, Co^{2+}, $Ni^{2+,}$ and Zn^{2+} interact with ligands having borderline bases like nitrogen as binding site, as represented in **Fig. 1.6.** Molecules/ligands that are covalently associated with fluorophores/chromophoric species have an open door for the sensing of these heavy metal ions.

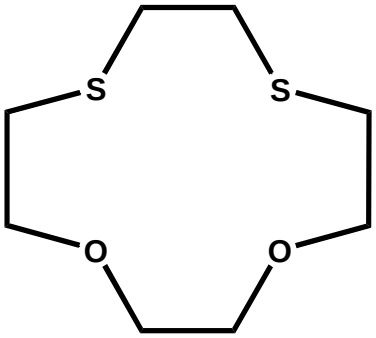

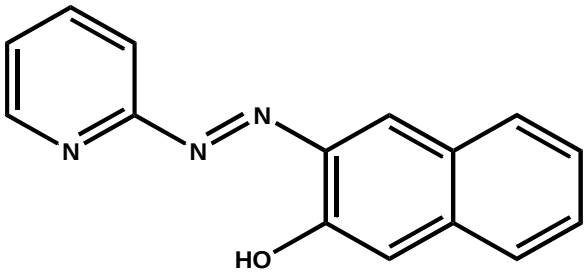

a. 1,4-dithia-12 crown-4 ionophore for Hg^{2+}

b. PAN sense in declining array to Ni^{2+}, Cu^{2+}, Zn^{2+}, Hg^{2+}, Pb^{2+} and Cd^{2+}

Fig. 1.6 Different types of **c**helators/ionophores for sensing of metal ions using in chemosensors

1.3.2. Design of chemosensor

The design of the chemosensors consists of three components, which are signalling unit, spacer, and binding site, as shown in (**Fig. 1.7**). Various research groups have used three different approaches in developing the synthetic receptors, which differ in a way the first two units are arranged concerning each other. a). Binding site-signalling, b). Displacement, c). Chemodosimeter approach.

In the "*binding site-signalling*" process, both the moieties (binding and signalling unit) are connected via covalent interaction. The "*displacement*" process takes place construction of molecular assemblies of binding site-signaling, which taking synchronization of a particular ion with the requisite, subsequently, in the discharge of the signaling unit into the media via producing a signal in the form of the optical signal (absorption/fluorescence). In the "*chemodosimeter approach*," a specific anion-induced chemical reaction occurs, which results in an optical signal. A chemosensor shall be designated as electrochemical, optical, and heat-sensitive sensors based on considering the type of signaling units. Generally, the electrochemical and optical types of chemosensors are widely used for cations detection. Nevertheless, optical chemosensors are superior to electrochemical devices.

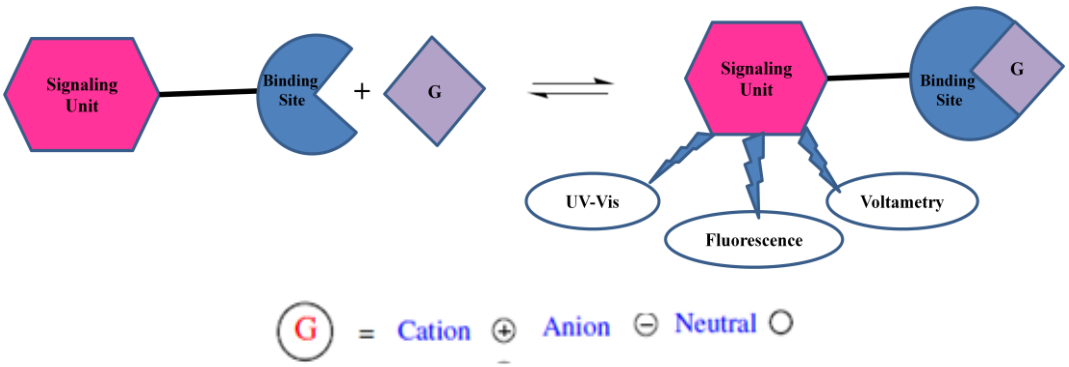

Fig. 1.7: Model illustration of a chemosensors structure

Signaling moiety is a distinctive organic compound having appropriate contributor atoms, which can selectively and efficiently form an interaction with target moiety and shall be termed as signaling unit (examples: macrocyclic units like calixarene, amides, crown ethers, cryptands, etc.,).

1.3.3. Fluorescent cation sensors

Fluorescent chemosensors have a significant value for their simplicity, easy processability, low cost, and high selectivity. IN fluorogenic/fluorescent chemosensors, the interaction between the coordination site and the guest moiety produces the changes in fluorescence behavior of the signaling unit. Generally, the fluoroionophore will have two parts and are as an ionophore and fluorophore. In the detection process of analytes, these will act as sensing and signaling units, respectively. The signaling unit transforms the signal information into an optical response by photo-physical changes of the fluorophore, and these changes can be monitored and processed in the right way to determine the presence and the concentration of a given analyte. Besides, the fluorophore associated with the ionophore through a spacer, which also works as efficient electronic contact between chromophores. Examples for signaling units: naphthalene derivatives, Pyrene, anthracene, etc. Examples for ionophores: Cyclodextrin calixarene, Crown ether, etc.

Fluorescent chemosensors posses an electron-withdrawing and an electron-donating species. The intramolecular charge transfer leads caused by when the guest molecule interacts with the sensor molecule, results in the change in the dipole moment at the excited state occurs. It brings the shift in the absorption/fluorescence, as depicted in **Fig. 1.8**.

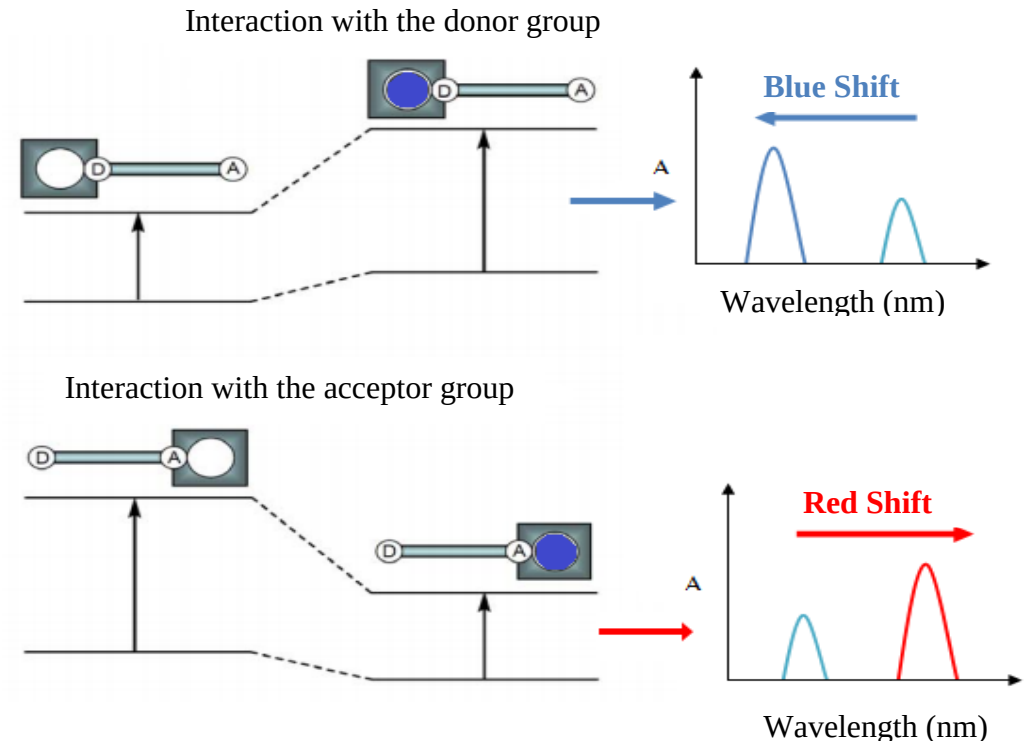

Fig. 1.8: Schematic representation of photo induced charge transfer process

The detection ability of chemosensor with hydroxy compounds, aza compounds, thiocarbazine, carbazole, pyrrole/imidazole/ indole, rhodamine functional groups where –OH, –N=N–, –C=S, –C=O acts as the binding site, depending on number of binding sites available in the sensor molecule the complex formation occurs by intramolecular charge transfer (ICT) or photo induced charge transfer (PCT), photo induced electron transfer (PET), metal-ligand or ligand-metal transfer complexes. As a result, significant color change of the solution with either a large red shift or blue shift will be achieved, and hence, the naked-eye detection of cations becomes feasible.

1.4. Conventional methods for the estimation of cations and application of chemosensors

A variety of analytical methods are available to measure exact amount of cations such as inductively coupled plasma emission or mass spectrometry (ICP-ES, ICP-MS), atomic absorption spectroscopy (AAS), furnace total reflection X-Ray fluorimetry (TXRF) and anodic stripping voltammetry (ASV) (Fegade et al. 2014;

Gattás-Asfura and Leblanc 2003; Hong et al. 2007; Kato et al. 1990; Küpper and Schultze 1997; Yin et al. 2010). Since the conventional methods are with few major limitations like difficulties in carrying analysis, high cost, time-consuming, need of well-practiced protocols, and need of sophisticated instruments that hampers spot analysis and thereby causing a necessity to develop a simple analytical technique like colorimetric chemosensors to determine the heavy metal ions. The key merits of chemosensors are user-friendly, do not require sophisticated instruments, possible spot analysis, inexpensive, and need a low quantity of sample. Due to all these merits, the chemosensors find an imperative role in the techniques that involve the determination of toxic ions in the environment.

1.5. Challenges in cation receptor chemistry

Heavy metal ions have a high toxicity effect on human beings, so; they have many adverse effects on living organisms. Numerous effects need to be put on the detection and removal of these toxic metal ions from the drinking water. The receptor metal chelation chemistry is an aged perception. However, the design of selective chemosensors for cations is still a challenging area due to the following reasons.

- High-cost spectroscopic techniques like inductively coupled plasma mass spectroscopy (ICP-MS), atomic absorption spectroscopy, and X-ray fluorescence are needed for the sensing of trace amounts of heavy metals.
- The instrumental methods have many limitations/drawbacks like time consumption, high cost for analysis, need of high skilled operator, the need for more sample quantity, sophisticated area, and complex analytical procedures, so difficult to use at field.
- Detection of metal ions in organic and organo-aqueous media with moderate sensitive and selective is well defined in the literature. Nevertheless, sensing these metal ions with high sensitivity and selective in water media is a more challenging task in the current field.
- The development of single-channel and analyte chemosensors is well defined in the literature. Whereas, developing multi-channel (i.c naked-eye, UV, fluorescence) and multi-analyte detecting chemosensors is a difficult task to the

researchers, and this has more advantages than the single analyte detecting chemosensors.

The chemosensors could be used as alternative analytical methods for the detection of heavy metal ions because these methods have several advantages than the conventional methods such as, simple operation, naked-eye detection, fast analyses (in a few minutes), low cost and allows field monitoring. However, definite improvements need for the applications, especially sensitivity at micromolar levels. Interference of other competitive metals also a hurdle task to develop highly selective and sensitive chemosensors.

On the other hand, the design and synthesis of small chemosensor molecules capable of detecting cations in aqueous conditions for real-life applications is a challenging task and yet to be explored by chemists.

1.6. Literature review

The development of chemosensors for selective cation binding is an area of excessive research interest in supramolecular and biological chemistry. Because a range of cations plays an imperative role in biological, chemical, environmental, and industrial processes. For an exemplification, Co^{2+} is a key component in Vitamin-$B_{12.}$ Zn^{2+} has a specific role to play activity as a series of biological enzymes.

Tang et al. developed 8-hydroxyquinoline-based chemosensor for Cd^{2+} at pH 7.0 in the H_2O-MeOH solution. The receptor exhibits slight emission from 397 to 410 nm. The DL for Cd^{2+} was found to be 9.0 ppm by the fluorimetric assay (Tang et al. 2008).

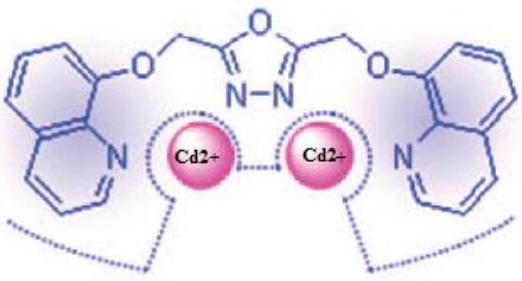

Wang and Wu developed mercury (II) ions sensor using a fluorescent signal with high selectivity and exhibits applications in living cell imaging. The detection limit found to be 1.74 μM (Wang and Wu 2013a).

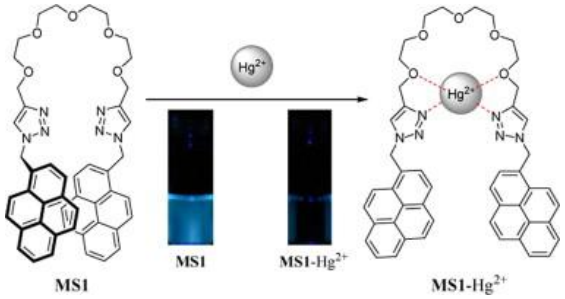

Lin et al. synthesized thiourea moiety as the binding site and nitrophenyl moiety as a signal group for the detection of Hg^{2+} ions. It exhibits color change from brown to colorless upon the addition of Hg^{2+}. The detection limits were found to be 5.0×10^{-6} M (Naked eye) and 1.0×10^{-7} M (UV-Vis) (Lin et al. 2013).

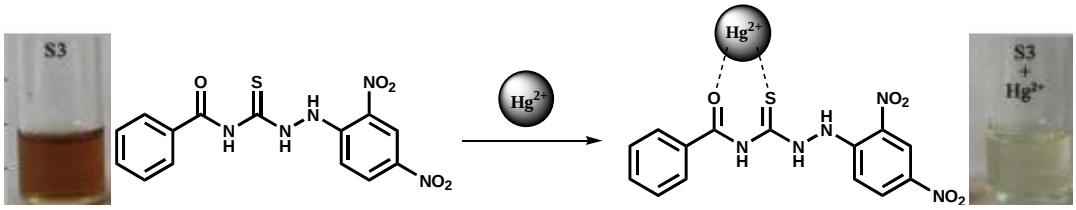

Sarkar et al. synthesized a pyrene-based, highly selective fluorescence sensor for Cu^{2+} ions via a static excimer process. The DL found to be 4×10^{-7} M (Sarkar et al. 2013).

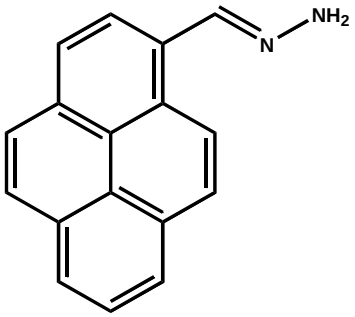

Wang and Wu synthesized a pyrene derivative sensor containing a benzothiazolenhydrazone moiety, which exhibits a highly selective turn-on fluorescence sensor for Cu^{2+} ions over the range of pH 2 to 8.5, and this was used as a fluorescent probe for detecting Cu^{2+} in living cells (Wang and Wu 2013a).

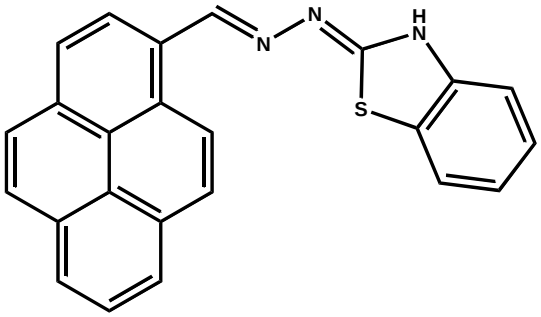

A highly sensitive and selective quinoline based colorimetric and flurosens chemosensor was reported for the sensing of Cd^{2+} ions in aqueous media **(Goswami et al. 2013)**. The DL found to be 10^{-7} M with a good color change from colorless to pink color in the presence of Cd^{2+} ions.

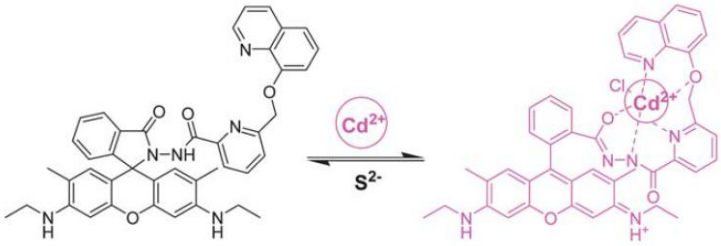

Udayakumari et al. reported thiophene–based Schiff base chemosensor R1 and R2 for toxic metal ions in the water media and its applicability in living cells. The receptor R1 exhibits selectivity towards Pb^{2+}, Hg^{2+}, and Sn^{2+} ions. R2 exhibits selectivity for Hg^{2+}, $Cu^{2+,}$ and Sn^{2+} ions in the aqueous medium (Udhayakumari et al. 2014).

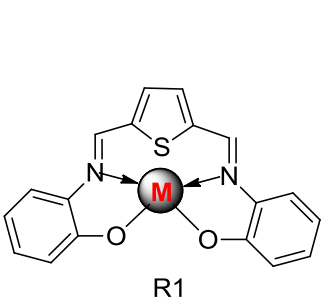

R1

M= Pb^{2+}, Hg^{2+} and Sn^{2+}

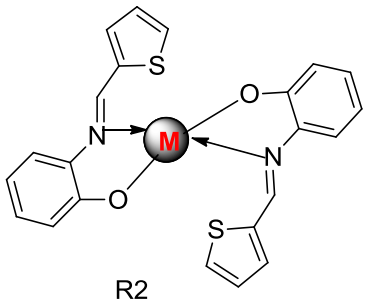

R2

M= Cu^{2+} and Hg^{2+}

Jo et al. synthesized a derivative of 2-hydroxy-1-naphthaldehyde Schiff base for colorimetric selective detection of Cu^{2+} in the aqueous medium and exhibited naked eye response from yellow to orange color in the attendance of Cu^{2+}(Jo et al. 2014).

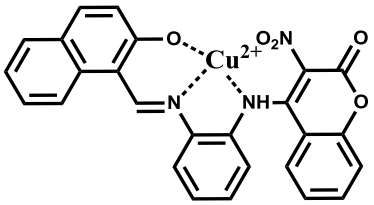

Wu et al. synthesized non-sulfur 1, 5-diaminonaphthalene Schiff base derivatives sensor for mercury ions. This sensor displayed a dual-channel (fluorescent and UV–Vis) response for Hg^{2+} ions. The sensor exhibits an ICT mechanism for the detection of mercury ions (Wu et al. 2014).

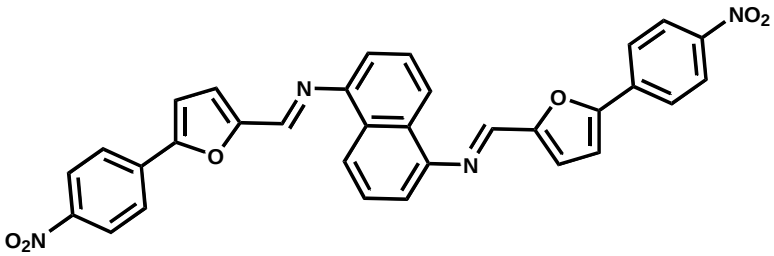

Singhal et al. reported thiophene based Schiff base chemosensor for the detection of Hg^{2+} ion by ‘naked eye’ and fluoresce ‘turn on' mechanism. The sensor displayed a yellow color from colorless in the attendance of Hg^{2+} ions. The DL found to be 20 μM in the aqueous medium (Singhal et al. 2015).

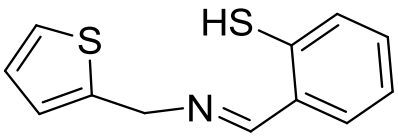

Xiong et al. developed 4-aminoantipyrine derivatives as a colorimetric chemosensor for the recognition of Cu^{2+} ions. Further, the sensor application developed using the test kit method for the detection of Cu^{2+} ions. The found DL to be 2.14×10^{-7} M, and it displayed purple color in the presence of Cu^{2+} from colorless solution (Xiong et al. 2016).

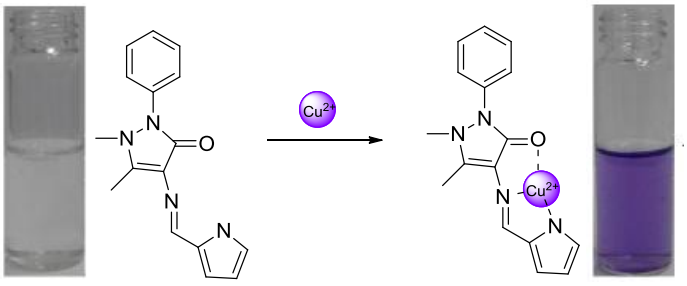

Huo et al. Have been reported five colorimetric chemosensors for the detection of Hg^{2+} ions in EtOH/H_2O (v/v = 4:1) system (Huo et al. 2016). All the receptors (1–5), displayed red-shift in the UV–Vis spectrum with the addition of Hg^{2+} ions. The stability constant and the detection limit was given below. R4 exhibits good stability constant, and DL compare to other receptors.

Name of receptor	Binding constants (K)	Detection limit (M)
R1	6.88×10^2	2.40×10^{-6}
R2	4.89×10^2	3.13×10^{-6}
R3	3.11×10^3	2.74×10^{-6}
R4	3.62×10^3	1.93×10^{-6}
R5	2.12×10^3	3.13×10^{-6}

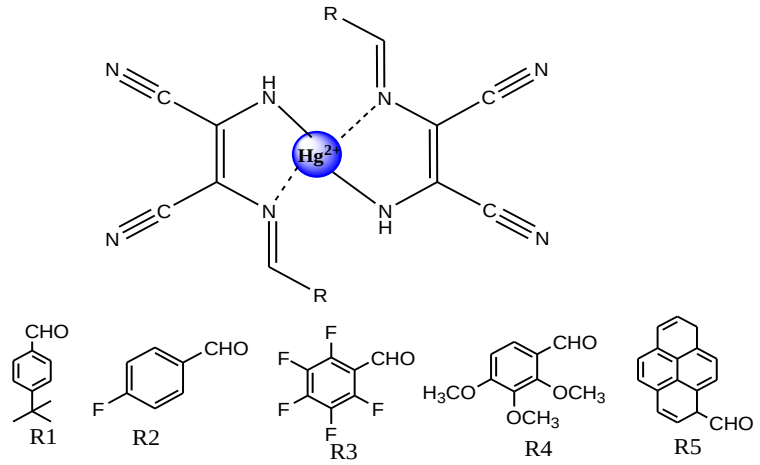

Ghorai et al. designed and synthesized reversible dual-channel response chemosensors based on azino *bis*-Schiff base for the detection of Pb^{2+} in water media (Ghorai et al. 2016). The sensor displayed sensing ability in a wide pH range of 4–10. The receptor exhibits 2:1 stoichiometric complexation. With the addition of Pb^{2+}, the sensor exhibits a redshift in the UV–Vis spec[illegible], and The DL found to be 8 nM.

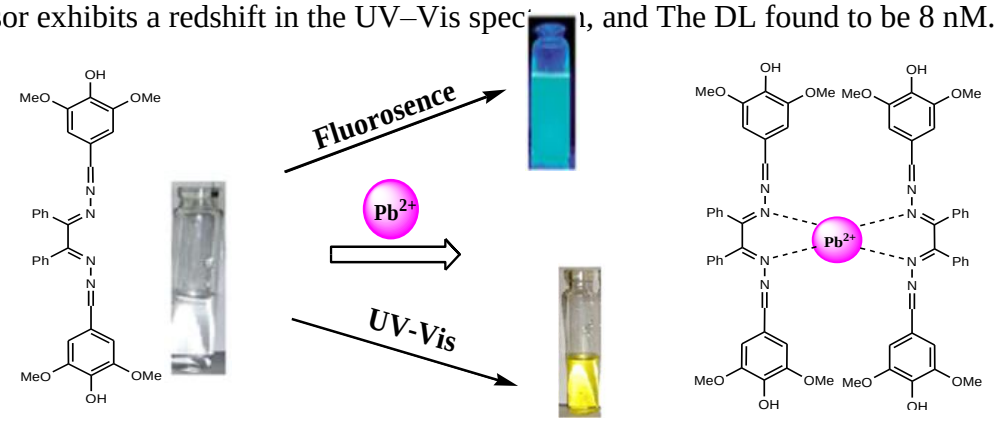

Lee et al. reported a fluorescence "turn-on" chemosensor for Hg^{2+} and Ag^{+} based on 7-nitrobenzo-2-oxa-1,3-diazolyl (Lee et al. 2017). It has shown high sensitivity toward Hg^{2+} with detection limits of 0.05 μM.

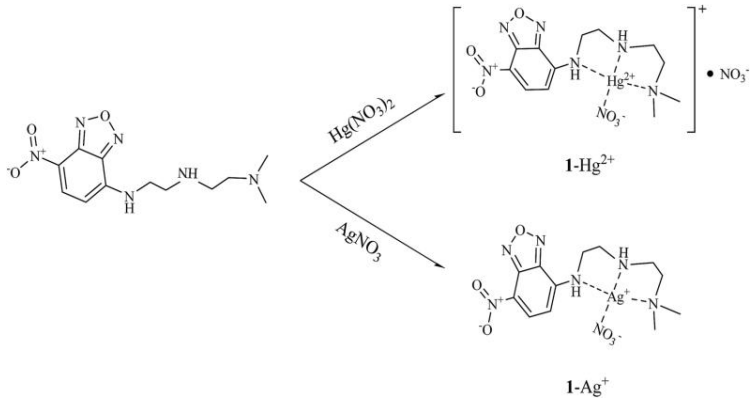

Zhang et al. developed a simple Schiff base chemosensor for multi-ions sensing of Cu^{2+}, $Ag^{+,}$ and Hg^{2+} in DMSO: H_2O (1:1, v/v) solution (Zhang et al. 2017). The sensor exhibits a 1: 2 binding ratio of sensor and metal ions. The calculated detection limit is 52.7 μM for Hg^{2+}, 63.7 μM for Ag^{+} and 64.8 μM for Cu^{2+} ions. The binding constant was calculated to be 9.27×10^4 M^{-1} for sensor-Hg^{2+}, 1.37×10^5 M^{-1} for sensor-Ag^{+}, and 1.64×10^5 M^{-1} for sensor-Cu^{2+}.

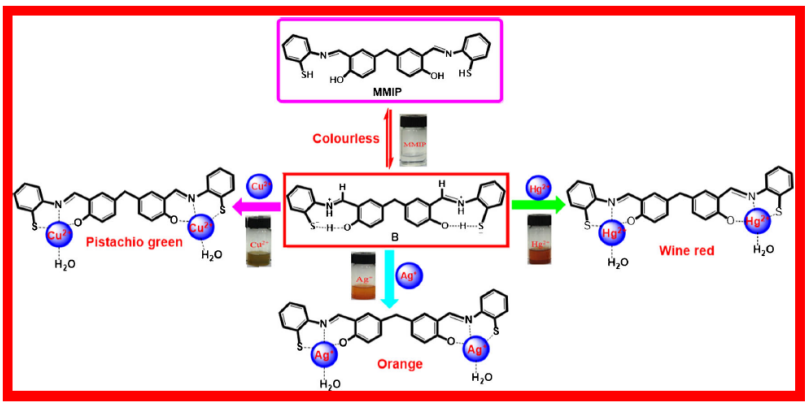

Chauhan et al. synthesized a new benzothiazole Schiff base chemosensor for colorimetric sensing of arsenic and utilized for on-site sensing at ppb level (Chauhan et al. 2017). The sensor displayed a naked eye response of brown-orange from light yellow in the addition of arsenic in an aqueous medium. The sensor exhibits a low naked eye detection limit of 7.2 ppb for As^{3+} and 6.7 ppb for As^{5+} without using any instrument.

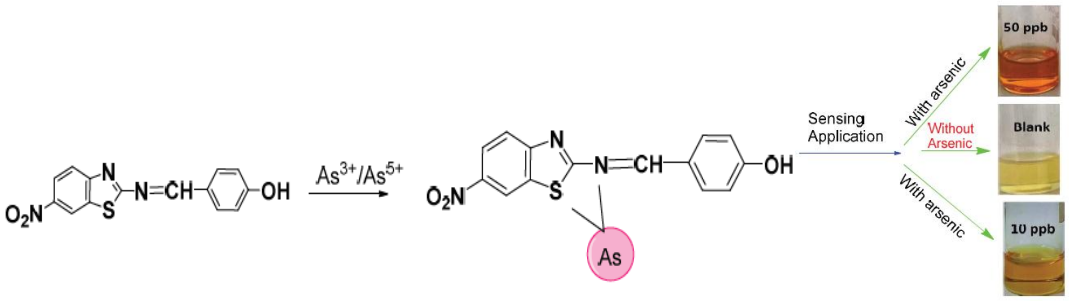

Yin et al. synthesized a derivative of carbazole chemosensor (fluorescence) for the detection of Cu^{2+} (Yin et al. 2018). The receptor exhibits the colorimetric and fluorometric response for the Cu^{2+} ions in the acetonitrile solution. The sensor displayed a 1:1 stoichiometric complex with Cu^{2+} ions, and the calculated DL was 2.74×10^{-8} M from the fluorescence method.

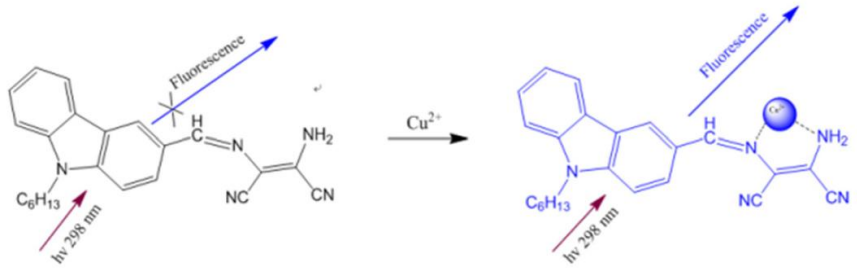

Kalyani Rout et al. have been a synthesis of new guanidine based bis Schiff base chemosensor for colorimetric detection of Hg(II) and fluorescent detection of Zn(II) ions **(Rout et al. 2019)**. The sensor displayed a naked eye response from yellow to red for Hg^{2+}. The detection limit for Hg^{2+} and Zn^{2+} is found to be 9.89×10^{-7} M and 1.23×10^{-6} M, respectively. Further, the chemosensor has applications in real sample analysis in environmental and biological samples and building molecular logical devices.

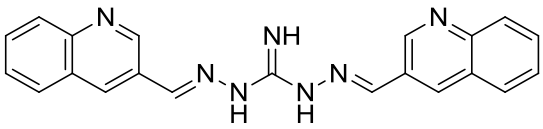

Thangaraj Anand and Suban K Sahoo have synthesized a new sensor, **N1.** In the 1:1 of CH_3OH:H_2O (v/v) medium, it exhibited selectivity and sensitivity for Hg^{2+} and Cu^{2+} ions by a distinct colorimetric change from pale yellow to pink color. It exhibits 1:1 stoichiometry with Cu^{2+}/Hg^{2+} ions. The N1 displayed a detection limit of 4.70×10^{-7} M and 1.23×10^{-7} M for Hg^{2+} and Cu^{2+} ions. Finally, the practicability of **N1**

to quantify Hg^{2+} and Cu^{2+} ions in real water samples was successfully validated by using both the UV–Vis and the smartphone (Anand and Sahoo 2019).

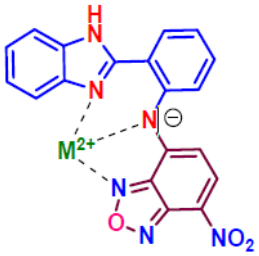

M^{2+} =Cu^{2+}, Hg^{2+} Sensor N1

1.7. Scope of work

Chemosensors have simple, selective, and cost-effective for the detection of environmental pollutants and biologically important cations compared to the other detection methods. The metal cations such as Hg^{2+}, Pb^{2+}, As^{3+} & Cd^{2+}, etc., are pollutants because of their high toxicity. The biologically important cations such as Cu^{2+}, Co^{2+}, Zn^{2+}, Fe^{2+} & $Mg^{2+,}$ etc., play a major role in the biological system. A wide range of cations present in the environment, among them the detection of environmentally hazardous and biologically harmful cations, has gained great attention because of their high toxicity and cause serious health illness. Literature reports reveal that the design and synthesis of the chemosensor are well-defined areas of supramolecular chemistry.

Nevertheless, the majority of researchers are having some limitations and drawback, which are described below:

- Most of the reported chemosensors in the literature are not cost-effective. Because these are synthesized by multistep synthesis with complicated chemistry
- The majority of the detection of heavy metal ions is achieved by the fluorometric method. Therefore, the detection process is complicated and need instrumental knowledge
- Majority of the chemosensors are limited to qualitative applications only
- Selectivity and sensitivity (at μM levels) of chemosensors are still needed to be enhanced

- Most of the chemosensors reported are without any real-time application
- Very few reports are available with analytical method validation and real-life applications

1.8. Objectives

The main objectives of the proposed work are as follows,

- Design and synthesis of organic molecules which can show colorimetric cation sensing property, even at low concentration of an analyte in organic, semi-aqueous and aqueous solution
- Characterization of the as-synthesized organic chemosensor by various spectroscopic techniques like ^{1}H-NMR, ^{13}C-NMR, FT-IR, Mass analysis, and SC-XRD (if possible)
- Determination of the stoichiometric ratio of receptor-cation complexation using Job's plot / B-H equation
- Qualitative analysis and quantitative analysis of heavy metal ions and finding their detection limits
- Calculation of binding constant using B-H equation
- Investigation of the binding mechanism of the cation with the chemosensor by FT-IR, Mass, and ^{1}H-NMR titration(if possible)
- To demonstrate real-time application by detecting various cations present in tap and drinking water samples

CHAPTER–2

MULTI-SIGNALING THIOCARBOHYDRAZIDE BASED COLORIMETRIC SENSORS FOR THE SELECTIVE RECOGNITION OF HEAVY METAL IONS IN AN AQUEOUS MEDIUM

CHAPTER–2

2. MULTI-SIGNALING THIOCARBOHYDRAZIDE BASED COLORIMETRIC SENSORS FOR THE SELECTIVE RECOGNITION OF HEAVY METAL IONS IN AN AQUEOUS MEDIUM

Abstract

In this chapter, the design, syntheses, and characterization of new thiocarbohydrazide derivatives as a colorimetric chemosensor for heavy metal ion detection have included. The colorimetric cation sensing properties and detection mechanism of these chemosensors have been discussed in detail.

2.1. Introduction

The design of new colorimetric chemosensors capable of the selective recognition of biologically and environmentally important metal ions, such as Hg^{2+}, Pb^{2+}, Cu^{2+}, and Cd^{2+}, has attracted much attention. Also, the application of new colorimetric chemosensors has extensively improved, mostly because it involves the detection through a less expensive technique in which the analyte is detected by a color change noticeable by direct optical observation. Nevertheless, colorimetric techniques also offer several advantages in comparison with others, such as high sensitivity, quick response, and they are non-destructive (Kim et al. 2012; Marbella et al. 2009). Hence, many artificial organic receptor molecules containing different channels such as imine, (Azadbakht et al. 2013; Ermakova et al. 2013; Jiang et al. 2012; Lauwerys et al. 1994), (Choi et al. 2014), coumarine, (Beer and Gale 2001; Que et al. 2008), quinolines(Jiang et al. 2011), (Vinod Kumar and Anthony 2014), rhodamine, (Labbé et al. 1999), (Zhang et al. 2015) have been developed as colorimetric cation sensors. Some metal ions have a very important role, namely in stabilization and reactivity of proteins. However, for human and environmental well-being, they must occur in optimal quantities. Otherwise, they can promote metabolic disorders since they are easily fascinated and accumulated from the environment (Zhang et al. 2015) (Wu et al. 2016). Metal ions, for instance, Hg^{2+}, Pb^{2+}, and Cd^{2+}

ions are extremely toxic and pollutant, and once present in water, they are carcinogenic (Nordberg 1992) (Malm 1998).

Recently, udhayakumari et al. developed an innovative Schiff base molecular sensor **1** for different metal ions using signalling channels based on a carbazole backbone, which exhibits a highly selective colorimetric response to Hg^{2+}, Cu^{2+}, Co^{2+} ions in DMSO solvent (Udhayakumari et al. 2014). The chromogenic 'naked eye' and fluorogenic sensor have been developed for mercury metal ion detection (Singhal et al. 2015) (Das et al. 2012), S.K Sahoo has been reported pyridoxal derived chemosensor for chromogenic sensing of Cu^{2+} and fluorogenic sensing of Fe^{3+} in semi-aqueous medium (Sahoo et al. 2016). R. S. Patil designed a simple uracil nitroso amine-based colorimetric chemosensor for Cu^{2+} ions in an aqueous environment (Patil et al. 2015).

With this background, in the present work, the thiocarbazide group has into the sensor molecule so that it can strengthen transition and heavy metals coordination ability. These chemosensor moieties comprise hydroxy (–OH), thio group (–C=S–), and imine group (–C=N) groups as a binding site for cation detection. The chemosensors were designed on the binding site, spacer, and signaling unit methodology, which are used for the recognition of different heavy metal ions. **S1R1** shows multi-colored for Hg^{2+}, Cu^{2+}, Cd^{2+}, and Pb^{2+} ions from colorless to pink, yellow, brownish-red, and orange, respectively, **S1R2** exhibits colorless to yellow in the presence of **Cu^{2+}** ions, and **S1R3** exhibits a significant color change Cu^{2+} ions from yellow to brown in an aqueous environment.

2.2. Experimental section

All chemicals and metal nitrate salts were purchased from commercial suppliers and used without any further purification. Chromatography grade solvents are used for synthesis and UV-Vis titrations without any further purification.

^{1}H-NMR (400MHz) and ^{13}C-NMR (100MHz) spectra were recorded on a Bruker spectrometer. Chemical shifts are reported in δ scale (in ppm) downfield from tetramethylsilane (TMS, δ 0.00) and DMSO-d_6 (39.50), respectively, as internal reference standards). The melting point was recorded on Bio-cote (SMP10) instrument and in open capillary and is uncorrected. Fourier Transform Infrared (FT-

IR) spectra were recorded on a Bruker Alpha, which is equipped with silicon carbide as IR source. All sample spectra were recorded using KBr pellet media. The samples under study were recorded with 16 scans with a sample resolution of 4 cm^{-1}. The background data collection was done with the KBr pallet before the analysis of samples. The UV–Vis titrations were carried out on UV–Vis spectrophotometer (Analytikjena Specord S600) in standard 3.0 mL quartz cells (2 optical windows) having a path length of 1.0 cm.

2.2.1. Colorimetric and UV–Vis studies

A Stock solution of various metal ions as their nitrate salts (1.0×10^{-2} M) was prepared in de-ionized water. An individual chemosensor stock solution of **S1R1-S1R3** was prepared in dimethylformamide (DMF). The stock solutions **S1R1**, S**R2,** and **S1R3** were further diluted to 5.0×10^{-6} M, 2.5×10^{-5} M, and 1.0×10^{-5} M with the same solvent, respectively. In colorimetric and UV–Vis titration experiments, metal ions were added by using a micropipette to a chemosensor solution **(S1R1-S1R3)**. UV–Vis spectral data were recorded after the addition of the metal ions using 3.0 mL quartz cells (2 optical windows) having a path length of 1.0 cm.

2.2.2. Synthesis of chemosensors S1R1–S1R3

The synthesis procedure of **S1R1–S1R3** has illustrated in the **scheme 2.1**. The synthesis of chemosensor **S1R1:** Thiocarbohydrazide (0.050g, 0.47mmol) and 8-hydroxy quinoline-2-carbaldehyde (0.163g, 0.95mmol) were separately dissolved in 10 mL ethanol. Then aldehydehyde solution was added drop-wise with constant stirring to the thiocarbohydrazide solution. To this a catalytic amount of acetic acid was added and the reaction mixture was stirred at room temperature for 3 hours. The progress of reaction was monitored by TLC. After the completion of reaction the reaction mixture was filtered and washed with hot ethanol. Similarly, the **S1R2** and **S1R3** were synthesized as stated above synthetic methodology. The **S1R2** was synthesized by the reaction of thiocarbohydrazide (0.050g, 0.47mmol) and 5-phenyl thiophene-2-carboxaldehyde (0.089, 0.95mmol). The **S1R3** was synthesized by the reaction of thiocarbohydrazide (0.047g, 0.47mmol) and 5-Nitro furfural-2-

carboxaldehyde (0.133g, 0.94mmol). The final obtained desired compounds were characterized by using standard spectroscopic methods as given below.

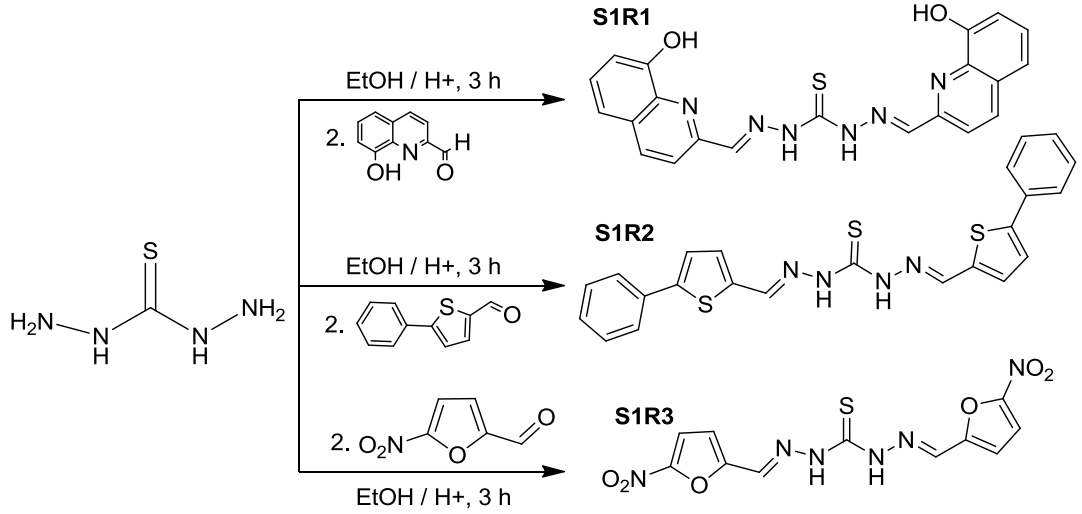

Scheme 2.1: Synthesis route for compounds **S1R1–S1R3**

(Z)-N'-((Z)-(8-hydroxyisoquinolin-3-yl)methylene)-2-((8-hydroxyquinolin-2-yl) methylene)hydrazine-1 (S1R1):

Yield: 94.3 %, **Melting point**: 243˚C. **FT-IR (KBr, cm^{-1}):** 3486, 3353, 2985, 1533, 1499, 1427, 1230, 1137, 1086, 892, 842, 760, 691 **(Fig. 2.1)**. **^{1}H NMR (400 MHz; DMSO-d_6, δ_{ppm}):** 9.925 (s 2H, phenolic –OH), 8.551 (s, 2H, –NH), 8.392 (m, 2H, imine (HC=N)), 7.962 (m, 2H, aromatic (–C=CH)), 7.453 (m, 4H, aromatic (–C=CH)), 7.140 (m, 2H, aromatic (–C=CH)) **(Fig. 2.2)**. **^{13}C-NMR (100 MHz; DMSO-d_6, δ_{ppm})):** 176.8 (–C=S), 153.0 (HC=NH), 152.1 (aromatic =C–OH), 139.2, 130.7, 128.7, 126.4, 126.2, 115.7, 114.0 (aromatic –C=C– (quinoline ring) **(Fig. 2.5)**. **LC-MS (ESI) m/z:** Calculated for $C_{21}H_{16}N_6O_2S$, 416.5, found, 417.51 (M+1) **(Fig. 2.8)**.

(Z)-2-((4-phenylthiophen-2-yl)methylene)-N'-((Z)-(4-phenylthiophen-2-yl)methylene) hydrazine-1-carbothiohydrazide (S1R2):

Yield: 97.5 %, **Melting point:** 212˚C; **FT-IR (KBr, cm^{-1}):** 3202, 2969, 1566, 1503, 1247, 1197, 1018, 911, 791, 744, 620 **(Fig. 2.1)**. **^{1}H NMR (400 MHz; DMSO-d_6, δ_{ppm}):** 9.474 (s, 2H, –NH), 8.168 (s, 2H, imine (HC=N)), 7.699 (d. 4H, aromatic thiophene (–C=CH) J= 2.8Hz), 7.528 (d. 2H, aromatic, phenyl (–C=CH), J=3.0 Hz), 7.455 (m, 6H, aromatic phenyl (–C=CH)), 7.359 (m, 2H, aromatic phenyl (–C=CH)) **(Fig. 2.3)**. **^{13}C-NMR (100 MHz; DMSO-d_6, δ_{ppm}):** 175.9 (–C=S), 145.7 (HC=NH), 138.57, 137.6, 133.8 (thiophene aromatic –C=C–), 132.0, 129.7, 128.7, 125.9, 124.8

(quinoline aromatic –C=C–) **(Fig. 2.6)**. **LC-MS (ESI) m/z:** Calculated for $C_{23}H_{18}N_4S_3$, 446.6, found, 447.71 (M+1) **(Fig. 2.9)**.

(Z)-2-((4-nitrofuran-2-yl)methylene)-N'-((Z)-(5-nitrofuran-2-yl)methylene) hydrazine-1-carbothiohydrazide (S1R3):

Yield: 97.4 %, **Melting point:** 208˚C. **FT-IR (KBr, cm^{-1}):** 3240, 3106, 1541, 1474, 1342, 1240, 1201, 1103, 1017, 810, 771, 689 **(Fig. 2.1)**. **^{1}H NMR (400 MHz; DMSO-d_6, δ_{ppm}):** 12.258 (s, 1H, –NH), 10.217 (s, 1H, –NH), 8.082 (s, 1H, imine (HC=N)), 7.850 (s, 1H aromatic (HC=N), 1H), 7.529–7.523 (d, 2H, aromatic (–C=CH), J=2.4Hz), 7.401–7.387 (d. 1H, aromatic Nitro furfural (–C=CH), J=5.2Hz), 7.247–7.234 (d. 1H, aromatic Nitro furfural (–C=CH), J=5.2Hz) **(Fig. 2.4)**. **^{13}C-NMR (100 MHz; DMSO-d_6, δ_{ppm}):** 180.8 (–C=S), 158.7 (HC=NH), 143.5 (furfuran =C–NO_2), 134.1 (furfuran C–O–C), 133.60, 123.1, 117.4 (aromatic furfural –C=C–) **(Fig. 2.7)**. **LC-MS (ESI) m/z:** Calculated for $C_{11}H_8N_6O_6S$, 352.3, found, 353.21 (M+1) **(Fig. 2.10)**.

2.2.3. Characterization spectra of chemosensor S1R1-S1R3

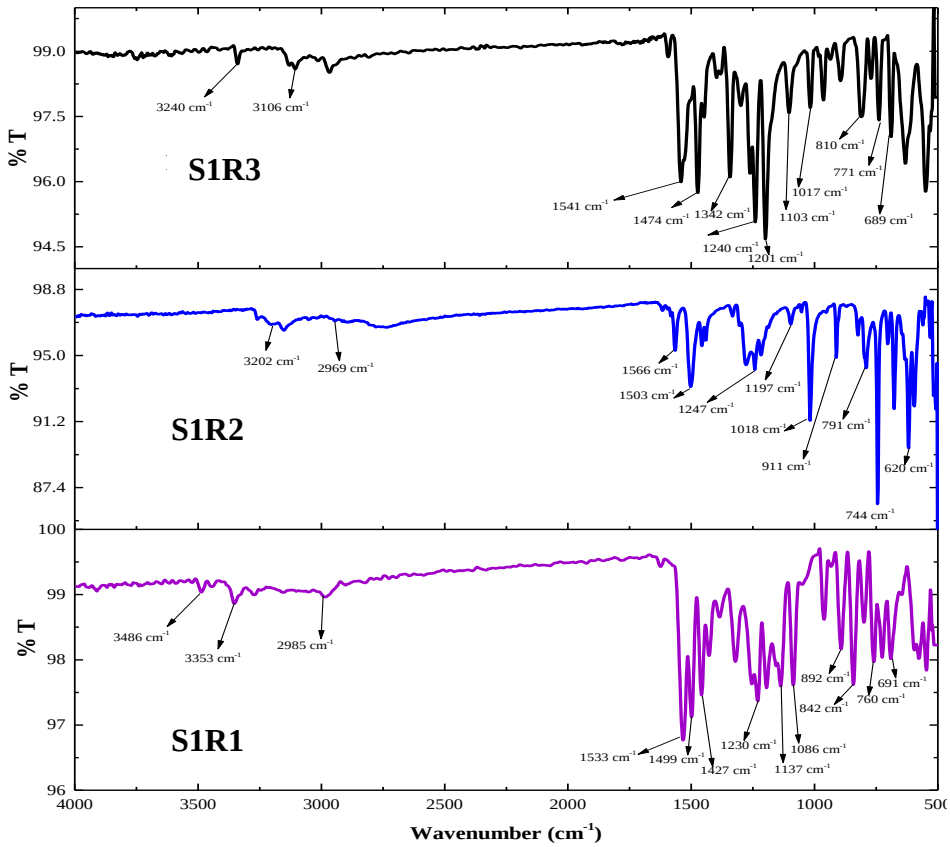

Fig. 2.1: FT-IR Spectra of chemosensors **S1R1–S1R3**

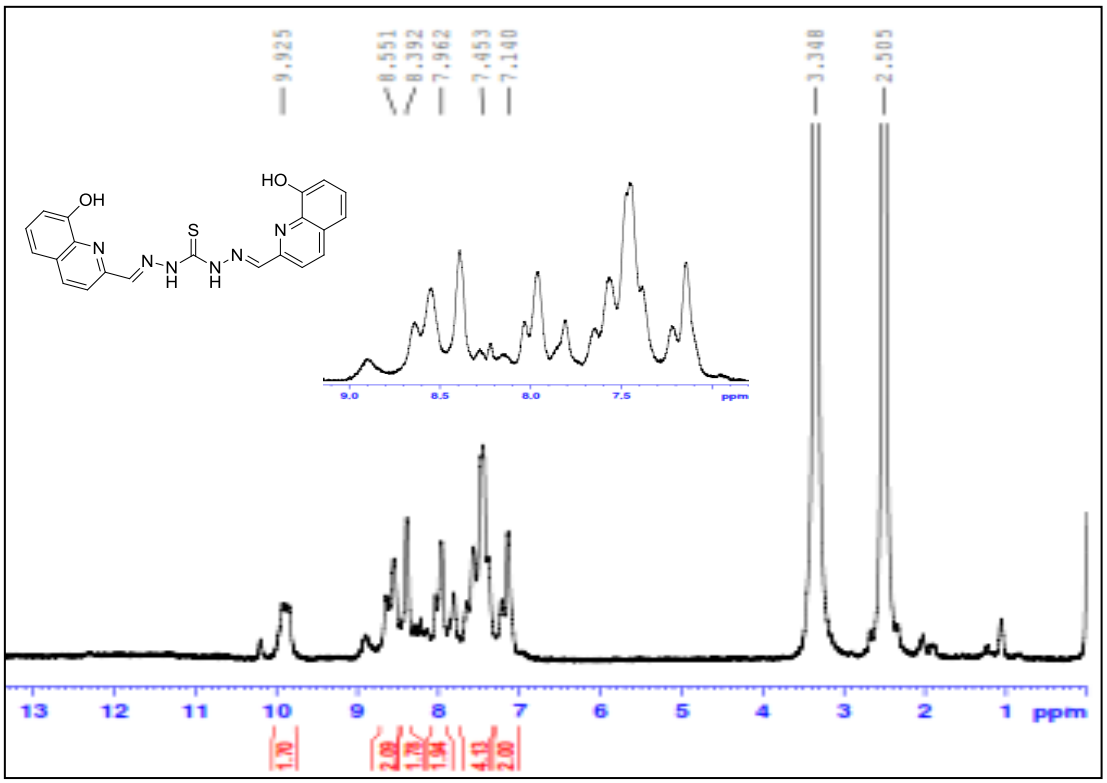

Fig. 2.2: ^{1}H NMR spectrum of chemosensor **S1R1**

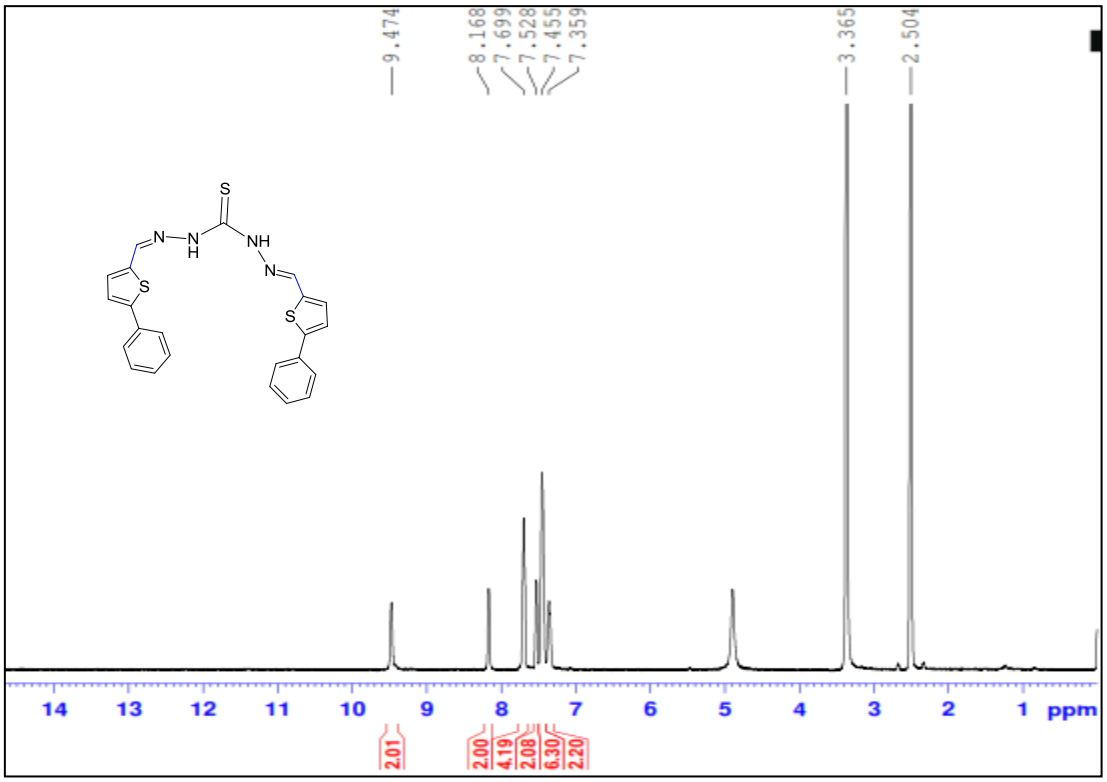

Fig. 2.3: ^{1}H NMR spectrum of chemosensor **S1R2**

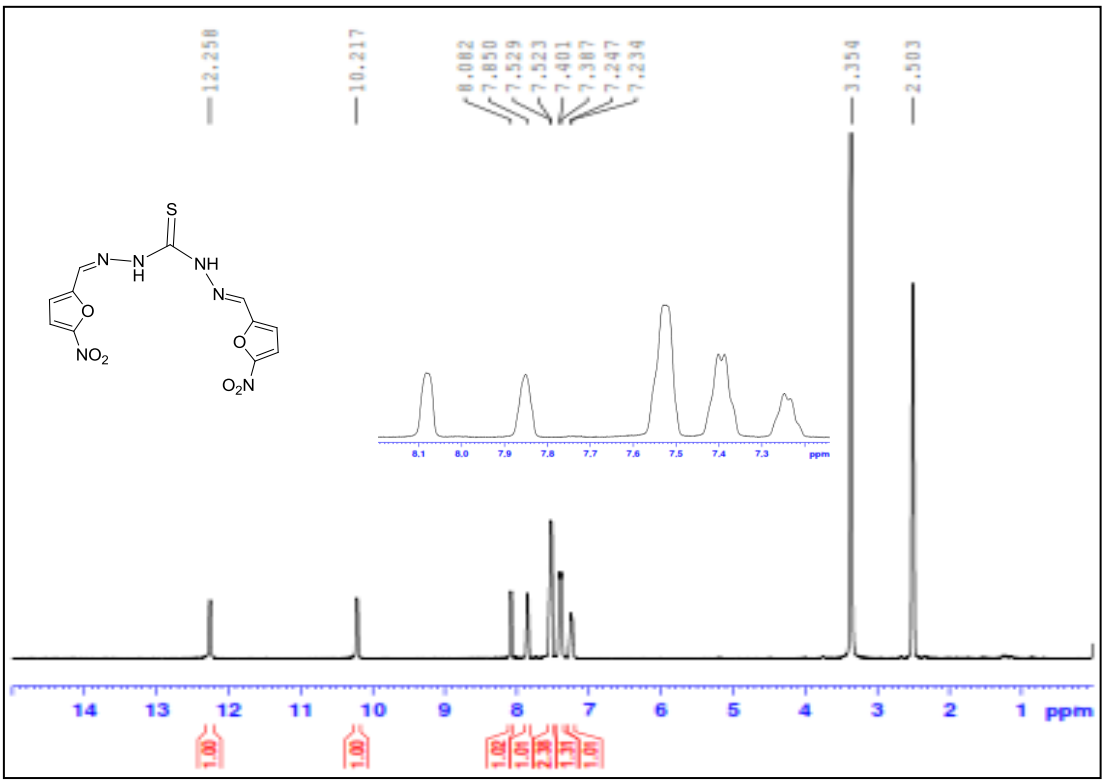

Fig. 2.4: ^{1}H NMR spectrum of chemosensor **S1R3**

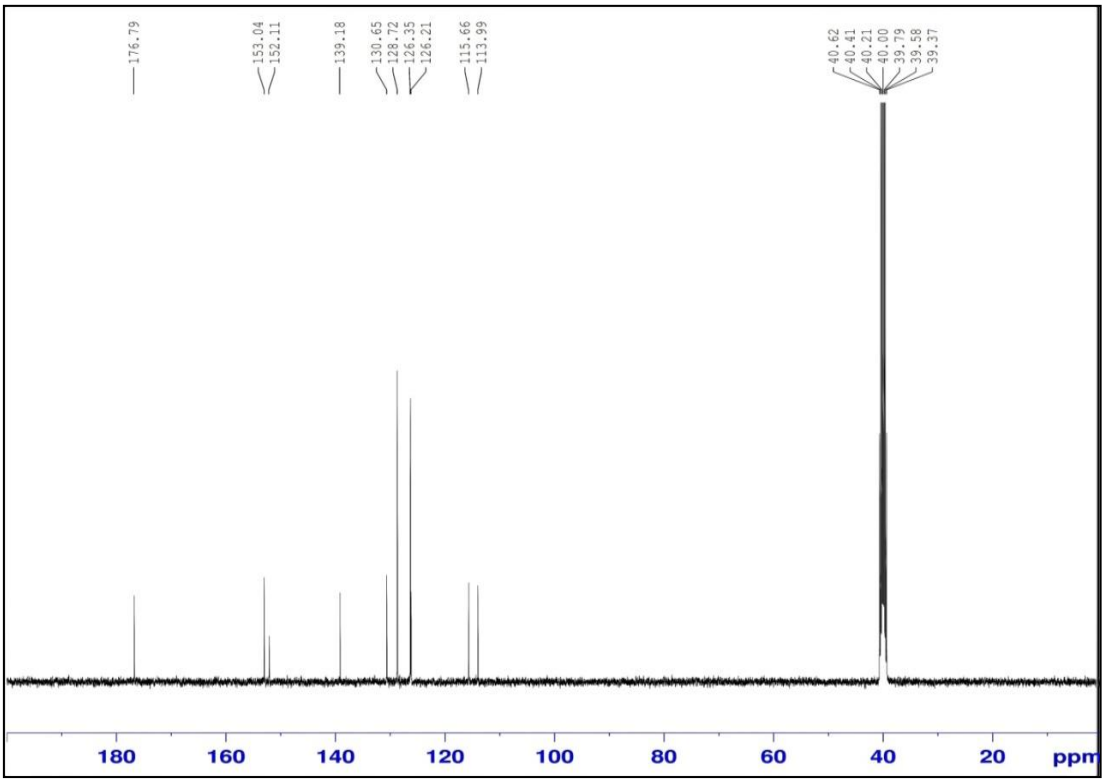

Fig. 2.5: ^{13}C NMR spectrum of chemosensor **S1R1**

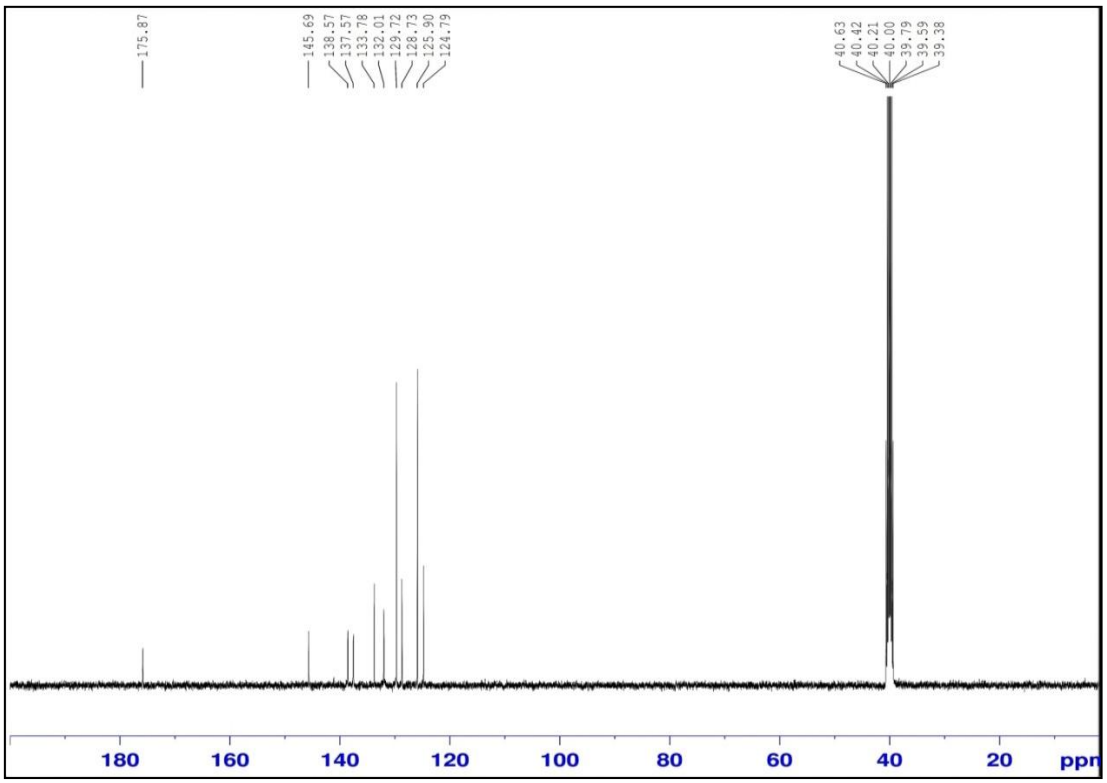

Fig. 2.6: ^{13}C NMR spectrum of chemosensor **S1R2**

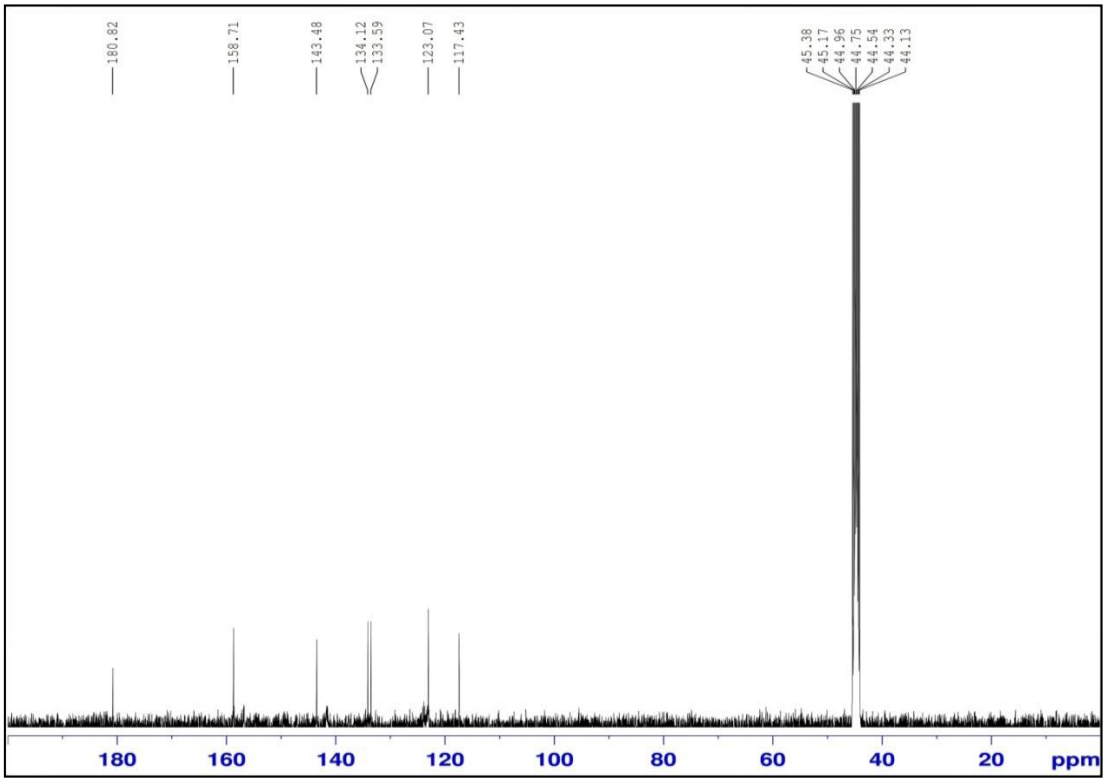

Fig. 2.7: ^{13}C NMR spectrum of chemosensor **S1R3**

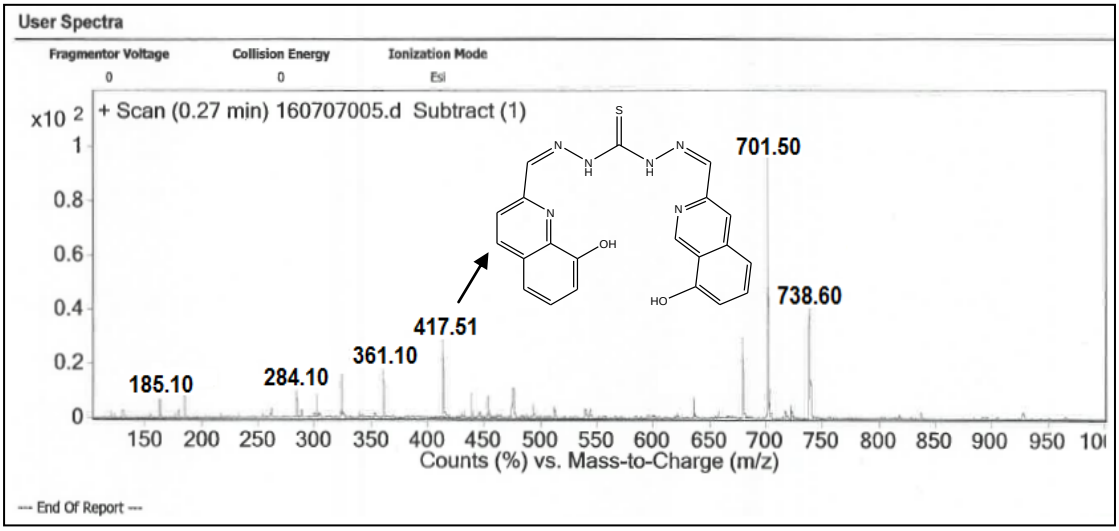

Fig. 2.8: ESI-mass spectrum of chemosensor **S1R1**

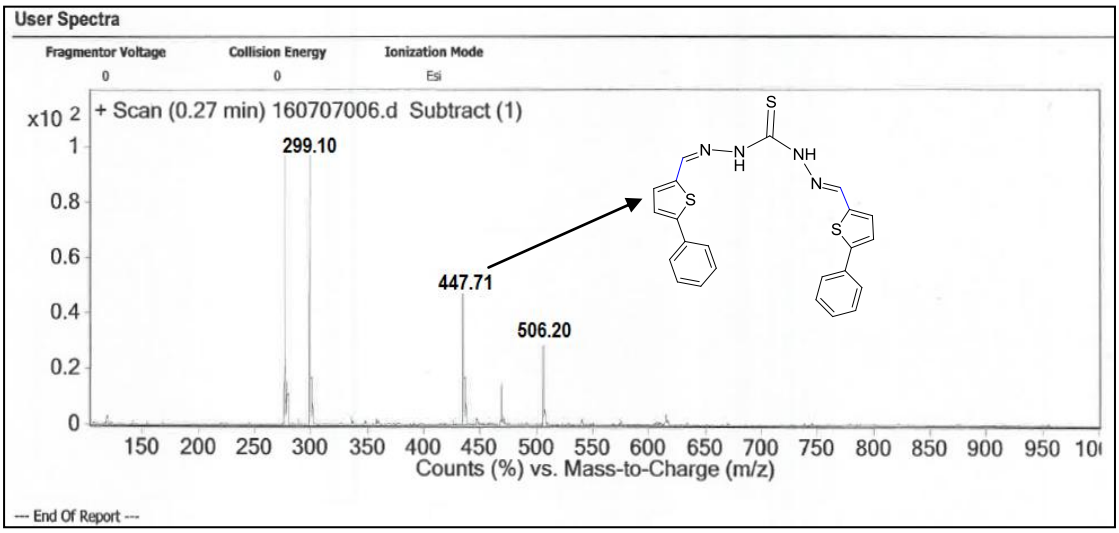

Fig. 2.9: ESI-mass spectrum of chemosensor **S1R2**

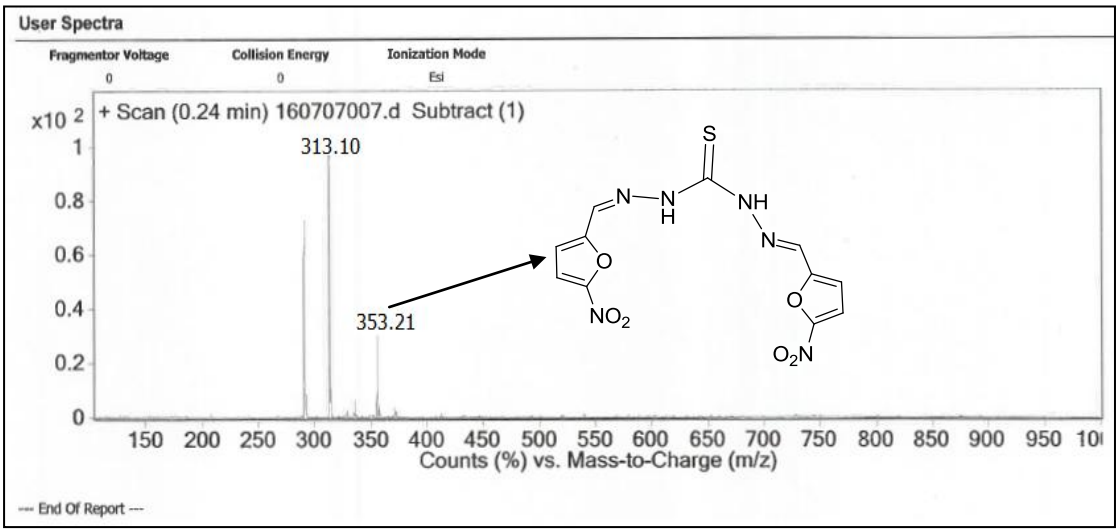

Fig. 2.10: ESI-mass spectrum of chemosensor **S1R3**

2.3. Results and discussion

2.3.1. Colorimetric studies

The colorimetric sensing abilities were initially examined by adding various nitrate salts of cations such as Fe^{3+}, Al^{3+}, Ag^{+}, Mn^{2+}, Mg^{2+}, Ca^{2+}, K^{+}, Na^{+}, Cu^{2+}, Hg^{2+},Cr^{3+}, Fe^{2+}, Co^{2+}, Zn^{2+}, Ni^{2+}, Cd^{2+} and Pb^{2+} ions to chemosensors **S1R1–S1R3** (**Fig. 2.11**). **S1R2** and **S1R3** did not show any significant color change in the presence of Fe^{3+}, Al^{3+}, Ag^{+}, Mn^{2+}, Mg^{2+}, Ca^{2+}, K^{+}, Na^{+}, Hg^{2+}, Cr^{3+}, Fe^{2+}, Co^{2+}, Zn^{2+}, Ni^{2+}, Cd^{2+} and Pb^{2+} ions apart from Cu^{2+} ions. **S1R1** did not show any color change in the presence of Fe^{3+}, Al^{3+}, Ag^{+}, Mn^{2+}, Mg^{2+}, Ca^{2+}, K^{+}, Na^{+}, Cr^{3+}, Fe^{2+}, Co^{2+}, Zn^{2+}, and Ni^{2+} ions. And however in the presence of Hg^{2+}, Cu^{2+}, Cd^{2+}, and Pb^{2+} ions, it exhibits multi-color response from colorless to pink, yellow, brownish-red, and orange. The color change of chemosensor **S1R1–S1R3** in the presence of different metal ions is displayed in **table 2.1.**

Table 2.1: Color change of chemosensor **S1R1–S1R3** in the presence of 2.0 equivalence of different metal ions

Chemosensor	Con. (M) of Receptor	Color of the	Volume of sensor(mL)	Metal ion	Color change
S1R1	5.0×10^{-6}	Colorless	2.0	Hg^{2+}	Pink
				Cu^{2+}	Yellow
				Cd^{2+}	Brownish red
				Pb^{2+}	Orange
S1R2	2.5×10^{-5}	Colorless	2.0	Cu^{2+}	Yellow
S1R3	1.0×10^{-5}	Yellow	2.0	Cu^{2+}	Orange

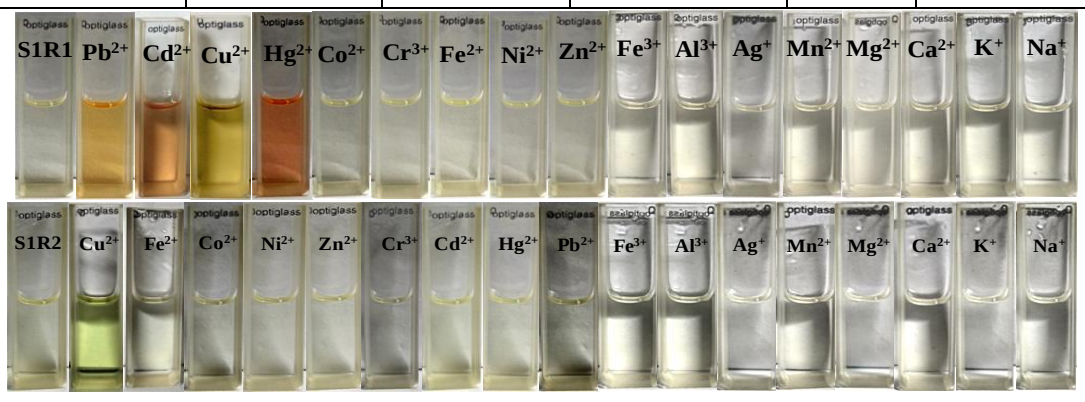

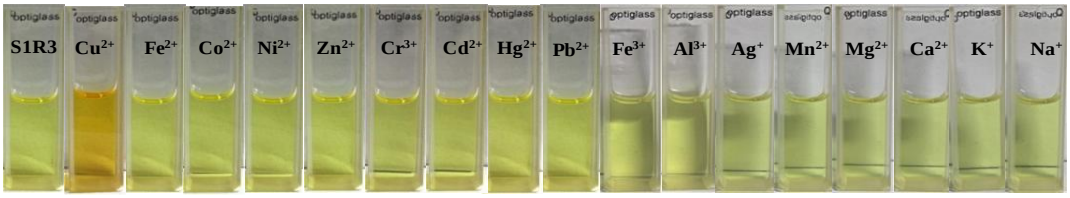

Fig. 2.11: The colorimetric changes observed by naked-eye of chemosensor **S1R1–S1R3** upon the addition of 2.0 equiv. of various cations in an aqueous solution

2.3.2. UV–Visible absorption studies

All the analytical solutions were prepared, as mentioned in the experimental section of colorimetric and UV–Vis studies.

A detailed UV–Vis titration and comparative study experiment were conducted to investigate the selectivity and binding properties of chemosensor **S1R1–S1R3** towards active and inactive metal ions based on the observation of colorimetric study. The **S1R1–S1R3** did not show any significant changes in the absorption spectrum with the addition of 2.0 equivalences of different metal ions except above stated selective metal ions (in Colorimetric) **(Fig. 2.12**). It suggests that the high selectivity of chemosensor **S1R1–S1R3** towards active metal ions in the presence of other interfering metal ions.

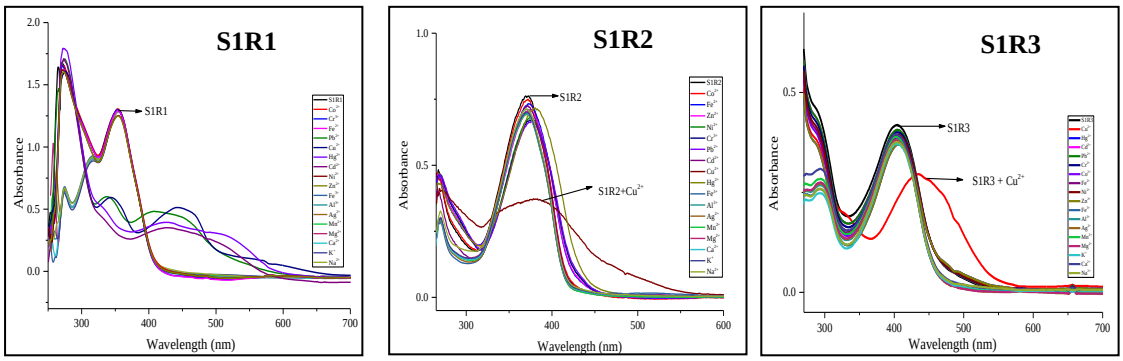

Fig. 2.12: Comparative UV-Vis spectra of chemosensor **S1R1, S1R2**, and **S1R3** in the presence of 2.0 equvi. of other cations.

In the UV–Vis titration experiment, chemosensor **S1R1** exhibits an absorption band at 354 nm in the absence of metal ions, and the solution is colorless. The absorption spectrum of **S1R1** exhibits redshift by 146 nm, 96 nm, 66 nm, and 96 nm fold increment, with multi-color signals (pink, yellow, brownish-red, and orange color) in the presence of Hg^{2+}, Cu^{2+}, Cd^{2+}, and Pb^{2+} ions respectively. It exhibits different isosbestic points centered at 445 nm, 397 nm, 393 nm, and 390 nm for Hg^{2+},

Cu^{2+}, Cd^{2+}, and Pb^{2+} ions, respectively. It suggests the formation of metal-complex **(Fig. 2.13a-d).** The multi-sensing ability of **S1R1** is due to the presence of hydroxy functionality of quinoline moiety, which has suitable binding sites (–OH, HC=N, and N in quinoline ring) to co-ordinate with the metal ions.

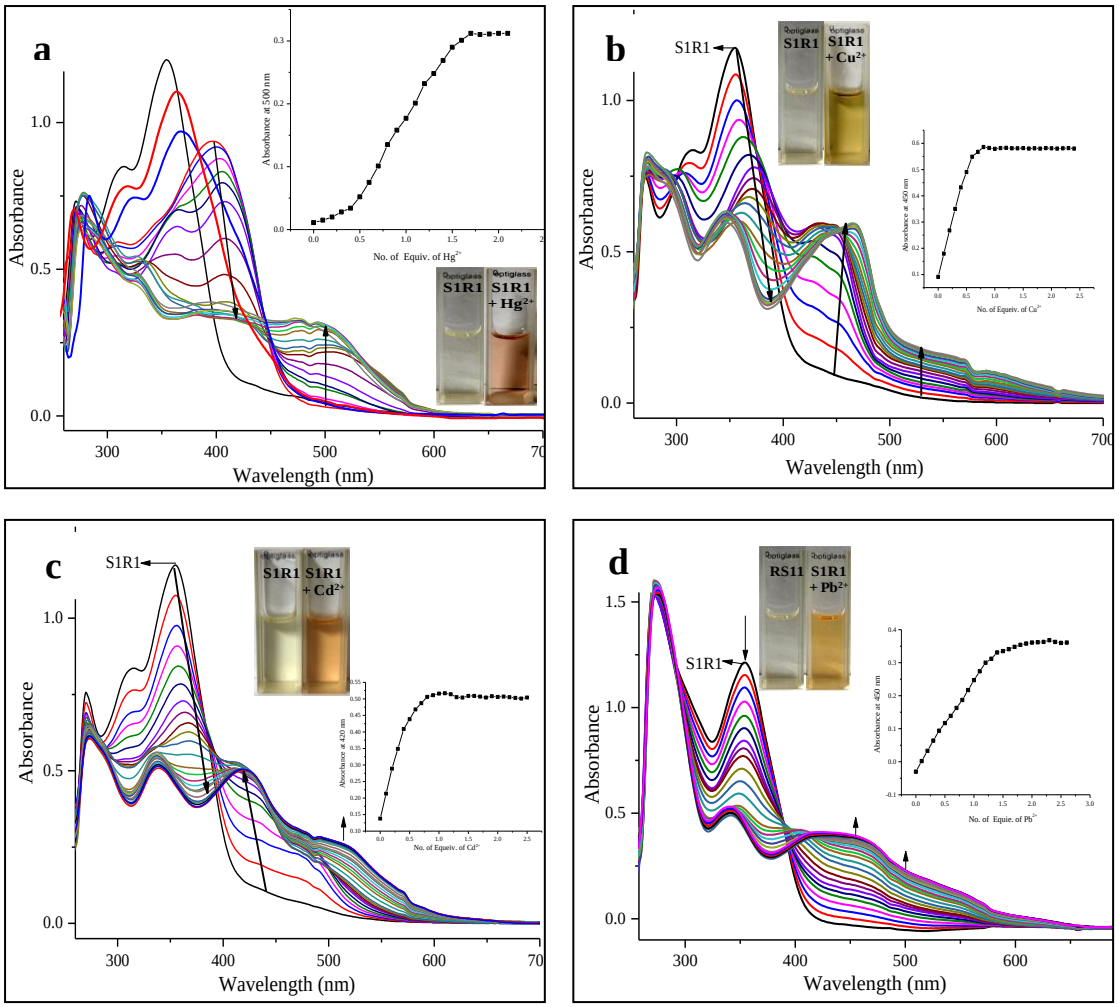

Fig. 2.13: UV–Vis titration and color change of **S1R1 (**5.0×10^{-6} M, DMF) with increasing concentration of metal ions (0 – 2.5 equiv.) in an aqueous medium. The inset graph shows binding isotherm at a selected wavelength, **a)**. **S1R1** vs. Hg^{2+} ions, at 500 nm, **b)**. **S1R1** vs. Cu^{2+} ions, at 450 nm, **c)**. **S1R1** vs. Cd^{2+} ions, at 420 nm, **d).** **S1R1** vs. Pb^{2+} ions, at 450 nm

The chemosensor **S1R2** and **S1R3** exhibit selectivity towards Cu^{2+} ions. In the absence of metal ions, **S1R2** and **S1R3** exhibit absorption wavelength maxima at 370 nm and 410 nm, whereas in the presence of Cu^{2+} ions, both the chemosensors exhibit red-shift toward longer wavelength by 80 folds **(S1R2)** and 60 folds **(S1R3)** in the

absorption spectrum, with the color change from colorless to yellow **(S1R2)**, yellow to orange **(S1R3)**. And also, **S1R2** and **S1R3** exhibit clear isosbestic points in the absorption spectra at 401 nm and 430 nm, respectively **(Fig. 2.14a-b).**

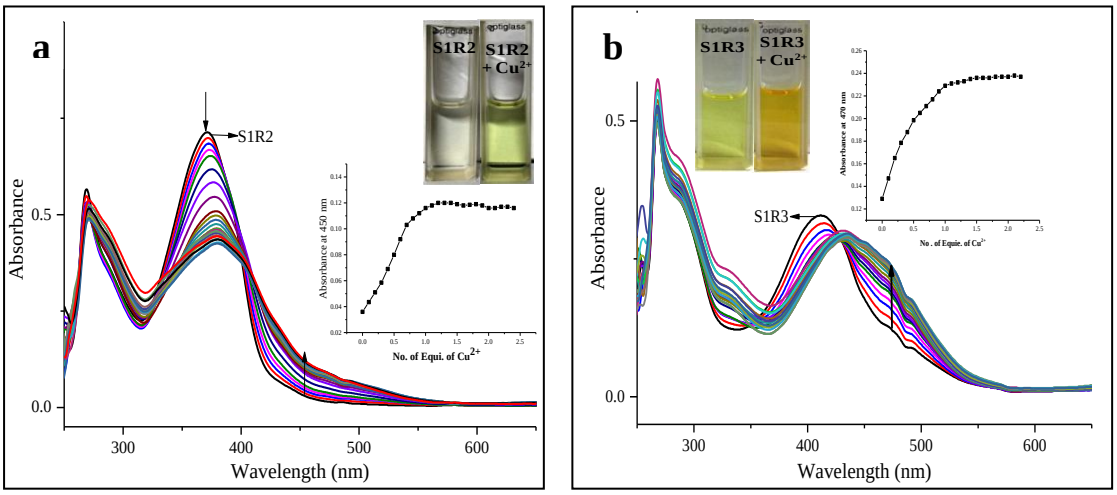

Fig. 2.14: UV–Vis titration and color change of **S1R2 (**2.5 × 10^{-5} M, DMF) and **S1R3 (**1.0 × 10^{-5} M, DMF) with increasing concentration of Cu^{2+} ions (0 – 2.5 equiv.) in an aqueous medium. The inset graph shows binding isotherm at a selected wavelength, **a)**. **S1R2** vs. Cu^{2+} ions, at 540 nm, **b)**. **S1R3** vs. Cu^{2+} ions, at 470 nm

2.3.3. Selectivity of chemosensor S1R1–S1R3 towards metal ions

The selectivity of reported chemosensors was confirmed by UV-Vis spectroscopy in the presence of different cations such as Fe^{3+}, Al^{3+}, Ag^{+}, Mn^{2+}, Mg^{2+}, Ca^{2+}, K^{+}, Na^{+}, Cu^{2+}, Hg^{2+}, Cr^{3+}, Fe^{2+}, Co^{2+}, Zn^{2+}, Ni^{2+}, Cd^{2+}, and Pb^{2+} ions. **S1R2** and **S1R3** exhibit selectivity towards Cu^{2+} ions in the presence of other tested cations. **S1R1** has shown multi-selective for Hg^{2+}, Cu^{2+}, Cd^{2+}, and Pb^{2+} ions in the absorption spectra and did not give any changes in the presence of other tested ions (**Fig. 2.12**). Further, a detailed UV-Vis study was conducted to confirm the selectivity of **S1R1** between Hg^{2+}, Cu^{2+}, Cd^{2+}, and Pb^{2+} ions. In the presence of 2.0 equivalences of Hg^{2+} ions, the color of **S1R1** changed to pink from colorless with the appearance of the new absorption band at 500 nm. Upon addition of an excess of Cu^{2+}, Cd^{2+}, and Pb^{2+} ions, there was no significant change in color and absorbance **(Fig. 2.15a)**; it shows **S1R1** has higher selectivity towards Hg^{2+} ions than the Cu^{2+}, Cd^{2+}, and Pb^{2+} ions. The high selectivity of **S1R1** towards Hg^{2+} ions may be due to soft-soft interaction

and presences of favourable active binding sites (hydroxyl and nitrogen atoms present in two quinoline ring) to form a stable four-member co-ordination ring with Hg^{2+}. Whereas Cu^{2+}, Cd^{2+} and Pb^{2+} forms stable six-member co-ordination rings. Similarly, in the absence of Hg^{2+} ions, **S1R1** exhibits high selectivity towards Cu^{2+} ions than the Cd^{2+} and Pb^{2+} ions **(Fig. 2.15b)**. In the absence of Hg^{2+} and Cu^{2+} ions, **S1R1** exhibits selectivity towards Cd^{2+} ions than Pb^{2+} ions **(Fig. 2.15c)**. **S1R1** exhibits selectivity towards Pb^{2+} ions in the absence of Cu^{2+}, Cd^{2+}, and Hg^{2+} ions. Based on the colorimetric, absorption study and binding constant results, the selectivity order of chemosensor **S1R1** towards active metal ions confirmed as $Hg^{2+} > Cu^{2+} > Cd^{2+} > Pb^{2+}$ ions.

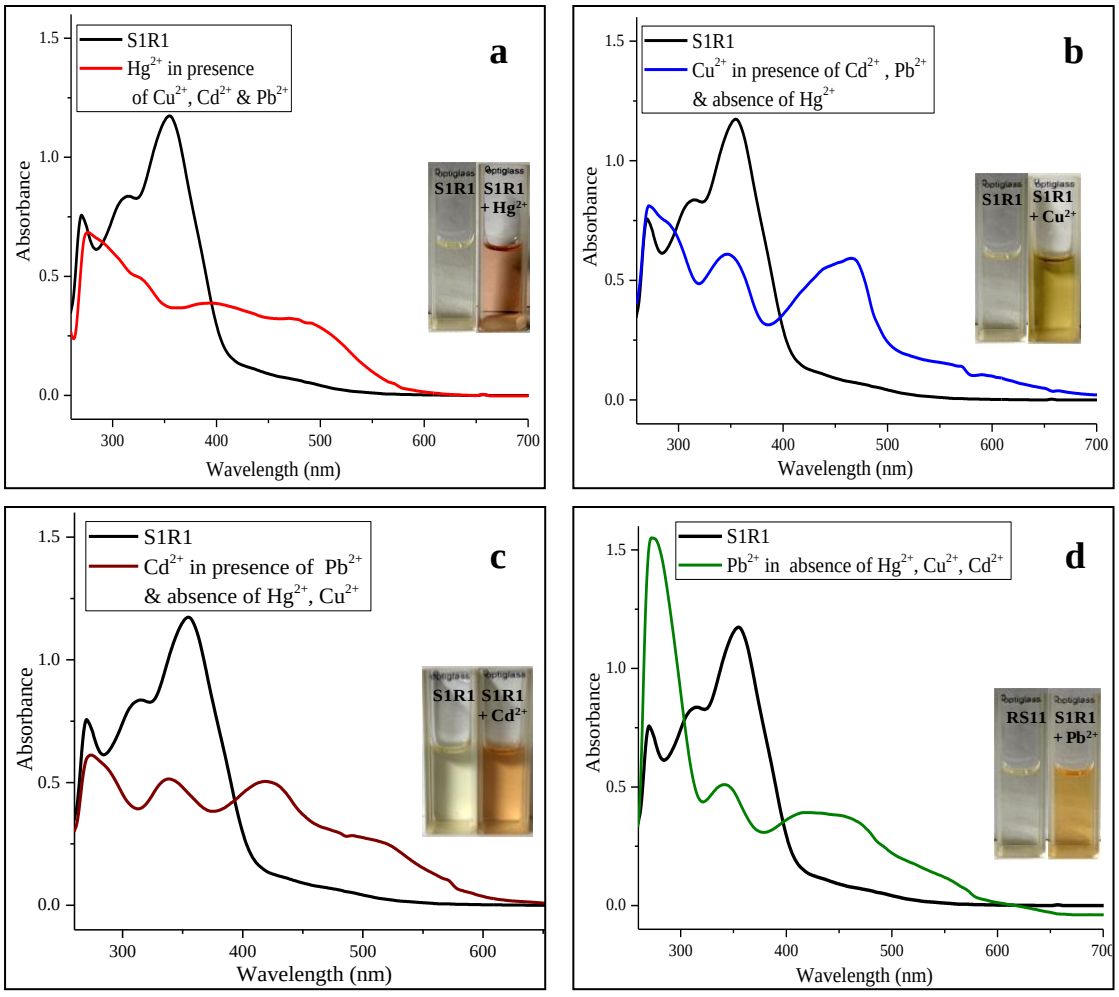

Fig. 2.15: UV–Vis and color change of **S1R1** (5.0×10^{-6} M, DMF), of 2.0 equiv. of Hg^{2+}, Cu^{2+} Cd^{2+} and Pb^{2+} ions in an aqueous medium. The inset graph shows the color change of **S1R1**, **a)**. **S1R1-Hg^{2+}** in the presence of Cu^{2+} Cd^{2+} and Pb^{2+} ions, **b)**. **S1R1-Cu^{2+}** in the presence of Cd^{2+}, Pb^{2+}, and absence of

Hg^{2+} ions, **c)**. **S1R1-Cd^{2+}** in the presence of Pb^{2+} and absence of Hg^{2+}, Cu^{2+} ions, **d)**. **S1R1-Pb^{2+}** in the absence of Hg^{2+}, Cu^{2+} and Cd^{2+} ions

The absorbance response (A_0/A) of **S1R1-S1R3** to various metal cations versus ionic radii/electronegativity is plotted (**Fig. 2.16 & 2.17**), and this furthermore illustrates clearly that Hg^{2+}, Cu^{2+}, Cd^{2+} and Pb^{2+} exhibit good response than other tested metal ions. This selective complexation and sensing of Hg^{2+}, Cu^{2+}, Cd^{2+}, and Pb^{2+} ions rationalized in principle by various factors like ionic radii, electronegativity as well as HSAB theory (Pearson 1963). When the (A_0/A) of **S1R1-S1R3** values are plotted against ionic radii, no significant correlation is observed (**Fig. 2.17)**. When the data are plotted against electronegativity (Shannon 1976), (Li and Xue 2006), (Suresh et al. 2010) of various metal cations, it is observed that cations Hg^{2+}, Cu^{2+}, Cd^{2+}, and Pb^{2+} bind more readily than that of other cations. According to Hard and Soft Acid-Base (HSAB) theory, Ag^{+}, Cu^{2+}, Cd^{2+}, Hg^{2+}, and Pb^{2+} classified as soft acid bind favorably to ligands containing sulfur it shows a selection of carriers bearing hetero-atomic groups for the recognition of heavy metal ions. On the other hand, this opens the door for the determination of heavy metal ions when this chemosensor molecule is covalently linked to chromophoric or fluorophore moieties. A closer look at the data shows that the results can be more readily explained based on Pearson's HSAB theory. The sulfur group can be considered as a relatively soft base. Analysis of the hardness and softness of various cations indicate that softer acids like Cd^{2+}, Pb^{2+}, Cu^{2+}, and Hg^{2+} have much more affinity towards **S1R1-S1R3**.

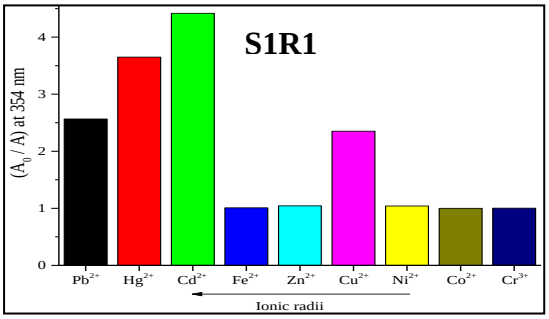

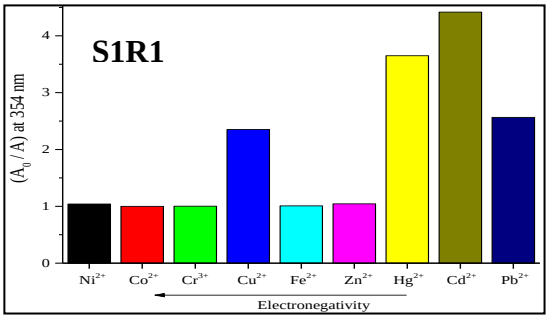

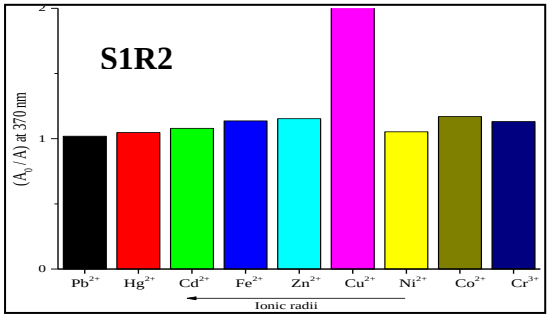

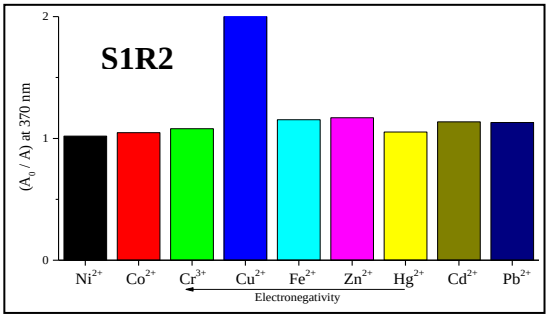

Fig. 2.16: Absorbance response (A_0 /A) of **S1R1–S1R3** at a selected wavelength (350 nm, 342 nm, 395 nm, 354 nm, 370 nm, and 410 nm) plotted against ionic radii (pm) of cations in decreasing order

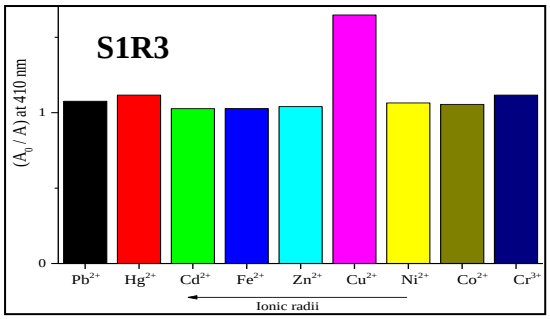

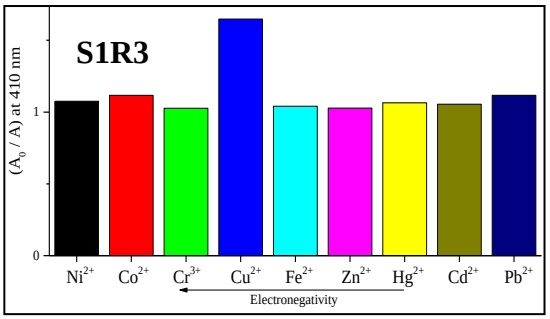

Fig. 2.17: Absorbance response (A_0/A) of **S1R1–S1R3** at a selected wavelength (350 nm, 342 nm, 395 nm, 354 nm, 370 nm, and 410 nm) plotted against electronegativity of cations in decreasing order

2.3.4. Binding constant and detection limit determination

The binding stoichiometry between chemosensor **S1R1–S1R3** with the different metal ions was determined by the Benesi-Hildebrand (B-H) method using UV-Vis spectrometric titration (Steed, J. W., and Atwood 2010)**.** The B-H plot confirms that all the chemosensors form 1:1 complexation with the metal ions **(Fig 2.18 & 2.20**). The association constant (K) was calculated for all the chemosensor metal complexes using the B-H equation, and results are tabulated in **Table 2.2.**

The detection limit (DL) was calculated based on the standard deviation of the measurement and the slope using the following equation mentioned by ICH quality guideline **Q2R1**(Guideline 2005).

$$DL\ \frac{C \times \sigma}{m}$$

Where, σ = standard deviation of the measurement**,** m = slope of the calibration curve, *C* = constant (3.0).

The DL for Hg^{2+}, Cu^{2+}, Cd^{2+}, and Pb^{2+} ions were determined using the calibration plot between metal ion concentration and the corresponding absorbance of chemosensor-metal complex measured at selective wavelengths (**Fig. 2.19**).

The calculated DL results, Regression analysis data of Hg^{2+}, Cu^{2+}, Pb^{2+}, Cd^{2+} ions by the proposed chemosensors **S1R1–S1R2** were tabulated in **table 2.2.**

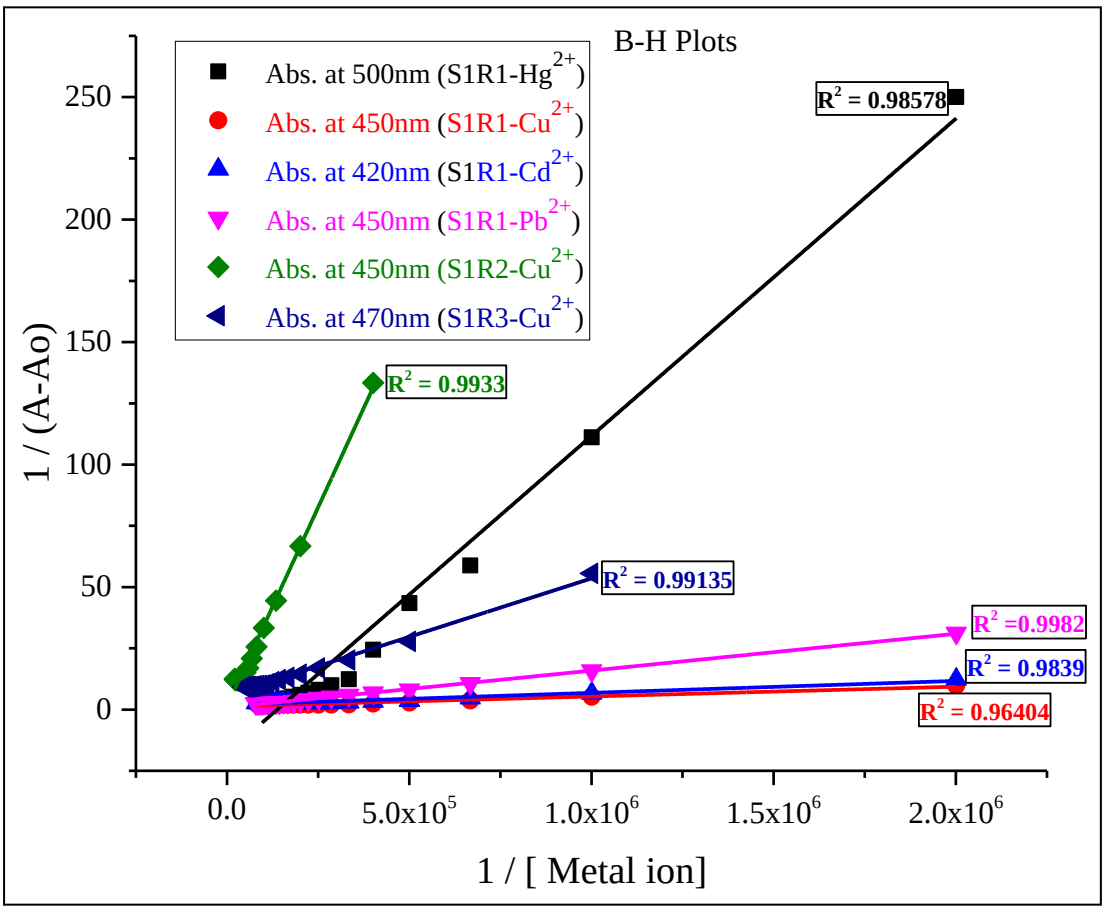

Fig. 2.18: Benesi-Hildebrand (B-H) plot of chemosensor binding with metal ions associated with absorbance change at a selective wavelength. **S1R1** (5.0×10^{-6} M, DMF) with Hg^{2+} ions at 500 nm**,** Cu^{2+} ions at 450 nm, Cd^{2+} ions at 420 nm, Pb^{2+} ions at 450 nm, **S1R2** (2.5×10^{-5} M, DMF) with Cu^{2+} ions at 450 nm and **S1R3** (1.0×10^{-5} M, DMF) with Cu^{2+} ions at 470 nm wavelength

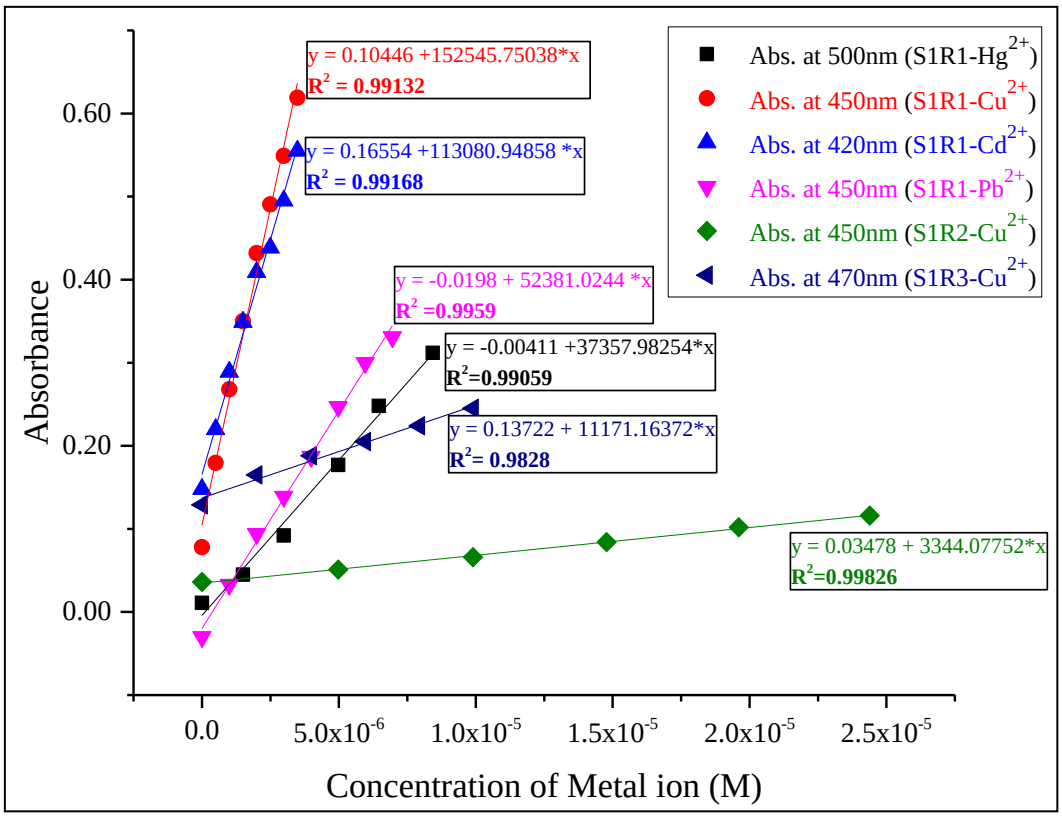

Fig. 2.19: Calibration curve plot of absorbance of complex (chemosensor-metal) versus concentration of metal ions in M. **S1R1**–Hg^{2+} vs. Hg^{2+} ions, **S1R1**–Cu^{2+} vs. Cu^{2+} ions, **S1R1**–Cd^{2+} vs. Cd^{2+} ions, **S1R1**–Pb^{2+} vs. Pb^{2+} ions, **S1R2**–Cu^{2+} vs. Cu^{2+} ions, **S1R3**–Cu^{2+} vs. Cu^{2+} ions

Table 2.2: Regression analysis data, stoichiometry, binding constant and detection limit of chemosensor S1R1–S1R3 with metal ions

Chemo sensor	**Metal ion**	**Stoichiometry**	**Binding constant (K) M^{-1}**	**Linear range (M)**	**R^2**	**Detection limit (ppb)**
S1R1	Hg^{2+}	1:1	3.0×10^5	$0.0 – 8.4\times10^{-6}$	0.9906	140
	Cu^{2+}	1:1	2.5×10^5	$0.0 – 3.5\times10^{-6}$	0.9913	13
	Cd^{2+}	1:1	1.8×10^5	$0.0 – 3.5\times10^{-6}$	0.9917	22
	Pb^{2+}	1:1	1.3×10^4	$0.0 – 7.0\times10^{-6}$	0.9959	32
S1R2	Cu^{2+}	1:1	4.1×10^4	$0.0 – 2.4\times10^{-5}$	0.9983	57
S1R3	Cu^{2+}	1:1	1.1×10^4	$0.0 – 9.9\times10^{-6}$	0.9828	76

Binding interaction:

From the UV-Vis spectrum, it is observed that the chemosensor **S1R1** displayed redshift by 146 nm, 96 nm, 66 nm, and 96 nm fold increment from 354 nm, in the presence of Hg^{2+}, Cu^{2+}, Cd^{2+}, and Pb^{2+} ions respectively. This red-shift in the absorption spectra could be n–π* transitions occurring in the molecule. Particularly the metal atoms interaction with the imine nitrogen (–C=N), hydroxy (–OH) in quinoline ring and nitrogen present in the quinoline ring (–C=N). (Tang et al. 2008) (Zhang et al. 2017) (Rout et al. 2019). Having like these more active binding sites (i.e., (–C=N), hydroxy (–OH), quinoline nitrogen) in the molecular structure of **S1R1** is responsible for multi-metal ion sensing (Udhayakumari et al. 2014). From the B-H plot confirms the 1:1 (**S1R1: M)** stoichiometry for the active metal ions. It confirms the formation of stable six-member rings with metal ions. Whereas the **S1R2** and **S1R3** did not have hydroxy (–OH) in their molecular structure and formed a stable four-member ring with the metal ions via Imine nitrogen (–C=N), and thiophene ring (–S–) for **S1R2** and imine nitrogen (–C=N), and furfural ring (–O–) for **S1R3** (Udhayakumari et al. 2014). This phenomenon was identified by the UV-Vis titration experiments. The **S1R2** and **S1R3** shows absorbance at 370 nm and 410 nm, whereas in the presence of Cu^{2+} ions, both the chemosensors exhibit red shift toward longer wavelength by 80 folds **(S1R2)** and 60 folds **(S1R3)** in the absorption spectrum, this red shift could be attributed due to n–π* transitions (i.e. imine nitrogen (–C=N), and thiophene ring **S1R2** and furfural ring).

This discriminating complexation and recognition of metal ions rationalized in principle like HSAB theory (Pearson 1963). The chemosensor **S1R1** has a hard group (–OH) and soft groups (HC=N–, quinoline ring) in its structure, this two different base functionalities (soft and hard), could be responsible for the multi sensitive to borderline (Cu^{2+}) and soft metals (Hg^{2+}, Cd^{2+}, Pb^{2+}). Whereas in the case of **S1R2, S1R2**, the hard group (–OH) is absent, could be due to this reason, it exhibits activity towards only Cu^{2+} ions. **Fig. 2.20** represents the binding interaction among **S1R1-S1R3** with different metal ions.

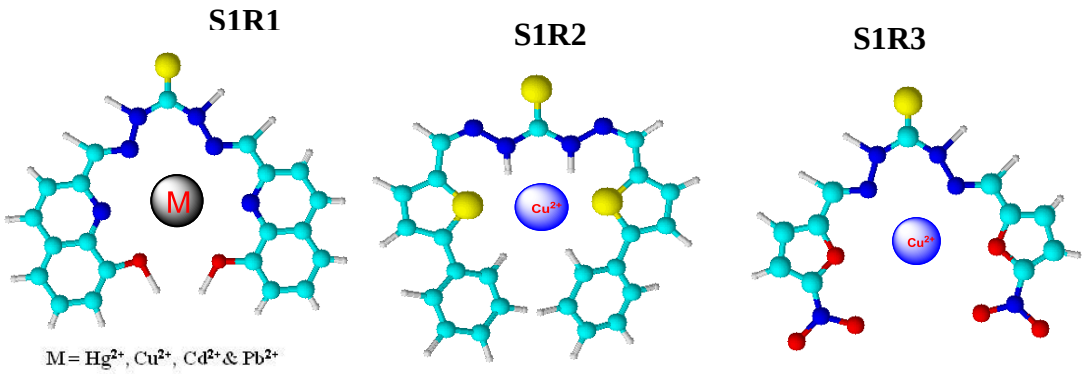

Fig. 2.20: Binding interaction between chemosensors and metal ions

2.4. Conclusions

To summarize, herein, three thiocarbohydrazide based chemosensors **S1R1–S1R3** have developed for the selective detection of Hg^{2+}, Cu^{2+}, Pb^{2+}, and Cd^{2+} ions over other tested cations. Among synthesized chemosensors, **S1R1** has shown response towards metal ions viz., Hg^{2+}, Cu^{2+}, Cd^{2+}, and Pb^{2+} in an aqueous medium with ppb detection limits of 140, 13, 22 & 32 ppb respectively. The multi-metal ion detection is due to the presence of the more active binding site in its molecular structure (hydroxyquinoline) than the other chemosensors. The **S1R2** and **S1R3** exhibit selective response towards Cu^{2+} ions at the ppb detection limit (57 & 76 ppb). All the chemosensors **S1R1–S1R3** exhibited good binding consent (10^3 to 10^5 M^{-1}) and 1:1 stoichiometric binding ratio with that of metal ions, based on the correlation study (absorption (A_0/A) versus ionic radii, electronegativity), comparative study results, high affinity of chemosensor **S1R1–S1R3** was confirmed towards Hg^{2+}, Cu^{2+}, Pb^{2+} and Cd^{2+} than other tested cations. Among all synthesized chemosensors, **S1R1** is versatile in its function binding Hg^{2+}, Cu^{2+}, Cd^{2+}, and Pb^{2+} ions with distinct colorimetric responses in an aqueous medium and the multi-metal ion sensing activity of **S1R1** gains significance in the field of colorimetric chemosensors for heavy metal ions detection. All the reported chemosensors have a good linear range from 0 to 10^{-6} M. It reveals that the chemosensors can be used for the quantitative determination of heavy metal ions in water media.

CHAPTER-3

Hg^{2+} INDUCED HYDROLYSIS OF THIAZOLE AMINE BASED SCHIFF BASE: COLORIMETRIC AND FLUOROGENIC CHEMODOSIMETER FOR Hg^{2+} IONS IN AN AQUEOUS MEDIUM

CHAPTER-3

3. Hg^{2+} INDUCED HYDROLYSIS OF THIAZOLE AMINE BASED SCHIFF BASE: COLORIMETRIC AND FLUOROGENIC CHEMODOSIMETER FOR Hg^{2+} IONS IN AN AQUEOUS MEDIUM

Abstract

In this chapter, the design, syntheses, and characterization of new Thiazole amine Schiff's base derivatives as a colorimetric chemosensor for mercury metal ion detection have been discussed in detail. The colorimetric cation sensing properties and detection mechanism of these chemosensors and real-life applications have been incorporated.

3.1. Introduction

Research in the detection and sensing of metal ions has received substantial attention in the last few decades in the field of chemosensors. Several strategies can be followed in the design and production of molecular sensors with optimal selectivity toward particular analyte, and the recognition process converted into a read-out signal, either in the form of spectroscopic (Optical / Fluorescence / NMR) or electrochemical signal. "*Cation Recognition*" as a research area has been actively pursued by many scientists, including chemists, biologists, clinical biochemists, and environmentalists in past decades. Environmental contamination is one of the most important concerns of modern research. Immense efforts have been put towards the production of molecular chemosensor for the determination of poisonous elements, like Hg^{2+}, Pb^{2+}, and Cd^{2+}, As^{2+}, and Cr^{3+} (Jeon et al. 2018; Jeong and Kim 2015; Kumar et al. 2017). Because these heavy metals damage human health as well as the environment (Malm 1998; Renzoni et al. 1998; Tchounwou et al. 2003). Therefore, early recognition and sensing of these metals are desirable.

The broad uses of mercury in chemical manufacturing industries and farming processes have led to its increased concentration in the environment (Malm 1998; Que et al. 2008; Renzoni et al. 1998; Tchounwou et al. 2003), thus the quantitative determination of the Hg^{2+} necessary. Mercury has more poisoning for human beings, and more than its permeable limit can cause the neurological syndrome. An excessive

amount of mercury can cause paralysis, coma, and death in human beings (Burdette and Lippard 2001, 2003).

From past decades, three different approaches are being used in the area of chemosensor for the recognition of metal ions such as i). *Binding site-signalling*, ii). *Displacement*, iii). *Chemodosimeter approach*. In the chemodosimeter approach, a specific ion-induced chemical reaction occurs, which results in an optical signal (Kaur et al. 2012; Quang and Kim 2010; Santra et al. 2009; Song et al. 2006). To date, numerous chemosensors have developed and reported using fluorescence "turn-on" mechanism, attributed to the quenching nature of the Hg^{2+} ions (Aragay et al. 2011; Lee et al. 2012; Srivastava et al. 2013; Wang and Wu 2013b; Yan et al. 2015). Recently, numerous 'turn-on' fluorescence chemosensors for the detection of Hg^{2+} ion have reported in organic and semi-aqueous media (Chen et al. 2012; Das et al. 2012; Srivastava et al. 2011, 2014; Xie et al. 2011; Yan et al. 2015). A few fluorescence and colorimetric chemosensors are available in the literature for the detection of Hg^{2+} ions in aqueous media (Jeon et al. 2018; Singhal et al. 2015). The international standards like WHO (Edition 2011) and US-EPA (United States Environmental Protection Agency 2013) have set the limit for their daily consumption, due to the more poisonous nature of heavy metal ions in drinking water. Present many advanced and accurate techniques are available which offer the quantification of heavy metal ions like ICP-MS and Atomic absorption spectroscopy (AAS) (De Jesus et al. 2013; Noël et al. 2015), which offers the quantification of heavy metal ions. The above mentioned sophisticated methods require high cost and maintenance, making it unsuitable for field monitoring.

In the present work, simple Schiff base chemosensors **S2R1**-**S2R3** (Scheme-3.1) have reported. The present developed chemosensor **S2R1** has N and S as interacting sites in its molecular structure, which help in selective binging of mercury ions (Chemosensor **S2R1**). It displayed qualitative and quantitative determination of Hg^{2+} ion through a dual-channel (colorimetric and fluorometric) response in a water medium. In chemosensor **S2R1**, thiazole moiety undergoes Hg^{2+} induced hydrolysis of –C=N–(imine) bond in water media whereas, pyrenecarboxaldehyde molecules act like 'Turn On' chemodosimeter for Hg^{2+} ions. The **S2R1** is more susceptible and efficient to detect mercury ions in the attendance of other tested competitive metals in an aqueous media.

3.2. Experimental details

3.2.1. General information

In the present study, all chromatography grade solvents, analytical grade metal salts, and chemicals that were procured from commercial sources and utilized as such. Melting point (M.P) was determined on Bio-cote (SMP10). Bruker Alpha (FT-IR) instrument was used to record the IR spectra of synthesized chemosensor **S2R1–S2R3**.

The ^{13}C NMR (100 MHz) and ^{1}H NMR (400 MHz) spectra were recorded using Varian mercury plus and Bruker FT-NMR, and DMSO-d_6 solvent was used. The ^{1}H NMR and ^{13}C NMR chemical shifts are reported on the δ scale (in ppm) relative to tetramethylsilane (TMS, δ 0.00) and DMSO-d_6 (39.50), respectively, as internal reference standards. The chemical shift in ppm and coupling constants (J) in Hz were represented. The Peak multiplicities are represented with s, d, t & m letters (s-singlet, d-doublet, t-triplet & m-multiplet). Agilent LC-MS 6410 instrument was used to record the mass spectra of reported chemosensors. Analytik Jena Specord S600 UV-Vis spectrophotometer was used for the titration experiments with quartz sample cell having 3.0 mL capacity and path length of 10 mm. Jasco-FP-6200 fluorescence spectrophotometer instrument was used for the fluorescence titration in 3.0 mL quartz cells having four transparent optical windows and path length of 10 mm.

3.2.2. Colorimetric, UV–Vis and fluorescence experiments

Individual metal ion stock solutions of 1.0×10^{-3} M were prepared in de-ionized water in 10 mL volumetric flasks. 1.0×10^{-3} M solutions of chemosensors **S2R1–S2R3** were made in dimethyl sulphoxide (DMSO) as stock solutions. Further, these stock solutions were diluted to 2.5×10^{-6} M using DMSO. The micropipette was used for additions of metal solution to the chemosensor solution during all the instrumental analysis such as colorimetric, UV–Vis and fluorescence studies. All the spectra were recorded after each addition of metal solution to the chemosensor solutions.

3.2.3. Synthesis of chemosensors S2R1–S2R3 and characterization

The synthesis procedure of **S2R1–S2R3** has illustrated in the **scheme 3.1**. The synthesis of chemosensor **S2R1:** Pyrene-1-carbaldehyde (0.2499g, 1.1mmol) and Thiazol-2-ylamine (0.3201g, 1.1mmol) were separately dissolved in10 mL ethanol. Then aldehydehyde solution was added drop-wise with constant stirring to the thiazol-2-ylamine solution. To this a catalytic amount of acetic acid was added and the reaction mixture was stirred at room temperature for 5 hours. The progress of reaction was monitored by TLC. After the completion of reaction the reaction mixture was filtered and washed with hot ethanol. Similarly, the **S2R2** and **S2R3** were synthesized as stated above synthetic methodology. The **S2R2** was synthesized by the reaction of Pyrene-1-carbaldehyde (0.2503g, 1.1mmol) and 1H-Benzoimidazol-2-ylamine (0.1457g, 1.1mmol). The **S2R3** was synthesized by the reaction of Pyrene-1-carbaldehyde (0.2505g, 1.1mmol) and Thiophene-2-carboxylic acid hydrazide (0.1503g, 1.1mmol). The final obtained desired compounds were characterized by using standard spectroscopic methods as given below.

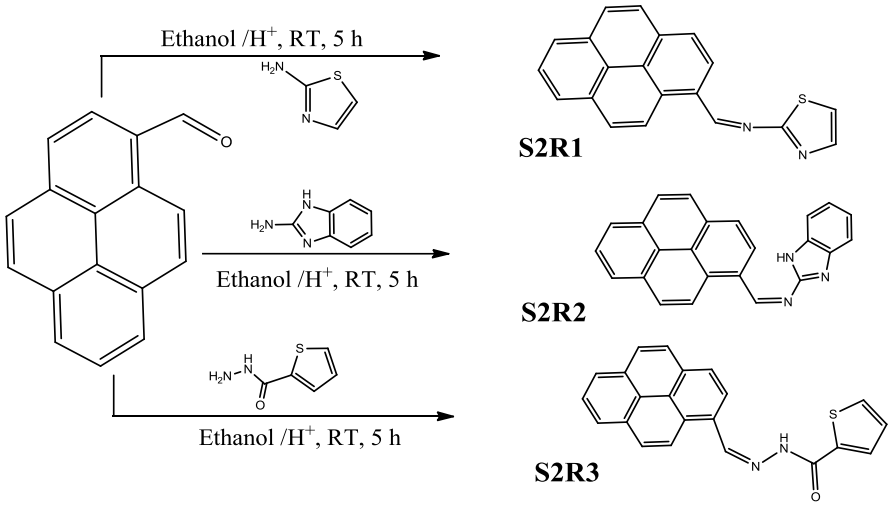

Scheme-3.1: General synthesis of the chemosensor **S2R1–S2R3**

Chemosensor S2R1 (Pyren-1-ylmethylene-thiazol-2-yl-amine):

Yield: 94.4%. **Melting range:** 206 – 208°C. **FT-IR: (KBr, cm^{-1})**: 3073.21 (Aromatic C–H, str), 1563.02 (imine C=N, str), 1478.01, 1384.08, 1316.86 (aromatic C=C, str), 1142.31 (C–N, str), 878.24 (C–H, bent), 712.61 (C–S, Str) **(Fig.3.1)**. **^{1}H-NMR (400 MHz, DMSO-d$_6$ δ$_{ppm}$):** 9.416 – 9.393 (d, 1H imine (HC=N), J=9.2 Hz), 9.253 – 9.229 (d, 1H (aromatic of pyrene), J=9.6 Hz), 8.823 – 8.803 (d, 1H (aromatic of pyrene, –C=CH), J=8.0 Hz), 8.607 – 8.586 (d, 1H (aromatic of pyrene, –C=CH),

J=8.4 Hz), 8.496 – 8.304 (m, 4H, aromatic of pyrene, –C=CH), 8.293 – 8.271 (m, 1H aromatic of pyrene, –C=CH), 8209 – 8.147 (m, 1H aromatic of pyrene, –C=CH), 7.821 – 7.813 (d, 1H (aromatic of thiophene, –C=CH), J=3.2 Hz), 7.722 – 7.714 (d, 1H (aromatic of thiophene, –C=CH), J=3.2 Hz) **(Fig.3.4)**.**^{13}C-NMR (100 MHz, DMSO-d$_6$ δ$_{ppm}$):** 173.2 (imine (HC=N), 162.7 (–C=N– thioazole), 142.0, 135.5 (thioazole aromatic (–C=C–), 131.5, 131.2, 131.0, 130.5, 130.2, 128.3, 127.9, 127.7, 127.4, 127.1, 125.7, 125.4, 124.5, 123.2, 123.1 (aromatic pyrene –C=C–), 120.1 (–C-S– thioazole ring) **(Fig.3.7)**. **LC-MS (ESI) m/z:** calculated for $C_{20}H_{12}N_2S$; 312.39, found, 313.10 (M+1) **(Fig.3.10)**.

Chemosensor S2R2 ((1H-Benzoimidazol-2-yl)-pyren-1-ylmethylene-amine):

Yield: 92.2%. **Melting range:** 141 – 143°C, **FT-IR: (KBr, cm^{-1})**: 3242.21(N–H str), 3085.33 (aromatic, C–H str), 1685.71 (Imine C=N, str), 1507.32, 1478.64, 1411.35, 1317.51 (aromatic C=C, str), 1220.16 (C–N, str), 844.06 (C–H, bent) **(Fig.3.3)**. **^{1}H-NMR (400 MHz, DMSO-d$_6$ δ$_{ppm}$):** 9.496 (s 1H, –NH), 8.846 (s, 1H, HC=N), 8.846 – 8.742 (d, 1H, aromatic pyrene –C=CH), 8.620 – 8.573 (m, 1H aromatic pyrene –C=CH), 8.393 – 8.373 (m, 4H, aromatic pyrene –C=CH), 8.301 – 8.321 (m, 2H aromatic pyrene –C=CH), 8.231 – 8.120 (m, 2H aromatic pyrene –C=CH), 8.033 – 8.005 (d, 2H (aromatic benzo imidazole –C=CH), J= 11.2Hz), 7.305 – 7.284 (t, 1H (aromatic benzo imidazole –C=CH), J=4.4Hz) **(Fig.3.5)**. **^{13}C-NMR (100 MHz, DMSO-d$_6$ δ$_{ppm}$):** 156.2 (HC=N), 130.8, 130.1 (aromatic benzo imidazole –C=C–), 128.7, 128.4, 127.4, 126.6, 126.1, 125.8, 123.8 (aromatic pyrene –C=C–) **(Fig.3.8)**. **LC-MS (ESI) m/z:** calculated for $C_{24}H_{15}N_3$; 345.40, found, 346.20 (M+1) **(Fig.3.11)**.

Chemosensor S2R3 (Thiophen-2-yl-acetic acid pyren-1-ylmethylene-hydrazide):

Yield: 93.0%. **Melting range:** 268 – 270°C. **FT-IR: (KBr, cm^{-1})**: 3217.15 (N–H, Str), 3070.17 (Aromatic C–H, Str), 1635.02 (amide C=O, Str), 1559.39 (imine C=N, str), 1418.57, 1359.68, 1294.23 (aromatic C=C, Str), 1135.15 (C–N, str), 845.08 (C–H, bent), 717.42 (C–S, Str) **(Fig.3.3)**. **^{1}H-NMR (400MHz, DMSO-d$_6$, δ$_{ppm}$):** 10.833 (s, 1H, (–NH), 9.420 – 9.397 (d, 1H, (aromatic of pyrene –C=CH), J=9.2Hz), 8.609 – 8.589 (d. 1H, imine (HC=N), J=8.0Hz), 8.496 – 8.408 (m, 3H, (aromatic of pyrene –C=CH), 8.305 – 8.283 (d, 1H (aromatic of pyrene –C=CH), J=8.8Hz), 8.220 – 8.182 (t, 1H (aromatic of thiophene –C=CH), (J=7.2), 7.125 – 7.085 (m, 2H (aromatic of pyrene –C=CH), 6.881 – 6.841 (m, 2H, aromatic of pyrene –C=CH), 6.219 (d, 2H, aromatic of thiophene –C=CH), J= 4.8Hz) **(Fig.3.6)**. **^{13}C-NMR (100MHz, DMSO-d$_6$,**

δ_{ppm}): 193.7 (–C=O), 172.2 (HC=N), 155.1 (thiophene =C–C=O), 130.9, 130.7, 130.6 (aromatic thiophene –C=C–), 127.3, 127.2, 127.2, 126.9, 126.9, 124.9, 122.5, 119.0 (aromatic pyrene –C=C–), 111.4 (–C-S– thioazole ring) **(Fig.3.9)**. **LC-MS (ESI) m/z:** calculated for $C_{22}H_{14}N_2OS$; 354.08, found, 355.10 $(M–H)^+$ **(Fig.3.12)**.

3.2.4. Characterization spectra of chemosensors S2R1– S2R3

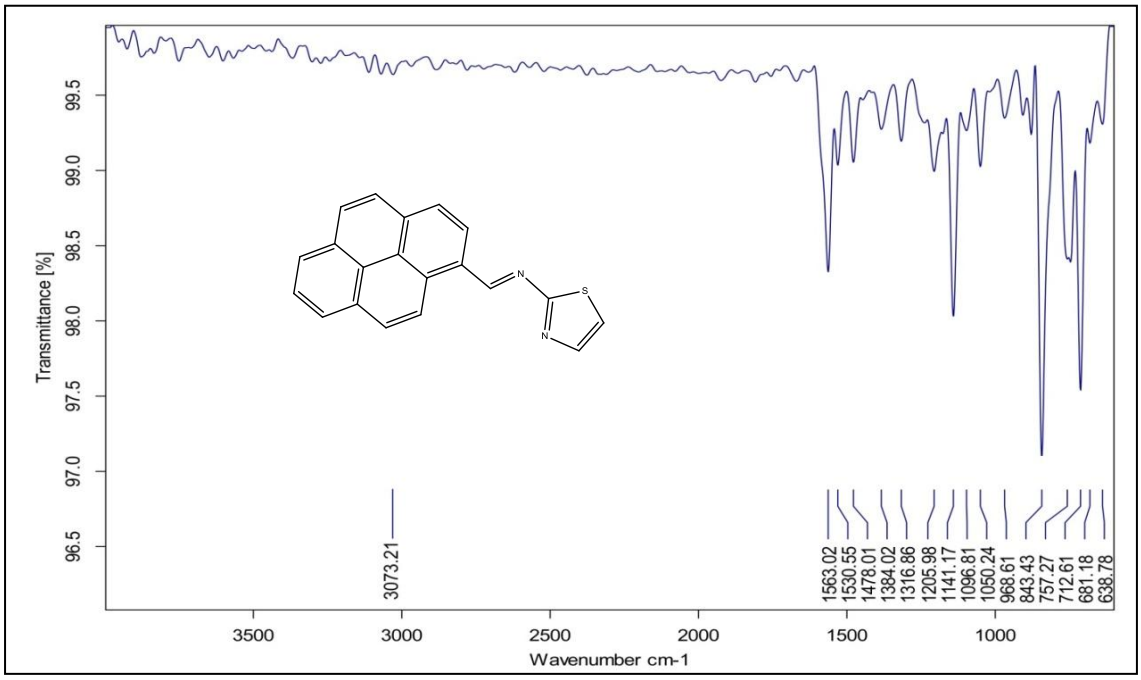

Fig. 3.1. FT-IR Spectrum of chemosensor **S2R1**

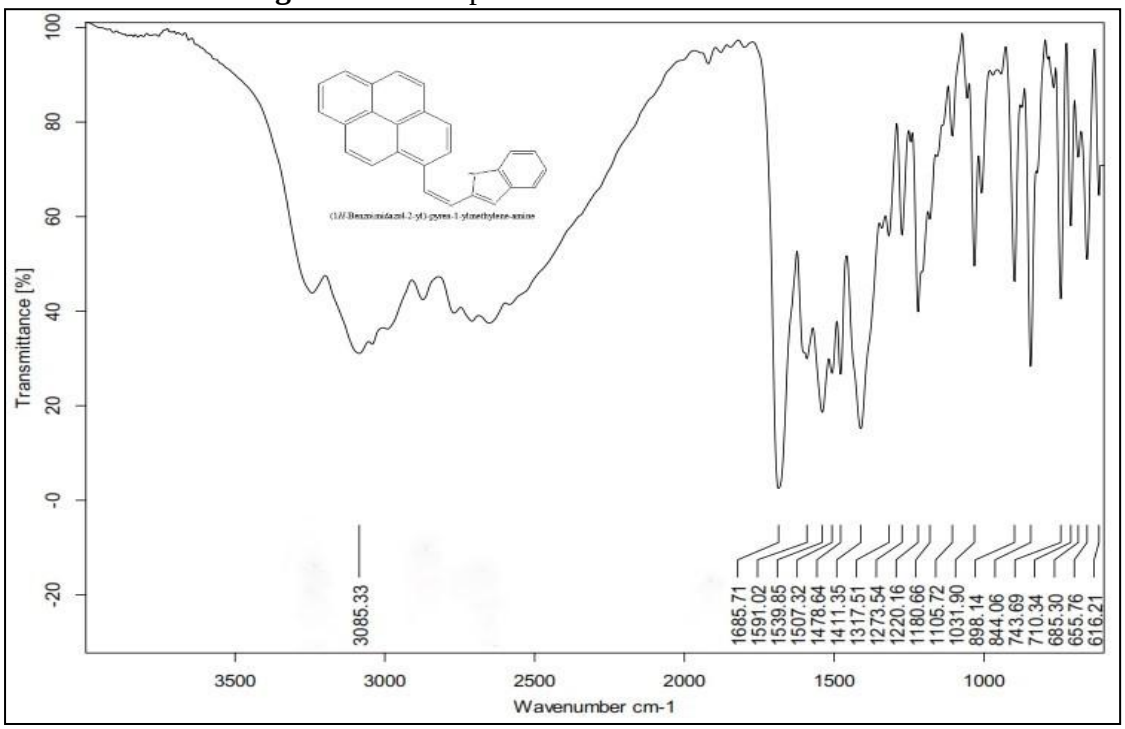

Fig. 3.2. FT-IR Spectrum of chemosensor **S2R2**

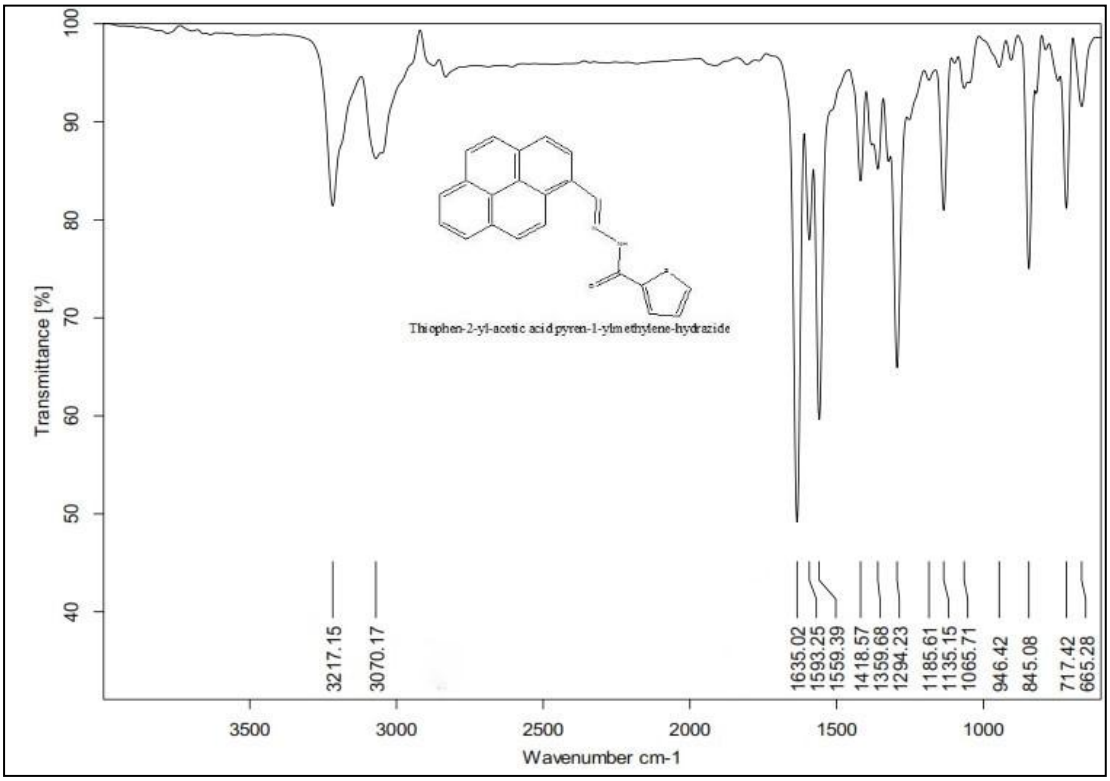

Fig. 3.3. FT-IR Spectrum of chemosensor **S2R3**

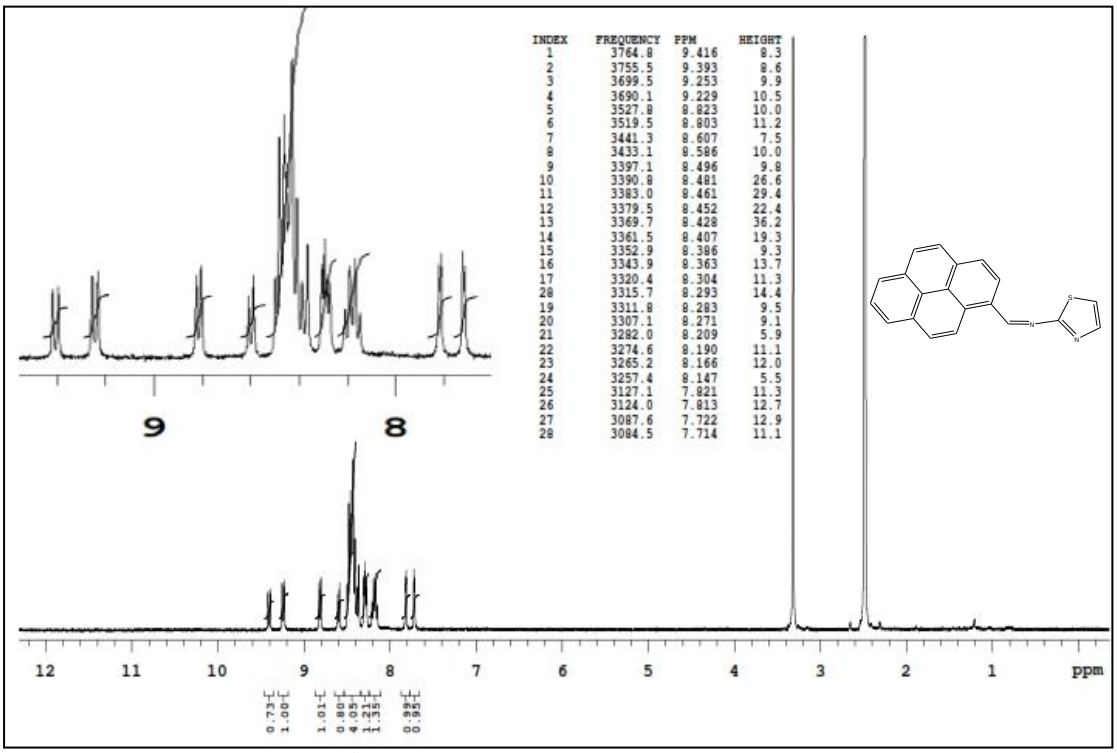

Fig. 3.4. ^{1}H NMR spectrum of chemosensor **S2R1**

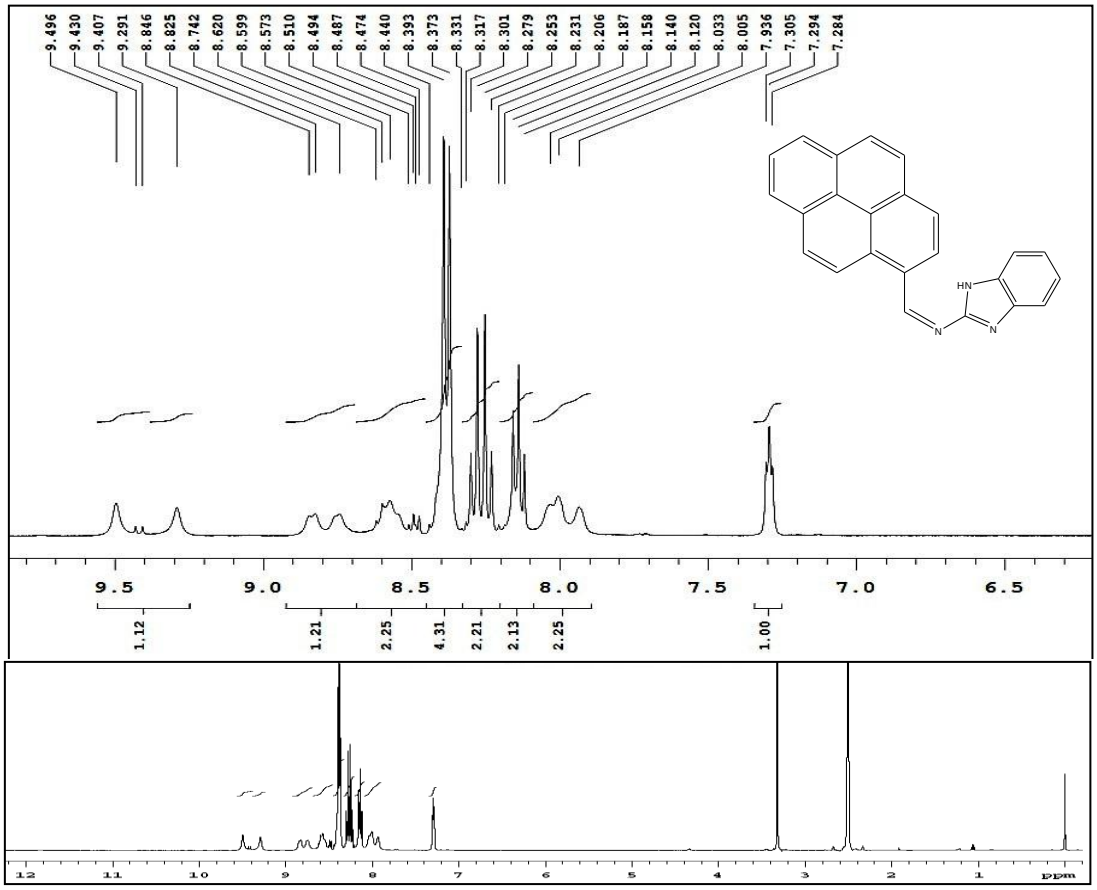

Fig. 3.5. ^{1}H NMR spectrum of chemosensor **S2R2**

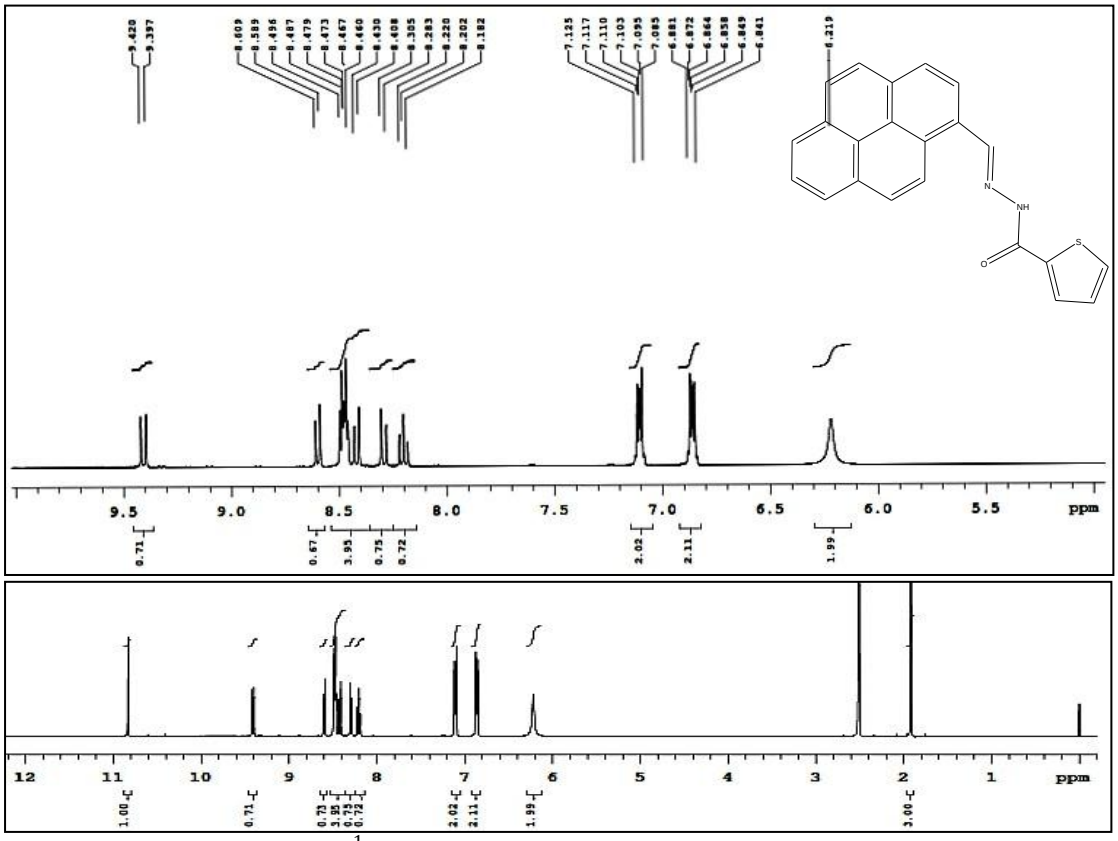

Fig. 3.6. ^{1}H NMR spectrum of chemosensor **S2R3**

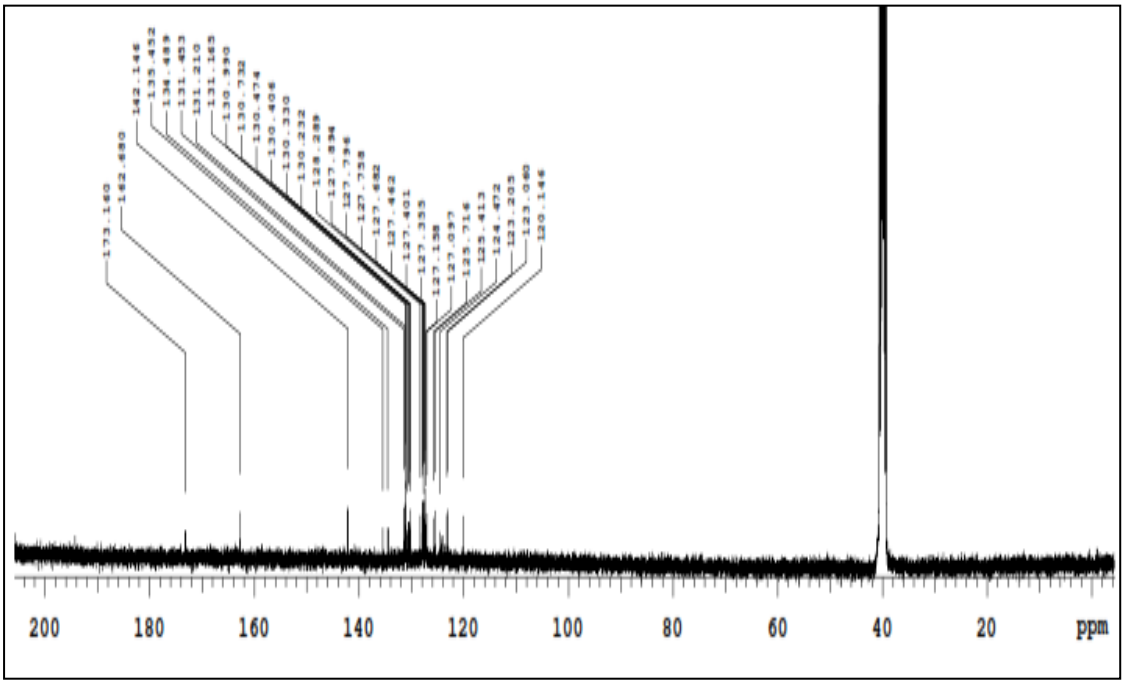

Fig. 3.7. ^{13}C NMR spectrum of chemosensor **S2R1**

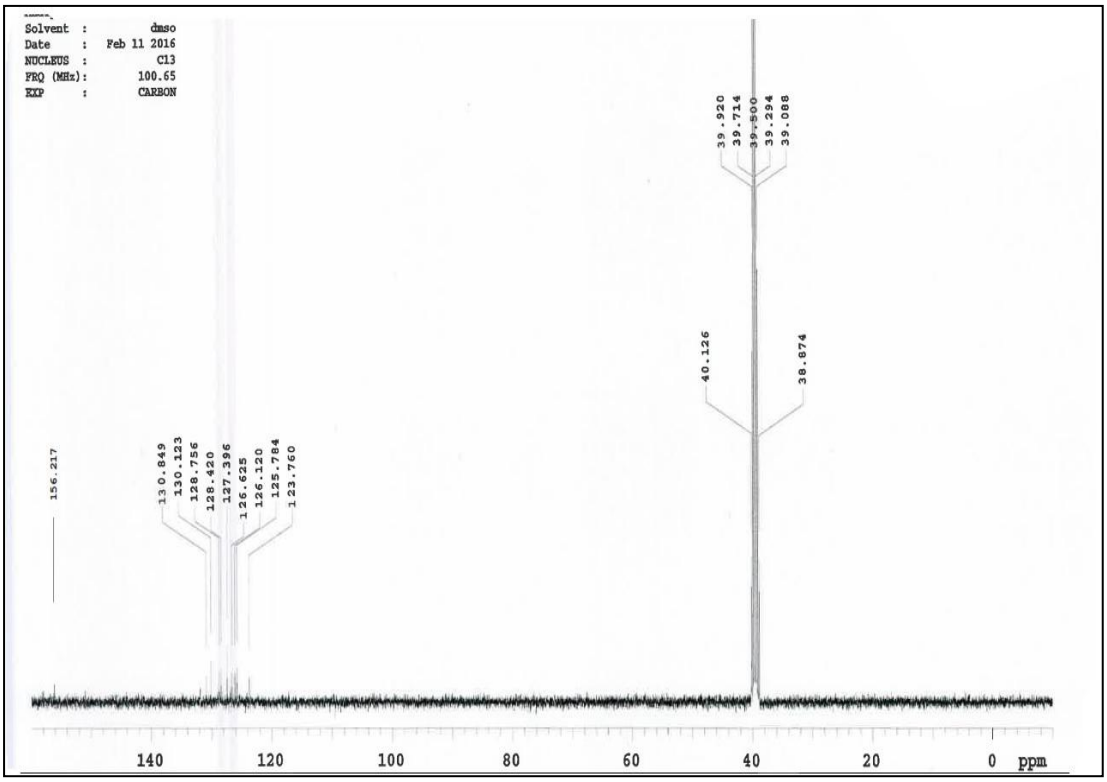

Fig. 3.8. ^{13}C NMR spectrum of chemosensor **S2R2**

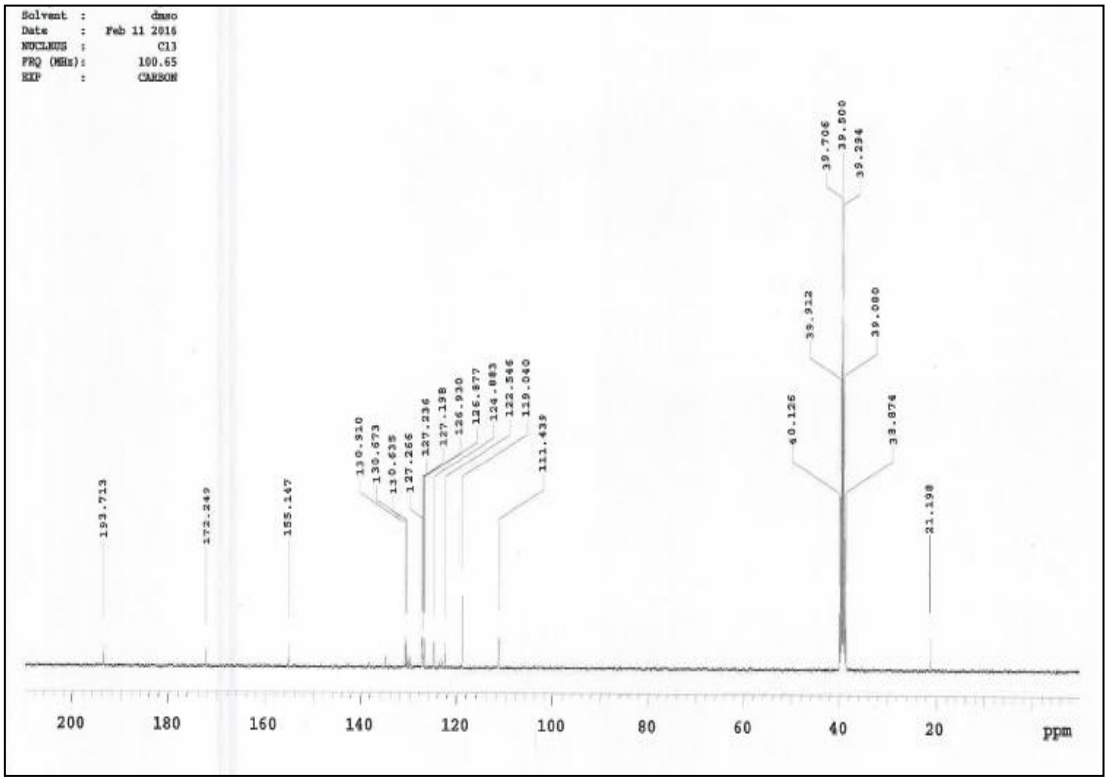

Fig. 3.9. ^{13}C NMR spectrum of chemosensor **S2R3**

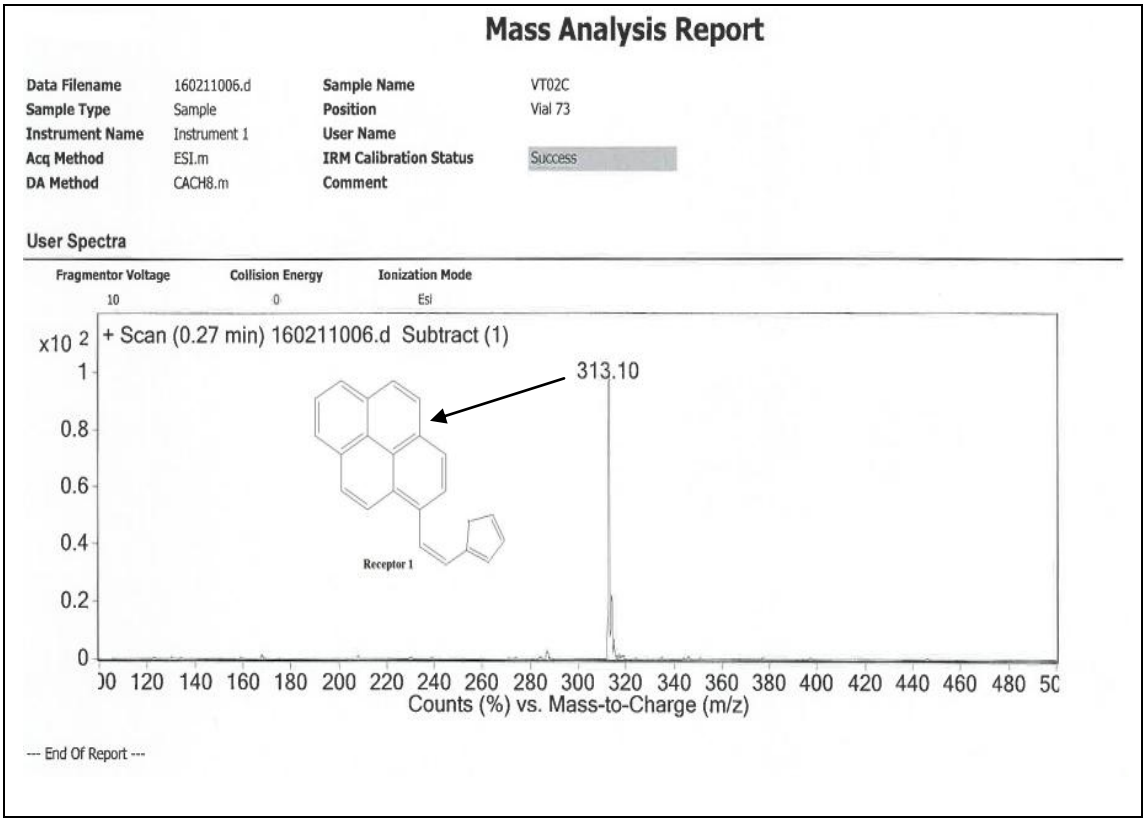

Fig. 3.10. The ESI-Mass spectrum of chemosensor **S2R1**

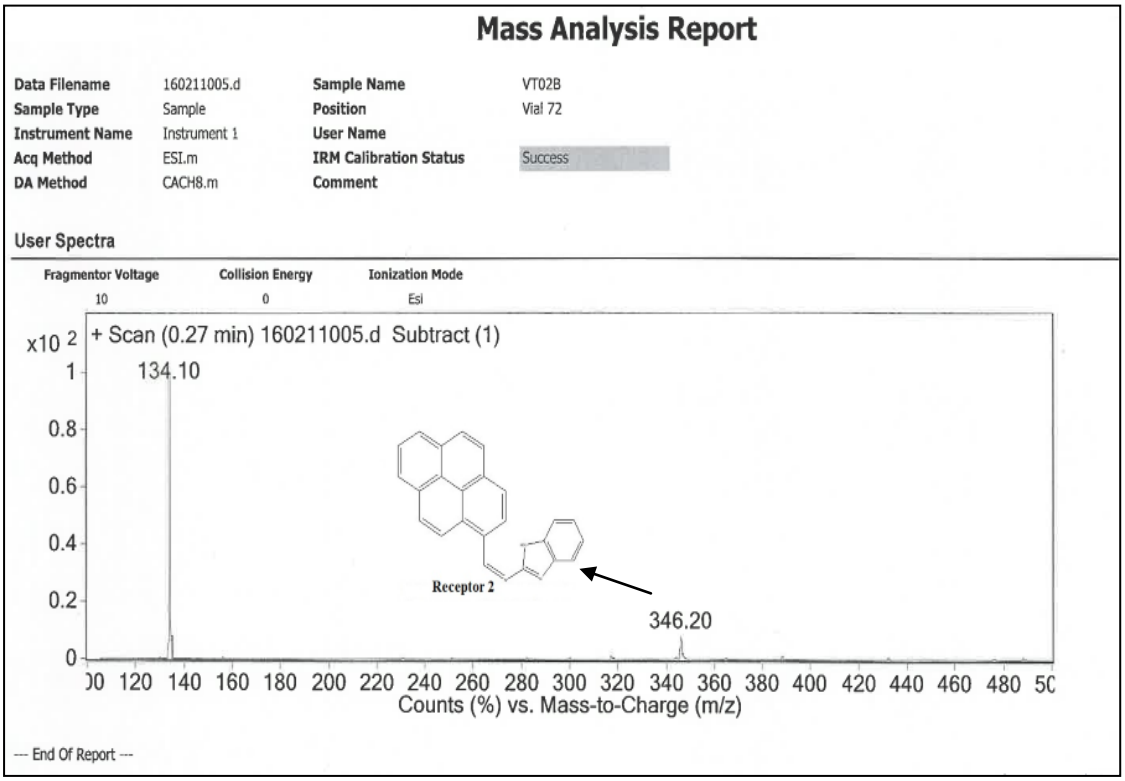

Fig. 3.11. The ESI-Mass spectrum of chemosensor **S2R2**

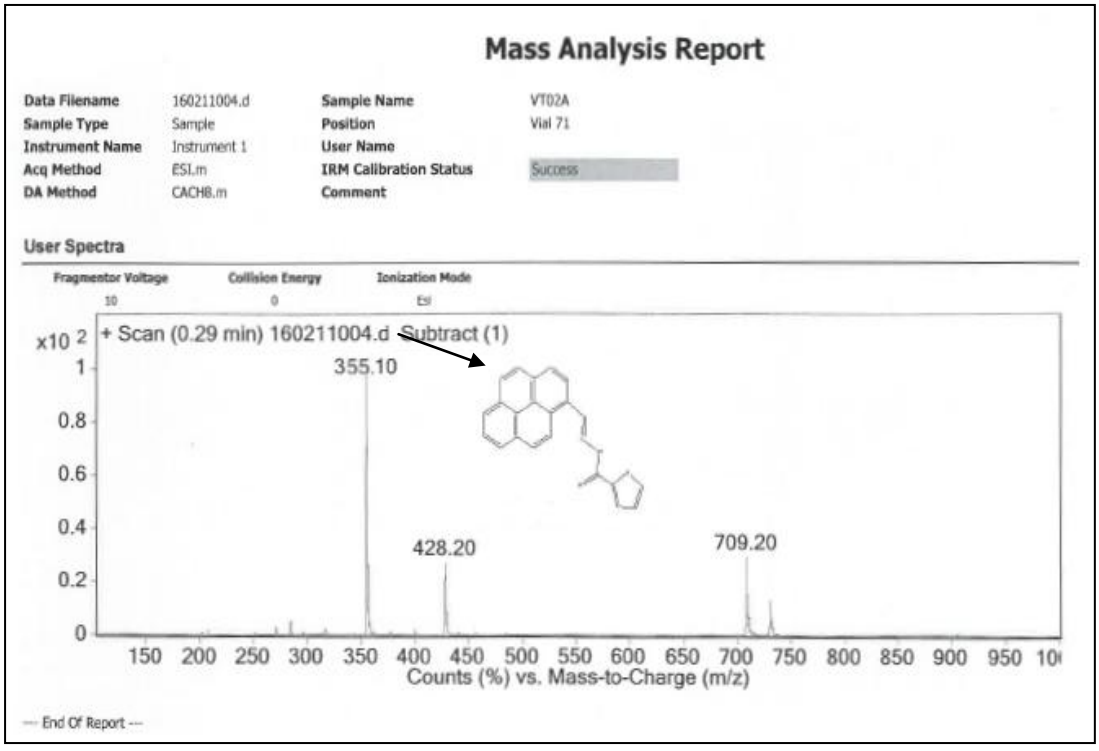

Fig. 3.12. The ESI-Mass spectrum of chemosensor **S2R3**

3.3. Results and discussion

3.3.1. Colorimetric detection of cations

The chemosensors **S2R1–S2R3** (2.5×10^{-6} M in DMSO) were tested for various metal ions like, Ni^{2+}, Cr^{3+}, Co^{2+} , Fe^{3+}, Al^{3+}, Cu^{2+}, Zn^{2+}, Ag^{+}, Hg^{2+}, Fe^{2+}, Cd^{2+}, Mn^{2+}, Mg^{2+}, Pb^{2+}, Ca^{2+}, Na^{+} and K^{+} in aqueous solution. Among them, the **S2R1** produced selectively color change yellow to colorless with the addition of two equivalence of $\mathbf{Hg^{2+}}$ ions. The **S2R2** and **S2R3** did not show any responses with the adding of other interfering metals and $\mathbf{Hg^{2+}}$ ions. A Linear colorimetric titration was conducted for the **S2R1.** The **S2R1** exhibits a linear decrement of color intensity (yellow to colorless) with the incremental addition of $\mathbf{Hg^{2+}}$ ions from 0, 0.5, 1.0, 1.5, and 2.0 equivalences, as shown in **Fig. 3.13**.

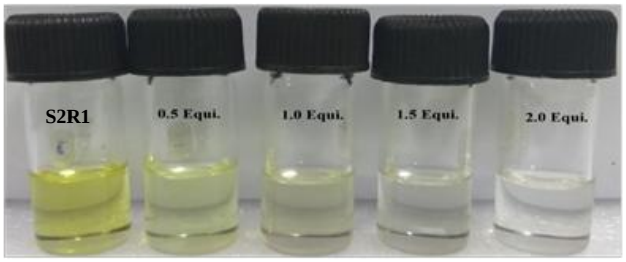

Fig. 3.13: Linear decreasing of color intensity of the chemosensor **S2R1** with the linear addition of Hg^{2+} ions (0.5, 1.0, 1.5 and 2.0 equivalence)

3.3.2. UV–Vis and fluorescence recognition of cations

The qualitative and quantitative determination of mercury ions, binding constant, interference of other metals, and the stoichiometric ratio between chemosensor-metal ions were carried out using UV–Vis and fluorescence titration experiments.

In the UV–Vis spectra of **S2R1**, absorption bands in the region at 290 nm and 417 nm were observed and are assigned to the π–π* and n–π*. Upon adding 2.0 equivalences of mercury ions, a new UV-Vis band was observed at 355 nm whereas, the band 417 nm was disappeared. This behavior can be explained by metal-chemosensor complex formation. Whereas, the **S2R1** did not produce any absorption or color changes in the attendance of 4.0 equivalences of interfering metals, as represented in **Fig. 3.14-3.16** in UV–Vis study experiments.

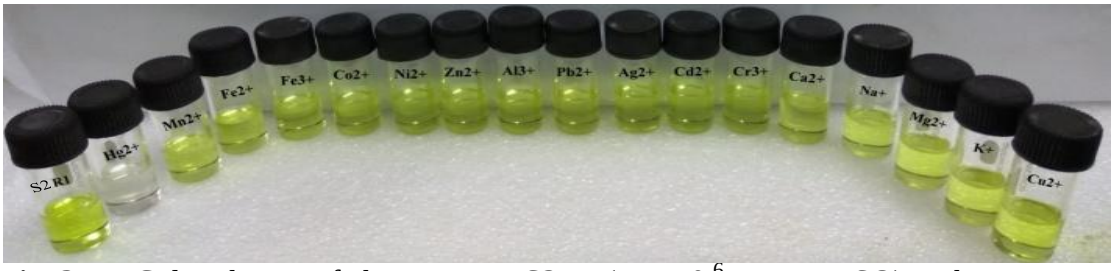

Fig. 3.14: Color change of chemosensor **S2R1** (2.5×10^{-6} M in DMSO) in the presence of 4.0 equivalences of different cations and 2.0 equivalence of $\mathbf{Hg^{2+}}$ ions

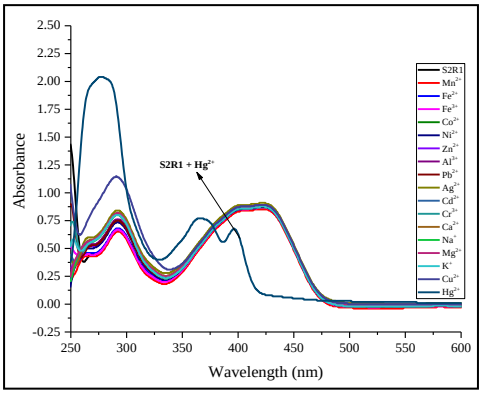

Fig. 3.15: UV-Vis absorption spectra of **S2R1** in the presence of 4.0 equivalence of various cations

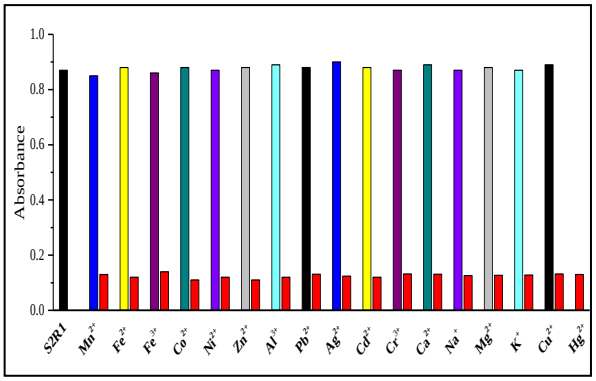

Fig. 3.16: A Bar-chart representation of UV–Vis absorption intensity changes of **S2R1** in the presence of various cations the measured wavelength at 417 nm

Titration experiments (UV–Vis) were performed with the incremental adding of $\mathbf{Hg^{2+}}$ ions (0.0–3.0 equivalences) to the **S2R1**. The UV–Vis maxima peak at 417 nm was linearly diminished, and a new absorption peak appears at 355 nm with the gradual addition of $\mathbf{Hg^{2+}}$ ions (**Fig. 3.17).** Similarly, fluorescence titration was performed with the incremental addition of mercury ions (0.0–3.0 equivalences) to the solution of **S2R1** (2.5×10^{-6} M) with excitation wavelength 355 nm. The emission band at 417 nm increased progressively, and the solution exhibits strong fluorescent in the emission spectra. (**Fig. 3.18).**

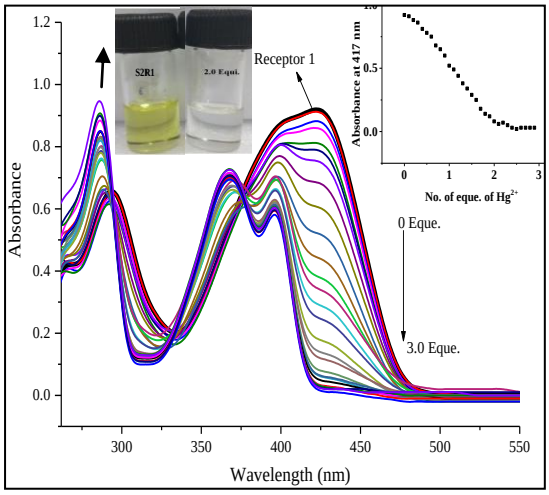

Fig. 3.17: UV-Vis titration spectra of **S2R1** (2.5×10^{-6} M) with the linear addition of **Hg^{2+}** ion (0.0–3.0 equivalence). Insert showing binding isotherm at a selected wavelength (417 nm)

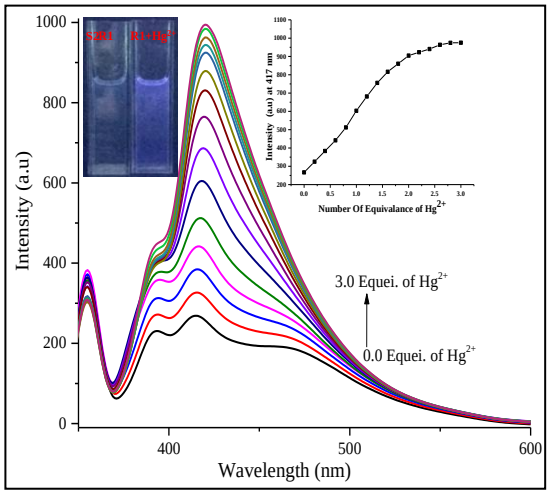

Fig. 3.18: Fluorescence titration spectra of **S2R1** (2.5×10^{-6} M) with incremental addition of Hg^{2+} ions (0.0–3.0 equivalence). Inset shows the number of equivalences of the metal solution vs. Intensity at 417 nm (Exited wavelength at 355 nm)

3.3.3. Determination of detection limit (DL) and quantization limit (QL)

According to ICH Q2R1guidlines (Ich 2005), defining the DL and QL for any quantification analytical methods is most important to understand the minimal quantification and detection of analyte present in the sample. The DL and QL were calculated with the help of a linear calibration curve drown between concentrations of **Hg^{2+}** ions (range from 0.0 to 5×10^{-6} M) versus the response of complex at 417 nm wavelength **(Fig. 3.19)**.

DL / QL = C * S_d / S

Where C = 3.0 for DL and 10.0 for QL (Ich 2005).

S_d = standard deviation of the response of the measurement, S = Slope.

UV-Vis

DL = 3 * 0.019681 / 179169.41
= 3.89×10^{-7} M ≈ 0.389 µM.

QL = 10 * 0.019681 / 179169.41
= 1.30×10^{-6} M ≈ 1.297 µM.

Fluorescence

DL = 3 * 11.954935 / 1.33×10^{8}
= 2.7×10^{-7} M ≈ 0.270 µM.

QL = 10 * 11.954935 / 1.33×10^{8}
= 8.99×10^{-7} M ≈ 0.899 µM.

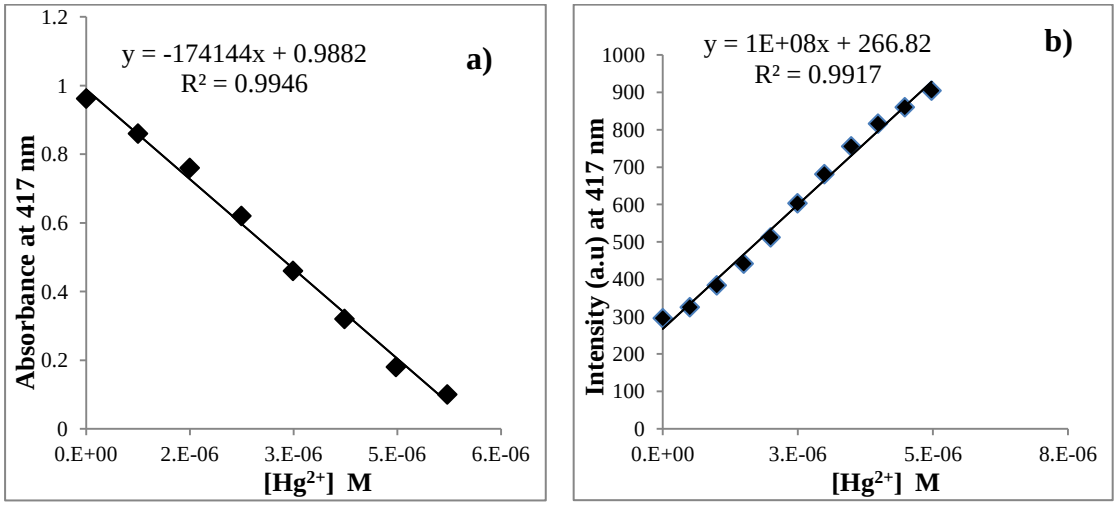

Fig. 3.19: Linear calibration plots, **a).** The concentration of Hg^{2+} and absorbance of **S2R1**– Hg^{2+} complex monitored wavelength at 417 nm, **b).** Emission of **S2R1**–Hg^{2+} vs. concentration of Hg^{2+} ions. (Exited wavelength at 355 nm)

3.3.4. Density functional theory (DFT)

Considering the experimental evidence on the hydrolytic cleavage of imine linkage of **S2R1** in the attendance of Hg^{2+} leading to the selective optical responses, the quantum mechanical calculations of **S2R1** and its starting reactant 1-pyrenecarboxaldehyde were done by adopting the density functional theory (DFT) method to complement the sensing mechanism. All calculations were done in the gas phase by applying the B3LYP exchange-correlation functional, and the 6-31G** basis set coded in the Gaussian 09W and Gaussview computational program (Frisch et al. 2009). Further, the time-dependent density functional theory (TD-DFT) calculations were done to complement the spectral changes at the same level of theory. As shown in **Fig. 3.20a**, the optimized geometry of **S2R1** was found to be planar, leading to a highly conjugated system resulting in the yellow colouration in the solution. The calculated UV-Vis spectrum of **S2R1** has three absorption bands at 426.74 nm (Oscillatory strength, f = 0.9315), 371.36 nm (f = 0.0826) and 336.33 (f = 0.0291) in the gas phase whereas at 455.34 (f =1.1237), 375.13 (f =0.1128) and 338.88 (f =0.0594) in the DMSO medium. The calculated band in the visible region complemented well with the experimental value (417 nm), which was responsible for the yellow coloration. The molecular electrostatic potential map (MEP) of **S2R1** indicates that the most negative sites shown in red color are observed over the

nitrogen atoms (**Fig. 3.20b**). Considering all the possible coordination sites of **S2R1**, we have tried to obtain the Hg^{2+} complex structure, but the structures are found to be energetically not favourable. Further, the reactant molecule 1-pyrenecarboxaldehyde was optimized, and its spectral data were obtained, which exhibit two bands at 370.88 (f = 0.3327) and 343.24 (f = 0.0445) in the gas phase whereas at 390.24 (f =0.4957) and 347.27 (f =0.0482) in the DMSO medium. The calculated absorption bands of 1-pyrenecarboxaldehyde are corroborated well with the experimental evidence obtained on the UV-Vis spectral changes that arise in **S2R1** upon binding with Hg^{2+}. Further, the blue spectral shift of **S2R1** in the attendance of Hg^{2+} was also complemented with the HOMO-LUMO energy levels, where the bandgap of **S2R1** was increased from 0.1114 eV to 0.1276 eV (**Fig. 3.20c**). Analyzing the molecular electrostatic potential (MEP) as well as the electron density in **S2R1**, the possible weak fluorescence from **S2R1** may be due to the PET (photoinduced electron transfer) occurred from the nitrogen atoms to the pyrene fluorophore. Upon interaction with Hg^{2+}, followed by the separation of 1- pyrenecarboxaldehyde and 2-aminothioazole, the PET process is inhibited, resulting in the vertical enhancement in the fluorescence.

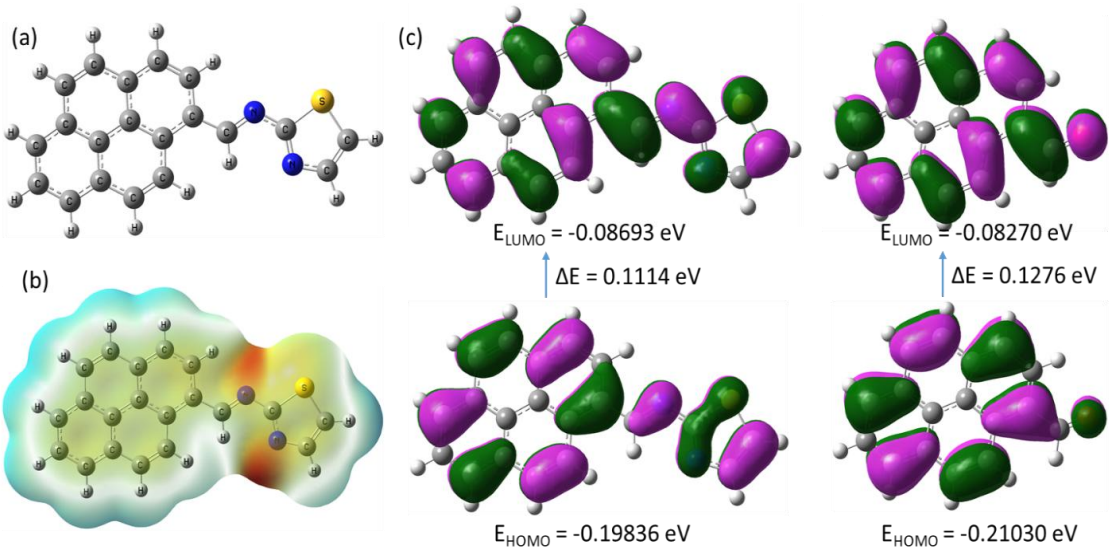

Fig. 3.20. (a) The DFT computed the structure of **S2R1** and, **(b) S2R1** MEP map. **(c)** The DFT computed HOMO–LUMO energy levels of **S2R1** and 1-pyrenecarboxaldehyde

3.3.5. Binding mechanism of S2R1 with mercury metal ion

The response (A_0/A) of **S2R1** to different metal ions verses ionic radii/electronegativity is depicted in **Fig. 3.21,** and it further substantiate that mercury

ion exhibits better response than other examined metals (Li and Xue 2006; Momidi et al. 2017; Shannon 1976; Suresh et al. 2010). This specific binding and recognition of mercury ions explained by different mechanisms like Hard and soft acid-base (HSAB) theory (Pearson 1963), electronegativity, and ionic radii. No correlation is noticeable when the (A_0/A) of **S2R1** in the presence of various metal ions are drowned against ionic radii (Li and Xue 2006; Momidi et al. 2017; Shannon 1976; Suresh et al. 2010) (**Fig. 3.21**) and same results were observed when data plotted against electronegativity. From the correlation study, it is observed that Hg^{2+} has more selectivity than that of other cations, and further, the results can be supported by Pearson's HSAB theory (Pearson 1963). The sulfur atom is a soft base, so it has a greater affinity to bind with mercury ion, which is soft acid; hence, the better response was shown by **S2R1**.

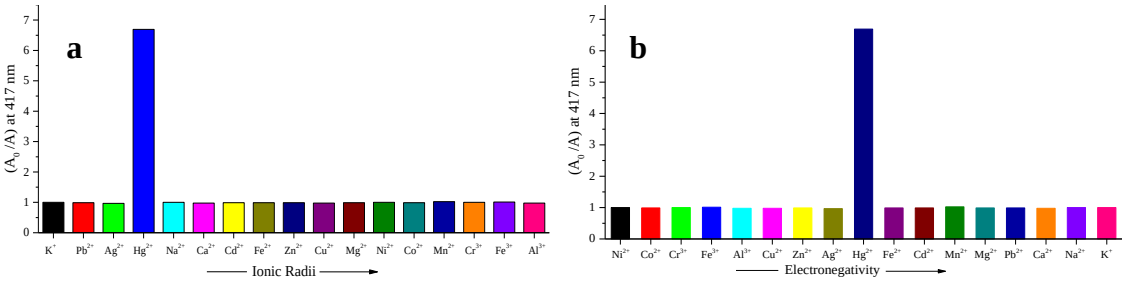

Fig. 3.21: a). Absorbance response (A_0 /A) of chemosensor **S2R1** at a selected wavelength (417 nm) plotted against ionic radii (pm) of cations in decreasing order. **b).** Absorbance response (A_0 /A) of **S2R1** at a selected wavelength (417 nm) plotted against electronegativity of cations in decreasing order

The fluorescence response of **S2R1** significantly increased at 417 nm when the Hg^{2+} ions were introduced to an **S2R1** solution. Enhancement at 417 nm in the fluorescence spectra was due to the chemodosimetric event of **S2R1** that produced a strong fluorescent moiety (1-Pyrenecarboxaldehyde). To prove the chemodosimetric reaction of **S2R1** with Hg^{2+}, spectroscopic, structural analysis of the reaction products, by FT-IR, LC-MS, and ^{1}H-NMR spectroscopy were investigated (Bhalla et al. 2013; Kim et al. 2010). FT-IR spectra were recorded for the **S2R1** in the presence and absence of Hg^{2+} ions (**Fig. 3.22**). When compared FT-IR spectra of **S2R1** with the chemosensor **S2R1**+Hg^{2+}, the imine (–C=N–) frequency at 1562 cm^{-1} was disappeared and aldehyde (–C=O) characteristic frequency at 1668 cm^{-1} was found after the addition of Hg^{2+} ions. From the FT-IR analysis, it was identified that the imine bond in **S2R1** undergone hydrolysis with the addition of Hg^{2+}. The mass peak

at m/z 313.08, 213.08, and 101.05 are corresponding to **S2R1**, aldehyde, and thiazole amine respectively were identified in the LC-MS spectra of **S2R1** in the attendance of Hg^{2+} ions. (**Fig. 3.23**). It indicates that the irreversible hydrolysis of the imine bond (in S2R1) in the attendance of Hg^{2+} ions. Direct evidence was obtained from the ^{1}H-NMR (**Fig. 3.24**); **S2R1** exhibits a proton peak at 10.9 ppm, which corresponding to pyrene aldehyde proton in the attendance of Hg^{2+} ions. These observations show that irreversible hydrolysis of imine bond in the attendance of Hg^{2+} ions.

The genesis of pyrenecarboxaldehyde as a result of Hg-promoted hydrolysis of the **S2R1** is confirmed by the absorption, fluorescence spectra (**Fig. 3.25**). The literature reports also support the proposed reaction mechanism (Bhalla et al. 2013; Kim et al. 2010). The absorption spectra of pyrenecarboxaldehyde and S2R1, **S2R1**+Hg^{2+} are closely undifferentiated, represent that hydrolysis of **S2R1** by Hg^{2+} ions affords pyrenecarboxaldehyde within a short reaction time.

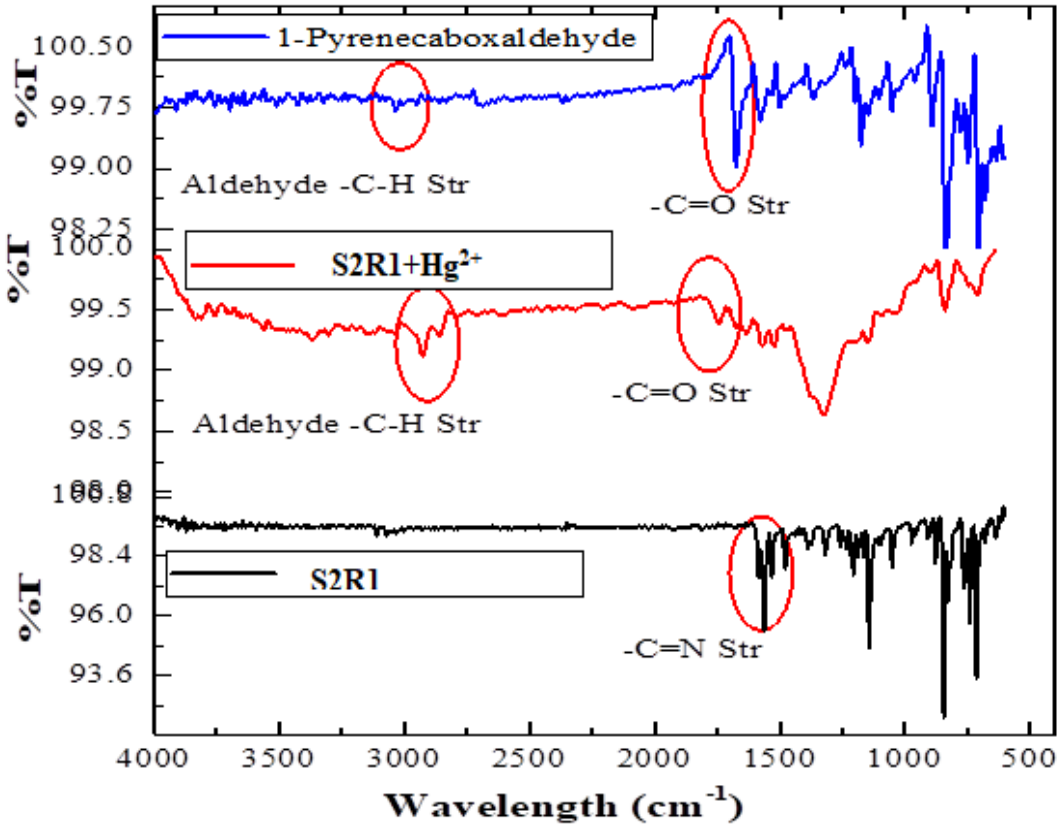

Fig. 3.22: FT-IR Spectra of **S2R1** and **S2R1**+Hg^{2+}, Pyrenecarboxaldehyde.

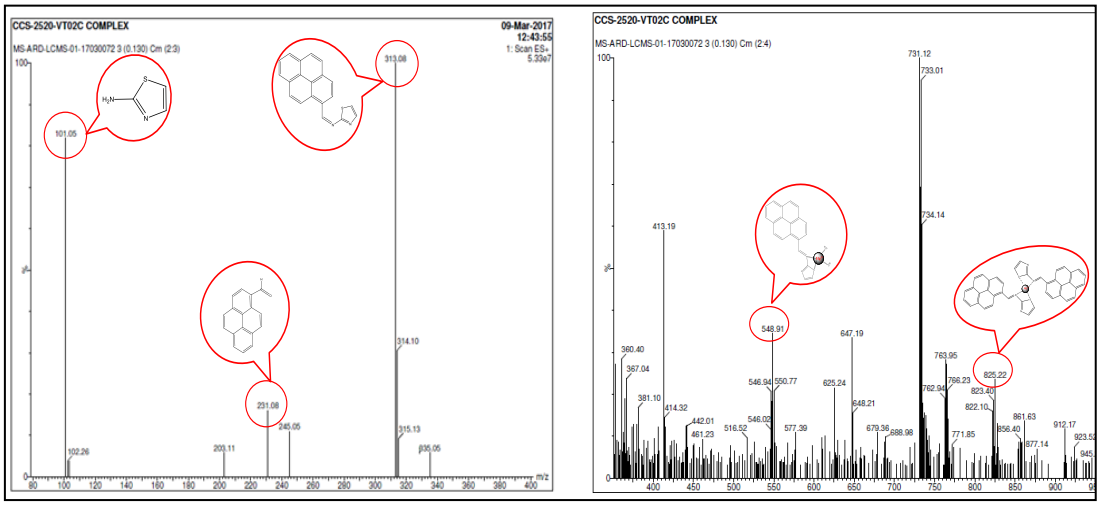

Fig. 3.23: LC-MS spectra of **S2R1** + Hg^{2+} complex (figure shows 0-400 m/z and 400 to 1000 m/z scale in ESI-MS from left to right)

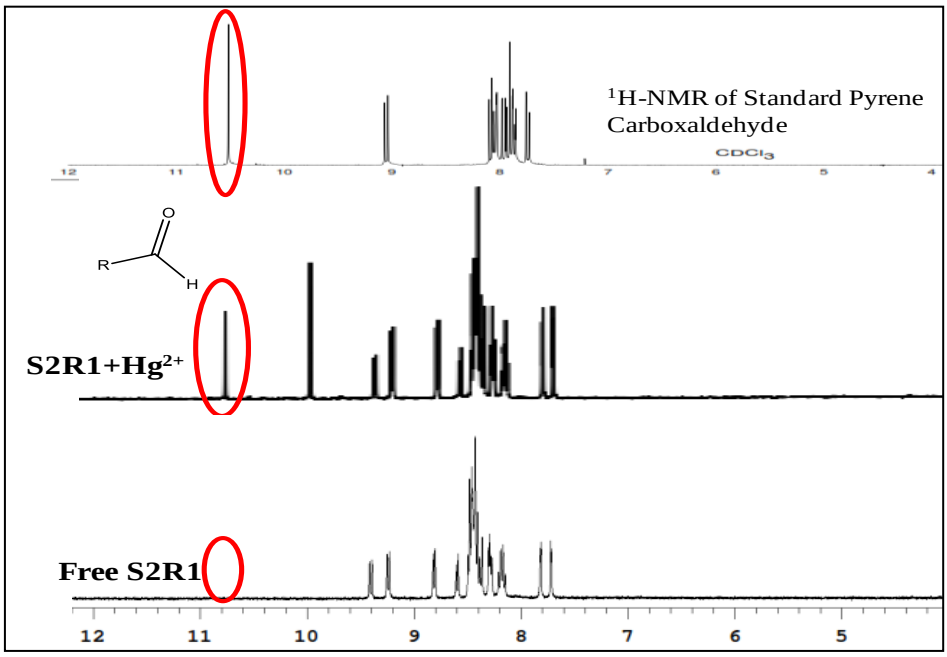

Fig. 3.24: ^{1}H-NMR spectra of **S2R1**, **S2R1**+Hg^{2+}, and Pyrenecarboxaldehyde

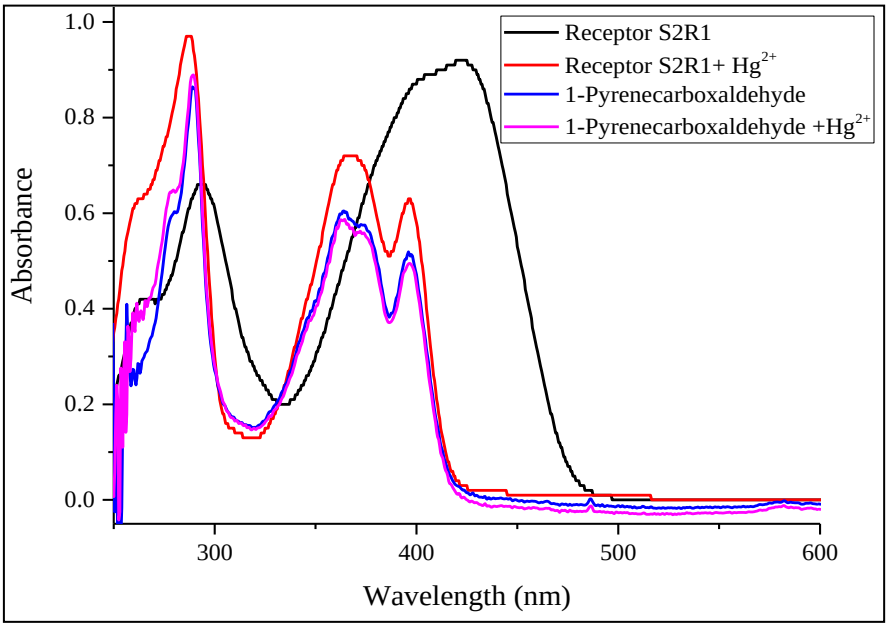

Fig. 3.25: UV-Vis Spectra of **S2R1** and **S2R1**+Hg^{2+}, Pyrenecarboxaldehyde, Pyrenecarboxaldehyde-Hg^{2+} in DMSO

The UV-Vis, FT-IR, LC-MS and ^{1}H-NMR results corroborate the proposed mechanism of Hg^{2+}-promoted imine hydrolysis of **S2R1** as represented in the **scheme -3.2.** Further, it was also supported by theoretical DFT studies.

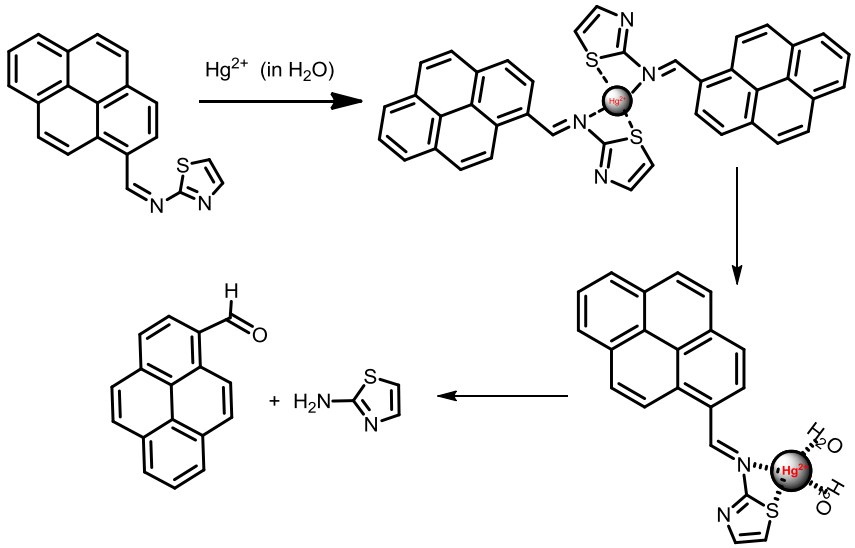

Scheme 3.2: Proposed mechanism of Hg^{2+}-promoted imine hydrolysis of **S2R1**

3.3.6. Real-life application

The chemosensor **S2R1** selectively binds with **Hg^{2+}** ions; with this mind, we tried to find the trace quantity of **Hg^{2+}** ions in drinking and tap water samples with a quantitative determination. Initially, linear calibration plots drown between the

absorbance of **S2R1-Hg^{2+}** vs. the amount of Hg^{2+} ions (0.0 to 7.0 μM) **(Fig. 3.26)**. From the linear plot, it was identified the absence of **Hg^{2+}** ions in the collected samples. Spiking studies were carried out to investigate the interference of the other competitive ions present in the collected water samples. Mercury spiked sample was prepared by adding a known quantity of **Hg^{2+}** ions (1.3 μM and 2.5 μM) to the water samples. The result is tabulated in **table 3.1**, and it shows a good % recovery between three replicate spiked samples during the analysis with good precession.

Table-3.1: Estimation of **Hg^{2+}** ions amount in water samples collected from different sources

Water sample type	Amount (μM) (n=3)	Spiked (μM)	Found (μM) & % RSD (n=3)	% Recovery (n=3)
Drinking	Not detected	1.30	1.31 ± 1.17	100.5
		2.50	2.49 ± 0.23	99.5
Tap	Not detected	1.30	1.31 ± 1.16	101.0
		2.50	2.48 ± 0.40	99.2

RSD: Relative standard deviation (RSD)

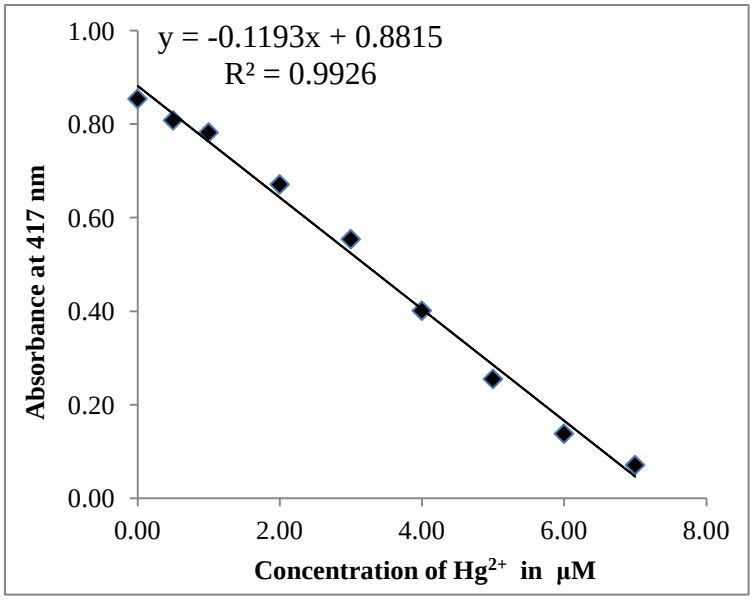

Fig. 3.26: A linear calibration plot of **S2R1**–Hg^{2+} vs. the amount of Hg^{2+} ions

From the spiking study experimental results, it is suggested that the quantitative estimation of **Hg^{2+}** ions in the tested two different water samples. This method can be utilized for regular analysis to measure the amount of **Hg^{2+}**.

3.4. Conclusions

Among the reported chemosensors, **S2R1** exhibits selectivity and sensitivity towards mercury ions by producing a noticeable color change, and this color change could be easily recognized by naked-eye. The **S2R1** was utilized for colorimetric detection and estimation of $\mathbf{Hg^{2+}}$ ions in the attendance of competitive tested metal ions qualitative and quantitatively. Through the optical studies (UV–Vis/ Fluoresce), spectroscopy (FT-IR, Mass, and ^{1}H-NMR) and theoretical DFT study results were confirmed the Hg^{2+}-induced hydrolysis of **S2R1.** The prepared **S2R1** was accomplished for the detection of 0.389 μM (UV-Vis) and 0.270 μM (Fluoresce) of $\mathbf{Hg^{2+}}$ ions in the water medium. The **S2R2** and **S2R3** did not show any activity towards other tested cations and $\mathbf{Hg^{2+}}$ ions, and this may be a lack of suitable binding sites in their molecular structure like **S2R1.** The **S2R1** has more acidic compared to the **S2R2,** and **S2R3** may be due to this the **S2R1** undergone hydrolysis with the Hg^{2+} ions**.** The real-time analysis results suggest that the **S2R1** could produce accurate and linear results for routine applications.

CHAPTER-4

A NEW COLORIMETRIC CHEMOSENSORS FOR Cu^{2+} AND Cd^{2+} IONS DETECTION: APPLICATION IN ENVIRONMENTAL WATER SAMPLES AND ANALYTICAL METHOD VALIDATION

CHAPTER-4

4. A NEW COLORIMETRIC CHEMOSENSORS FOR Cu^{2+} AND Cd^{2+} IONS DETECTION: APPLICATION IN ENVIRONMENTAL WATER SAMPLES AND ANALYTICAL METHOD VALIDATION

Abstract

In this chapter, the design, syntheses, and characterization of new thiophene carboxylic acid hydrazine derivatives as a colorimetric chemosensor for Cu^{2+} and Cd^{2+} metal ions, have been discussed in detail. The colorimetric cation sensing properties, detection mechanism, application in environmental water samples, and analytical method validation have been incorporated.

4.1. Introduction

The development of colorimetric chemosensors capable of recognizing biologically important and environmentally pollutant metal ions such as Mn^{2+}, Fe^{2+}, Fe^{3+}, Co^{2+}, Cu^{2+}, Ni^{2+}, Zn^{2+}, Ag^{2+}, Cd^{2+}, Hg^{2+} Pb^{2+}, Cr^{3+}, Al^{3+}, K^{+}, Na^{+}, $Ca^{2+,}$ and Mg^{2+} has been an important research topic over the last two decades (Ma et al. 2012), (Singhal et al. 2015), (Li et al. 2012a), (Tharmaraj and Pitchumani 2012), (Wang et al. 2005), (Tang et al. 2016),(Li et al. 2008). Copper is the third most abundant essential transition metal ion in the human body. Many proteins use copper ions as a cofactor for electron transport, or as a catalyst in oxido-reduction reactions. Copper distribution in the human body is highly controlled because of its cellular toxicity. Excess of copper ions in living cells can catalyze the production of reactive oxygen species (ROS) and can damage lipids, nucleic acids, proteins and cause several serious diseases, including Alzheimer's disease (Emerit et al. 2004), Indian childhood cirrhosis (ICC) (Hahn et al. 1995), Prion disease (Brown 2001) and Menkes and Wilson diseases (Waggoner et al. 1999) which are associated with the cellular toxicity of copper ions. Due to its extensive applications in our daily lives, copper is also a common metal pollutant. The limit for copper in drinking water, as set by the WHO and US Environmental Protection Agency (EPA) is 1.3 ppm (Edition 2011), (Chapter 2016).

Fegade U reported selective dual-channel chemosensor for Cu^{2+} in semi-aqueous media (Fegade et al. 2014). Kato T has developed isotope dilution inductively coupled plasma mass spectrometry for the determination of nickel, copper, zinc, silver, cadmium, and lead in seawater (Kato et al. 1990), Hong. S developed surface plasmon resonance analysis of aqueous copper ions with amino-terminated self-assembled monolayers (Hong et al. 2007), different techniques like fluorescence anisotropy assay, Peptide-coated CdS quantum dots for the optical detection and microelectrode for copper ion detection (Gattás-Asfura and Leblanc 2003; Küpper and Schultze 1997; Yin et al. 2010). Lin. W have used a ratiometric fluorescent probe for Cu^{2+} ion detection (Lin et al. 2009). Among various detection methods, optical detection methods (via fluorescence or colorimetric changes) are the most promising detection technique showing to their low cost, simplicity, low detection limit and useful application in environmental, biological, and industrial areas (Dutta and Das 2012; Hammud et al. 2015; Liu et al. 2015; Nair et al. 2015; Narayanaswamy and Govindaraju 2012; Sarkar et al. 2013; Xiong et al. 2016). The development of colorimetric chemosensors for the detection of Cu^{2+} ions has much attention due to its toxic effect on human health.

Cadmium is widely distributed in the Earth's crust and mostly associated with zinc and copper and is produced commercially only as a by-product of zinc smelting. It is highly toxic to the human organism like mercury. Its derivatives enter the environment only from geological or human activities (metal mining, smelting, and fossil fuel combustion). Cadmium and its compounds are blacklisted materials, which by international agreement, may not be discharged or dumped into the environment. A high exposure level of cadmium is associated with increased risks of cardiovascular diseases, cancer mortality, and damage to the liver and kidney (Lauwerys et al. 1994; Nordberg 1992). In literature Kim et al. have reported a fluorescent and colorimetric sensor for detection of lead, cadmium, and mercury ions (Kim et al. 2012), tang et al. has reported a new semirigid molecule as a selective fluorescent chemosensor for recognition of Cd (II) (Tang et al. 2008). Li et al. have used a turn-on fluorescent sensor for selective detection of Zn^{2+}, Cd^{2+}, and Hg^{2+} in water (Li et al. 2012b). Another problem with Cd^{2+} sensitive sensors is the interference of Zn^{2+} that provides false-positive spectral signals after interaction with the sensor (Dutta and Das 2012). As a solution to this problem, (Lu et al. 2007) have synthesized a sensor based on 4,5-

diamino-1,8-naphthalimide as the fluorophore, which, by undergoing two reverse ICT processes, in sensing Cd^{2+} and Zn^{2+}, discriminated between this ion pair efficiently.

The majority of literature reports reveal the sensitivity for the detection of metal ions in organic media. However, to achieve selectivity and sensitivity in aqueous media in the presence of other common interfering anions /cations, method validation is more important for the quantitative application. Very few reports are available in the literature wherein the method validation has been used to confirm the efficacy of the sensor. With this in view, in the present chapter designed, new thiophene-2-caboxylic acid hydrazine based colorimetric chemosensor **(S3R1-S3R4)** for metal ion detection. Chemosensor **S3R3** exhibits selectivity towards Cu^{2+} ions and chemosensor **S3R4** towards Cd^{2+} over the other metal cations and anions in aqueous media with a significant color change from colorless to yellow in the presence of Cu^{2+} and Cd^{2+} ions respectively, which can be detected through naked-eye. The reported chemosensors **S3R3** and **S3R4** have the advantage over the other published methods in terms of method validation, real-time applications, selectivity in the presence of other competitive cations, and anions in an aqueous medium.

4.2. Experimental section

4.2.1. Materials and methods

All chemicals and metal nitrate salts were purchased from commercial suppliers and used without any further purification. Chromatography grade solvents have been used for synthesis and UV–Vis titrations without any further purification.

4.2.2. Colorimetric and UV–Vis studies

A Stock solution of various metal ions as their nitrate salts (1.0×10^{-2} M) was prepared in de-ionized water. An individual chemosensor stock solution of **S3R1–S3R4** (1.0×10^{-3} M) were prepared in dimethylformamide (DMF). The stock solutions **S3R1–S3R4** were further diluted to 2.5×10^{-5} M with the same solution. In UV-Vis and colorimetric titration experiments, metal ions were added by using a micropipette to a solution of **S3R3** and **S3R4** (2.5×10^{-5} M). UV-Vis spectral data were recorded after the addition of the metal ions using 3.0 mL quartz cells (2 optical windows) having a path length of 1.0 cm.

4.2.3. General synthesis procedure for chemosensors S3R1–S3R4

The synthesis procedure of **S3R1–S3R4** has illustrated in the **scheme 4.1**. The synthesis of chemosensor **S3R1:** Thiophene-2-carboxylic acid hydrazide (0.5004g, 3.5mmol) and thiophene-2-carboxaldehyde (0.3965g, 3.5mmol) were separately dissolved in 10 mL ethanol. Then aldehydehyde solution was added drop-wise with constant stirring to the thiophene-2-carboxylic acid hydrazide solution. To this a catalytic amount of acetic acid was added and the reaction mixture was stirred at room temperature for 2 hours. The progress of reaction was monitored by TLC. After the completion of reaction the reaction mixture was filtered and washed with hot ethanol. Similarly, the **S3R2, S3R3** and **S343** were synthesized as stated above synthetic methodology. The **S3R2** was synthesized by the reaction of thiophene-2-carboxylic acid hydrazide (0.5012g, 3.5mmol) and furfural-2-carboxaldehyde (0.3393g, 3.5mmol). The **S3R3** was synthesized by the reaction of thiophene-2-carboxylic acid hydrazide (0.5007g, 3.5mmol) and pyrrol-2-carboxaldehyde (0.335g, 3.5mmol). The **S3R4** was synthesized by the reaction of thiophene-2-carboxylic acid hydrazide (0.3003g, 2.1mmol) and quinoline-2-carbaldehyde (0.6001g, 2.1mmol). The final obtained desired compounds were characterized by using standard spectroscopic methods as given below.

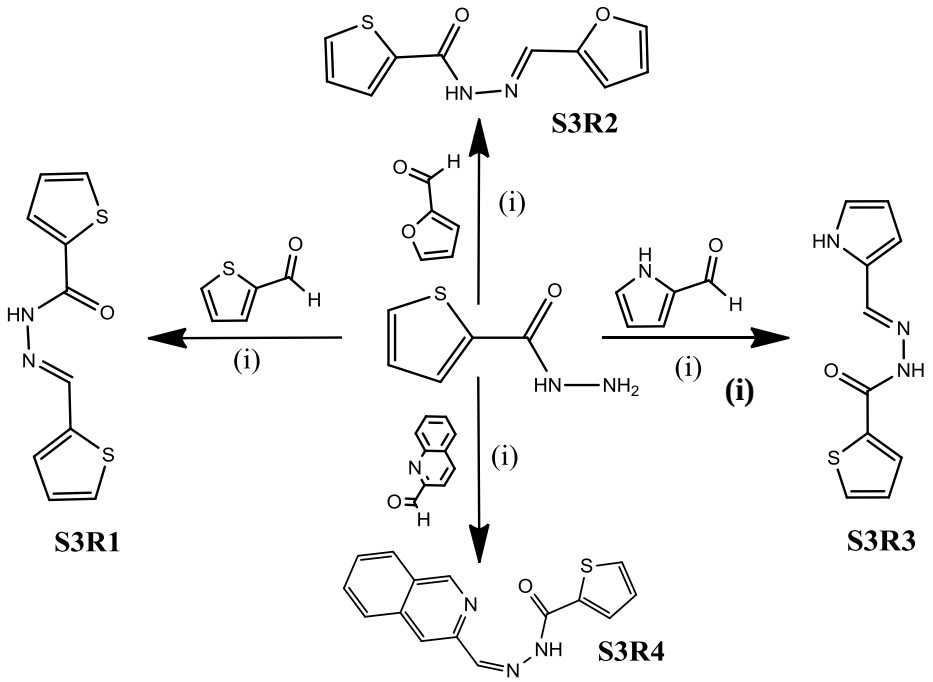

(i) = Ethanol / Acetic acid, 2 h

Scheme-4.1: Synthesis of chemosensor **S3R1** to **S3R4**

4.2.4. Characterization

The melting point was recorded on Bio-cote (SMP10) instrument and in open capillary and is uncorrected. Fourier Transform Infrared (FT-IR) Spectra was recorded on a Bruker Alpha, which is equipped with silicon carbide as IR source. All sample spectra were recorded using KBr pellet media. The samples under study were recorded with 16 scans with a sample resolution of 4 cm^{-1}. The background data collection was done with the KBr pallet before the analysis of samples. ^{1}H-NMR (400 MHz) and ^{13}C-NMR (100MHz) spectra were recorded on 400 MHz Varian Mercury plus FT-NMR spectrometer and DMSO-d_6 solvent was used. The ^{1}H NMR and ^{13}C NMR chemical shifts are reported on the δ scale (in ppm) relative to tetramethylsilane (TMS, δ 0.00) and DMSO-d_6 (39.50), respectively, as internal reference standards. The coupling constants (J) mentioned in Hz. Resonance multiplicities are described as s (singlet), d (doublet), t (triplet), and m (multiplet). Mass spectra were recorded on Agilent LC-MS 6410. Single X-ray Diffraction data for synthesized molecules collected on a Bruker Apex II duo diffractometer with a CCD detector. As a source of radiation for the experiment, monochromatic Molybdenum (Mo) Kα radiation (λ=0.7107Å) was used. Data collection was done at ambient temperature (296K). All the crystal structures were solved by direct methods using SHELXL-2007/2014 software, and the refinement was carried out by full-matrix least-squares technique using SHELXL-2007/2014. For all the non-hydrogen atoms, anisotropic displacement parameters were calculated. The UV-Vis titrations were carried out on a UV-Vis spectrophotometer (Analytikjena Specord S600, GBC-Cintra 101 double beam UV-Visible Spectrometer and ocean optics SD2000) in standard 3.0 mL quartz cells (2 optical windows) having a path length of 1.0 cm. The characterization data of chemosensor S3R1-S3R4 is given below:

S3R1 (Thiophene-2-carboxylic acid thiophen-2-ylmethylene-hydrazide):

Yield: 99.5%. **Melting range:** 215 – 216°C. **FT-IR: (KBr, cm^{-1})**: 3443.63, 3146.07, 1653.85, 1512.83, 1423.19, 1382.68, 1307.47, 1220.30, 1162.76, 1031.41, 859.17, 782.51, 726.80 **(Fig.4.1)**. **^{1}H NMR: (400 MHz; DMSO-d_6 δ_{ppm}):** 8.654 (s, 1H, –NH), 8.297 (s, 1H, HC=N), 8.047 – 7.887 (m, 2H, aromatic thiophene –C=CH), 7.697 – 7.683 (d, 1H, aromatic thiophene –C=CH, J=5.6 Hz). 7.496 – 7.488 (d, 1H,

aromatic thiophene –C=CH, J=3.2Hz), 7.238 – 7.217 (t, 1H, aromatic thiophene carboxylic acid –C=CH, J=8.4Hz), 7.164 – 7.142 (t, 1H, aromatic thiophene –C=CH), J=8.8Hz, **(Fig.4.5)**. **^{13}C NMR: (100 MHz; DMSO-d$_6$ δ$_{ppm}$):** 161.1 (–C=O), 142.7 (HC=N), 139.0, 135.0, 134.7, 131.9, 131.0, 129.1 (aromatic thiophene –C=C–), 128.2, 126.7 (thiophene =C–S–) **(Fig.4.9)**. **LC-MS (ESI) m/z:** calculated for $C_{10}H_8N_2OS_2$ 236.008, found, 237.10 $(M+1)^+$ **(Fig.4.13)**.

S3R2 (Thiophene-2-carboxylic acid furan-2-ylmethylene-hydrazide):

Yield: 89.9%. **Melting range:** 163 – 165°C. **FT-IR: (KBr, cm^{-1})**: 3263.97, 3138.94, 3099.56, 1629.29, 1606.02, 1445.55, 1418.95, 1358.74, 1305.76, 1245.11, 1131.57, 1131.57, 1063.18, 1034.36, 878.88, 842.99, 754.85, 713.06 **(Fig.4.2)**. **^{1}H NMR: (400 MHz; DMSO-d$_6$ δ$_{ppm}$):** 8.320 (s, 1H, –N–H), 8.085 (s, 1H, HC=N), 7.995 – 7.879 (m, 3H aromatic thiophene –C=CH), 7.228 (t, 1H aromatic furfural –C=CH, J=8.2Hz), 6.964 – 6.959 (d, 1H, aromatic furfural –C=CH, J=2.0Hz), 6.66 (d, 1H, aromatic furfural –C=CH, J=2.2Hz) **(Fig.4.6)**. **^{13}C NMR: (100 MHz; DMSO-d$_6$ δ$_{ppm}$):** 157.7 (–C=O), 149.3 (HC=N), 145.3 furfuran –C–O–C–), 137.3, 135.0, 133.4, 131.9 (aromatic thiophene –C=C–), 129.0, 126.8 (aromatic furfural –C=C–), 112.3 (=C–S–) **(Fig.4.10)**. **LC-MS (ESI) m/z:** calculated for $C_{10}H_8N_2O_2S$ 220.031, found, 221.10 $(M+1)^+$ **(Fig.4.14)**.

S3R3 (Thiophene-2-carboxylic acid (1H-pyrrol-2-ylmethylene)-hydrazide):

Yield: 92.0%. **Melting range:** 239 – 241°C. **FT-IR: (KBr, cm^{-1})**: 3263.9, 3099.56, 3048.38, 1629.29, 1606.02, 1557.26, 1445.55, 1418.95, 1358.74, 1305.76, 1131.57, 1096.11, 1063.18, 1034.36, 943.23, 878.88, 718.83 **(Fig.4.3)**. **^{1}H NMR: (400 MHz; DMSO-d$_6$ δ$_{ppm}$):** 11.515 (s, 2H, –NH), 8.258 (s, 1H, HC=N), 7.971 – 7.837 (m, 2H, aromatic thiophene –C=CH), 7.212 – 7.191 (t, 1H, aromatic thiophene –C=CH, J=8.4Hz), 6.967 – 6.915 (m, 1H, aromatic pyrrole –C=CH), 6.496 (d, aromatic pyrrole –C=CH, J=3.4Hz), 6.149 (s, 1H, aromatic pyrrole –C=CH) **(Fig.4.7)**. **^{13}C NMR: (100 MHz; DMSO-d$_6$ δ$_{ppm}$):** 157.4 (–C=O), 140.7 (HC=N), 138.4, 131.2, 128.4 (thiophene aromatic –C=C–), 127.9, 126.9, 122.6 (pyrrole aromatic –C=C–), 113.4 (pyrrole –C–NH), 109.2 (=C–S–) **(Fig.4.11)**. **LC-MS (ESI) m/z:** calculated for $C_{10}H_9N_3OS$ 219.047, found, 220.20 $(M+1)^+$ **(Fig.4.15)**.

S3R4 (Thiophene-2-carboxylic acid isoquinolin-1-ylmethylene-hydrazide):

Yield: 97.8%. **Melting range** 228 – 232°C. **FT-IR: (KBr, cm^{-1})**: 3290.38, 3067.80, 1642.63, 1589.55, 1504.88, 1418.46, 1374.91, 1300.21, 1216.05, 1156.41, 821.08,

760.84, 723.71 **(Fig.4.4)**. **^{1}H NMR: (400 MHz; dmso-d_6 δ_{ppm}):** 12.187 (s, 1H, –NH), 8.580 – 8.444 (m, 1H, aromatic quinoline –C=CH), 8.303 – 8.220 (m, 1H, aromatic quinoline –C=CH), 8.100 (s, 1H, HC=N), 8.025 – 7.998 (m, 3H, aromatic quinoline –C=CH), 7.815 – 7.811 (m, 1H, aromatic quinoline –C=CH), 7.794 – 7.773 (t, 1H, aromatic thiophene –C=CH, J=8.4Mz), 7.659 – 7.622 (m, 1H, aromatic thiophene –C=CH), 7.269 - 7.247 (t, 1H, aromatic thiophene –C=CH, J=8.8Hz) **(Fig.4.8)**. **^{13}C NMR: (100 MHz; DMSO-d_6 δ_{ppm}):** 147.8 (–C=O), 130.6 (HC=N), 129.4, 128.5, 127.9 (aromatic –C=C– in thiophene and quinoline ring), 118.0 (=C–S–) **(Fig.4.12)**. **LC-MS (ESI) m/z:** calculated for $C_{15}H_{11}N_3OS$ 281.3, found, 282.3 $(M+1)^+$ **(Fig.4.16)**.

4.2.5. Characterization spectra of chemosensors S3R1–S3R4

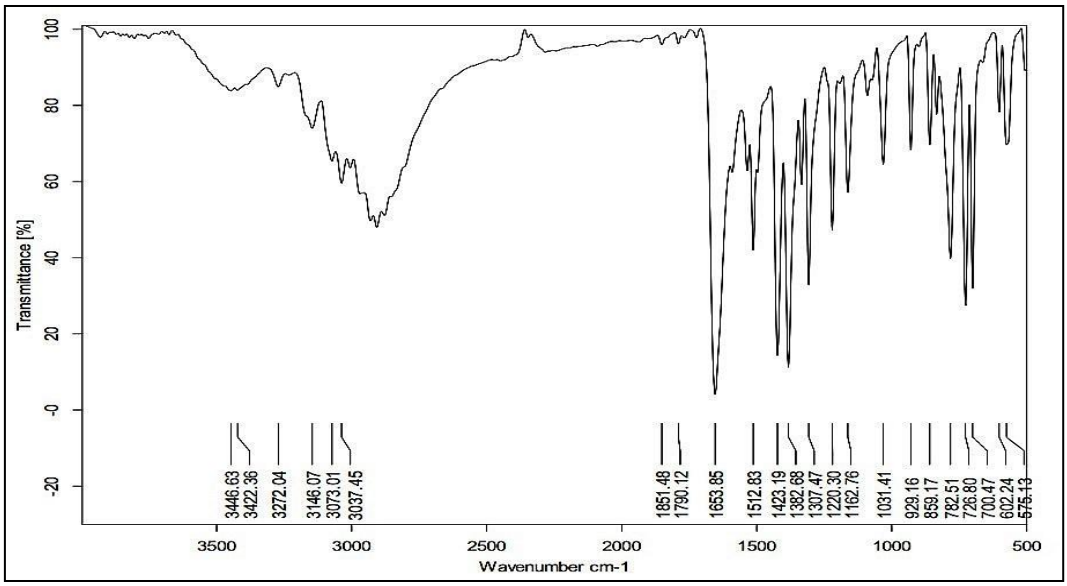

Fig. 4.1: FT-IR spectrum of chemosensor **S3R1**

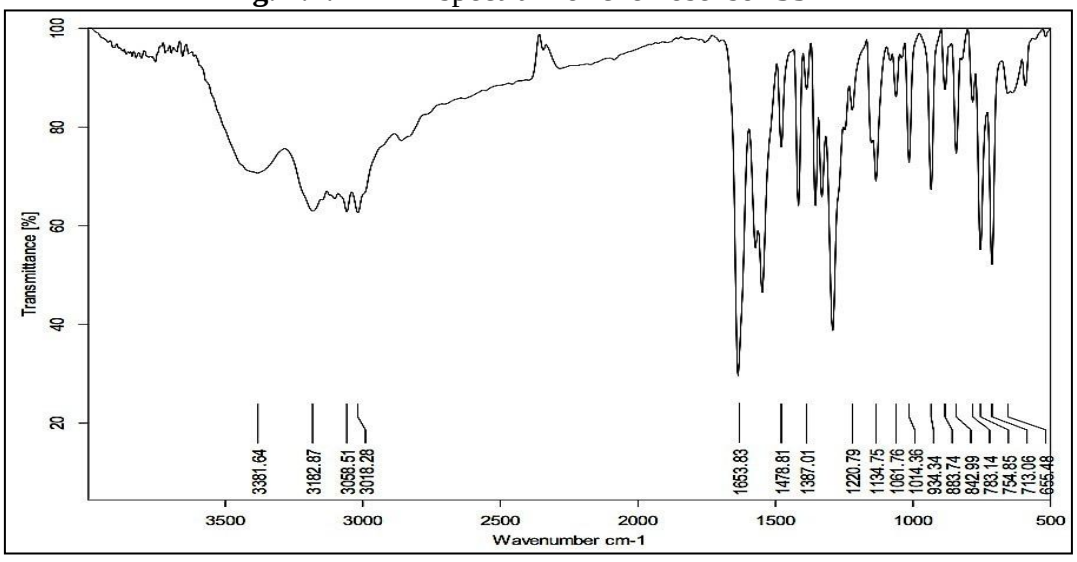

Fig. 4.2: FT-IR spectrum of chemosensor **S3R2**

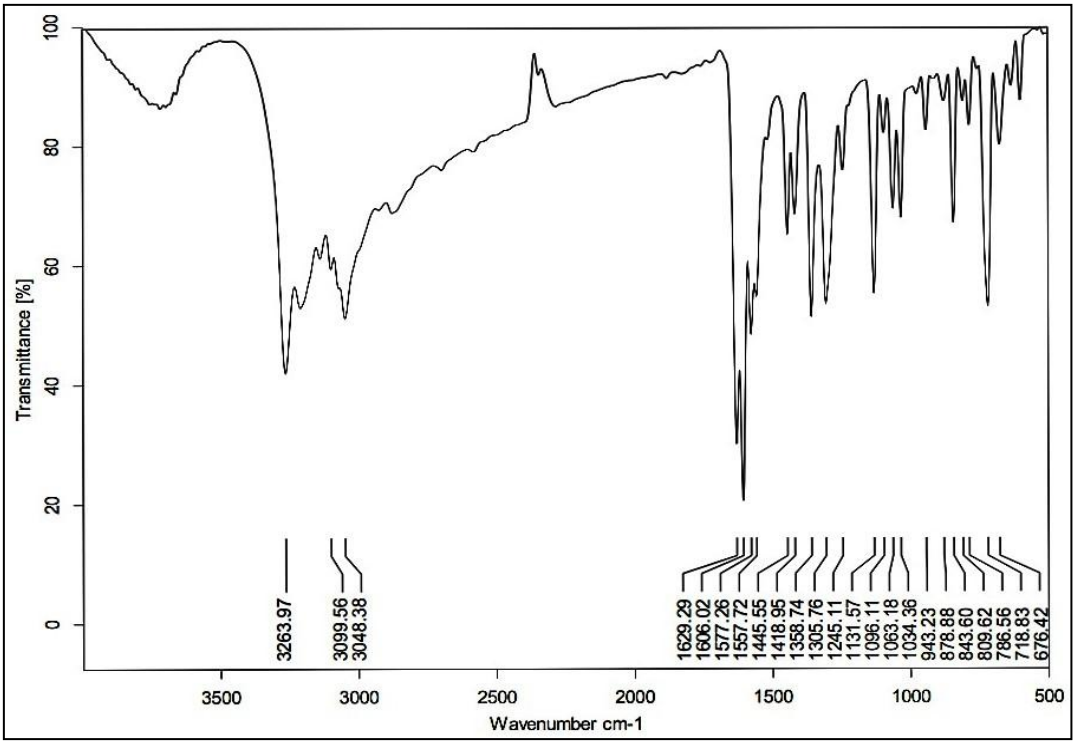

Fig. 4.3: FT-IR spectrum of chemosensor **S3R3**

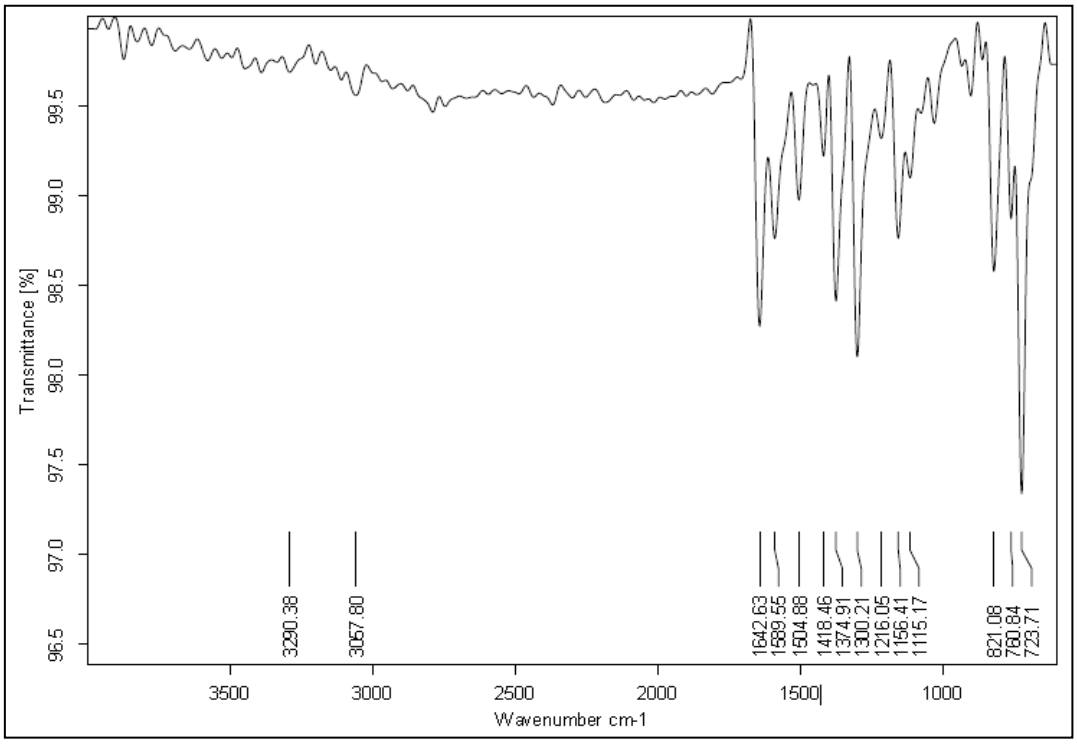

Fig. 4.4: FT-IR spectrum of chemosensor **S3R4**

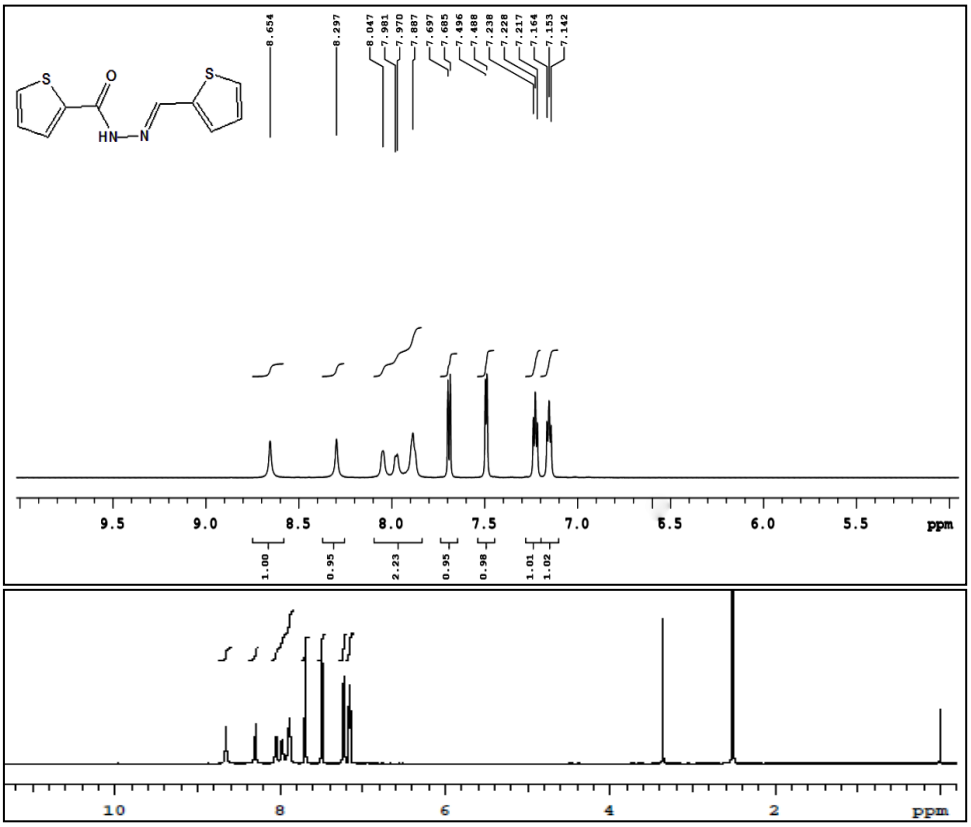

Fig. 4.5: ^{1}H NMR spectrum of chemosensor **S3R1**

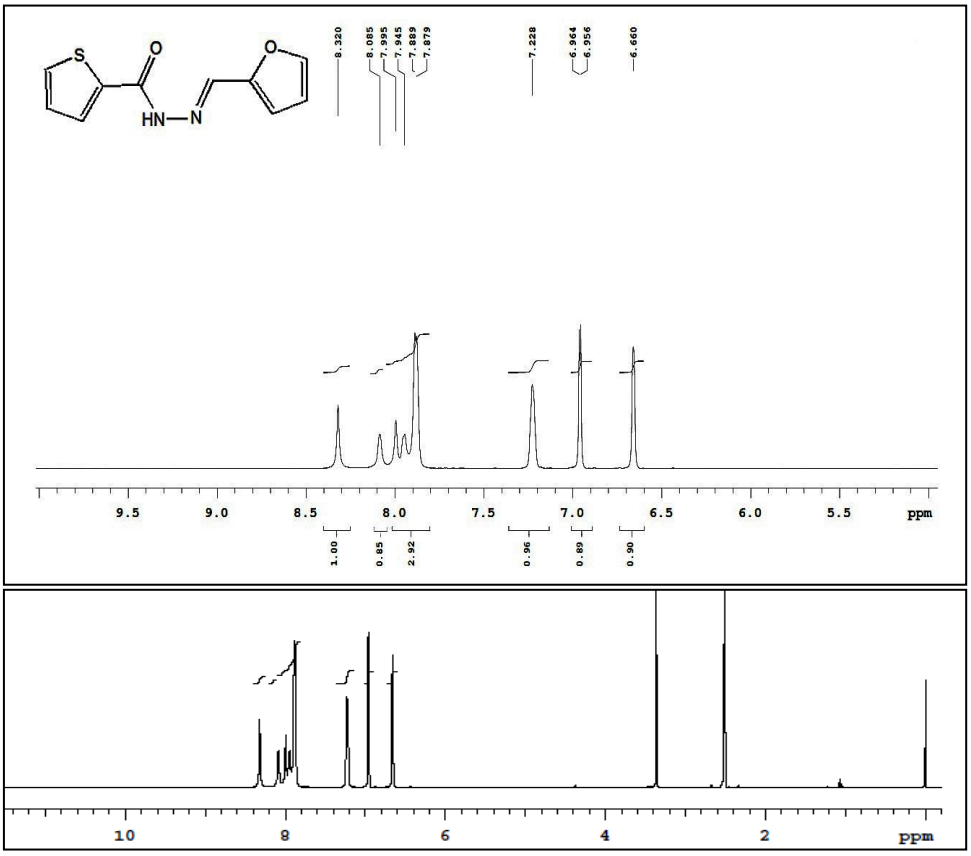

Fig. 4.6: ^{1}H NMR spectrum of chemosensor **S3R2**

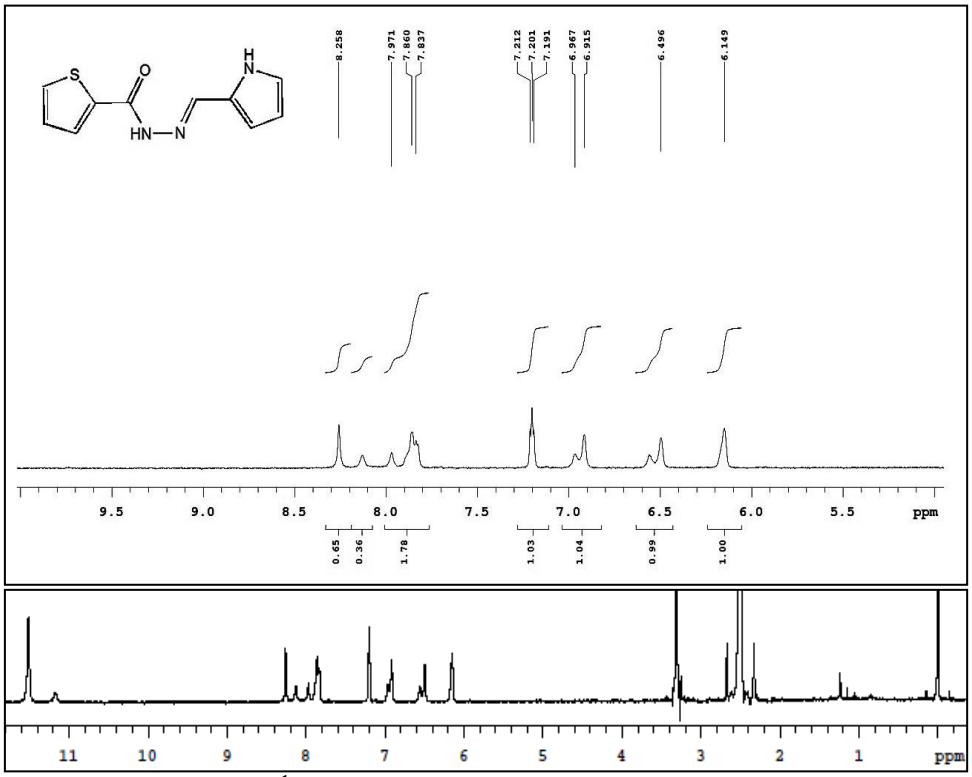

Fig. 4.7: ^{1}H NMR spectrum of chemosensor **S3R3**

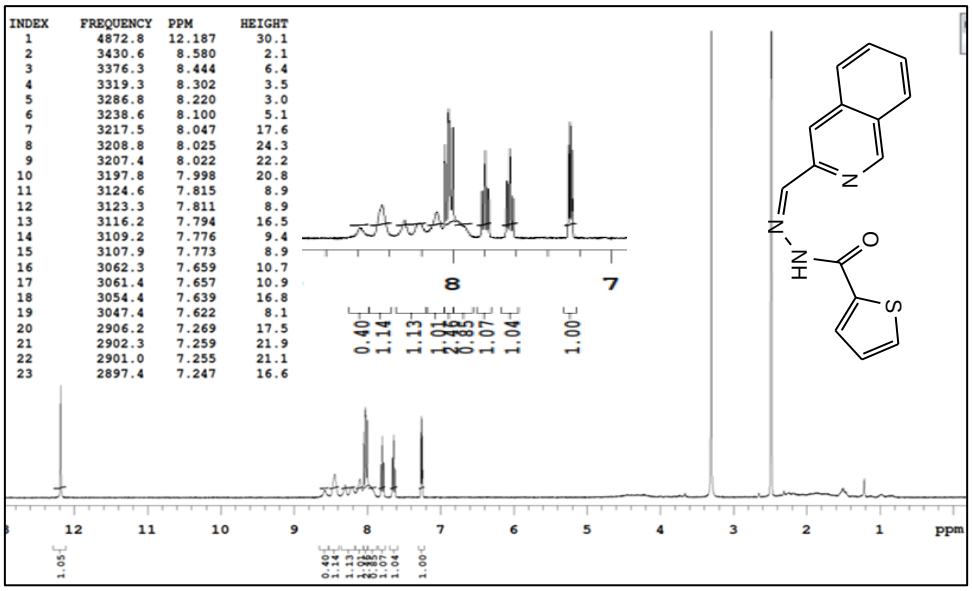

Fig. 4.8: ^{1}H NMR spectrum of chemosensor **S3R4**

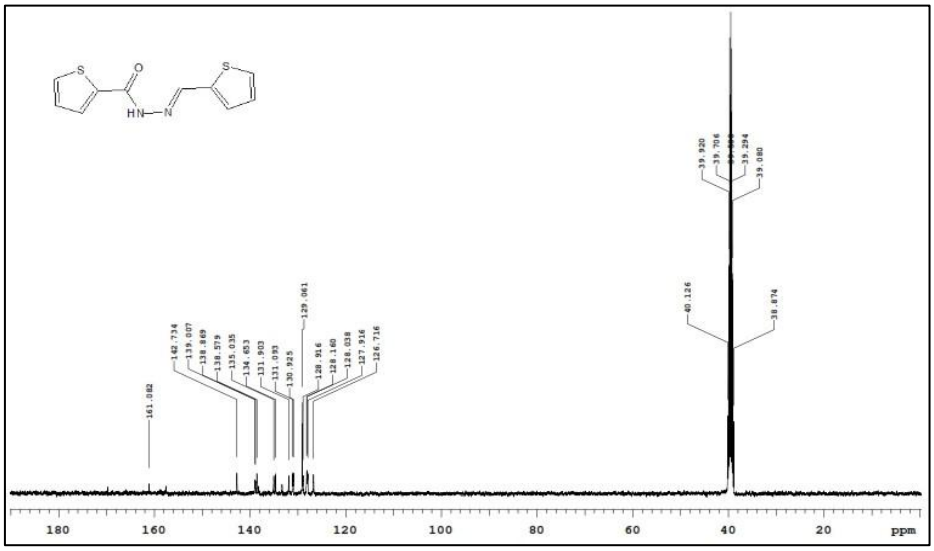

Fig. 4.9: ^{13}C NMR spectrum of chemosensor **S3R1**

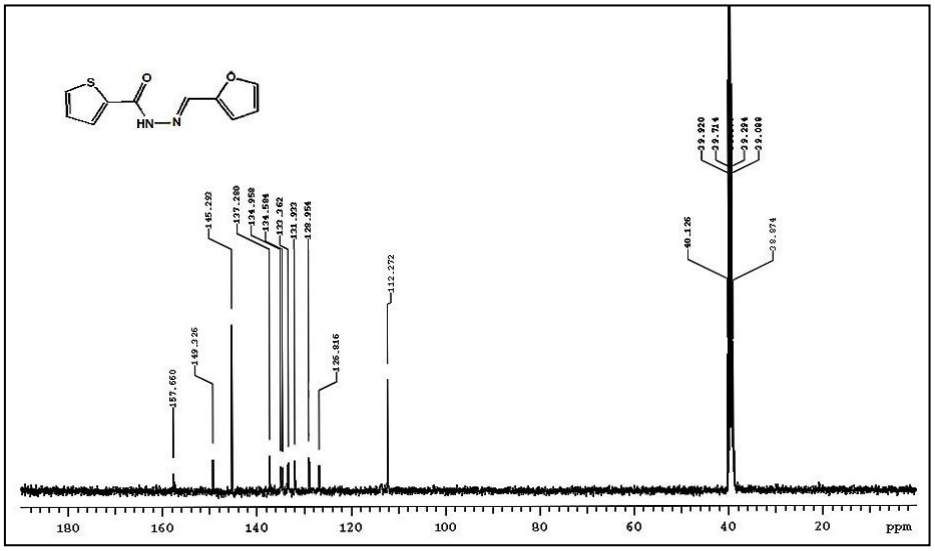

Fig.4.10: ^{13}C NMR spectrum of chemosensor **S3R2**

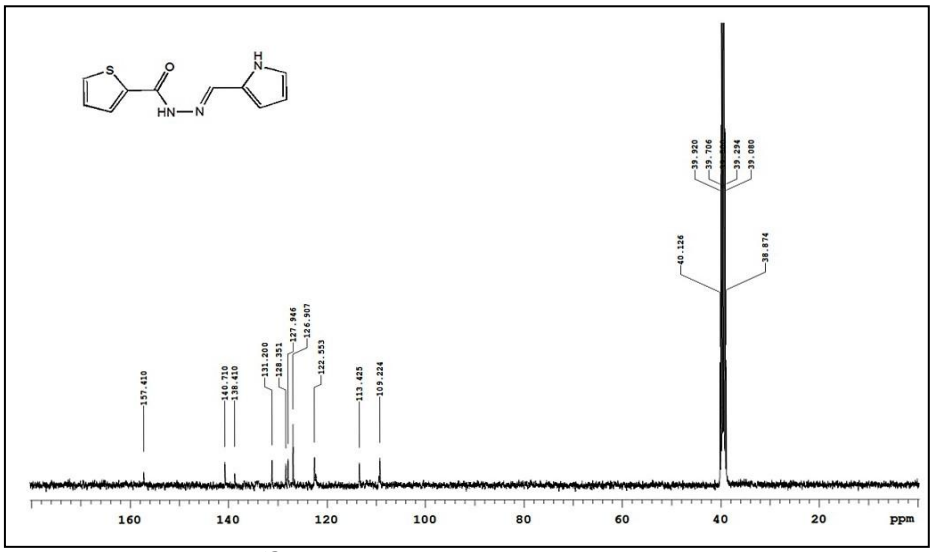

Fig.4.11: ^{13}C NMR spectrum of chemosensor **S3R3**

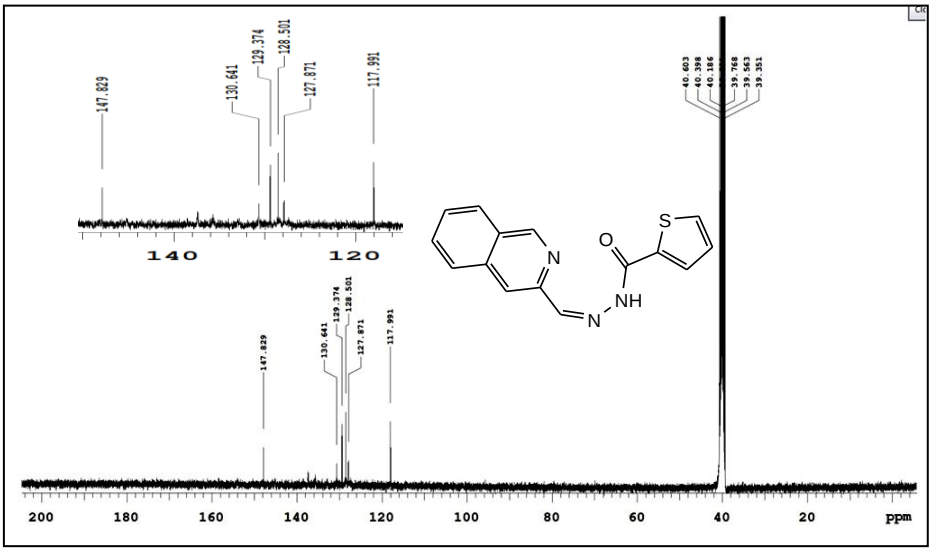

Fig.4.12: ^{13}C NMR spectrum Chemosensor **S3R4**

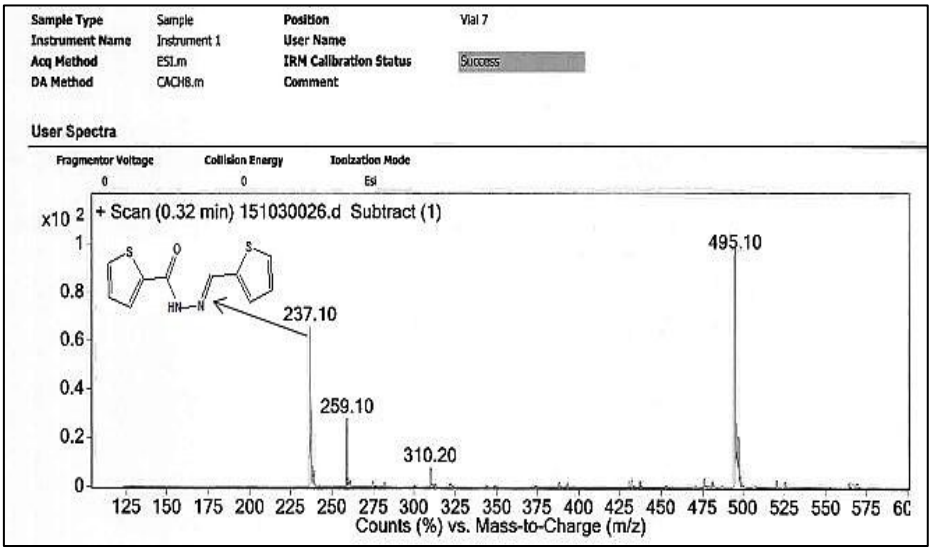

Fig.4.13: The ESI-mass spectrum of chemosensor **S3R1**

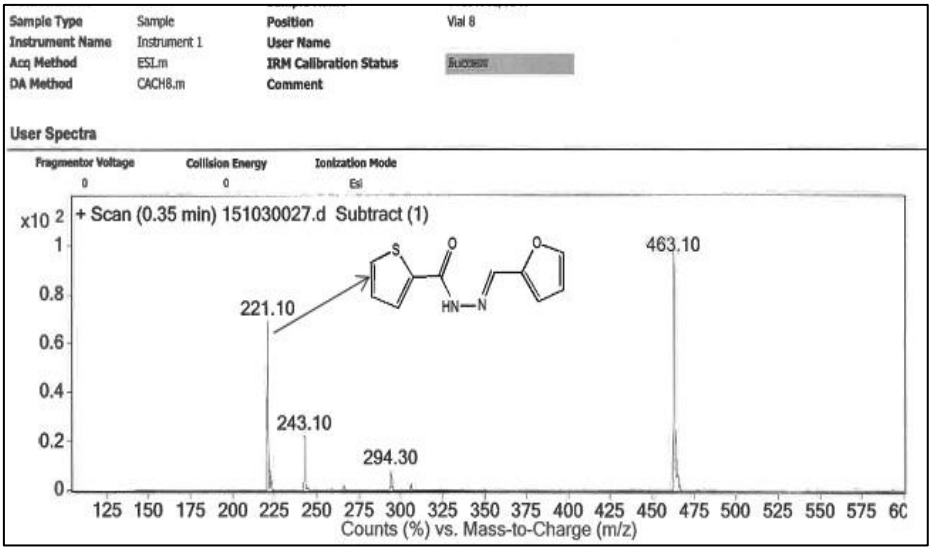

Fig.4.14. The ESI-mass spectrum of Chemosensor **S3R2**

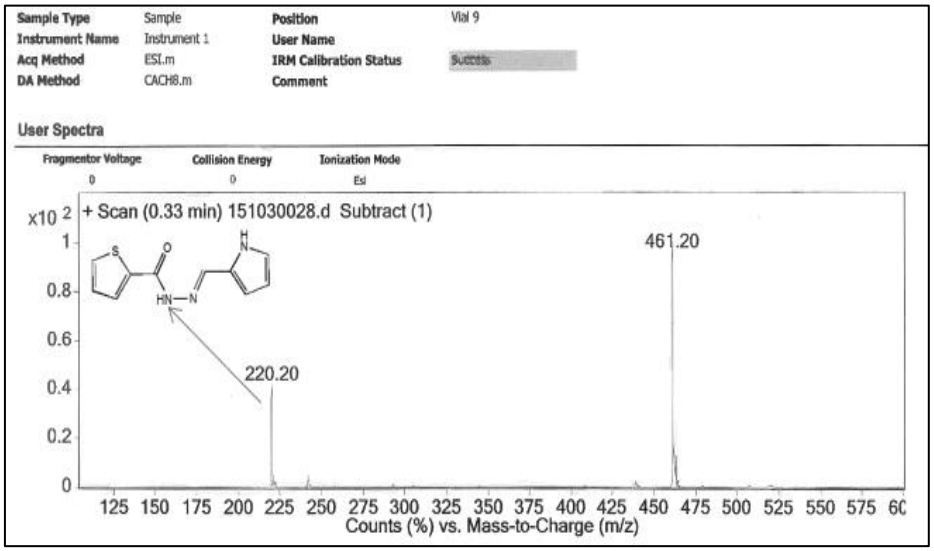

Fig.4.15 ESI-mass spectrum of chemosensor **S3R3**

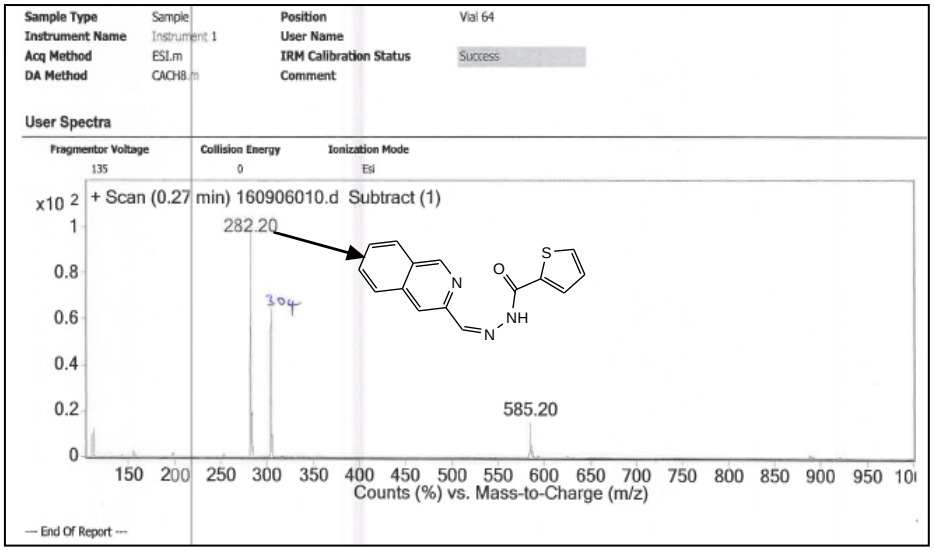

Fig.4.16. The ESI-mass spectrum of chemosensor **S3R4**

4.3. Results and discussion

4.3.1. Colorimetric study

The colorimetric study was conducted for the synthesized chemosensors **S3R1–S3R4**. A solution of 2.5×10^{-5} M concentration of **S3R1–S3R4** chemosensors was prepared in dimethyl sulfoxide (DMF). The chemosensor **S3R1** and **S3R2** did not show any color change after the gradual addition (0 to 3.0 equivalences) of metal ions such as Cu^{2+} Cr^{3+}, Mn^{2+}, Fe^{2+}, Fe^{3+}, Co^{2+}, Ni^{2+}, Zn^{2+}, Ag^{+}, Cd^{2+}, Hg^{2+}, Pb^{2+}, Al^{3+}, K^{+}, Ca^{2+} and Mg^{2+}. The chemosensor **S3R3** exhibits remarkable color change from colorless to yellow upon addition (0.6 equivalence) of **Cu^{2+}** ions and the color

intensity was increased with the incremental addition of **Cu^{2+}** ions (up to 3.0 equivalence). The chemosensor **S3R4** exhibits color change from colorless to yellow upon addition (0.4 equivalence) of **Cd^{2+}** ions, and the color intensity was increased with the incremental addition of **Cd^{2+}** ions (up to 2.0 equivalence). The **S3R3** did not show any color change even at 3.0 equivalences of other tested metal ions such as, Cr^{3+}, Mn^{2+}, Fe^{2+}, Fe^{3+}, Co^{2+}, Ni^{2+}, Zn^{2+}, Ag^{+}, Al^{3+}, Pb^{2+}, Cd^{2+}, Hg^{2+}, Ca^{2+}, Mg^{2+} and K^{+} (**Fig. 4.17**). Similarly, **S3R4** did not show any color change even at 3.0 equivalences of other tested metal ions such as Cr^{3+}, Mn^{2+}, Fe^{2+}, Fe^{3+}, Co^{2+}, Ni^{2+}, Zn^{2+}, Ag^{+}, Al^{3+}, Pb^{2+}, Cu^{2+}, Hg^{2+}, Ca^{2+}, Mg^{2+} and K^{+} (**Fig. 4.18**). This significant color change of **S3R3** and **S3R4** can be utilized for the "naked-eye" detection of **Cu^{2+}** and **Cd^{2+}** ions in an aqueous medium.

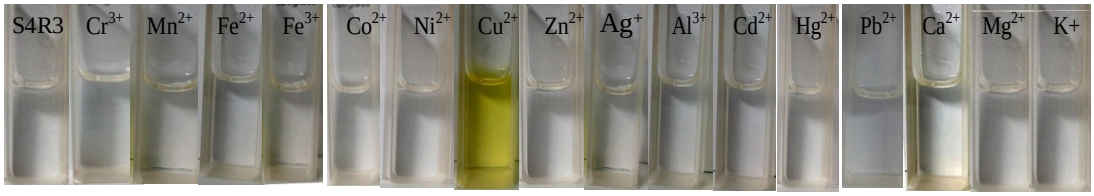

Fig. 4.17: Colorimetric selectivity of **S3R3** (2.5×10^{-5} M) after the addition of 3.0 equivalences of a different metal cation and 2.0 equivalences of **Cu^{2+}** ions

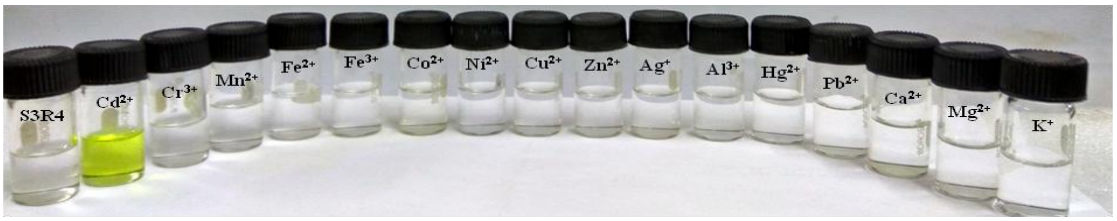

Fig. 4.18: Colorimetric selectivity of **S3R4** (2.5×10^{-5} M) after the addition of 3.0 equivalences of a different metal cation and 2.0 equivalences of **Cd^{2+}** ions

4.3.2. UV–Vis absorption spectroscopy studies

4.3.2.1. Effect of different solvents on absorbance

The absorption response of chemosensors **S3R3**, **S3R4, S3R3-Cu^{2+}** (3.0 equivalences of Cu^{2+}), and **S3R4-Cd^{2+}** (3.0 equivalences of Cd^{2+}) was studied in the presence of various solvents such as methanol, acetonitrile, dimethyl sulfoxide, and dimethylformamide. The free chemosensors **S3R3**, **S3R4,** and their complexes **(S3R3-Cu^{2+}** and **S3R4-Cd^{2+}**) exhibit good absorbance shifts and absorption intensity in the DMF solution compared to other solvents (**Fig. 4.19 and 4.20**), and therefore DMF was used as a solvent for all UV–Vis spectral studies.

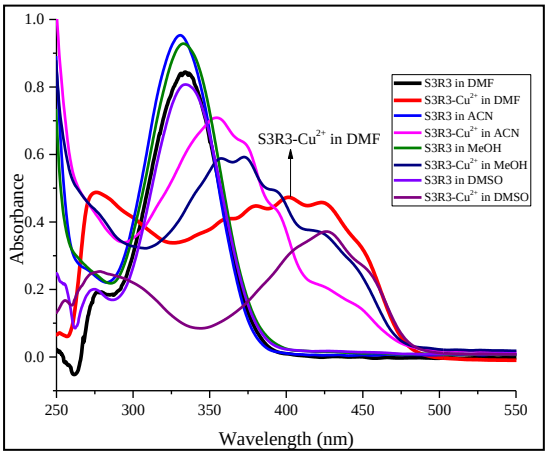

Fig. 4.19. UV–Vis absorption spectra of chemosensor **S3R3** (2.5×10^{-5} M) and S3R3-Cu^{2+} complex (2.0 equivalences of Cu^{2+} ions) in different solvents

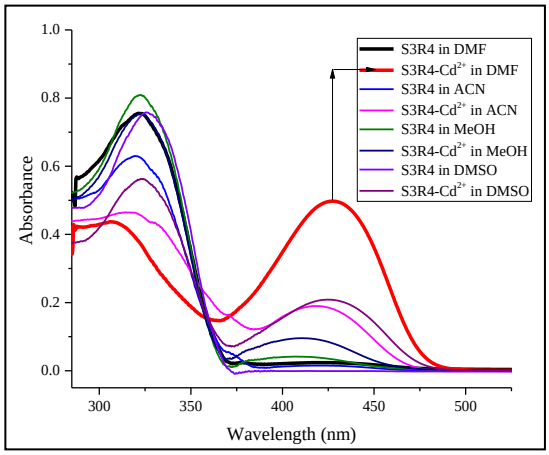

Fig. 4.20. UV–Vis absorption spectra of chemosensor **S3R4** (2.5×10^{-5} M) and S3R4-Cd^{2+} complex (2.0 equivalences of Cd^{2+} ions) in different solvents

A detailed UV–Vis absorption study was performed for **S3R3** and **S3R4** to find the stoichiometric binding between **S3R3–Cu^{2+}** and **S3R4–Cd^{2+}** and the selective reorganization of **S3R3** toward **Cu^{2+}** and **S3R4** toward **Cd^{2+}** ions over the other metal ions. The **S3R3** (2.5×10^{-5} M) exhibited major absorption peak wavelength at 335 nm in DMF solution (**Fig. 4.21**), which could be due to the n–π^* transition of –C=N– chromophore. The **S3R4** (2.5×10^{-5} M) exhibited major absorption peak wavelength at 320 nm in DMF solution **(Fig. 4.22),** which could be due to the n–π^* transition involving molecular orbital's particularly localized on the –C=N– chromophore and quinoline ring.

Competition experiments were performed by recording the changes of the UV–Vis absorbance intensity before and after adding the interferants into the **S3R3** and **S3R4** solution. Addition of 250 μM of aqueous solution of Cr^{3+}, Mn^{2+}, Fe^{2+}, Fe^{3+}, Co^{2+}, Ni^{2+}, Zn^{2+}, Ag^{+}, Pb^{2+}, Hg^{2+}, Al^{3+}, K^{+}, Ca^{2+} and Mg^{2+} ions, did not produce significant absorption intensity changes. Nevertheless, upon addition of 20 μM of **Cu^{2+}** to the **S3R3** solution and 25 μM of **Cd^{2+}** to the **S3R4** solution, it immediately exhibits a redshift in the absorption spectra (**S3R3** from 335 nm to 402 nm and **S3R4** from 320 nm to 425 nm). The absorbance intensity of **S3R3** and **S3R4** towards the surveyed metal ions is displayed in **Figs. 4.21 and 4.22**. Therefore, the **S3R3** and **S3R4** have better selectivity for **Cu^{2+}** and **Cd^{2+}** over other tested metal ions with the remarkable color change from colorless to yellow, which is useful in the naked-eye

detection of **Cu**$^{2+}$ and **Cd**$^{2+}$ ions. The competition experiment results reveal the high selectivity of **S3R3** towards **Cu**$^{2+}$ and **S3R4** towards **Cd**$^{2+}$ ions over the tested cations.

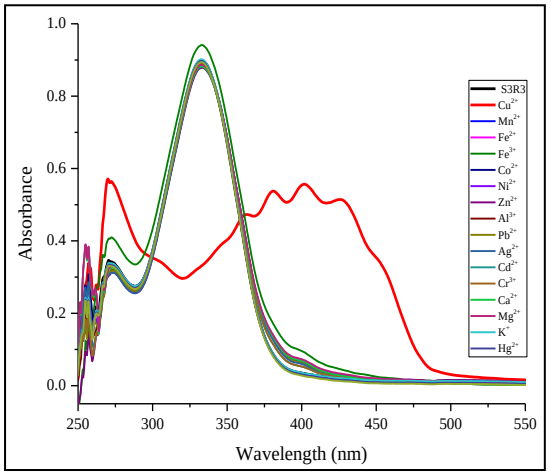

Fig. 4.21. Changes in the absorption intensity of **S3R3** (2.5×10^{-5} M in DMF) after the addition of 250 μM of different cations, in the presence of 20 μM of Cu^{2+} ions in an aqueous solution

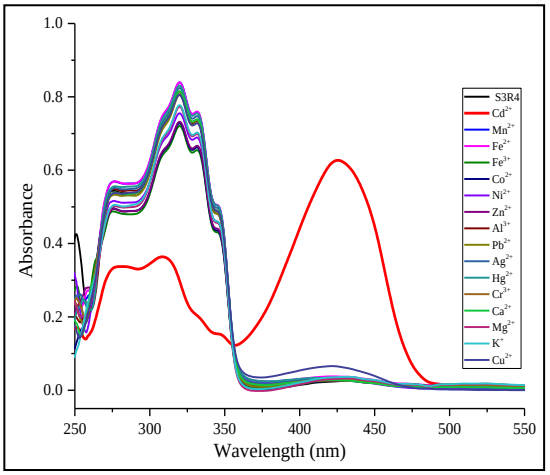

Fig. 4.22. Changes in the absorption intensity of **S3R4** (2.5×10^{-5} M in DMF) after the addition of 250 μM of different cations and 25 μM of Cd^{2+} ions in an aqueous solution

The UV–Vis titration study was performed at different concentrations of **Cu**$^{2+}$ ions to the **S3R3** and **Cd**$^{2+}$ ions to the **S3R4** solution to determine the binding stoichiometric ratio between **S3R3–Cu**$^{2+}$ and **S3R4–Cd**$^{2+}$ ions **(Fig. 4.23 and 4.24)**. The absorption intensity was decreased dramatically at 335 nm (in **S3R3**), 320 nm (in **S3R4**), and a new absorbance band appears at 402 nm (in **S3R3**), 425 nm (in **S3R4**) upon titration with **Cu**$^{2+}$ and **Cd**$^{2+}$ ions. These results exhibit that the absorption intensity was linearly changed with increasing concentration of metal ions, these changes may be due to chemosensor metal chelation formation, and it is caused for the color change. A small amount of chemosensor 25 μM of **S3R3** and **S3R4,** in this case, was sufficient to detect **Cu**$^{2+}$ and **Cd**$^{2+}$ ions, which make these chemosensors (**S3R3 and S3R4**) potentially useful in environmental practice, due to high selectivity.

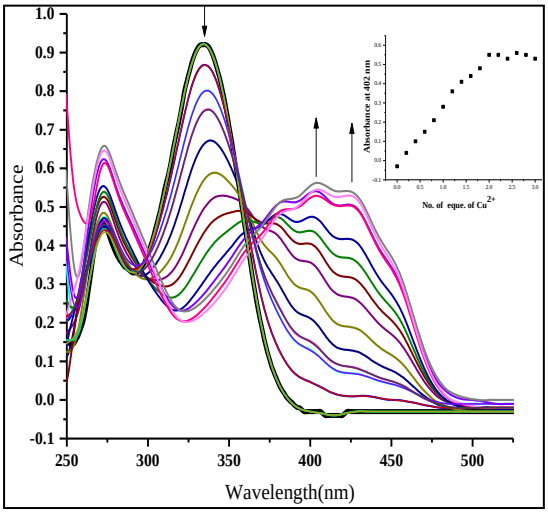

Fig. 4.23. UV–Vis spectra for the gradual addition of **Cu^{2+}** (0 to 3.0 equivalences) to **S3R3** (2.5×10^{-5} M in DMF). Inset showing the number of equivalence of **Cu^{2+}** vs. absorbance selected wavelength at 402 nm

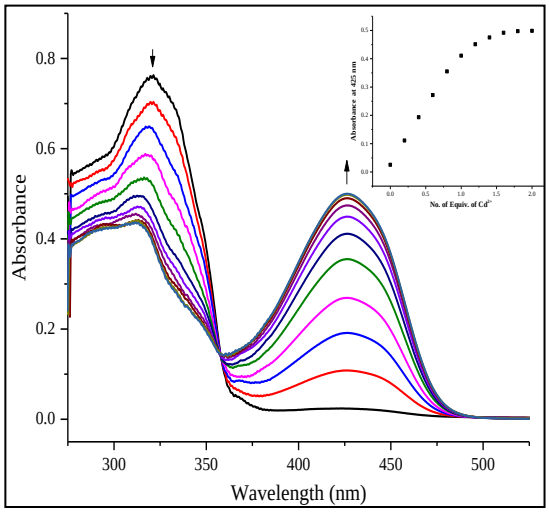

Fig. 4.24. UV-Vis spectra for the gradual addition of **Cd^{2+}** (0 to 2.0 equivalences) to **S3R4** (2.5×10^{-5} M in DMF). Inset showing the number of equivalence of **Cd^{2+}** vs. absorbance selected wavelength at 425 nm

4.3.3. Benesi-Hildebrand Plot, determination of association constant (K)

The association constant (K) was calculated for the **S3R3** and **S3R4** from the Benesi-Hildebrand equation (Lu et al. 2007) using UV–Vis absorption spectroscopy study data, and it was found to be 7.8×10^{3} M^{-1} for **S3R3–Cu^{2+}** and 3.7×10^{4} M^{-1} for **S3R4–Cd^{2+}**. The K was calculated using the formula below.

$$\frac{1}{A-A_0} = \frac{1}{K\,(A_{max}-A_0)\,[M_x^{+}]^n} + \frac{1}{(A_{max}-A_0)}$$

Where, A_0, A, A_{max} are the absorption considered in the absence of metal, at an intermediate, and at a concentration of saturation, K is binding constant, $[M_x^{+}]$ is a concentration of metal ions and n is the stoichiometric ratio.

The stoichiometry of the complex formed between the **S3R3** and **Cu^{2+}** metal ion was found to be 1:1 stoichiometry using the B-H Plot **(Fig. 4.25)**. The stoichiometry of the complex formed between the **S3R4** and **Cd^{2+}** metal ion was found to be 1:1 stoichiometry using the B-H Plot **(Fig. 4.26)**.

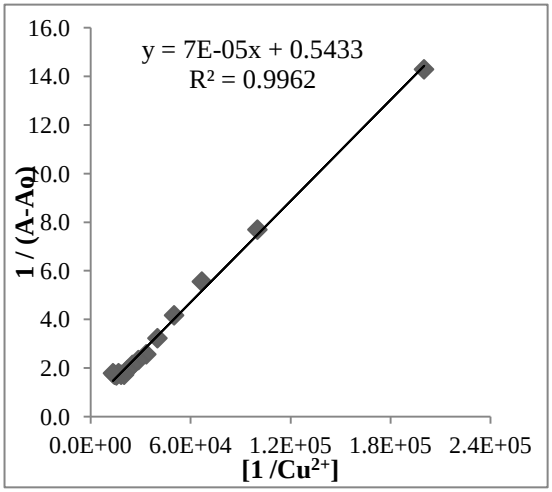

Fig. 4.25. Benesi-Hildebrand plot of **S3R3** (2.5×10^{-5} M in DMF) binding with **Cu^{2+}** ions associated with absorbance change at 402 nm

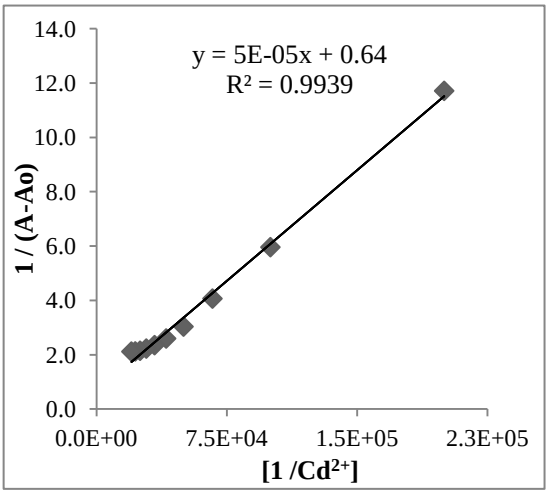

Fig. 4.26. Benesi-Hildebrand plot of **S3R4** (2.5×10^{-5} M in DMF) binding with **Cd^{2+}** ions associated with absorbance change at 425 nm

4.3.4. Method validation for determination of Cu^{2+} and Cd^{2+} ions

The analytical method validation was performed following guidelines put forth by ICH to standardize the analytical method for the routine analysis (Ich 2005).

4.3.4.1. Specificity / Selectivity

Specificity refers to ensure the identity of an analyte and that all the analytical procedures performed to allow an accurate statement of the content or assay of an analyte. The method specificity/selectivity was performed by preparing two separate blend stock solutions (**Cu^{2+}** absent in 1st blendstock and **Cd^{2+}** absence in 2nd blend stock solution) containing competitive cations Cr^{3+}, Mn^{2+}, Fe^{2+}, Fe^{3+}, Co^{2+}, Ni^{2+}, Zn^{2+}, Ag^{+}, Hg^{2+}, Pb^{2+}, Al^{3+}, K^{+}, Ca^{2+} Mg^{2+}, Cu^{2+}, Cd^{2+} and anions, sulphate, F^{-}, Cl^{-}, Br^{-}, I^{-}, NO_3^{-}, $H_2PO_4^{-}$ as their tetra butyl ammonium salts, NaF and NaOAc. The chemosensor **S3R3** did not show any absorption change after the addition of blend solution (3.0 equivalence of all cations and anions), and upon addition of 2.0 equivalences of **Cu^{2+}** ions, **S3R3** exhibits a specific absorption band at 402 nm selectively as shown in **Fig 4.27.** The chemosensor **S3R4** did not show any absorption change after the addition of blend solution (3.0 equivalences of all cations and anions), and upon addition of 2.0 equivalences of **Cd^{2+}** ions, **S3R4** exhibits a specific new absorption band at 425 nm selectively as depicted in **Fig 4.28**. It indicates that the chemosensor **S3R3** has

selectivity and specificity towards **Cu^{2+}** ions and **S3R4** have towards **Cd^{2+}** ions sensing in the presence of other interfering metal ions and anions.

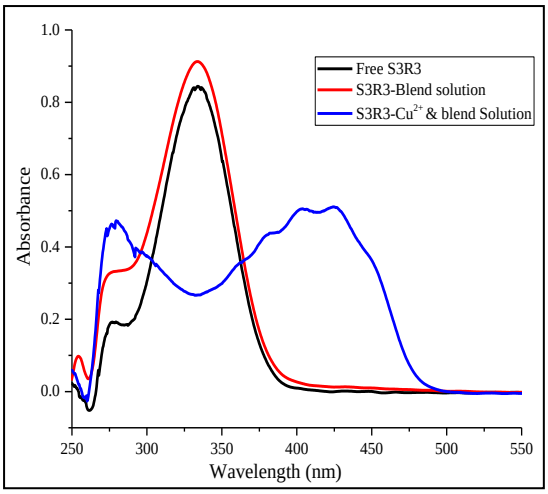

Fig. 4.27: Specificity/selectivity of chemosensor **S3R3** (2.5×10^{-5} M in DMF) towards **Cu^{2+}** ions in the blend solution containing 3.0 equivalences of different cations, anions and 2.0 equivalences of **Cu^{2+}** ions in an aqueous solution

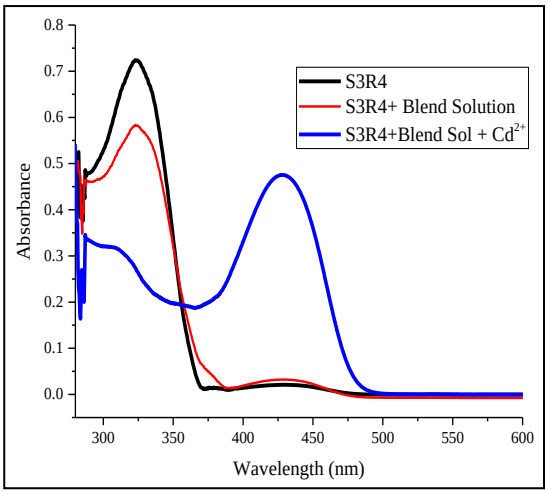

Fig. 4.28: Specificity/selectivity of chemosensor **S3R4** (2.5×10^{-5} M in DMF) towards **Cd^{2+}** ions in the blend solution containing 3.0 equivalences of different cations, anions and 2.0 equivalences of Cd^{2+} ions in an aqueous solution

4.3.4.2. Precision

The precision was determined by repeatability. Repeatability expresses the precision under the same operating conditions over a short interval of time. The repeatability study was investigated at three different concentration levels in triplicate preparation of **Cu^{2+}** at low (0.953 ppm, triplicates), at middle (1.271 ppm, triplicates) and at high (1.906 ppm, triplicates) concentrations and **Cd^{2+}** at low level (10 µM, triplicates) middle (25 µM, triplicates) and at high (30 µM, triplicates) were determined. The % relative standard deviation (% RSD) was calculated at each level of **Cu^{2+}** and **Cd^{2+}** spiked samples, and the results are reported in **table-4.1**.

4.3.4.3. Linearity

The linearity of an analytical procedure is its ability (within a given range) to obtain test results which are directly proportional to the concentration (amount) of analyte in the sample. The linearity of the method was evaluated by analyzing different concentrations of working standard solutions of **Cu^{2+}** and **Cd^{2+}** in the ranges

listed in **table-4.1**. Calibration curves were plotted between absorbance versus concentration of **Cu^{2+}** standard (**Fig. 4.29**) and **Cd^{2+}** working standard (**Fig. 4.30**).

Table-4.1: Regression analysis data and summary of analytical method validation parameters for determination of **Cu^{2+}** and **Cd^{2+}** ions by the proposed method

Parameters	**Results of Cu^{2+}**	**Results of Cd^{2+}**
Absorption wavelength	402 nm	425 nm
Concentration range (µM)	5.0 - 50	5.0 to 30
Regression equation	y = 11434x - 0.0139	y = 14669x + 0.0467
Correlation coefficient (R^2)	0.9976	0.9950
Detection Limit (µM)	2.8	0.20
Quantification Limit (µM)	9.4	0.70
Precision (% RSD) a) at low Con. level (n=3) b) at middle Con. level (n=3) c) at high Con. level (n=3)	----- ± 0.72 ± 0.59 ± 0.73	----- ± 0.07 ± 0.90 ± 0.76

RSD: Relative standard deviation

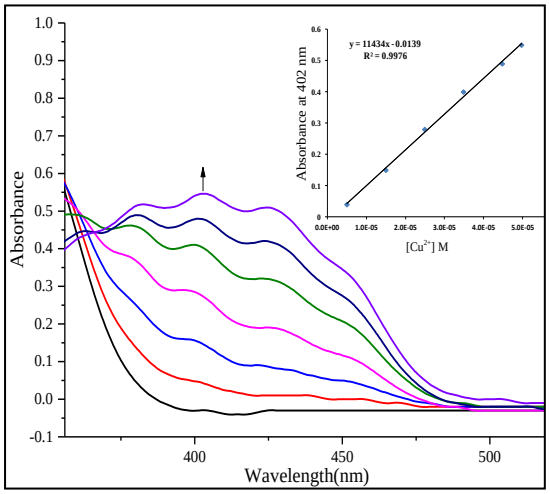

Fig. 4.29. Linear UV–Vis absorption spectra of complex (**S3R3–Cu^{2+}**). Insert showing linear calibration plot between the concentration of **Cu^{2+}** and absorbance wavelength at 402 nm

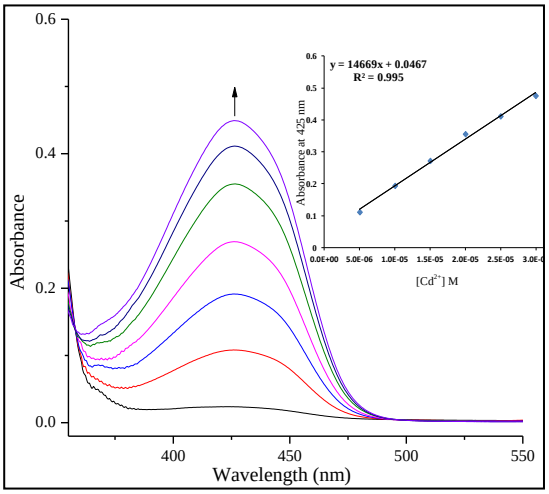

Fig. 4.30. Linear UV–Vis absorption spectra of complex (**S3R4–Cd^{2+}**). Insert showing linear calibration plot between the concentration of **Cd^{2+}** and absorbance wavelength at 425 nm

4.3.4.4. Accuracy

Recovery studies demonstrated the accuracy of the analytical method. The recovery study was done over three concentration levels where known amounts of the analyzed cation were added to known concentrations of the sample in triplicate at low, high, and middle concentration levels, respectively. The amount was obtained from the corresponding regression equations, and then the % recoveries were calculated for each spiked levels, and the results obtained were compared with the added amounts, as given in **table-4.2 & 4.3**. The good % recoveries of the standard addition/spiking method demonstrate the accuracy of the proposed analytical methods.

Table-4.2: Accuracy / recovery study of **Cu^{2+}** ion detection using **S3R3**

Cu^{2+} Spiked (ppm)	**Cu^{2+} found (ppm)**	**% Recovery & $\pm$ % RSD**
0.953	0.939 (n=3)	98.6 $\pm$ 1.04 (n=3)
1.271	1.259 (n=3)	99.0 $\pm$ 0.59 (n=3)
1.906	1.884 (n=3)	98.4 $\pm$ 0.88 (n=3)

Table-4.3: Accuracy / recovery study results of **Cd^{2+}** ion detection using **S3R4**

Cd^{2+} Spiked (µM)	**Cd^{2+} (µM)**	**% Recovery & $\pm$ % RSD**
10.41	10.55 (n=3)	101.3 $\pm$ 0.07 (n=3)
26.03	25.29 (n=3)	97.2 $\pm$ 0.90 (n=3)
31.23	30.52 (n=3)	97.7 $\pm$ 0.76 (n=3)

4.3.4.5. Detection limit (DL) and Quantization limit (QL) determination

The DL and QL for **Cu^{2+}** ions were determined using the calibration plot between **Cu^{2+}** metal ion concentration (range from 5.0×10^{-6} M to 5.0×10^{-5} M) and the corresponding absorbance of **S3R3–Cu^{2+}** complex at 402 nm wavelength (**Fig. 4.29)**. The DL and QL for **Cd^{2+}** ion were determined using the calibration plot between **Cd^{2+}** metal ion concentration (range from 5.0×10^{-6} M to 3.0×10^{-5} M) and the corresponding absorbance of **S3R4–Cd^{2+}** complex at 425 nm wavelength (**Fig. 4.30)**. The DL and QL were determined based on the standard deviation of the response or blank and the slope, using the below-mentioned formula as per ICH guidelines (Ich 2005)

$$DL / QL = \frac{c \times \sigma}{m}$$

Where,

c = constant (3.0 for DL and 10.0 for QL)

σ = Standard deviation of measurement (**STEYX) or** Standard deviation of the blank

m = Slope of the calibration plot

The calculated DL was found to be 2.8 µM for $\mathbf{Cu^{2+}}$ and 0.20 µM for $\mathbf{Cd^{2+}}$**.** QL was found to be 9.4 µM for $\mathbf{Cu^{2+}}$ and 0.70 µM for $\mathbf{Cd^{2+}}$ ions in an aqueous medium.

The analytical method validation summary results suggest that the proposed analytical method for the determination of $\mathbf{Cu^{2+}}$ and $\mathbf{Cd^{2+}}$ ions by UV–Vis spectroscopy would produce linear, precise, accurate results with selectivity for the qualitative and quantitative in the environmental water samples.

4.3.5. Application to different environmental water samples

Chemosensor **S3R3** selectively binds with $\mathbf{Cu^{2+}}$, and **S3R4** binds with $\mathbf{Cd^{2+}}$ ions, and due to this selective reorganization, detection of trace amount of $\mathbf{Cu^{2+}}$ and $\mathbf{Cd^{2+}}$ ions in drinking water, tap water and river water samples qualitative and quantitatively has aimed. Primarily, a calibration curve of absorption vs. concentration was obtained. From the graph, a linear equation was obtained to examine and quantify the concentration of $\mathbf{Cu^{2+}}$ and $\mathbf{Cd^{2+}}$ ions in the different water samples. To the investigation of the interference, if any, in the different water samples collected from various sources in the Surathkal, Mangalore, Karnataka, India, was also carried out by spiking a known quantity of $\mathbf{Cu^{2+}}$ (1.27 ppm ≈ 20 µM) and $\mathbf{Cd^{2+}}$ (1.19 ppm ≈ 10.56 µM) in the all collected samples. The obtained result are represented in **table-4.4 & 4.5**, and it exhibits good % relative standard deviation (% RSD) between replicate of unspiked samples or as such samples and % recovery in the spiked samples during the analysis. The spiked water sample also further analyzed by Atomic Absorption Spectroscopy (AAS) method to demonstrate the accuracy of the proposed analytical method, and the obtained results are tabulated in **table-4.4 & 4.5**.

Table-4.4: Determination of Cu^{2+} in different water samples collected from different sources by using **S3R3**

Water sample type	Cu^{2+} in water samples (ppm) (n=3)	Cu^{2+} Spiked (ppm)	Cu^{2+} found (ppm) & % RSD (n=3)	% Recovery	
				UV-Vis	AAS
Drinking	BDL	1.27	1.250 ± 0.80	98.4	99.8
Tap	BDL		1.247 ± 0.46	98.1	99.3
River	BDL		1.240 ± 0.81	97.6	99.1

Table-4.5: Determination of Cd^{2+} in different water samples collected from different sources by using **S3R4**

Water sample type	Cd^{2+} in water samples (ppm) (n=3)	Cd^{2+} Spiked (ppm)	Cd^{2+} found (ppm) & %RSD (n=3)	% Recovery	
				UV-Vis	AAS
Drinking	BDL	1.19	1.165 ± 1.51	97.9	99.7
Tap	BDL		1.135 ± 1.32	95.4	99.3
River	BDL		1.077 ± 2.56	90.5	99.2

RSD: Relative standard deviation, **BDL:** Below detection limit, **AAS:** Atomic absorption spectroscopy.

Therefore, the experimental and alternative analytical method (AAS) result suggests the identification and quantification of Cu^{2+} and Cd^{2+} in the collected different water samples and this could be used for routine analysis for determination of Cu^{2+} and Cd^{2+} in water samples.

4.3.6. Binding mechanism

Mechanistically, maximum red-shift in **S3R3** and **S3R4** can be attributed to the change in structural conformation of chemosensors on interaction with Cu^{2+} and Cd^{2+} indicating the coordinative interaction between the lone pair of the donor hetero-atoms carbonyl group oxygen and imine nitrogen in **S3R3**, hetero-atoms sulfur, nitrogen (imine & quinoline) which are conjugated to the π system of the chemosensors and the cations. Accordingly, there is an enhance in the conjugation of the chemosensor in a tightly bound complex with Cu^{2+} and Cd^{2+}, resulting in the planarization of complex and red-shift (Yadav et al. 2014). On the other hand, no such

considerable change was induced by the addition of other metal ions to the chemosensor **S3R3** and **S3R4**.

Based on the UV–Vis absorption study and the FT-IR analysis of **S3R3** and **S3R3–Cu^{2+}** complex, **S3R4**, and **S3R4–Cd^{2+}** complex, the binding sites were identified in chemosensor **S3R3** & **S3R4**. The FT-IR spectrum of **S3R3** exhibited some characteristic bands in the region 1626 and 1290 cm^{-1} corresponding to –C=O and C–N groups, respectively (**Fig. 4.31**). When compared to FT-IR spectrum of **S3R3–Cu^{2+}** with that of free chemosensor **S3R3**, some noticeable observations can be inferred, the stretching vibration of the –C=O group at 1626 cm^{-1} shift to 1603 cm^{-1} and the stretching vibration of the –C–N group at 1290 cm^{-1} shifted to 1304 cm^{-1}. The shift in the FT-IR frequencies of **S3R3-Cu^{2+}** suggests the secondary amine and carbonyl groups are participating in the binding with **Cu^{2+}** ions (Xiong et al. 2016). The colorimetric response of **S3R3** toward Cu^{2+} may be attributed to the **S3R3-Cu^{2+}** complex formation. It was indicated that Cu^{2+} coordinated with the oxygen atom of –C=O, the nitrogen atom of –C=N, and pyrrole. More direct evidence was observed by correlating the ESI-MS spectra of **S3R3** and **S3R3-Cu^{2+}**. For **S3R3**, the prominent peak at m/z = 220.2 (calculated = 219.0) corresponded to [S3R3+H]$^{+}$. With excess Cu^{2+} added to S3R3, the peak at m/z = 283.0 (calculated = 281.8) corresponding to [S3R3-Cu^{2+} + H]$^{+}$ was clearly observed, which indicated the formation of the complex S3R3-Cu^{2+} (**Fig. 4.32**) (Sun et al. 2015; Xiong et al. 2016). A proposed binding mechanism was represented in **Fig. 4.35**.

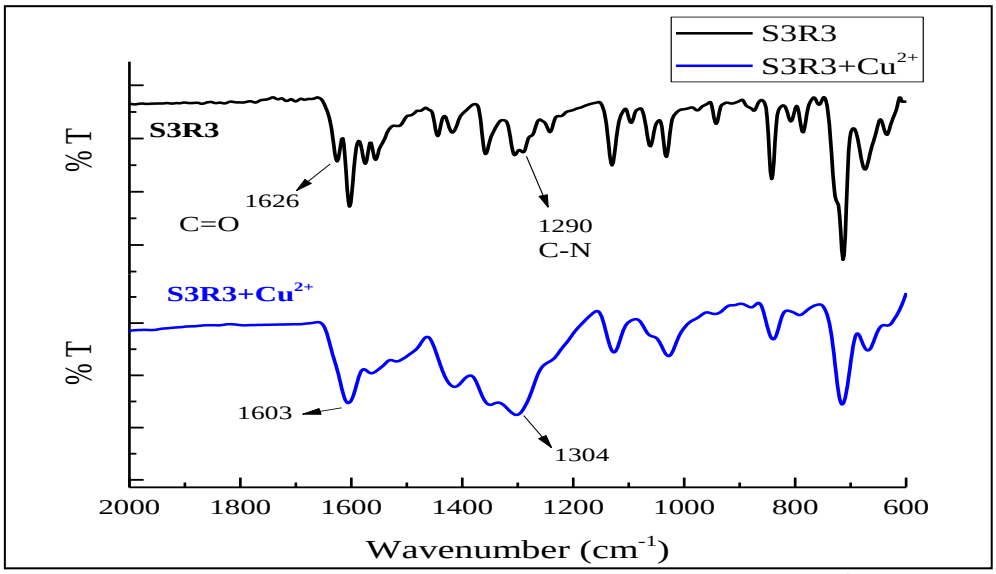

Fig. 4.31. FT-IR spectra of the chemosensor **S3R3** and **S3R3**–Cu^{2+} complex

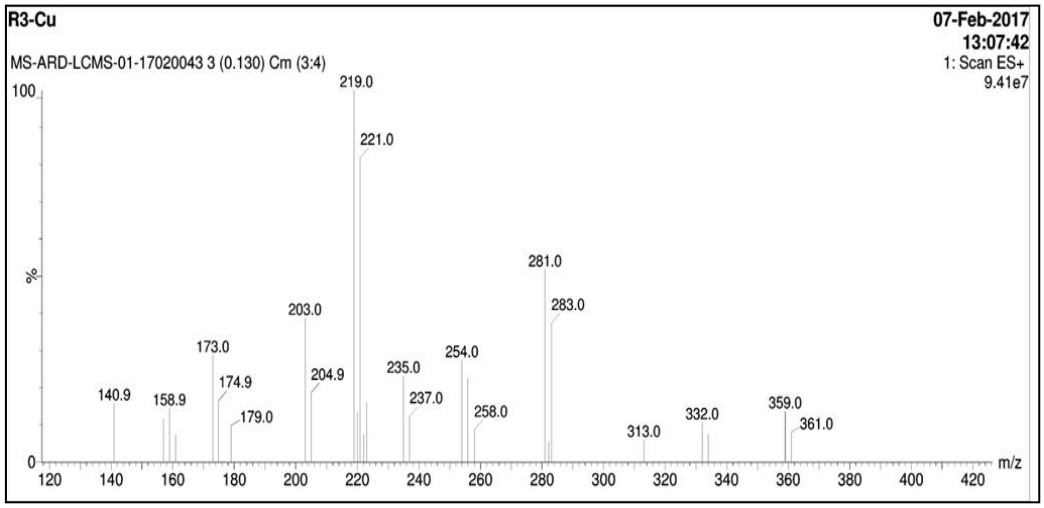

Fig. 4.32. ESI-MS for the complex **S3R3**–Cu^{2+}

The FT-IR spectrum of **S3R4** exhibited some characteristic bands in the region, 1300 cm^{-1} corresponding to C–N (**Fig. 4.33**). When compared to the FT-IR spectrum of **S3R4–Cd^{2+}** with that of free chemosensor **S3R4**, some noticeable observations can be inferred, the stretching vibration of the –C–N group at 1300 cm^{-1} shifted to 1313 cm^{-1}. These FT-IR differences suggest that the secondary amine group took part in coordination with **Cd^{2+}**. Another direct evidence was observed by correlating the ESI-MS spectra of S3R4 and S3R4–Cd^{2+}. For S3R4, the peak at m/z = 282.2 (calculated = 281.1) corresponded to $[S3R4+H]^+$. With excess Cd^{2+} added to S3R4, the peak at m/z 395.0 (calculated = 393.8) corresponding to $[S3R4\text{-}Cd^{2+} + H]^+$ was observed, which indicated the formation of the complex **S3R4–Cd^{2+}** (**Fig. 4.34**) (Choi et al. 2001; Liu et al. 2007). A proposed binding mechanism was represented in **Fig. 4.36**.

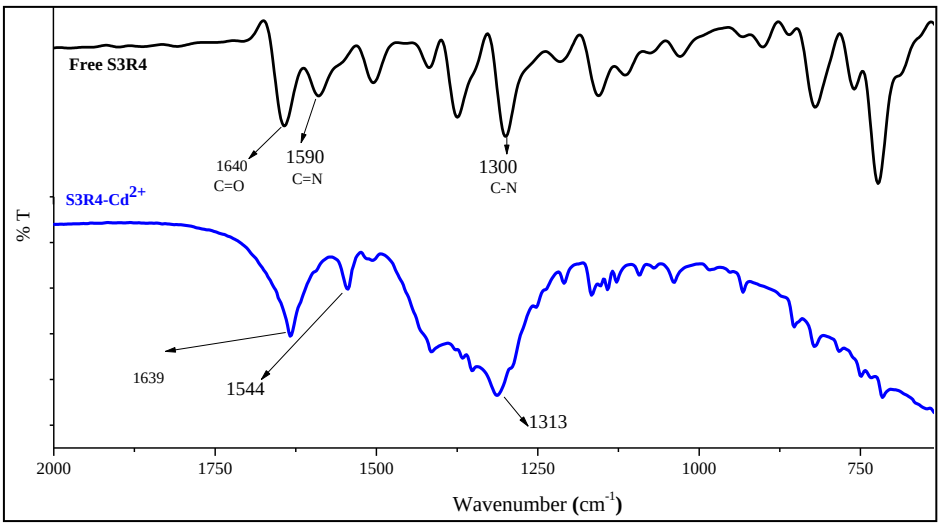

Fig. 4.33. FT-IR study for the chemosensor **S3R4** and **S3R4**–Cd^{2+}complex

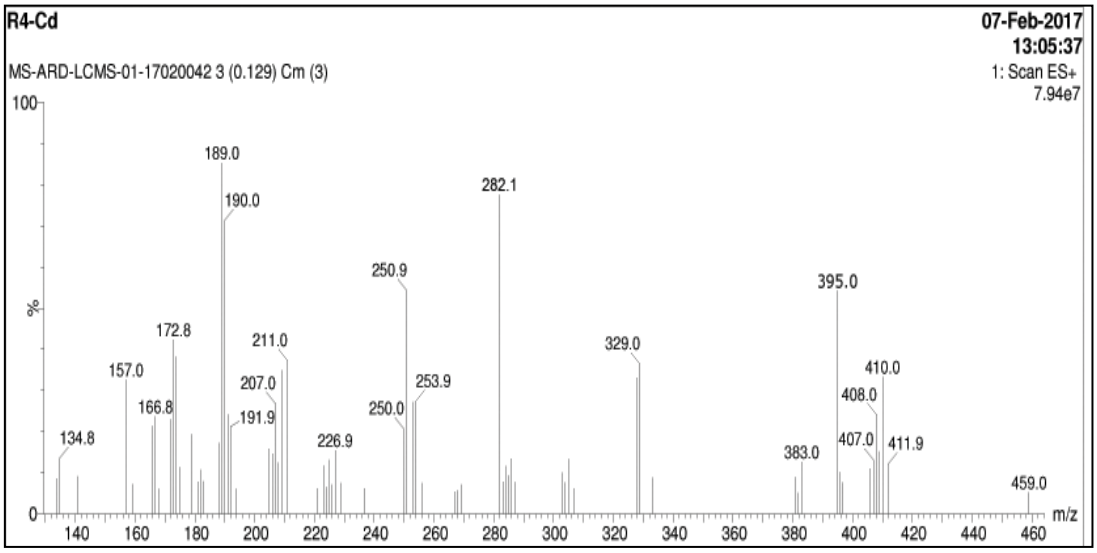

Fig. 4.34. ESI-MS for the complex **S3R4**–Cd^{2+}

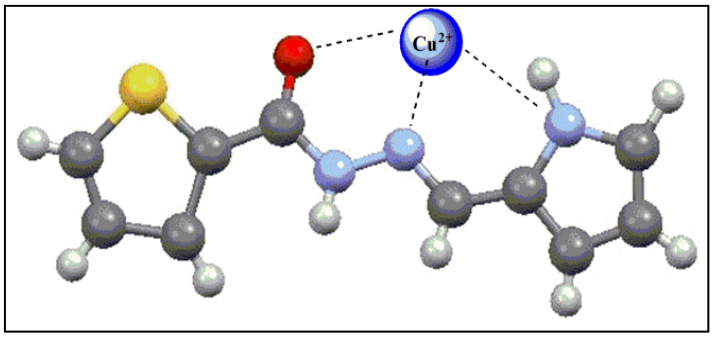

Fig. 4.35: A proposed binding mechanism of **S3R3** with Cu^{2+}

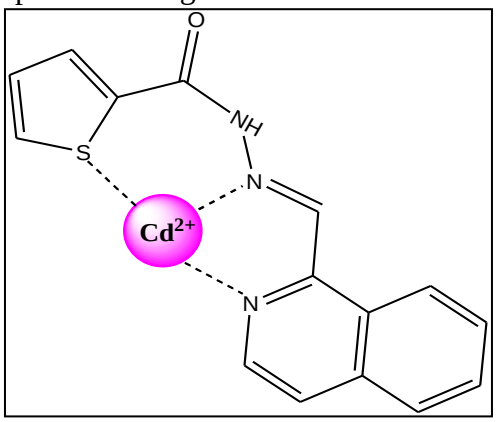

Fig. 4.36: A proposed binding mechanism of **S3R4** with Cd^{2+}

4.3.7. Comparison with other Cu^{2+} and Cd^{2+} sensing chemosensors

The newly designed chemosensors **S3R3** and **S3R4** have some specific features for the detection of **Cu^{2+}** and **Cd^{2+}** ions by colorimetrically. Further, the chemosensors (**S3R3 and S3R4**) were compared with some other literature reports

(i.e., **Cu^{2+}** and **Cd^{2+}** selective colorimetric / UV-Vis and fluorescent sensors). The comparison of the present method has listed in the below **table-4.6**. Each reported sensor exhibits some advantages such as low limit of detection(Huang et al. 2009; Kao et al. 2014; Kim et al. 2015; Wang et al. 2011a; Ye et al. 2014), simple synthesis (Kim et al. 2015; Sarkar et al. 2013; Sun et al. 2015; Xiong et al. 2016). According to ICH guidelines, analytical method validation is one of the most important tools for the standardization of methods, which is used in real-life applications. Present reported chemosensor **S3R3** and **S3R4** exhibited quite appealing analytical features as follows: (1) a facile one-step synthetic methodology; (2) Selectivity in the presence of other interfering cation and anions; (3) Analytical method validation; (4) Application to different water samples with good % recovery; (5) Comparable detection limit. The results are tabulated in **Table 4.6**.

Table-4.6: Comparison of the present developed method with other Cu^{2+} and Cd^{2+} ions sensitive sensors

Detection method	**Detection limit**	**Selectivity**	**Method Validation**	**Application**	**Reference**
		(Yes or No)			
Cu^{2+}					
UV-Vis	--	No	No	No	(Duan et al. 2012)
fluorescent and UV-Vis	--	No	No	No	(Yu et al. 2013)
UV-Vis	2.14×10^{-7} M	No	No	Yes	(Xiong et al. 2016)
Fluorescent	2.73 μM	No	No	Yes	(Wang and Wu 2013a)
Fluorescent and UV-Vis	4.83×10^{-7} M	No	No	No	(Sun et al. 2015)
Fluorescent	4×10^{-8} M	No	No	Yes	(Sarkar et al. 2013)
UV-Vis	5.24×10^{-7}M	No	No	No	(Liu et al. 2015)
Fluorescent	--	No	No	No	(Shi et al. 2013)
UV-Vis	0.3 μM	No	No	No	(Huang et al. 2009)
Fluorescent	0.25 μM	No	No	No	(Wang et al. 2011a)

UV-Vis	0.9 μM	No	No	No	(You et al. 2015a)
UV-Vis	1.2 μM	No	No	No	(Sheng et al. 2008)
UV-Vis	0.37 μM	No	No	Yes	(Kim et al. 2015)
Fluorescent	0.2 μM	No	No	No	(Ye et al. 2014)
UV-Vis	0.26 μM	No	No	No	(Kao et al. 2014)
UV-Vis	2.1 μM	No	No	No	(Jo et al. 2015)
UV-Vis	2.8×10^{-6} M	Yes	Yes	Yes	S3R3 (Present work)
Cd^{2+}					
Fluorescent	10^{-7} M	No	No	No	(Goswami et al. 2013)
Fluorescent	6.47×10^{-7} M	No	No	No	(Samanta et al. 2016)
Fluorescent	--	No	No	No	(Prodi et al. 2001)
Fluorescent	--	No	No	No	(Choi et al. 2001)
Fluorescent	1×10^{-6} M	No	No	--	(Bronson et al. 2005)
Fluorescent	--	No	No	Yes	(Peng et al. 2007)
Fluorescent	1×10^{-9} M	No	No	No	(Cockrell et al. 2008)
Fluorescent	--	No	No	Yes	(Yang et al. 2011)
Fluorescent	--	No	No	No	(Zhou et al. 2008)
Fluorescent	1×10^{-7} M	No	No	No	(Lu et al. 2007)
Fluorescent	--	No	No	No	(Gunnlaugsson et al. 2004)
UV-Vis	1.03×10^{-6} M 4.00×10^{-7} M 3.82×10^{-7} M	No	No	No	(Arabahmadi et al. 2014)
UV-Vis	2.0×10^{-7} M	Yes	Yes	Yes	S3R4 (Present work)

4.3.8. Crystallographic data of chemosensor S3R1–S3R3

The single crystal for chemosensor **S3R1–S3R3** was yielded in acetonitrile solvent by a solvent evaporation method. Unfortunately, **S3R4** did not yield good quality crystal for SC-XRD analysis. The **S3R1** and **S3R2** were crystallized in the monoclinic crystal system with P 21/c (**S3R1**) and C c (**S3R2**) space group. The **S3R3** was crystallized in the orthorhombic crystal system with P c a 21 space group (Crystalographic information is depicted in **table-4.7**). The crystal structure of chemosensor **S3R1–S3R3** was represented in **Fig. 4.37**.

In the crystal structure of chemosensor **S3R1**, adjacent molecular units are interconnected through strong complementary N–H···O hydrogen bond with distance of 2.876 Å (∠174.53°), in the crystal structure intramolecular S···N chalcogen bond has observed (2.762 Å), adjacent dimer units are interconnected through various C–H···π interactions resulting in 3D sandwich-like structure of chemosensor **S3R1** (**Fig. 4.38**). Primary synthon in the crystal structure of chemosensor **S3R2** involves the strong N–H···O hydrogen bond between the molecules with distances 2.843 Å and 2.965 Å (∠156.99°, ∠ 155.58°) respectively. Between two adjacent molecular units apart from strong N–H···O hydrogen bond, weak secondary hydrogen bonds are observed like C–H···O (3.263 Å & 3.352 Å), C–H···N (3.515 Å) and C–H···S (3.765 & 3.546 Å). This dimer connected to the neighboring dimer through weak C–H···O (3.316 Å, 3.548 Å & 3.466 Å), N–H···N (3.177 Å), C–H···S (3.546 Å) hydrogen bond and C–H···π (3.560 Å) interaction which further continuous resulting in 3D network like the structure of chemosensor **S3R2** (**Fig. 4.39**).

In chemosensor **S3R3**, the primary synthon involves the strong N–H···O hydrogen bond between the molecules with distance 2.835 Å (∠145.69°), (**Fig. 4.40**). In two adjacent molecular units other than strong N–H···O hydrogen bond, weak secondary hydrogen bonds like, C–H···O (2.999 Å & 3.330 Å), C–H···N (3.264 Å) and C–H···S (3.426 Å) are observed which further continuous resulting in 3D sandwich like a structure of chemosensor **S3R3** (**Fig. 4.41**).

Comparison of the crystal structure of S3R1, S3R2, and S3R3:

In all three crystal structures, a strong N–H···O hydrogen bond was the primary supramolecular synthons. However, the crystal packing and the secondary interactions involved with the molecular units are found to be different. An intramolecular S···N chalcogen bond is observed only in the case of **S3R1** crystal

structure, whereas in other two crystal structures twisting of the thiophene group is observed. The **S3R1** has high density compare to **S3R2** and **S3R3**; this could be closed packing in **S3R1** crystal structure due to more C–H···π interactions and strong intramolecular S···N chalcogen bond. The observed results prove that the crystal packing in these systems (**S3R1–S3R3**) differ among themselves, due to different types of secondary interaction involve in three crystal packing via C–H···π in **S3R1**, C–H···π, C–H···O, C–H···S, C–H···N in **S3R2** and C–H···O, C–H···S, C–H···N in **S3R3**.

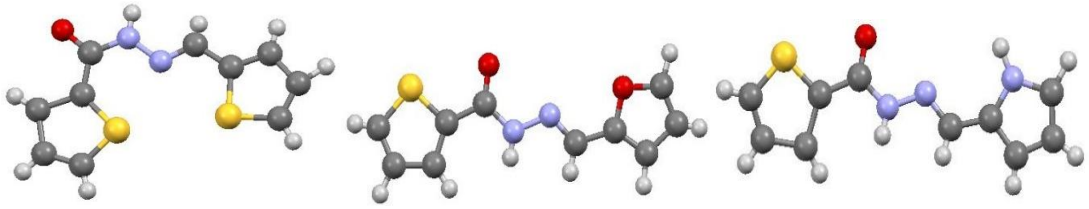

S3R1 **S3R2** **S3R3**

Fig. 4.37: Crystal structure of chemosensors **S3R1–S3R3**

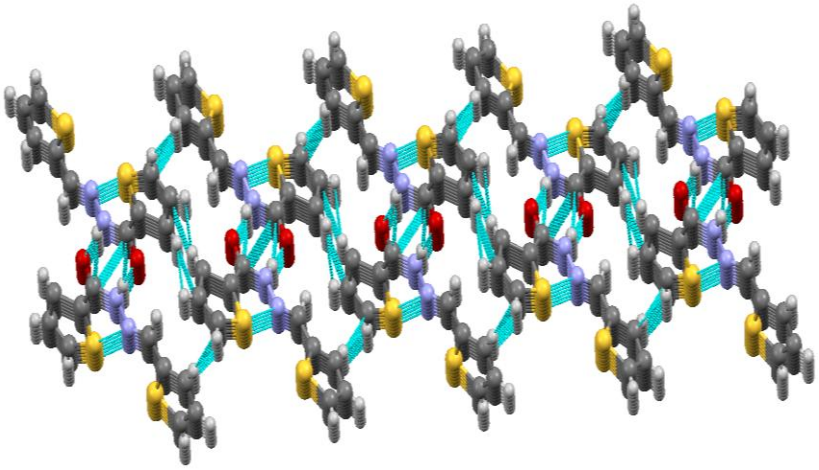

Fig. 4.38: 3D representation of chemosensor **S3R1**

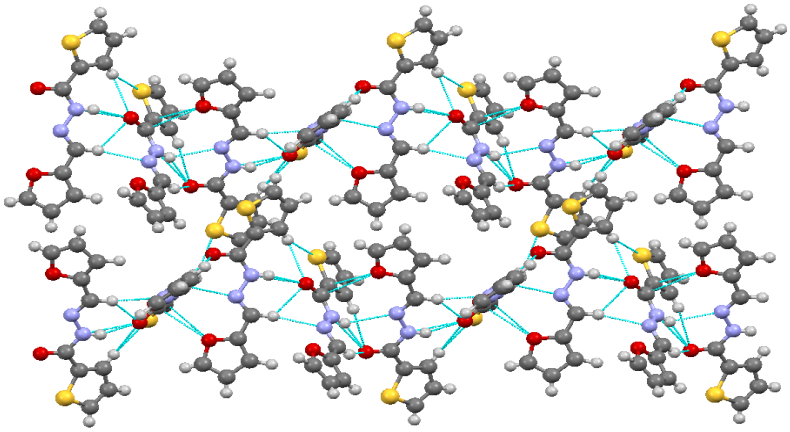

Fig. 4.39: 3D representation of chemosensor **S3R2**

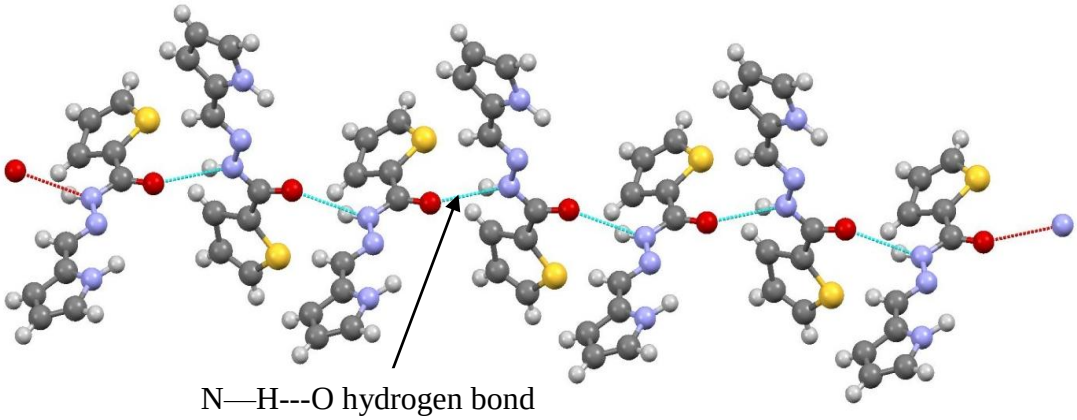

Fig. 4.40: 1D representation of chemosensor **S3R3**

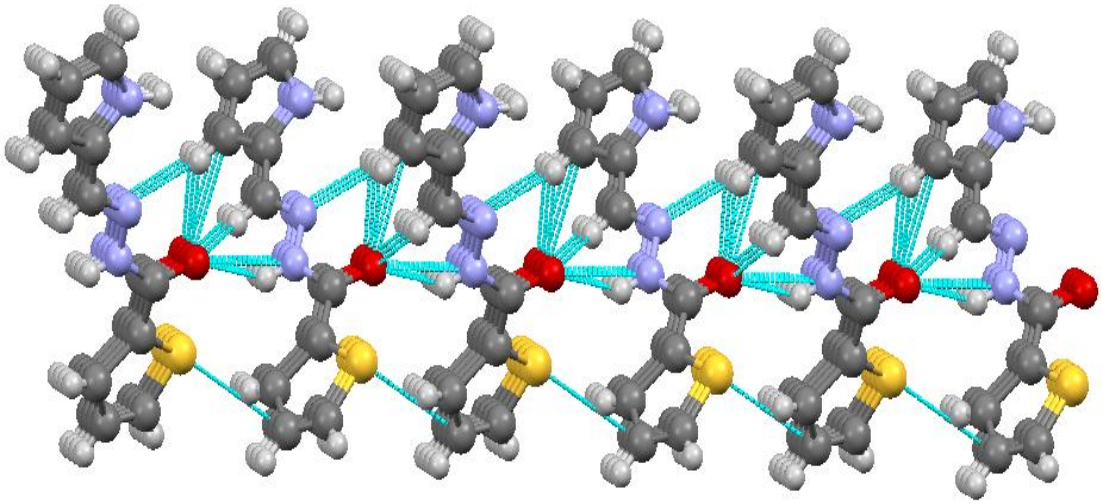

Fig. 4.41: 3D representation of chemosensor **S3R3**

Table- 4.7: Crystallographic data of chemosensor **S3R1, S3R2**, and **S3R3**

Parameters	**S3R1**	**S3R2**	**S3R3**
CCDC NO.	1444013	1443901	1443900
Chemical formula	C_{10} H_8 N_2 O S_2	C_{10} H_8 N_2 O_2 S	C_{10} H_9 N_3 O S
Formula weight	236.30	220.24	219.16
Crystal system	Monoclinic	Monoclinic	Orthorhombic
Space group	'P 21/c'	'C c'	'P c a 21'
a (Å)	13.4059(5)	17.0982(7)	9.7712(2)
b (Å)	5.3673(2)	16.9527(7)	5.22660(10)
c (Å)	15.5451(5)	7.7874(4)	19.8716(5)
α [°]	90	90	90
β [°]	110.985(2)	112.618(2)	90

γ [°]	90	90	90
V [Å]^3	1044.34(7)	2083.65(16)	1014.85(4)
Z	4	8	4
Density [g/cm^3]	1.503	1.404	1.435
μ (MoKα) [mm^{-1}]	0.71073	0.71073	0.71073
T/ °K	296(2)	296(2)	296(2)
Reflns collected	2061	3399	1850
Unique rflns	1777	3065	1975
Parameter refined	140	327	140
Color	Pale yellow	Cream	Colorless
R_1 (I>2σ)	0.1168	0.0376	0.0717
wR_2 (I>2σ)	0.3742	0.1070	0.2272
GOF	1.230	0.869	1.051

4.4. Conclusion

In this chapter, a new thiophene-2-carboxylic acid hydrazine Schiff base derivative as a colorimetric chemosensor for both qualitative and quantitative determination of **Cu^{2+}** and **Cd^{2+}** ions in an aqueous medium have described. The reported chemosensors can be easily synthesized in a single-step reaction. Among as-synthesized chemosensors, the **S3R3** and **S3R4** have shown selectivity and sensitivity towards **Cu^{2+}** and **Cd^{2+}** ions in an aqueous solution through a remarkable color change from colorless to yellow color. It can be easily identified by naked-eye. The proposed analytical method was validated and successfully applied to the environmental samples. The method validation results demonstrate that the proposed analytical method would produce precise, accurate, and linear results for the determination of **Cu^{2+}** and **Cd^{2+}** ions in environmental water samples. The chemosensors **S3R1** and **S3R2** did not show any activity towards **Cu^{2+}** and **Cd^{2+}** ions and other tested cations due to a lack of suitable heteroatom in the thiophene ring-like **S3R3** and **S3R4**. The present reported chemosensors **S3R3** and **S3R4** have the advantage over the other published methods in terms of method validation and selectivity in the presence of other competitive cation and anions.

CHAPTER 5

5. SMART COLORIMETRIC RESPONSE FOR HEAVY METAL DETECTION: SYNTHESIS, SPECTRAL RESPONSE AND DFT STUDIES

Abstract

In this chapter, the design, syntheses, and characterization of new carbohydrazide derivatives as a colorimetric chemosensor for heavy metal ion detection have included. The colorimetric cation sensing properties, DFT studies, detection mechanism of these chemosensors, and test strips applications have discussed in detail.

5.1. Introduction

The improvement of new capable colorimetric chemosensors for elective detection of environmentally pollutant metals, like Hg^{2+}, Cu^{2+}, Zn^{2+}, Pb^{2+}, Co^{2+} and Cd^{2+} has fascinated more interest (Ma et al. 2012; Singhal et al. 2015; Tang et al. 2016; Tharmaraj and Pitchumani 2012; Wang et al. 2005). Generally, chemosensors detect the presence of analyte through a lesser amount of inexpensive technique in which the analyte is recognized by naked-eye. On the other hand, colorimetric sensing offers numerous advantages than other instrumental methods (Fegade et al. 2014; Gattás-Asfura and Leblanc 2003; Hong et al. 2007; Kato et al. 1990; Küpper and Schultze 1997; Yin et al. 2010), in terms of sensitivity, fast results and they are non-destructive (Hammud et al. 2015; Kim et al. 2012; Liu et al. 2015; Marbella et al. 2009; Nair et al. 2015; Narayanaswamy and Govindaraju 2012; Sarkar et al. 2013; Xiong et al. 2016).

In the human body, copper is a useful transition metal ion because it involves many biological processes like a catalyst in oxido-reduction, in an electron transfer mechanism like co-factor. The distribution of copper in the human body should be maintained in the limit due to its cellular toxicity. Above its acceptable limit, it harm living cells, lipids, nucleic acids, proteins and origin for the numerous diseases, like Alzheimer's, Indian childhood cirrhosis (ICC), Prion, Menkes and Wilson diseases (Brown 2001; Emerit et al. 2004; Hahn et al. 1995; Waggoner et al. 1999).

International standards like WHO, US-EPA put the permeable limit in drinking water is 1.3 ppm for copper (Chapter 2016; Graham 1999).

Generally, heavy metals are distinct as metal elements, and they are comparatively high density than water (Chaney 1991) like Cd^{2+}, Hg^{2+} Pb^{2+}, and Cr^{3+}. In current times, there has been rising environmental pollution by toxic heavy metal ions, and it leads to many health problems for human beings. Paul B Tchounwou et al., in the year 2012, repotted about environmental pollution by heavy metals (Tchounwou et al. 2012). Present human contact has increased radically as a result of these heavy metals utilize in several manufacturing, farming, household, and industrial applications (He et al. 2005; Tchounwou et al. 2012). Environmental contamination is very important in point cause areas like mining, smelters, and other metal-based engineering operations. Metal ions like Hg^{2+}, Pb^{2+}, Cd^{2+} ions are very toxic, contaminant, and their presence in water is carcinogenic.

Hence, numerous synthetic organic chemosensor having various binding moieties like imine, coumarine, quinolines, rhodamine (Beer and Gale 2001; Ermakova et al. 2013; Jiang et al. 2011; Udhayakumari et al. 2014; Vinod Kumar and Anthony 2014; Zhang et al. 2015)(Lauwerys et al. 1994; Que et al. 2008) have been reported as chemosensor. Recently Momidi, B. K et al., S.K Sahoo et al. and S R. Patil et al. were repotted very simple organic molecule (thiocarbohydrazide based, pyridoxal derived and uracil nitroso amine-based)as a chemosensors (Momidi et al. 2017; Patil et al. 2015; Sahoo et al. 2016).

The literature reports reveal that the function of colorimetric chemosensors for the detection of pollutant metal ions. From the literature, herein, the carbohydrazide group has introduced into the sensor molecule containing hydroxy (–OH), imine (–C=N), quinoline, and furfural groups as a binding site for the quick naked eye responds towards heavy metal ions. The **S4R1** shows noticeable enrichment in naked eye color change from colorless to different colors for dissimilar metal ions like Hg^{2+}, Cu^{2+}, Cd^{2+}, and Pb^{2+}. In the presence of Hg^{2+}, Cu^{2+} ions, the **S4R2** shows colorless to yellow color and pink color. **S4R3** displayed pale yellow color to light orange in the attendance of Cu^{2+} ions in water media. All the synthesized sensors **S4R1–S4R3** exhibit a good detection limit and linear range.

5.2. Experimental section

All chromatography grade solvents, metal nitrate salts, and chemicals were procured from commercial distributors and utilized as such.

Varian NMRS-400 MHz and Bruker-400 MHz spectrometer used to record all the ^{1}H NMR, ^{13}C NMR spectra, and DMSO-d_6 solvent was used. The ^{1}H NMR and ^{13}C NMR chemical shifts are reported on the δ scale (in ppm) relative to tetramethylsilane (TMS, δ 0.00) and DMSO-d_6 (39.50), respectively, as internal reference standards. Bio-cote (SMP10) used to record the melting point for the reported sensors. Bruker Alpha (silicon carbide as IR source) instrument used to record the Fourier Transform Infrared (FT-IR) spectra using KBr pellet media. The UV-Vis study experiments were done on Analytikjena Specord S600 UV-Vis spectrophotometer using a 3.0 mL quartz sample holder having two optical transparent windows with a path length of 10 mm.

All the metal solutions are prepared separately in de-ionized water, having a concentration of 1.0×10^{-3} M from their nitrate salts. Three separate chemosensor S4R1-S4R3 solutions were prepared in DMSO having a concentration of 1.0×10^{-3} M. Further, these chemosensor solutions diluted to 2.5×10^{-6} M (S4R1–S4R2) and 2.5×10^{-5} M (S4R3) using the same solvent. The micropipette was for the addition of metal solutions to respective chemosensor solutions in an instrumental study and naked-eye detection methods. All the spectra were recorded after the mixing of chemosensor and metal solution immediately at room temperature.

5.2.1. Synthesis of chemosensor S4R1-S4R3

The synthesis procedure of **S4R1–S4R3** has illustrated in the **scheme 5.1**. The synthesis of chemosensor **S4R1:** Carbohydrazide (0.0321g, 0.35mmol) and 8-hydroxy quinoline-2-carbaldehyde (0.1231g, 0.71mmol) were separately dissolved in 10 mL ethanol. Then aldehydehyde solution was added drop-wise with constant stirring to the thiophene-2-carboxylic acid hydrazide solution. To this a catalytic amount of acetic acid was added and the reaction mixture was stirred at room temperature for 3 hours. The progress of reaction was monitored by TLC. After the completion of reaction the reaction mixture was filtered and washed with hot ethanol. Similarly, the **S4R2** and **S4R3** were synthesized as stated above synthetic methodology. The **S4R2**

was synthesized by the reaction of carbohydrazide (0.1001g, 1.1mmol) and quinoline-2-carbaldehyde (0.3501g, 2.2mmol). The **S4R3** was synthesized by the reaction of carbohydrazide (0.1002g, 1.1mmol) and 5-Nitro furfural-2-carboxaldehyde (0.3131g, 2.2mmol). The final obtained desired compounds were characterized by using standard spectroscopic methods as given below.

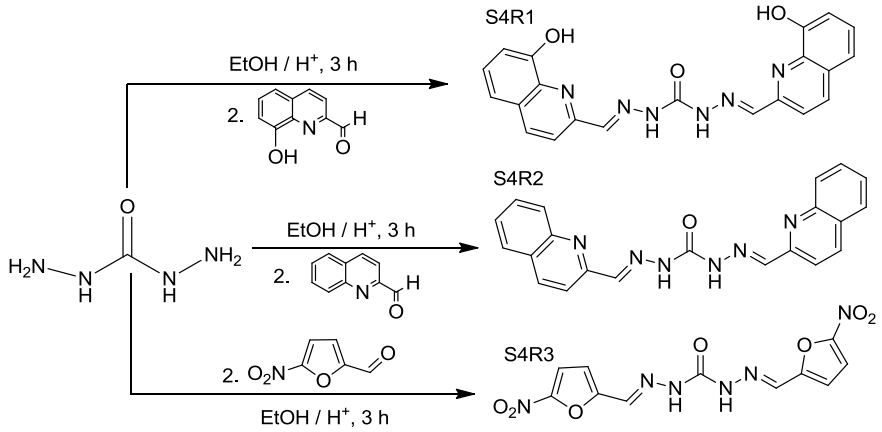

Scheme 5.1: Synthesis of chemosensors **S4R1 – S4R3**

(Z)-2-((8-hydroxyquinolin-2-yl)methylene)-N'-((Z)-(8-hydroxyquinolin-2-yl)methylene)hydrazine-1-carbohydrazide (S4R1): Yield: 94.9%. **M.P:** 244–246˚C. **FT-IR (ATR, cm^{-1}):** 3335, 3075, 1681, 1529, 1327, 1227, 1082, 764 **(Fig. 5.1)**. **^{1}H-NMR (400MHz, DMSO-d$_6$, δ$_{ppm}$):** 11.371 (s, 2H, –NH of carbohydrazide nitrogen), 8.291–8.481 (m, 6H imine (HC=N) and aromatic (–C=CH), 7.436 (m, 4H, aromatic (–C=CH), 7.131 (s, 2H, aromatic –OH) **(Fig. 5.2)**. **^{13}C-NMR (100MHz, DMSO-d$_6$, δ$_{ppm}$):** 153.8 (–C=O), 152.4 (aromatic –C–OH), 152.2 (HC=N), 138.5 136.8, 129.1, 128.5, 118.3, 111.5 (aromatic quinoline –C=C–) **(Fig. 5.5)**. **LC-MS (ESI) m/z:** Cald. for $C_{21}H_{16}N_6O_3$, 400.39 and found, 401.20 (M+1) **(Fig. 5.8)**.

(Z)-N'-((Z)-quinolin-2-ylmethylene)-2-(quinolin-2-ylmethylene)hydrazine-1-carbohydrazide, (S4R2): Yield: 92.9%. **M.P:** 221–223˚C. **FT-IR (ATR, cm^{-1}):** 3300, 3096, 1705, 1546, 1283, 1136, 746 **(Fig. 5.1)**. **^{1}H-NMR (400MHz, DMSO-d$_6$, δ$_{ppm}$):** 11.326 (s, 2H, –NH of carbohydrazide nitrogen), 8.318–8.441 (m, 6H, aromatic (–C=CH) and imine (HC=N), 8.029 (m, 4H, aromatic (–C=CH)), 7.798 (s, 2H, aromatic (–C=CH)), 7.642 (s, 2H, aromatic (–C=CH)), **(Fig. 5.3)**. **^{13}C-NMR (100MHz, DMSO-d$_6$, δ$_{ppm}$):** 154.4 (–C=O), 152.1 (imine HC=N), 147.8 (quinoline HC=N), 136.9, 130.5, 129.3, 128.4, 128.2, 127.6, 118.2 (aromatic quinoline –C=C–)

(Fig. 5.6). **LC-MS (ESI) m/z:** Cald. for $C_{21}H_{16}N_6O$, 368.39 and found, 369.20 (M+1) **(Fig. 5.9)**.

(Z)-2-((5-nitrofuran-2-yl)methylene)-N'-((Z)-(5-nitrofuran-2-yl)methylene)hydrazine-1-carbohydrazide (S4R3): Yield: 93.8%. **M.P:** 248–250˚C. **FT-IR (ATR, cm^{-1}):** 3217, 3017, 1689, 1542, 1460, 1336, 1234, 1077, 794 **(Fig. 5.1)**. **^{1}H NMR (400MHz, DMSO-d_6, δ_{ppm}):** 11.371 (s, 2H, –NH of carbohydrazide nitrogen), 8.159 (s, 2H, imine (HC=N)), 7.591–7.830 (m, 2H, aromatic (–C=CH) 2H)), 7.249–7.344 (m, 2H, aromatic (–C=CH)) **(Fig. 5.4)**. **^{13}C-NMR (100MHz, DMSO-d_6, δ_{ppm}):** 152.7 (–C=O), 152.1 (imine HC=N), 151.6 (furfural =C–NO_2), 132.3 (furfural =C–O–), 115.4, 114.4 (aromatic furfural –C=C–) **(Fig. 5.7)**. **LC-MS (ESI) m/z:** Cald. for $C_{11}H_8N_6O_7$, 336.22 and found, 337.20 (M+1) **(Fig. 5.10)**.

5.2.2. Characterization data of chemosensors S4R1–S4R3

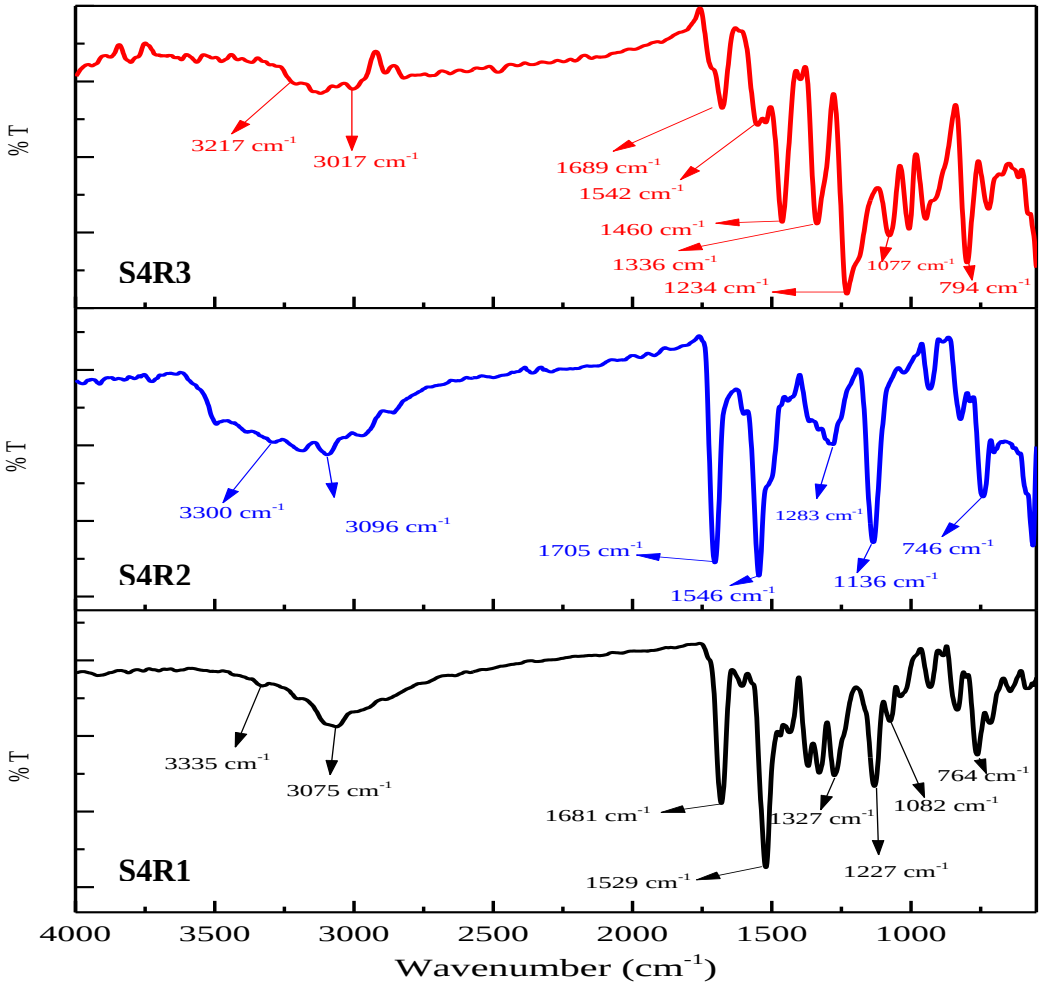

Fig. 5.1: FT-IR Spectra of chemosensor **S4R1–S4R3**

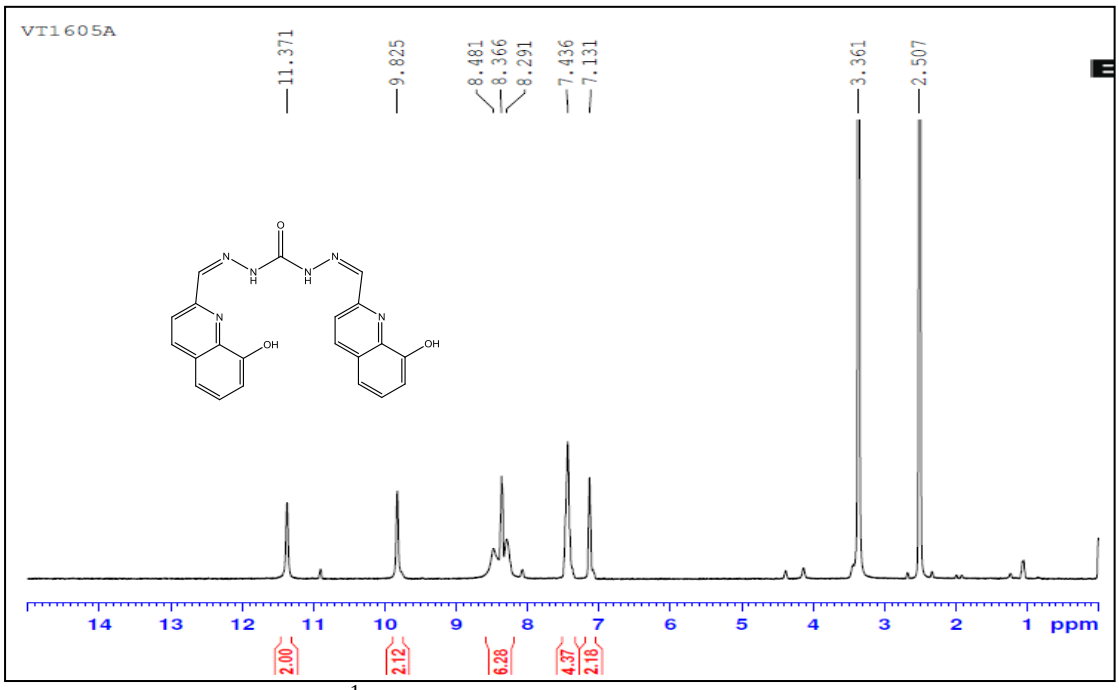

Fig. 5.2: ^{1}H NMR spectrum of chemosensor **S4R1**

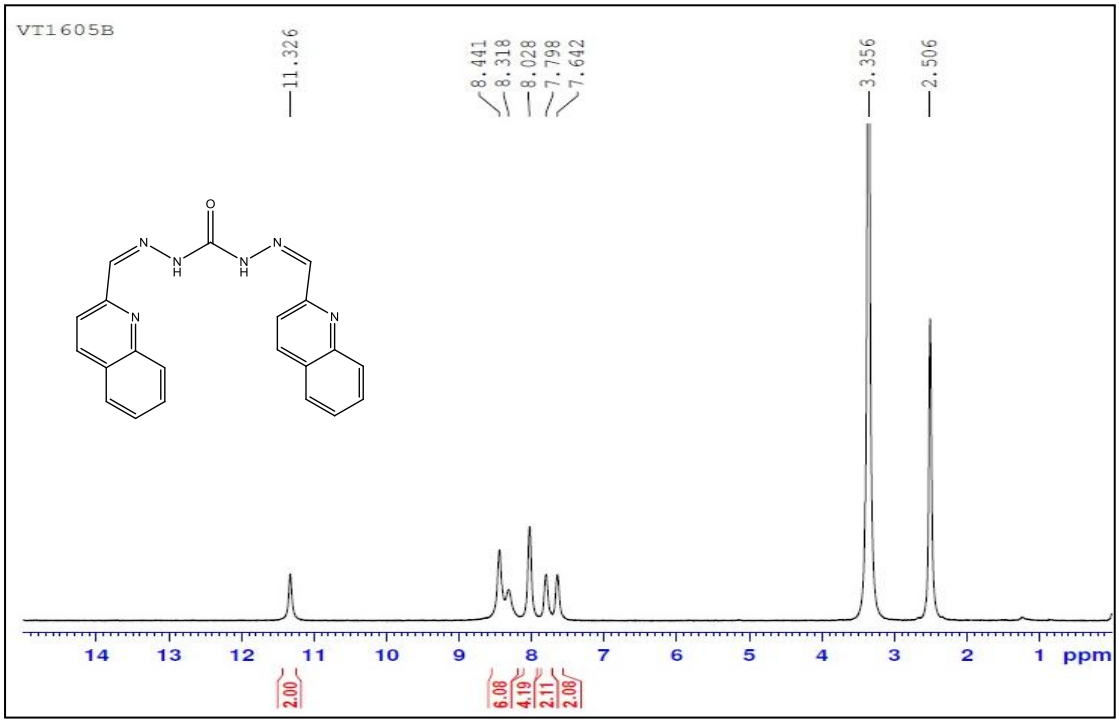

Fig. 5.3: ^{1}H NMR spectrum of chemosensor **S4R2**

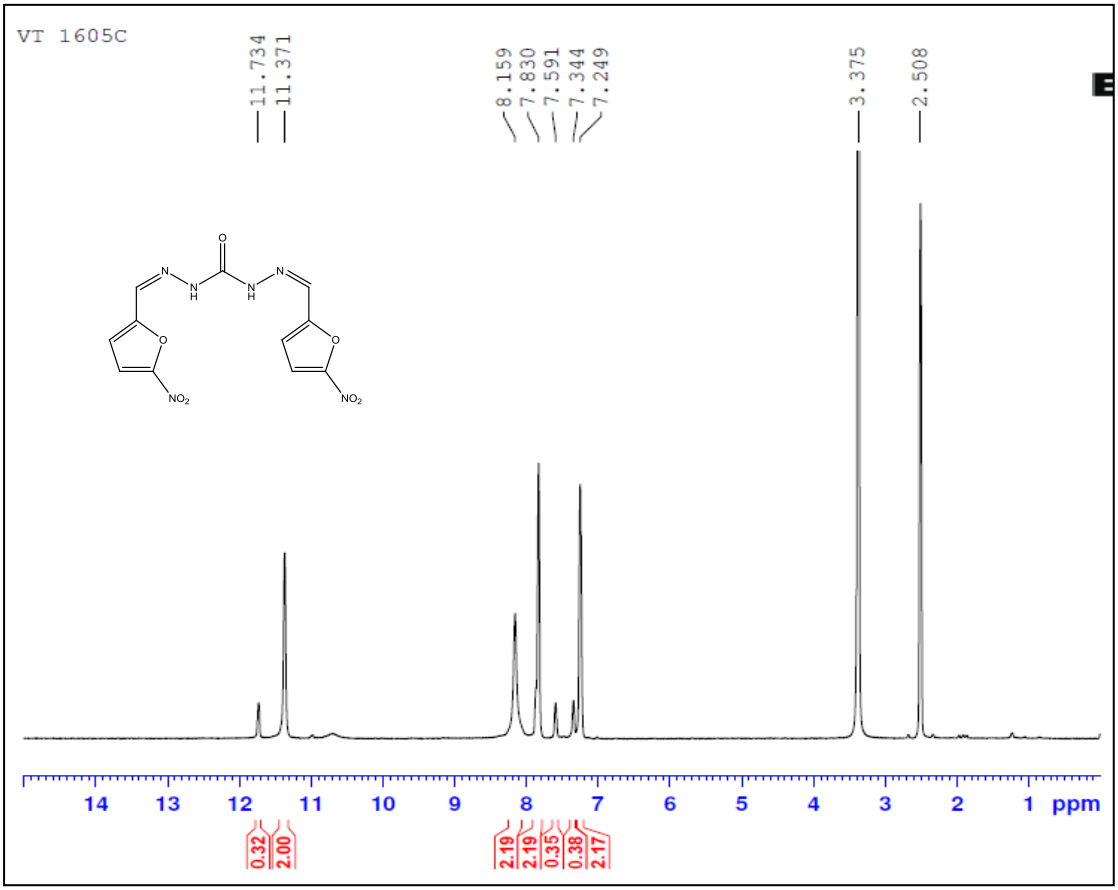

Fig. 5.4: ^{1}H NMR spectrum of chemosensor **S4R3**

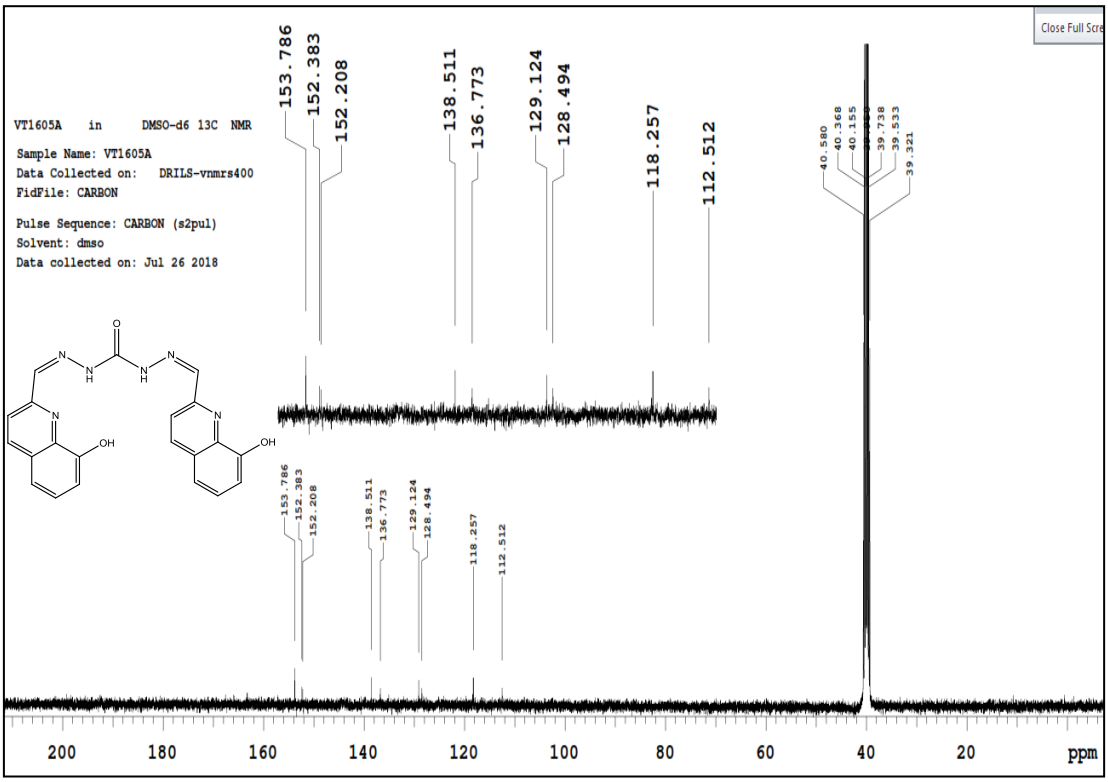

Fig. 5.5: ^{13}C NMR spectrum of chemosensor **S4R1**

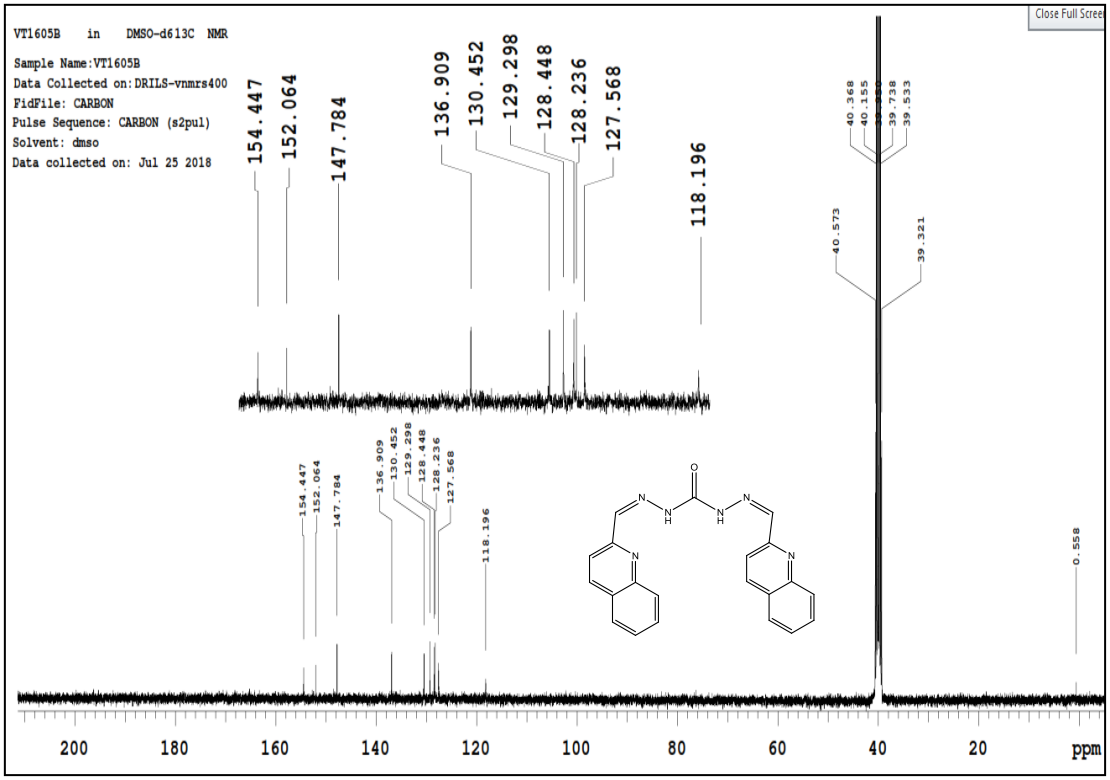

Fig. 5.6: ^{13}C NMR spectrum of chemosensor **S4R2**

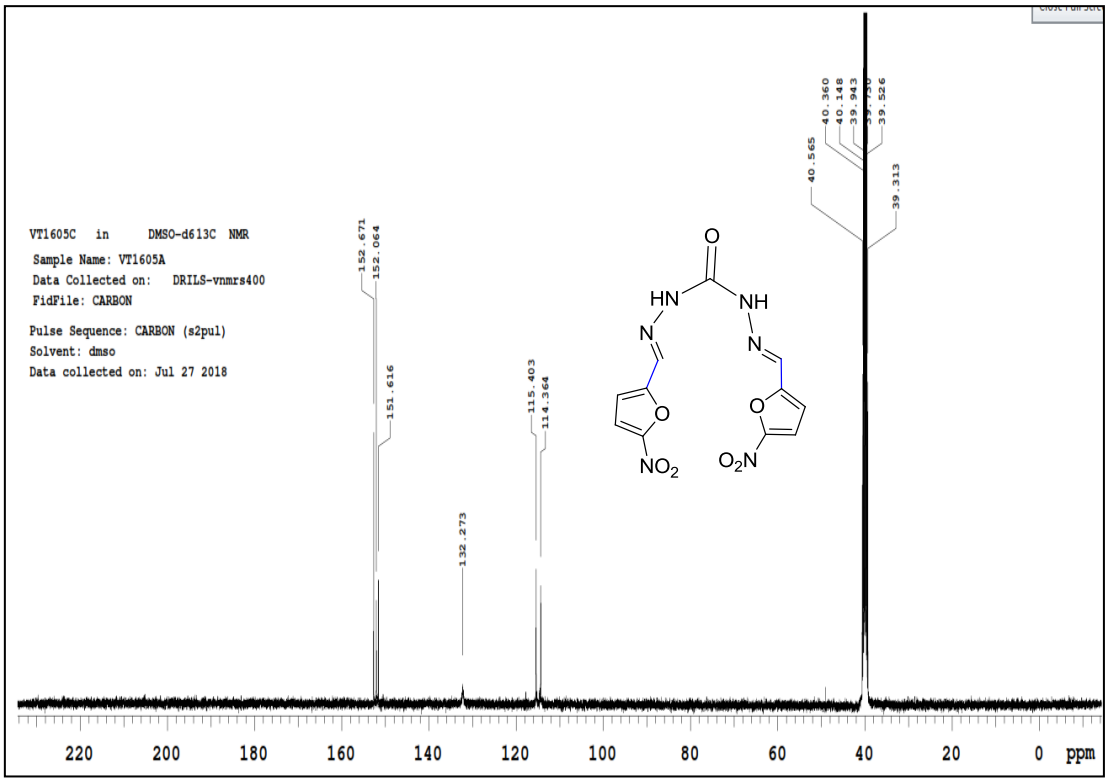

Fig. 5.7: ^{13}C NMR spectrum of chemosensor **S4R3**

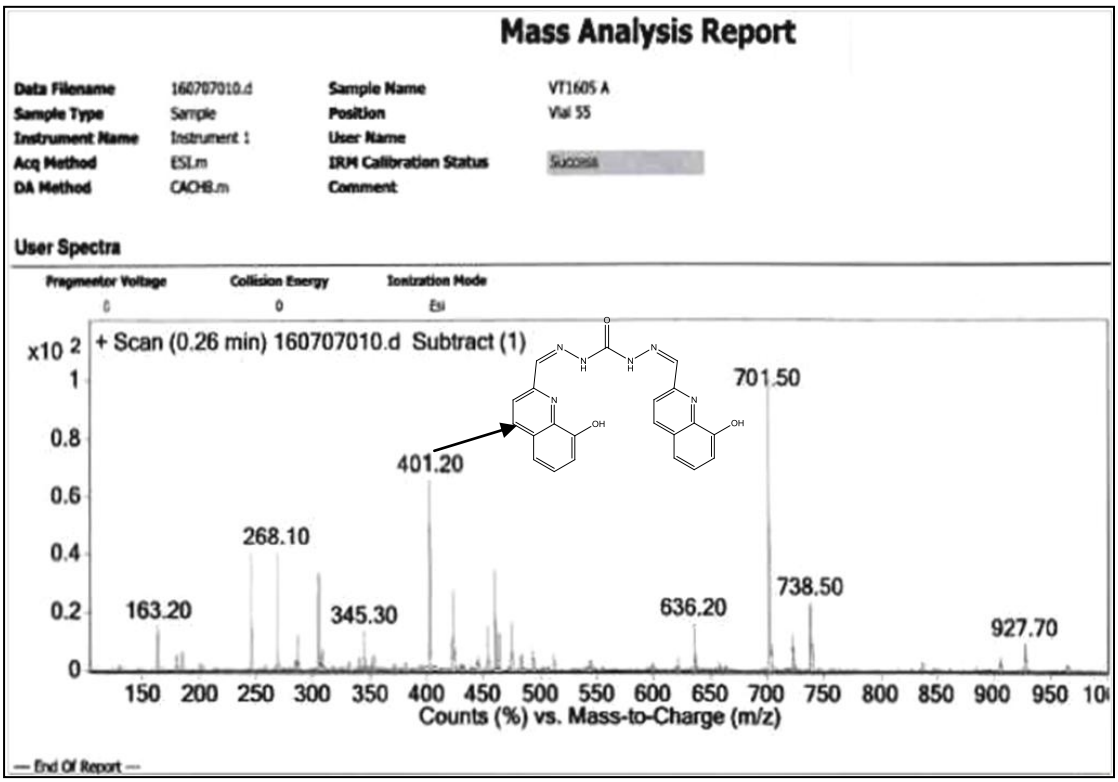

Fig. 5.8: ESI-mass spectrum of chemosensor **S4R1**

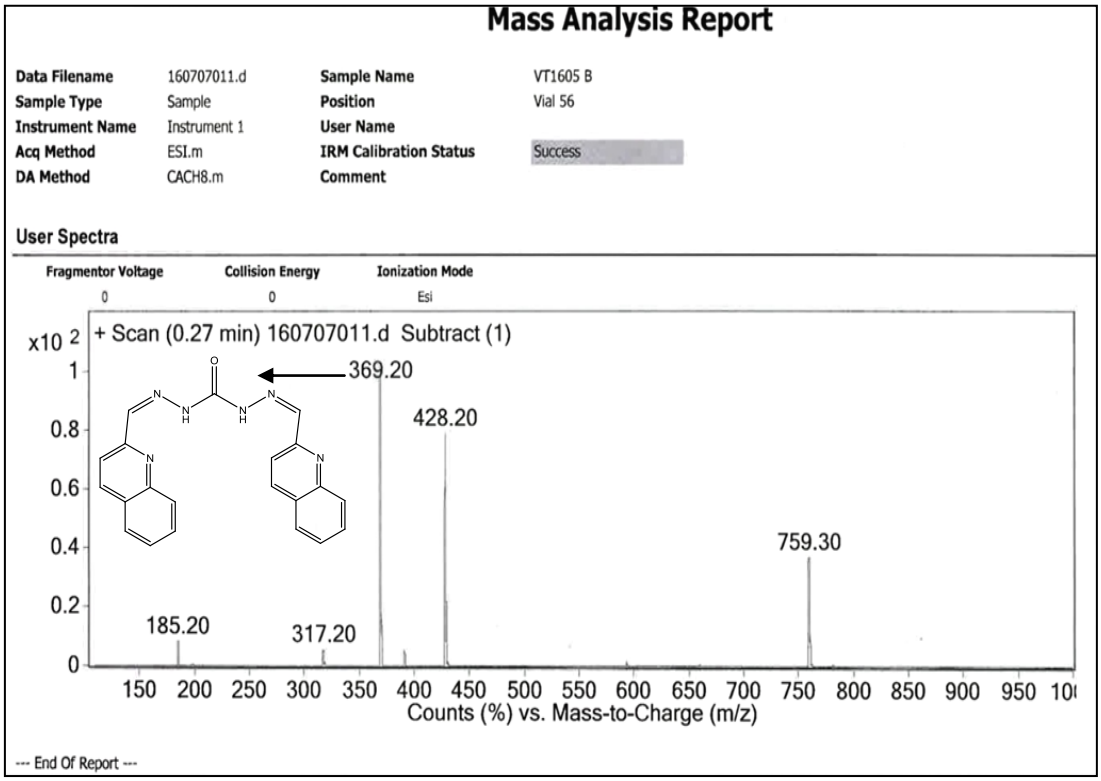

Fig. 5.9: ESI-mass spectrum of chemosensor **S4R2**

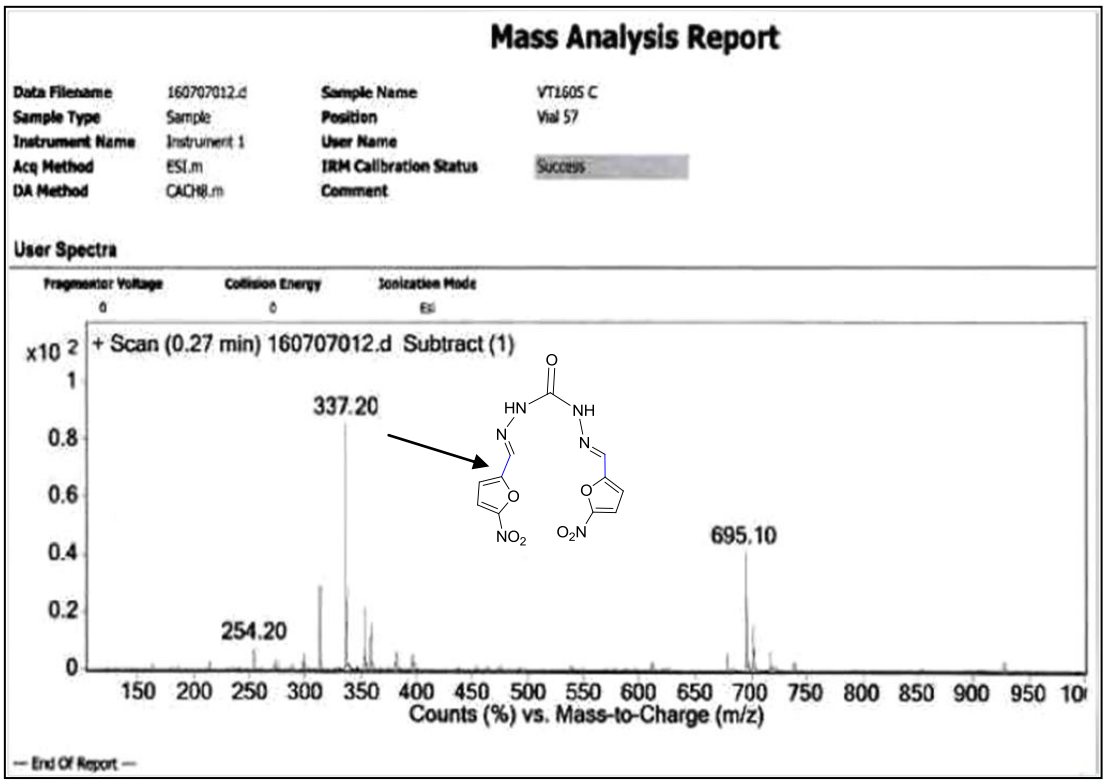

Fig. 5.10: ESI-mass spectrum of chemosensor **S4R3**

5.3. Results and discussion

5.3.1. Colorimetric sensing experiments

Initially, the sensing ability of chemosensors **S4R1–S4R3** is examined in the presence of various cations like Co^{2+}, Hg^{2+}, Fe^{2+}, Cu^{2+}, Cd^{2+}, Pb^{2+}, Cr^{3+}, Ni^{2+}, Zn^{2+}, Ag^{+}, Fe^{3+}, Al^{3+}, Mn^{2+}, and AsO_2^{-} ions (**Fig. 5.11**). **S4R1** did not show any activity towards Co^{2+}, Fe^{2+}, Cr^{3+}, Ni^{2+}, Zn^{2+}, Ag^{+}, Fe^{3+}, Al^{3+}, Mn^{2+}, and AsO_2^{-}cations, whereas, it exhibits a different color response for the dissimilar metal ions, Pb^{2+}, Cu^{2+}, $Hg^{2+,}$ and Cd^{2+} ions as shown in **table 5.1** and **Fig. 5.11**. In similarly, the **S4R2** exhibits a noticeable dual-color change towards Hg^{2+} and Cu^{2+} ions; **S4R3** exhibits dual-color change for Cu^{2+}, AsO_2^{-} ions, and both the **S4R2, S4R3** produced no remarkable color response with the other tested ions except above said selective ions.

Table 5.1: Naked eye response of **S4R1-S4R3** in the presence of active metals

Chemosensor	Concentration (M)	Visible color	Analyte (2.0equi)	Visible color change
S4R1	2.5×10^{-6}	Colorless	Hg^{2+}	Orange
			Cu^{2+}	Dark yellow
			Cd^{2+}	Yellowish orange
			Pb^{2+}	Pink
S4R2	2.5×10^{-6}	Colorless	Hg^{2+}	Yellow
			Cu^{2+}	Pink
S4R3	2.5×10^{-5}	Pale yellow	Cu^{2+}	Orange
			AsO_2^-	Pale violet-blue

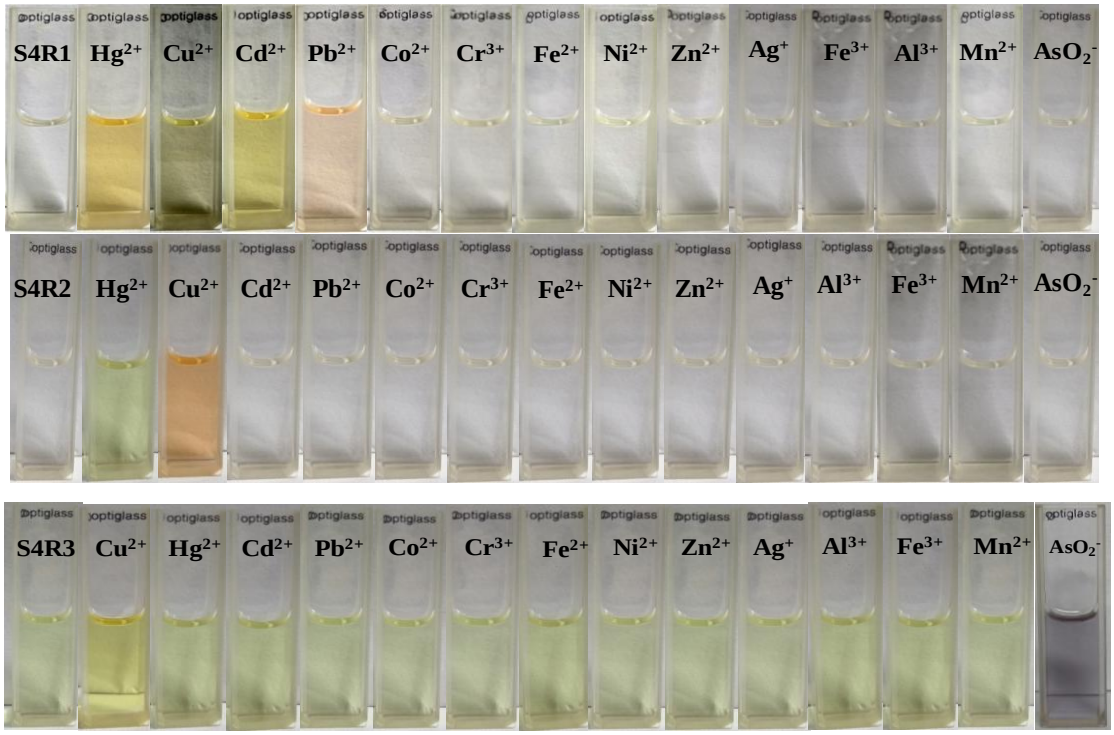

Fig. 5.11: The colorimetric changes observed by naked-eye of chemosensor **S4R1–S4R3** upon addition of 3.0 equivalences of various cations in an aqueous solution

5.3.2. UV–Visible sensing studies

With the colorimetric experimental study background further, the selectivity of **S4R1–S4R3** was determined using optical studies (UV–Vis) with a variety of metal ions, as stated in the colorimetric studies. There was no

remarkable response observed for **S4R1**, except active metal ions (Hg^{2+}, Cu^{2+}, Pb^{2+}, and Cd^{2+}) in the absorption studies (**Fig. 5.12**). Further, the order of selectivity of **S4R1** confirmed as Hg^{2+} > Cu^{2+} > Cd^{2+} > Pb^{2+} using UV–Vis experimental data. Initially, 2.0 equivalences of Hg^{2+} ions were added to the **S4R1**. Resulting in a new peak at 475 nm have found in the absorption spectrum, to confirm this high selectivity of **S4R1** with Hg^{2+} ions, added 2.0 equivalences of Cd^{2+}, $Pb^{2+,}$ and Cu^{2+} ions to the chemosensor S4R1-Hg^{2+} solution. Resulting no considerable changes were found in the color of the solution and absorption of **S4R1,** it reveals that the **S4R1** more preferable to sense the mercury ions compare to other active metals (Cd^{2+}, Cu^{2+}, and Pb^{2+}). Similar experiments were done to confirm the order of selectivity with other active metal ions in the existence and nonexistence of mercury ions. From these experiments and binding constant values, the selectivity order of metals, as stated above, has confirmed **(Fig. 5.13)**. The selectivity preference of **S4R1-S4R3** in the presence of other interfering metals and selectivity order of Hg^{2+}, Pb^{2+}, Cd^{2+}, and Cu^{2+} metal ions could be supported by the HSAB theory (Momidi et al. 2017; Pearson 1963).

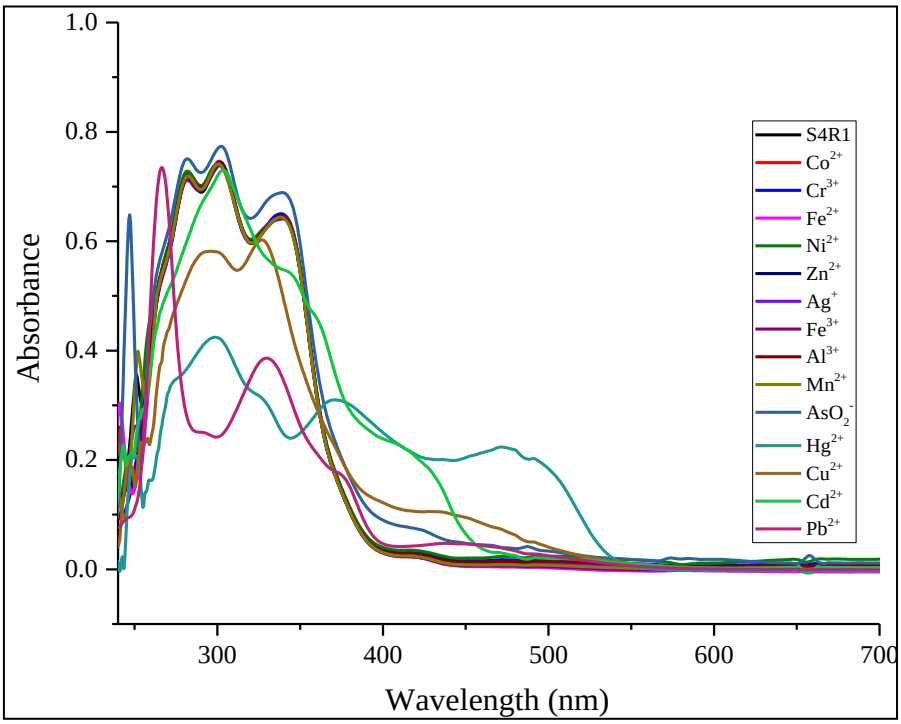

Fig. 5.12: UV–Vis comparative spectrum of chemosensor **S4R1** (2.5×10^{-6} M, DMSO) in the existence of 3.0 equivalences of other cations

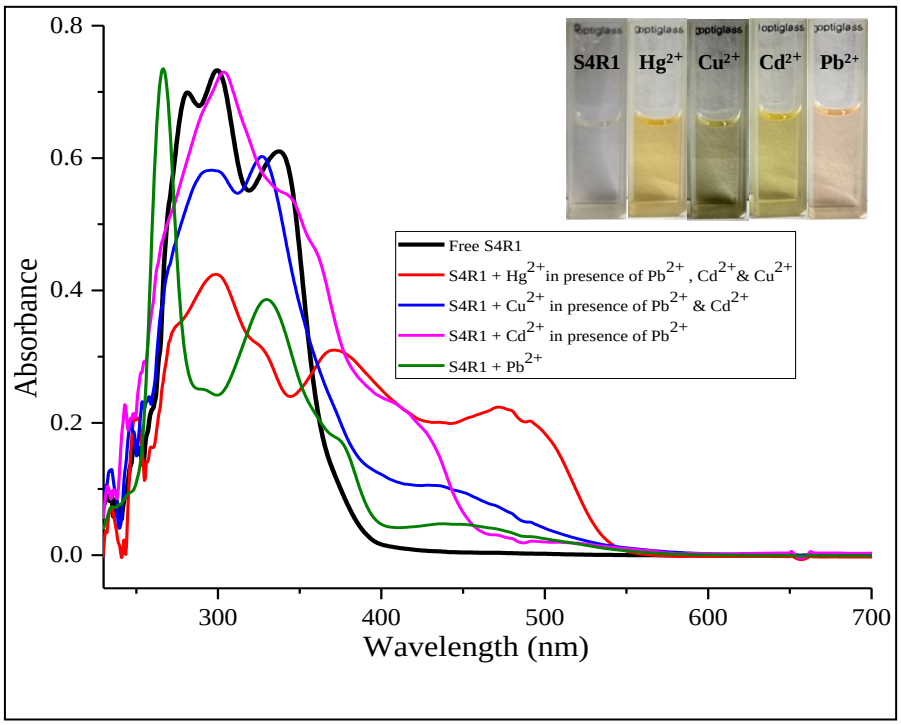

Fig. 5.13: Absorption and naked eye response of **S4R1** (2.5×10^{-6} M, DMSO), with the addition of 2.0 equivalences of Pb^{2+}, Cd^{2+}, Cu^{2+} and Hg^{2+} ions in water. Inset: naked eye response of **S4R1** towards metal ions.

Similarly, the **S4R2** & **S4R3** was tested with different metal ions, as above stated. The **S4R2** exhibits selectivity for Hg^{2+}, Cu^{2+} ions, and a reliable response was observed in the presence of other competitive ions (**Fig. 5.14**). Further, **S4R3** also tested for the selectivity of metal ions as earlier stated competitive metals; it was observed that the **S4R3** give a remarkable response with the Cu^{2+} and AsO_2^- ions and the un-noticeable response was observed in case of other competitive metals (**Fig. 5.15**). This result indicates the high selectivity of **S4R2, S4R3** towards selected ions.

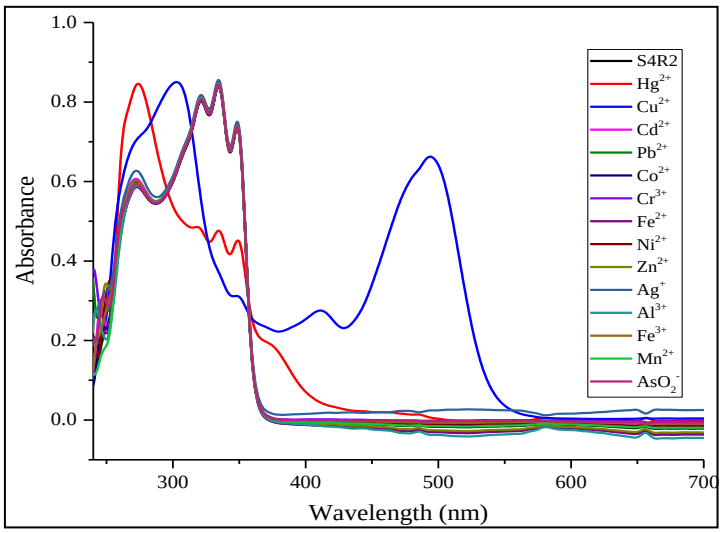

Fig. 5.14: UV–Vis comparative spectra of **S4R2** (2.5×10^{-6} M, DMSO) in the existence of 3.0 equivalences of other cations

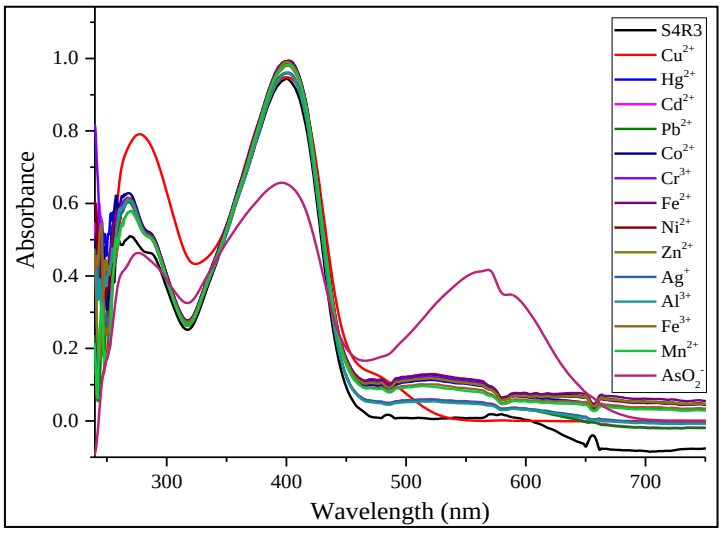

Fig. 5.15: UV–Vis comparative spectra of **S4R3** (2.5×10^{-5} M, DMSO) in the existence of 3.0 equivalences of other cations

From the above experimental results further, the sensitivity, binding rations of **S4R1–S4R3** with the selective metal ions (i.e., Pb^{2+}, Cd^{2+}, $Cu^{2+,}$ and AsO_2^- ions) have investigated. The absorption spectrum of **S4R1** exhibits major bands at 300 nm and 340 nm was assigned to n–π* transition. With the addition of Hg^{2+}, Pb^{2+}, Cd^{2+}, and Cu^{2+}ions to the **S4R1** show red-shift by 135 nm, 95 nm, 75 nm and 110 nm respectively in the absorption spectrum with a clear isobestic points centered at 357 nm for Hg^{2+}, Cu^{2+}, 350 nm, 381 nm for Cd^{2+} and Pb^{2+}. It indicated that the metal to ligand charge transfer metal-complex formation **(Fig. 5.16a-d).** The molecular structure of **S4R1** possessed appropriate binding sites like hydroxy, imine, and

quinoline sites) and a suitable cavity for the metal ions is responsible for multi-signal of **S4R1**.

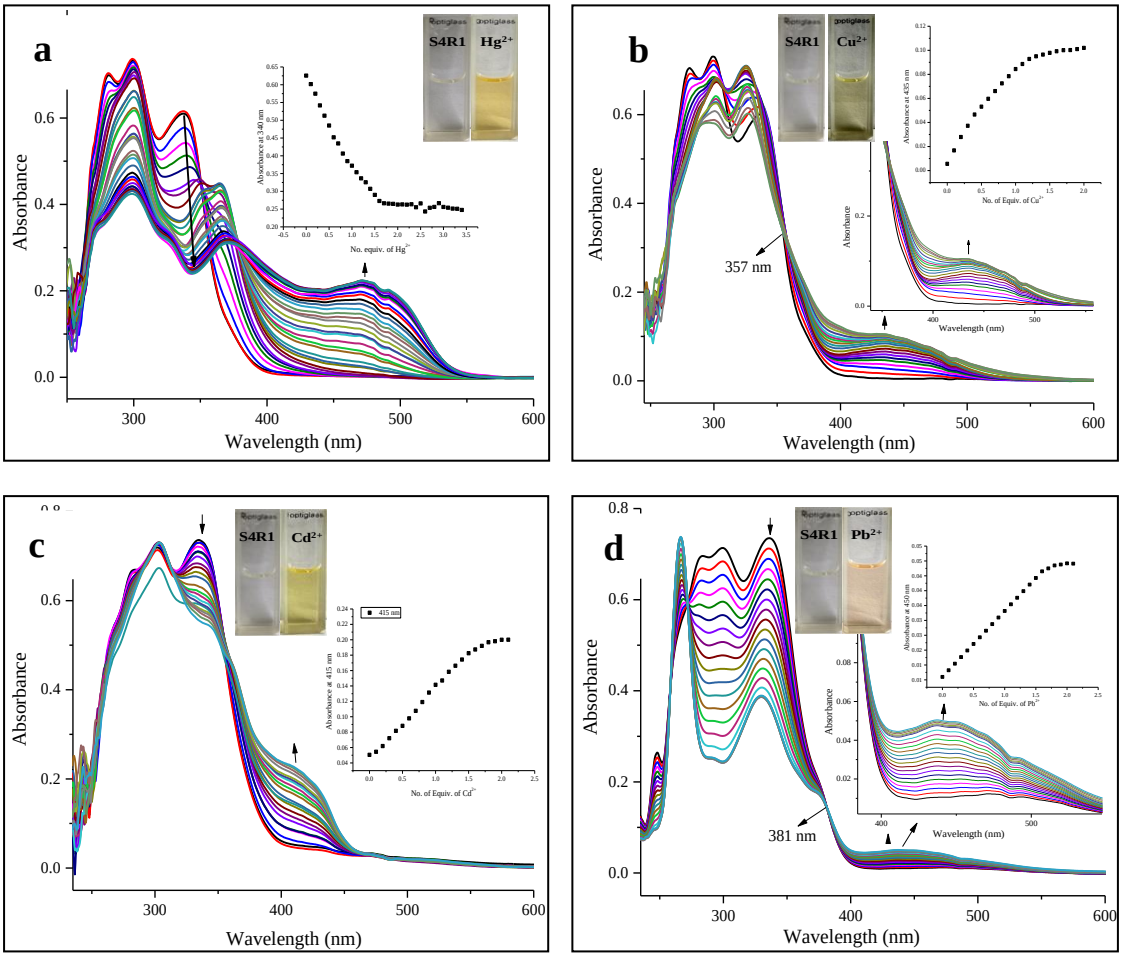

Fig. 5.16: Absorption and naked eye responses of **S4R1 (**2.5 × 10^{-6} M, DMSO) with the rising amount (0 – 2.5 equiv.) of metal ions in water. The inset diagram represents the color & absorption changes at a particular wavelength, **a)**. At 340 nm, **S4R1** vs. Hg^{2+}, **b)**. At 435, nm **S4R1** vs Cu^{2+} , **c)**. At 415 nm, **S4R1** vs. Cd^{2+} ions, d**)**. At 450 nm, **S4R1** vs. Pb^{2+} ions

In the absorption spectrum, the **S4R2** possessed wavelength maxima at 275 nm 335 nm, which are due to π–π* and n–π* electronic transitions occur in the **S4R2**. While, the attendance of Cu^{2+} and Hg^{2+} ions displayed a red-shift by 159 nm and 40 nm, respectively, with the clear isobestic point centered at 358 nm **(Fig. 5.17a–b).** This behavior attributes the metal to ligand charge transfer in the complex. The titration profile confirms the linear relationship between the response of sensor–metal

complex and concentration of analytes; this could help in the quantitative analysis of Cu^{2+} and Hg^{2+} ions.

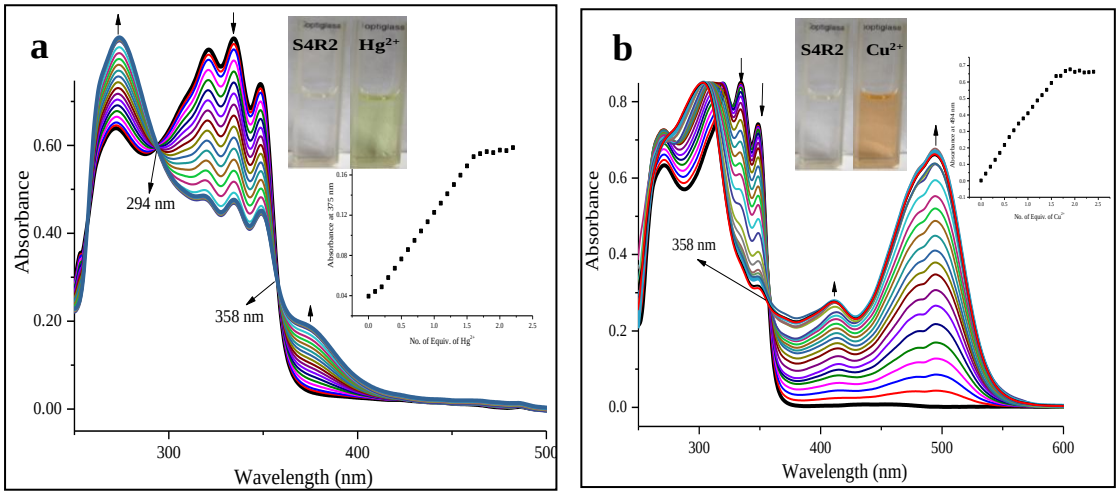

Fig. 5.17: Absorption and naked eye color observation of **S4R2 (**2.5×10^{-6} M, DMSO) upon gradual addition (0 – 2.5 equiv.) of Hg^{2+} and Cu^{2+} ions in water. Inset diagram represents photographs of naked-eye response and absorption change at selected wavelengths, **a)**. At 375 nm, **S4R2**–Hg^{2+}, **b)**. At 494 nm, **S4R2**–Cu^{2+}

S4R3 has absorption wavelength maxima at 400 nm, which can be attributed to the n–π* transitions of free **S4R3**. In the UV–Vis titration study, the **S4R3** displayed a red-shift by 164 nm and 75 nm, with the incremental addition of AsO_2^- and Cu^{2+} ions, respectively, and were observed a clear isobestic point centered at 350 and 410 nm **(Fig. 5.18a-b).** This behavior attributes the metal to ligand charge transfer in the complex. The titration profile confirms the linear relationship between the response of sensor–metal complex and concentration of analytes; this could help in the quantitative analysis of Cu^{2+} and AsO_2^- ions.

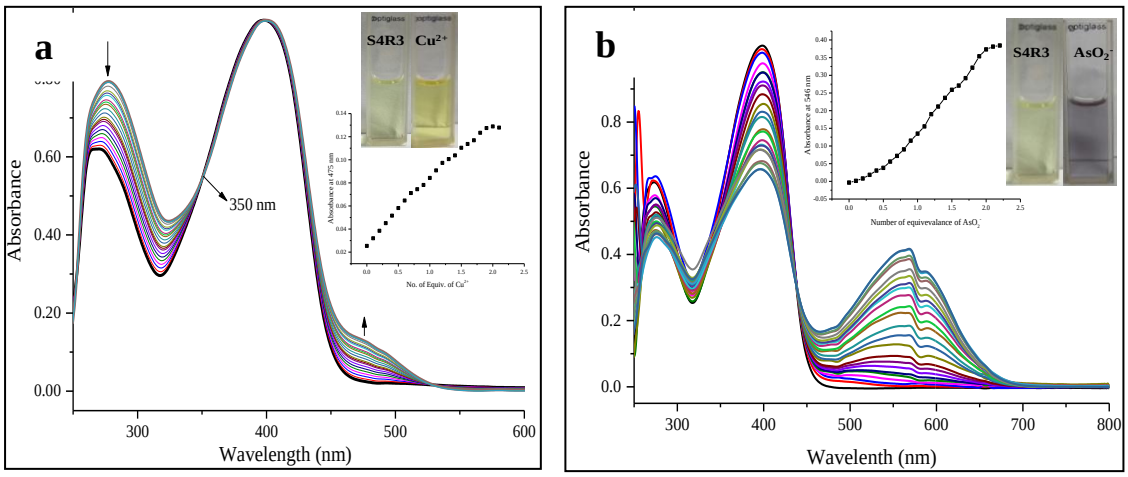

Fig. 5.18: Absorption and naked eye observation of **S4R3 (**2.5×10^{-5} M, DMSO) with the rising amount (0 – 2.5 equiv.) of Cu^{2+} and AsO_2^- ions in water. Inset shows color and absorption changes of the complex at particular wavelengths. **a)**. **S4R3**–Cu^{2+} at 475 nm, **b)**. **S4R3**–AsO_2^- at 564 nm

5.3.3. Binding properties and determination of detection limit (DL)

Based on the UV–Vis titration study results, the 1:1 and 1:2 stoichiometry of the chemosensor and metal ions (R+M) have determined using the Benesi-Hildebrand (B-H) plots **(Fig 5.19**). All the chemosensors (**S4R1–S4R3**) exhibited a good binding constant (k) with that of metal ions, and the results are tabulated in **Table 5.2**. It represents the good stability of the formed complexes. Further, linear calibration plots were drowned between the concentration of metal ions versus UV–Vis response of complex (R+M) to determine the linear range and minimal amount of metal ions using formula given by ICH quality guideline **Q2R1** (Ich 2005) (**Fig. 5.20a-b**). The R^2 values >0.99 indicate the good linear relationship between the obtained response and the concentration of analytes; this helps to get more linear results during quantitative analysis. Further, the chemosensors **S4R1–S4R3** wide linear range, as mentioned in **table 5.2**. The regression analysis data, association constant, and detection limits of metal ions using chemosensors **S4R1–S4R3** by UV–Vis method are tabulated in **table 5.2**.

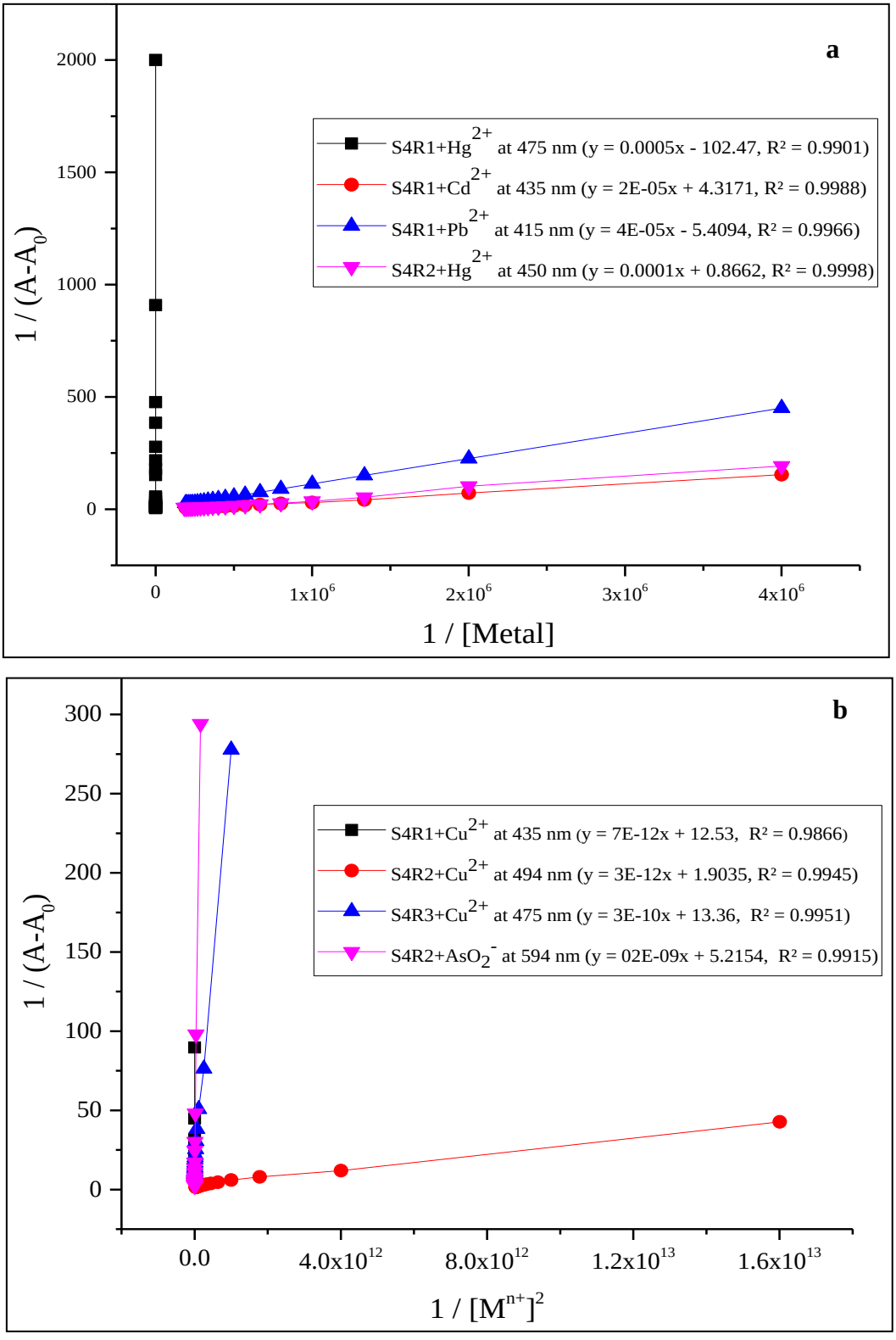

Fig. 5.19: Benesi-Hildebrand (B-H) plot of chemosensor **S4R1–S4R3** binding with metal ions, associated with absorbance change at selective wavelengths **a).** 1:1 and **b).** 1:2 ratio of chemosensor: metal ion

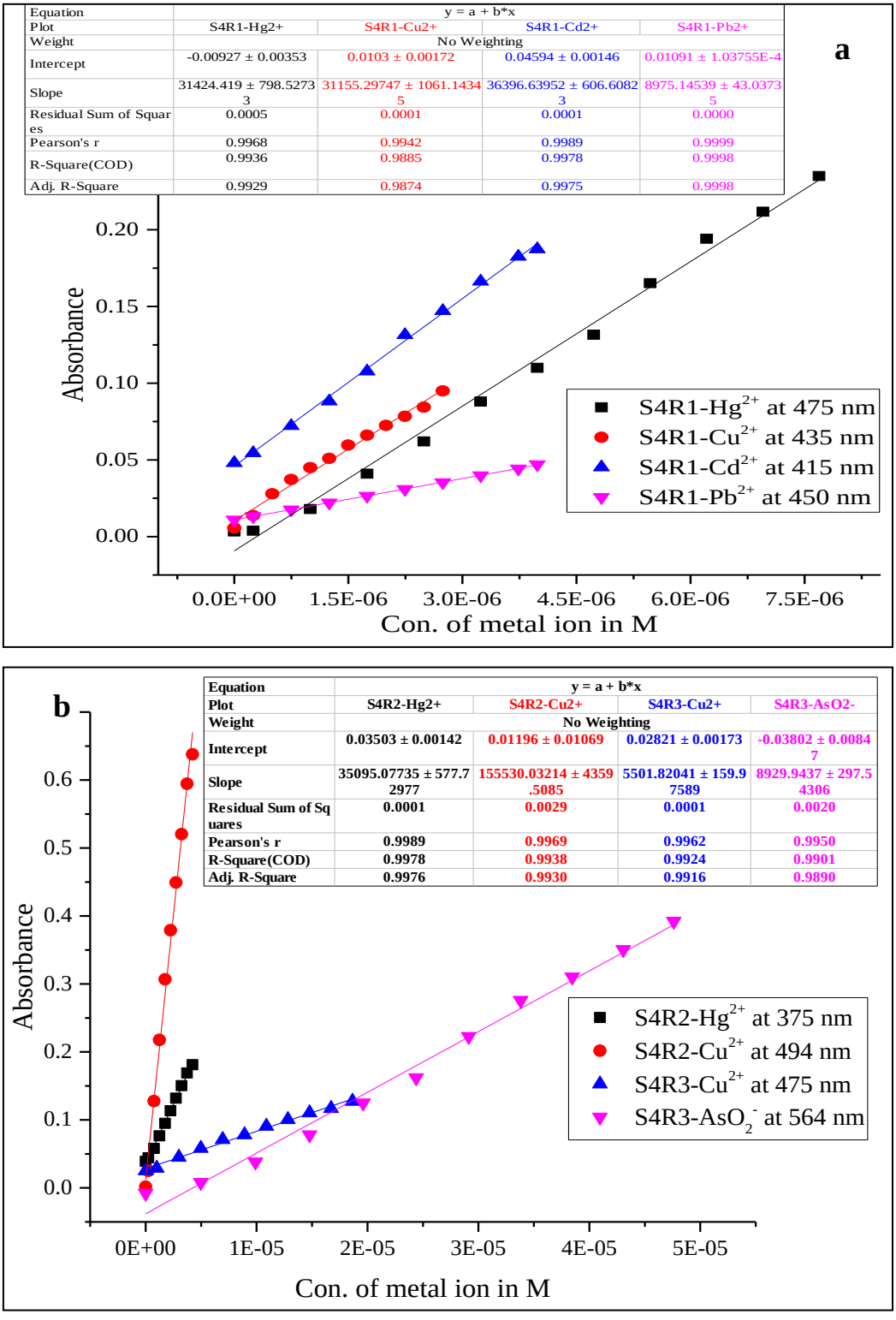

Fig. 5.20: Linear plots between response of complex (chemosensor-metal) verses amount of metal ions in molar. **a). S4R1**–Hg^{2+} vs. Hg^{2+}, **S4R1**–Cu^{2+} vs. Cu^{2+}, **S4R1**–Cd^{2+} vs. Cd^{2+}, **S4R1**–Pb^{2+} vs. Pb^{2+} ions. **b). S4R2**–Hg^{2+} vs. Hg^{2+}, **S4R2**–Cu^{2+} vs. Cu^{2+}, **S4R3**–Cu^{2+} vs. Cu^{2+}, **S4R3**–AsO_2^- vs. AsO_2^- ions

Table 5.2: Regression data, association constant, and DL of metal ions using **S4R1–S4R3** by UV–Vis.

Sensor	Ions	λ (nm)	Association constant(k)	Range (μM)	Intercept (y)/ slope (m)	Sd* of blank (σ)	R^2	DL (ppb)
S4R1	Hg^{2+}	475	$2.7\times10^5\ M^{-1}$	0.0–7.7	–0.00927 / 31424	0.00010	0.9936	2
	Cu^{2+}	435	$1.0\times10^5\ M^{-2}$	0.0–2.7	0.01030/ 31155	0.00172	0.9885	11
	Cd^{2+}	415	$7.5\times10^4\ M^{-1}$	0.0–4.0	0.04594/ 36397	0.00020	0.9978	2
	Pb^{2+}	450	$2.3\times10^4\ M^{-1}$	0.0–4.0	0.01091/ 8975	0.00021	0.9998	14
S4R2	Hg^{2+}	375	$1.2\times10^5\ M^{-1}$	0.0–4.2	0.03503/ 35095	0.00013	0.9978	2
	Cu^{2+}	494	$6.8\times10^4\ M^{-2}$	0.0–4.2	0.01196/ 155530	0.01069	0.9938	13
S4R3	Cu^{2+}	475	$7.3\times10^4\ M^{-2}$	0.0–19	0.02821/ 5502	0.000583	0.9924	20
	As^{3+}	564	$2.0\times10^4\ M^{-2}$	0.0–48	–0.03802 /8930	0.00847	0.9901	213

***Sd -** Standard deviation.

5.3.4. DFT Study of S4R1–S4R3

The Gaussian 09 program package was used for the determined calculations were. Ground state optimization for the chemosensors **S4R1–S4R3** in the gas phase followed by the solvent phase was obtained using the DFT method with B3LYP functional. Metals and anions were optimized using the nonrelativistic effective core potential (ECP) (Häussermann et al. 1993; Peterson 2003) with LanL2DZ (Lee et al. 1988) basis set in combination with 6-31G (d, p)(Hariharan and Pople 1973; Hehre et al. 1972) for C, N, O, S and H atoms. To study the solvent effect on the energy parameters of the molecules self-consistent reaction field with conductor polarizable continuum model (SCRF-CPCM) (Tomasi and Persico 1994) was incorporated and DMSO selected as a solvent medium. Vibrational frequency calculations follow the geometry optimization, and nonattendance of unreal frequency in the computed vibrational spectra confirms the true energy minimum of the geometry optimized. Ground state optimized geometries in gas and solvent phase did not contain any negative vibrational frequency confirming the true energy minimum of the structures.

The excited-state electronic properties of these optimized complexes have also been computed by TD-DFT estimate at the same B3LYP level with the first six excited singlet states that were computed in a solvent medium. The molecular orbital representing HOMO and LUMO of the metal complexes and the chemosensors were visualized using Avogadro software (Hanwell et al. 2012).

Molecular orbitals, especially HOMO and LUMO, play a significant role that governs chemical reactivity (Selvaganapathi et al. 2017). The kinetic stability, chemical hardness, and chemical reactivity are determined by the energy gap between HOMO and LUMO; it further provides an overall understanding of the reaction pathway and molecular activity of the complex. The nodal properties of the complexes studied exhibit a strong orbital delocalization and good orbital overlap possessing a minimal number of nodal planes. These features result in a longer wavelength with a higher value of oscillator strength in the electronic transition spectrum undergoing charge transfer transitions. The energy bandgap between HOMO and LUMO for all the complexes studied varies by the nature of metal ion interaction (El-Shwiniy and Zordok 2018). Chemosensor shows good color change on binding towards Hg^{2+}, Pb^{2+}, Cd^{2+}, As^{3+}, and Cu^{2+}, as discussed earlier.

The HOMO and HOMO–1 are delocalized on the entire molecular network mainly accumulated on the quinolone moiety for the bare chemosensor **S4R1** and **S4R2**, and on nitrofuran moiety for chemosensor **S4R3**. HOMO is concentrated on the metal atom upon binding with the complex, and HOMO–1 is majorly localized on one of the quinolone moiety and partially on the other. The molecular orbital distribution trend observed for the entire metal-bound complex is similar unless otherwise mentioned. LUMO and LUMO+1 of the complex are highly delocalized on the entire molecular network. HOMO contained on the metal atom, and LUMO on the chemosensor molecule suggests that the charge-transfer is happening from the metal center to the ligand, indicating metal to ligand charge transfer. The bandgap energy E_G for the bare chemosensor and the complexes, with their HOMO–LUMO energy value, is provided in the table. The energy bandgap of the metal complex is reduced in comparison with that of the bare chemosensor. The energy value for **S4R1** upon binding with the metal Hg^{2+} and Cu^{2+} shows a bandgap reduction by 0.3 eV and with

Pb^{2+} and Cd^{2+} shows a bandgap value of 1.724 eV and 2.071 eV highly reduced in comparison with the bare chemosensor showing a value of 2.727 eV. Molecular orbitals of copper bound **S4R2** shows a similar pattern with that of S4R1, except that HOMO is concentrated on copper and a small fragmental electron cloud over the quinoline moiety as shown in **Fig**. **5.21-5.26.** The energy band gap values of the Hg^{2+} and Cu^{2+} complex exhibit a bandgap value of 2.394 eV and 1.95 eV in comparison with the chemosensor possessing a bandgap of value 3.9 eV. Molecular orbitals of arsenic bound chemosensor **S4R3** shows a complete delocalization of HOMO and LUMO, as shown in **Fig. 5.27–5.28,** the linear structure of the chemosensor is sterically hindered upon complex formation. The bandgap energy of chemosensor **S4R3** shows a value of 2.908 eV and, upon binding with arsenic, predicts a value of 2.671 eV and 1.603 eV for copper. The value of HOMO for the arsenic bound complex hikes to a value of –6.682 eV with that of the **S4R3,** whose HOMO is –6.465 eV. The HOMO, LUMO, and E_G values are depicted in **table-5.3**.

TD-DFT calculations were computed on chemosensors and anion bound complex to superior value the excited state properties of the system and to arrive at theoretical absorption spectra. The graph providing the oscillator strength versus the excitation wavelength for all the chemosensors and complexes is provided in the supplementary. TDDFT exhibited a redshift in the excitation wavelength for most of the complexes, in comparison with that of the bare chemosensor, but unable to reproduce the experimental results accurately.

Table 5.3: Molecular orbital energy levels for chemosensor (**S4R1–S4R3**) and its complexes

	HOMO–1 (eV)	**HOMO (eV)**	**LUMO (eV)**	**LUMO+1 (eV)**	**E_G (eV)**
S4R1	–5.990	–5.097	–2.370	–2.059	2.727
S4R2	–6.429	–6.168	–2.268	–1.949	3.900
S4R3	–6.932	–6.465	–3.557	–3.382	2.908
S4R1+Hg^{2+}	–5.726	–4.598	–2.182	–1.900	2.416
S4R1+Cu^{2+}	–5.726	–4.598	–2.182	–1.900	2.416
S4R1+Cd^{2+}	–5.735	–4.263	–2.192	–1.913	2.071

S4R1+Pb^{2+}	–5.597	–3.818	–2.094	–1.300	1.724
S4R2+Hg^{2+}	–6.051	–4.551	–2.157	–1.915	2.394
S4R2+Cu^{2+}	–5.214	–4.290	–2.340	–2.396	1.950
S4R3+AsO_2^-	–6.877	–6.682	–4.011	–3.809	2.671
S4R3+Cu^{2+}	–6.022	–5.054	–3.451	–3.178	1.603

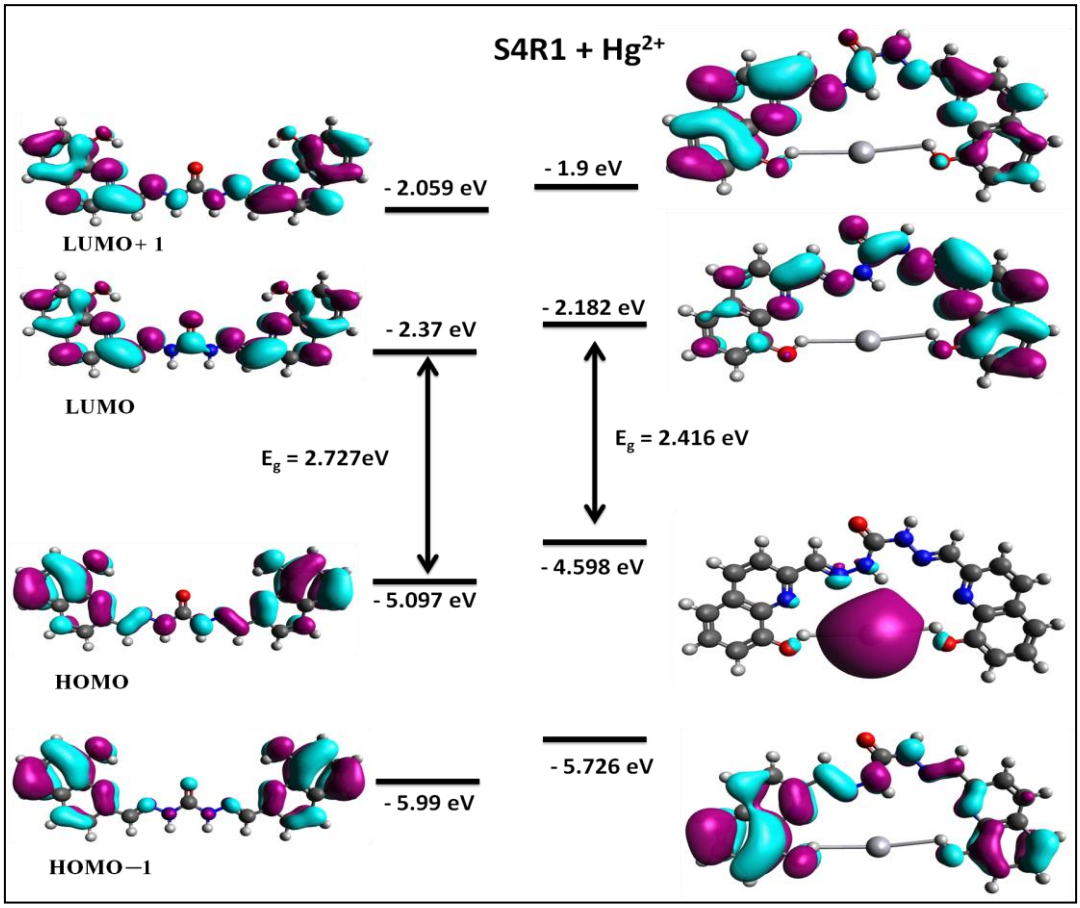

Fig. 5.21: Illustration of calculated HOMO and LUMO molecular orbitals for chemosensors **S4R1** and **S4R1**–Hg^{2+} complex

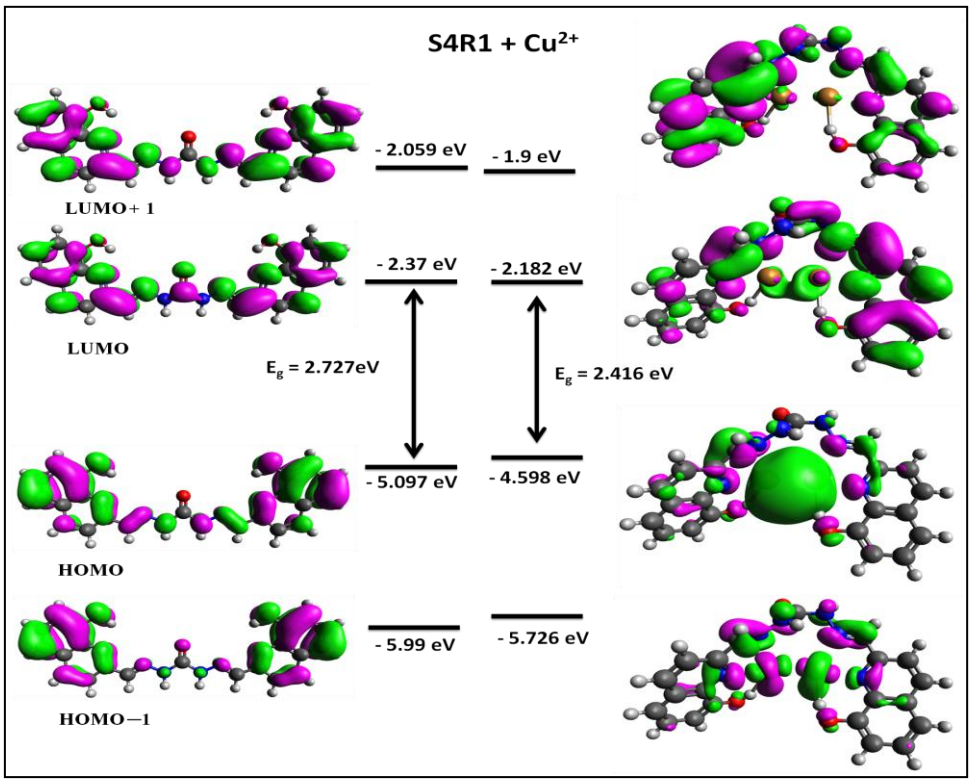

Fig. 5.22: Illustration of calculated HOMO and LUMO molecular orbitals for chemosensors **S4R1** and **S4R1**–Cu^{2+} complex

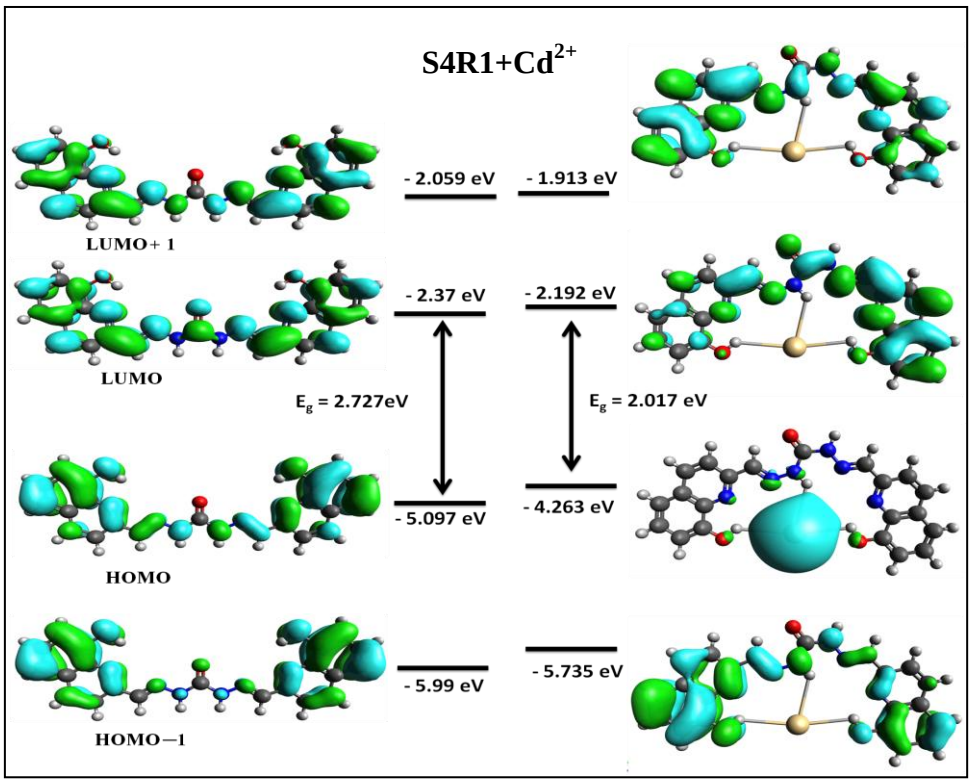

Fig. 5.23: Illustration of calculated HOMO and LUMO molecular orbitals for chemosensors **S4R1** and **S4R1**–Cd^{2+} complex

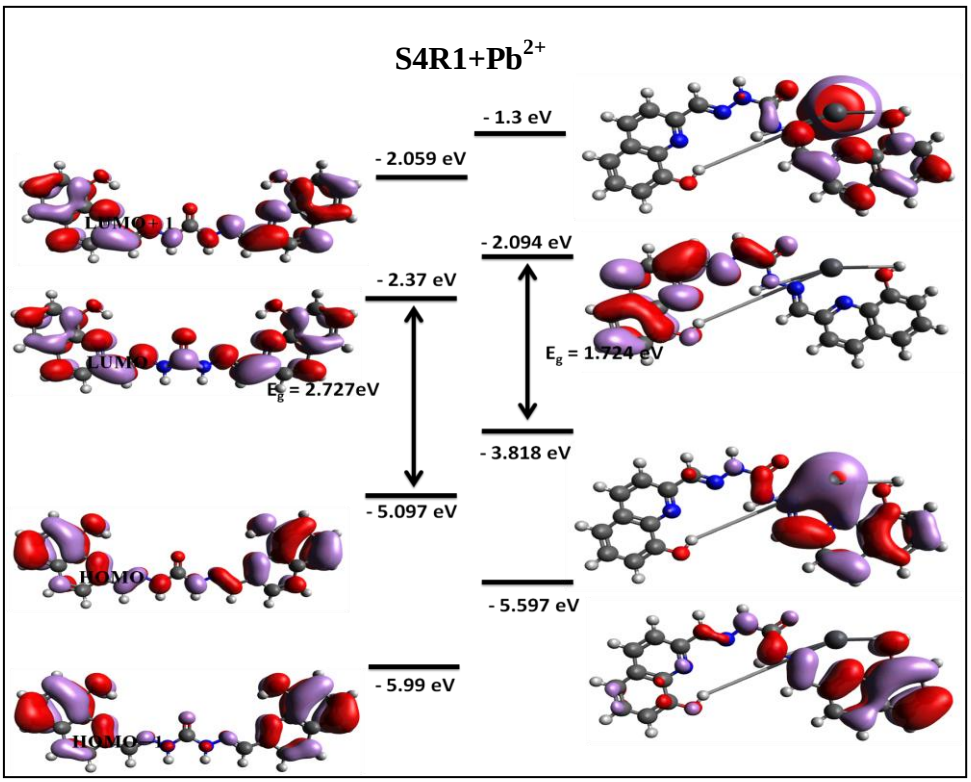

Fig. 5.24: Illustration of calculated HOMO and LUMO molecular orbitals for chemosensors **S4R1** and **S4R1**–Pb^{2+} complex

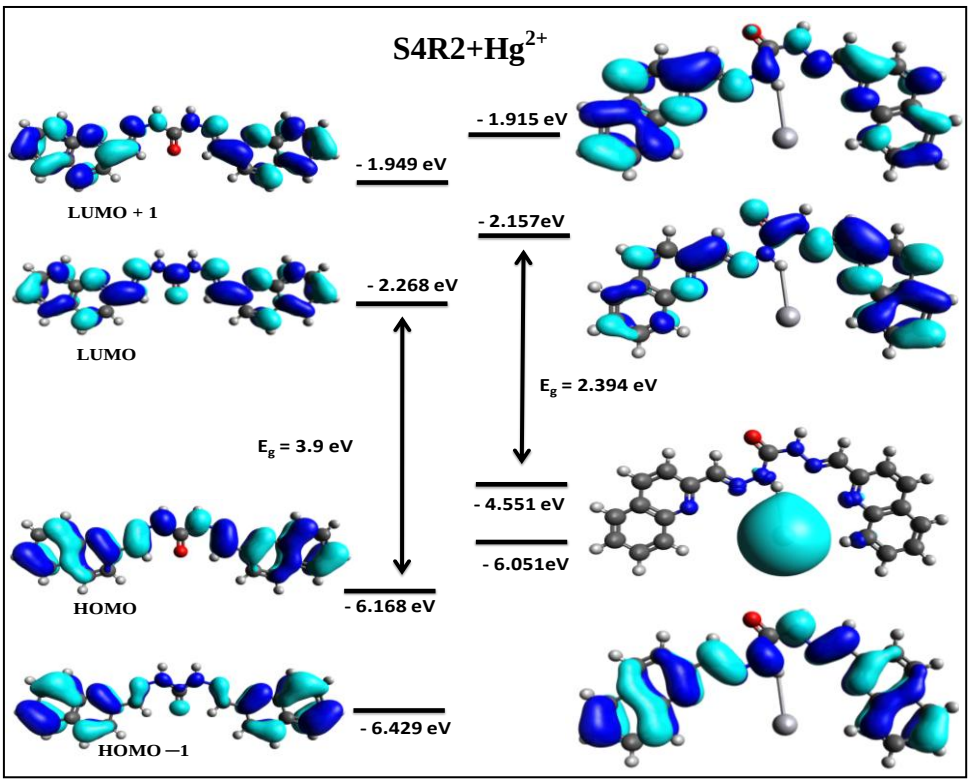

Fig. 5.25: Illustration of calculated HOMO and LUMO molecular orbitals for chemosensors **S4R2** and **S4R2**–Hg^{2+} complex

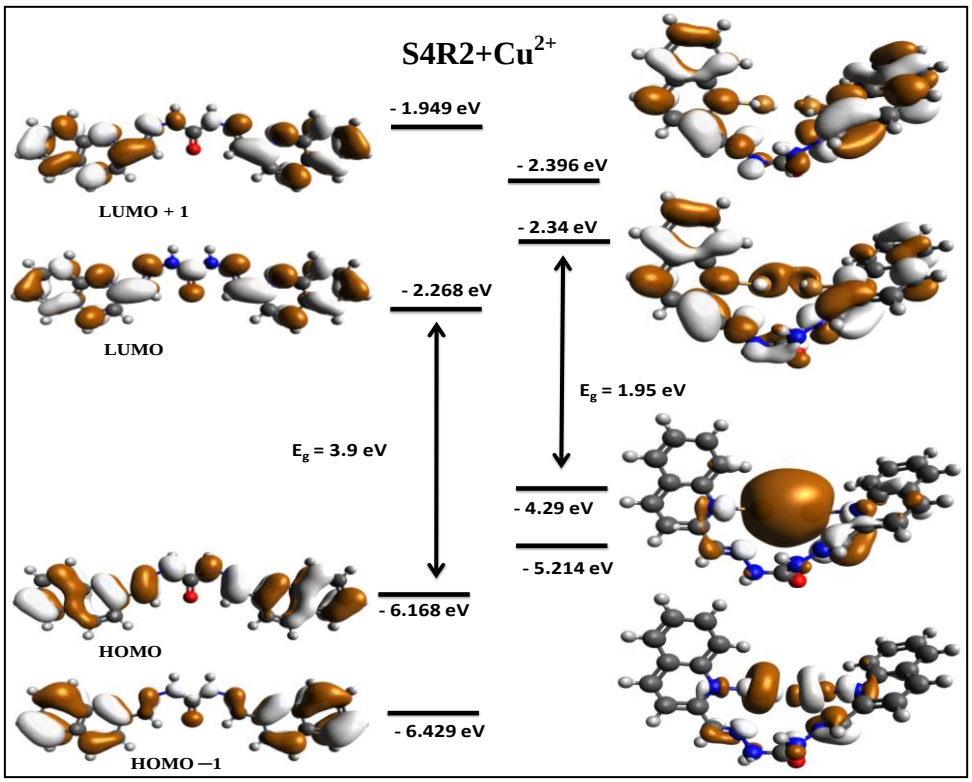

Fig. 5.26: Illustration of calculated HOMO and LUMO molecular orbitals for chemosensors **S4R2** and **S4R2**–Cu^{2+} complex

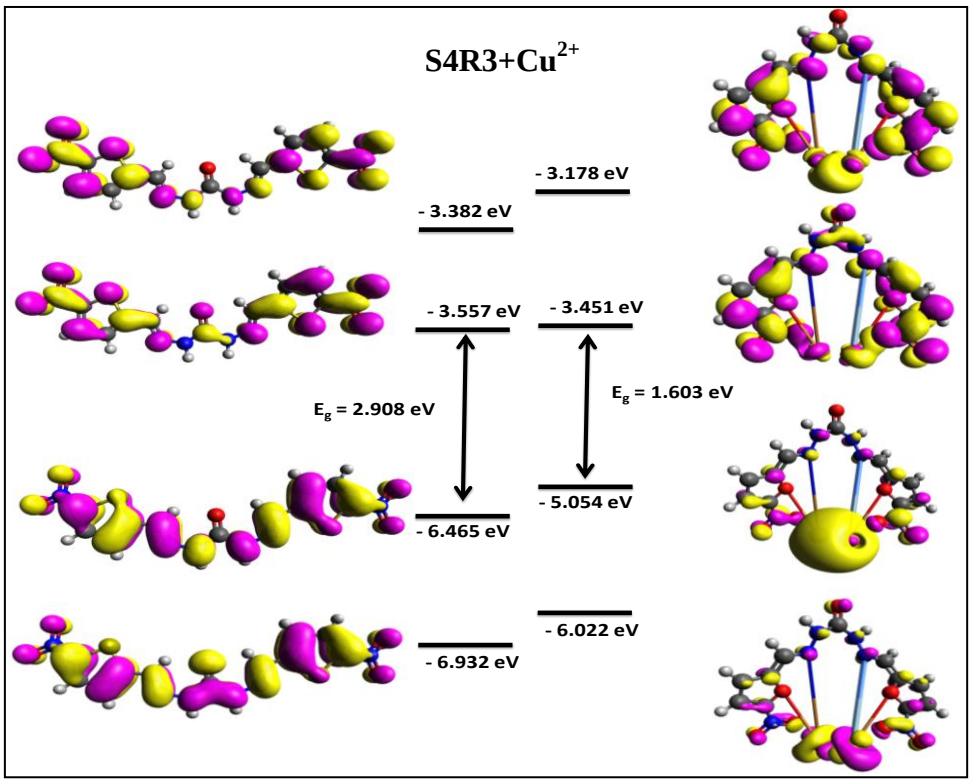

Fig. 5.27: Illustration of calculated HOMO and LUMO molecular orbitals for chemosensors **S4R3** and **S4R3**–Cu^{2+} complex

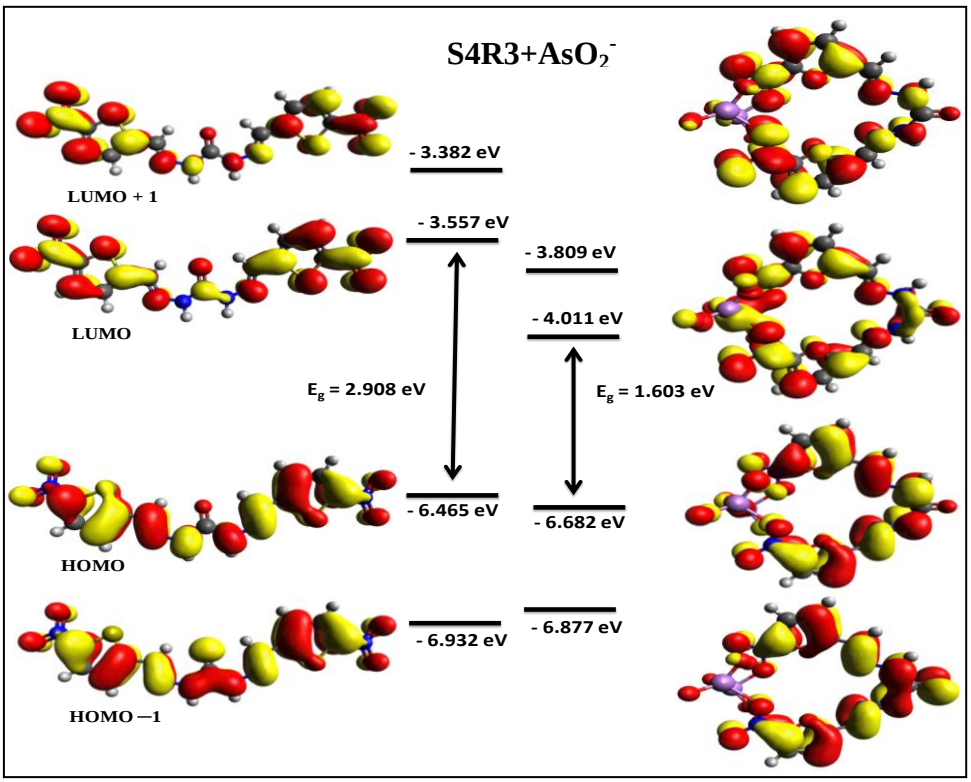

Fig. 5.28: Illustration of calculated HOMO and LUMO molecular orbitals for chemosensors **S4R3** and **S4R3**–AsO_2^- complex

5.3.5. Proposed binding interaction between metal ions and chemosensors

From the UV-Vis spectrum, it is observed that decreasing the intensity of chemosensor **S4R1** at 340 nm and appearance of new bands at 435 nm, 415 nm, 450 nm upon binding with metal ions (Hg^{2+}, Cu^{2+}, Pb^{2+}, and Cd^{2+}), this may due to interaction of imine nitrogen, hydroxy (–OH), nitrogen present in the quinoline ring with the metal ions. Having like these more active binding sites in the molecular structure of **S4R1** is responsible for multi-metal ion sensing. The B-H plot confirms the 1:1 (**S4R1: M)** stoichiometry for S4R1–Hg^{2+}, S4R1–Pb^{2+}, S4R1–Cd^{2+} and 1:2 for S4R1–Cu^{2+} ions. The **S4R2** exhibits decreasing the absorbance of the band at 335 nm, and new bands appear at 375 nm, 494 nm, with the addition of Cu^{2+} and Hg^{2+} ions to the **S4R2.** These spectral changes (Red-shift) or may be due to the interaction of imine nitrogen and nitrogen having in the quinoline ring. **S4R2** exhibits 1:1 (**S4R2: M**) stoichiometry for Hg^{2+} ions and 1:2 for Cu^{2+} ions. Addition of Cu^{2+} and AsO_2^- ions the **S4R3** exhibits red-shift in the absorption spectrum; this may be due to the

interaction of imine nitrogen and furfural ring. **S4R3** exhibits 1:2 (**S4R3: M**) stoichiometries for Cu^{2+} and AsO_2^- ions.

This discriminating complexation and recognition of metal ions rationalized in principle like HSAB theory (Pearson 1963). The chemosensor **S4R1** has a hard group (–OH) and soft groups (HC=N–, pyridine ring) in its structure, maybe due to the presence of these two different base functionalities (soft and hard), **S4R1** exhibits sensitive to borderline (Cu^{2+}) and soft metals (Hg^{2+}, Cd^{2+}, Pb^{2+}). Whereas in the case of **S4R2**, the hard group (–OH) is absent, maybe due to this reason, it exhibits activity towards only Hg^{2+} and Cu^{2+} ions. In the case of chemosensor **S4R3**, the nitro-furfural group in its molecular structure has introduced; due to this, it exhibits activity towards Cu^{2+} and AsO_2^- ions.

The binding interaction between the chemosensor and different metal ions also confirmed by the FT-IR and mass analysis of free chemosensor and their complexes. When compared the FT-IR spectrum of **S4R1** with that of chemosensor–metal complexes (**S4R1**–Hg^{2+}, **S4R1**–Cu^{2+}, **S4R1**–Cd^{2+} and **S4R1**–Pb^{2+}), some significant changes were found in the vibration frequencies of hydroxy (–OH), imine (–C=N), carbonyl (–C=O) and C–N functional groups of the chemosensor **S4R1,** upon complexation with metal ions **(Fig. 5.29)**. It suggests these groups of **S4R1** involved in binding with the metal ions. Particularly, imine, hydroxy peak intensity decreased, and broadening of peaks was observed upon complexation with Hg^{2+}, Cu^{2+}, Cd^{2+}, and Pb^{2+} ions. Similarly, changes were found when compared the free **S4R2** with that of Hg^{2+} and Cu^{2+} complexes **(Fig 5.30)**. The vibration peak of imine and carbonyl intensity almost diminished in complex FT-IR spectra of **S4R2**–Hg^{2+}, **S4R2**–Cu^{2+}, it gives the significant role of these functional groups in the binding with the metal ions. The chemosensor **S4R3** exhibits similar changes in the FT-IR spectrum for the imine, –C–N, and carbonyl groups with the complexation of Cu^{2+} ions **(Fig. 5.31)**. Whereas, when **S4R3** binds with the AsO_2^- ions, a specific change was identified in the –C–O str. frequency of **S4R3,** and there were no significant changes in the imine, carbonyl and –C–N frequencies **(Fig. 5.31)**. It indicates that the AsO_2^- ions interact with the oxygen of furfural moiety.

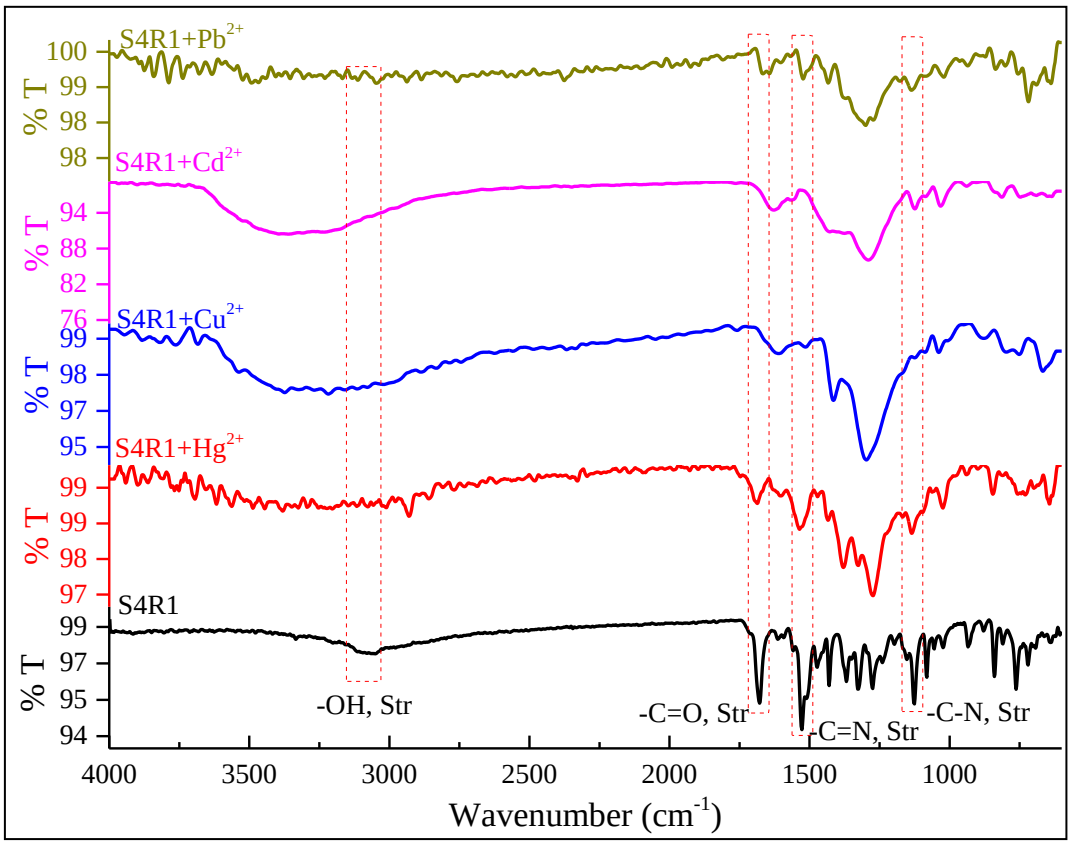

Fig. 5.29: FT-IR spectra of **S4R1** and their complexes

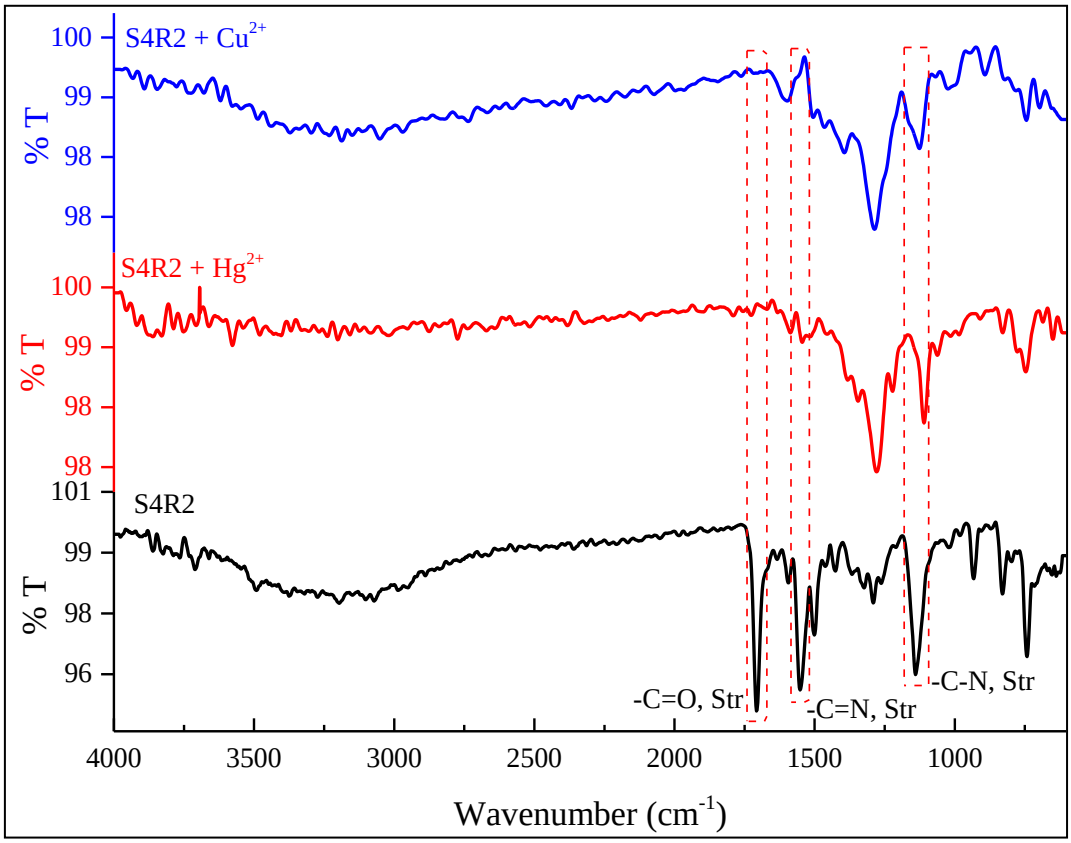

Fig. 5.30: FT-IR spectra of **S4R2**, **S4R2**–Hg^{2+} and **S4R2**–Cu^{2+} complexes

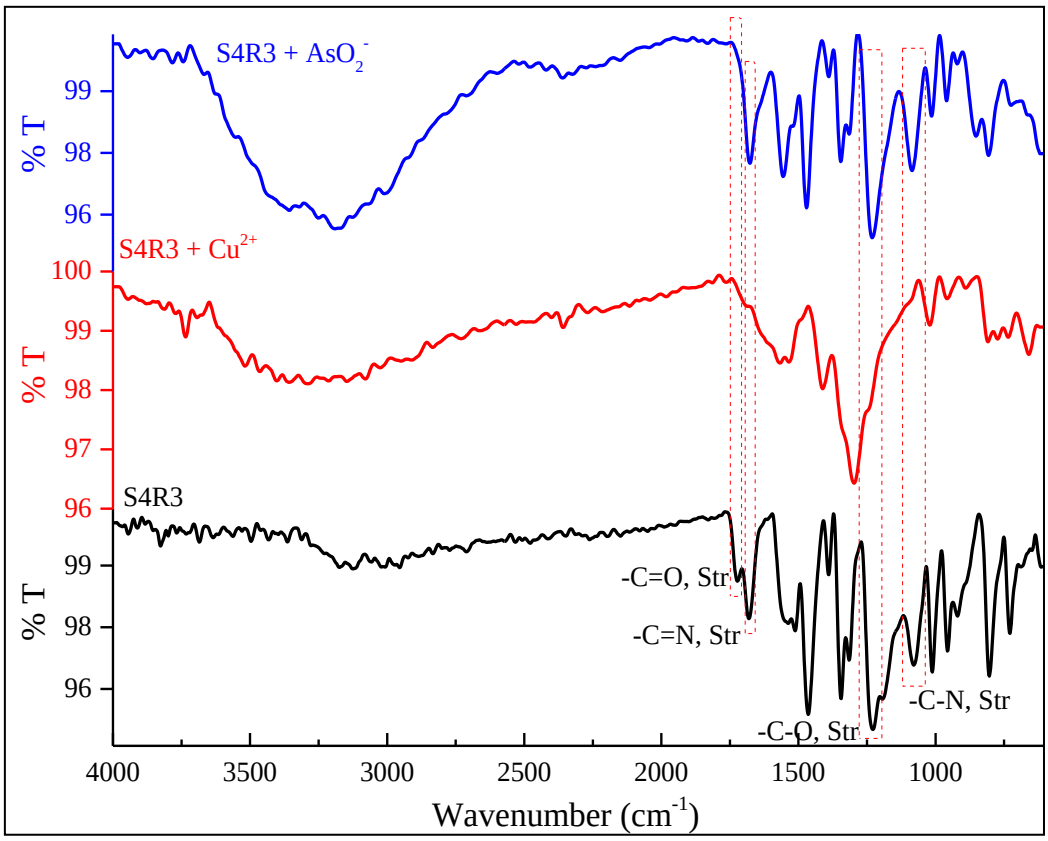

Fig. 5.31: FT-IR spectra of **S4R3**, **S4R3**–Cu^{2+} and **S4R3**–AsO_2^- complexes

Direct evidence was found from the mass analysis of chemosensor-complexes **(Fig. 5.32-5.34)**. From the mass spectra of **S4R1** complexes, the mass peak at m/z 601.70 (M+1) for **S4R1**–Hg^{2+}, m/z at 513.60 (M+1) for **S4R1**–Cd^{2+} and m/z at 608.50 (M+1) for **S4R1**–Pb^{2+} represents the for formation of 1:1 ration of chemosensor and metal ions complex **(Fig. 5.32a, 5.32c, and 5.32d)**, like **S4R1**–Hg^{2+}, the chemosensor **S4R2** forms 1:1 ratio complex with Hg^{2+} ions, it was identified from the mass peak at m/z 569.70 (M+1) for the **S4R2**–Hg^{2+}complex **(Fig. 5.33a).** The chemosensors **S4R1–S4R3** exhibits 1:2 ratios of chemosensor and Cu^{2+}ions, it was confirmed by the mass peaks at m/z 527.90 (M+1) **(Fig. 5.32b)** for **S4R1**–Cu^{2+}, m/z at 956.60 (M+1) for **S4R2**–Cu^{2+} **(Fig. 5.33b)** and 464.40 (M+1) **S4R3**–Cu^{2+} ions **(Fig. 5.34a)**. Similarly, the chemosensor **S4R3** also binds 1:2 ratio of chemosensor, and AsO_2^- ion, was confirmed by the mass peak at m/z 551.07 (M+1) for **S4R3**–AsO_2^- complex as depicted in the **Fig. 5.34b.**

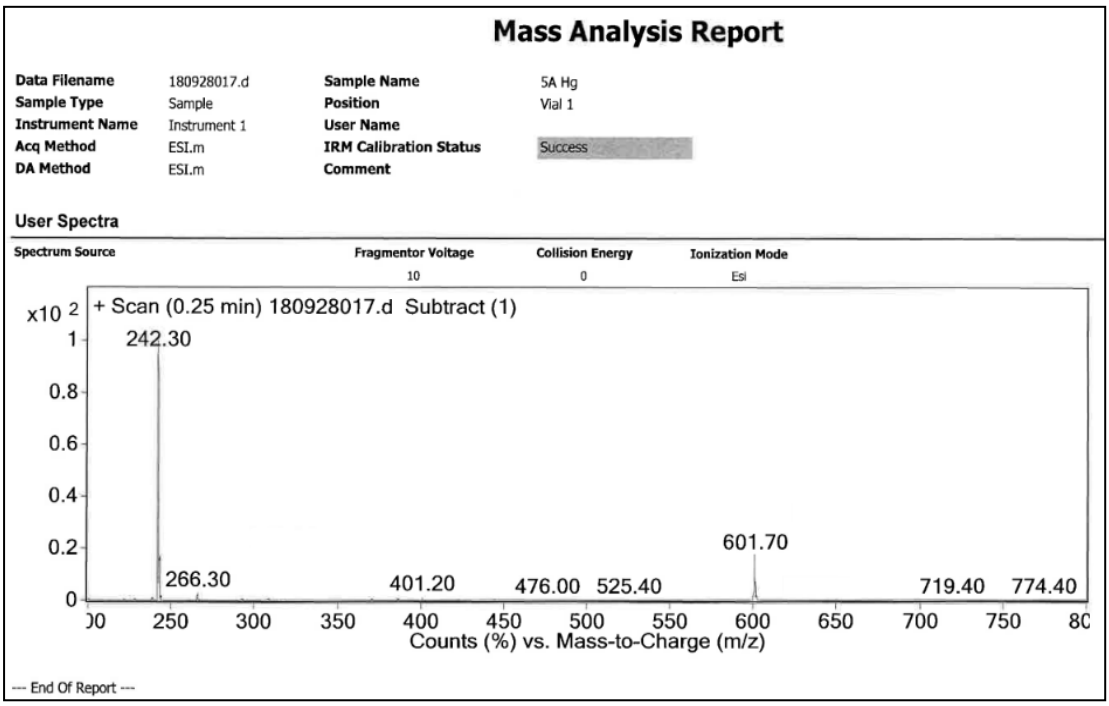

Fig. 5.32a: ESI-mass spectrum of **S4R1**–Hg^{2+} complexes

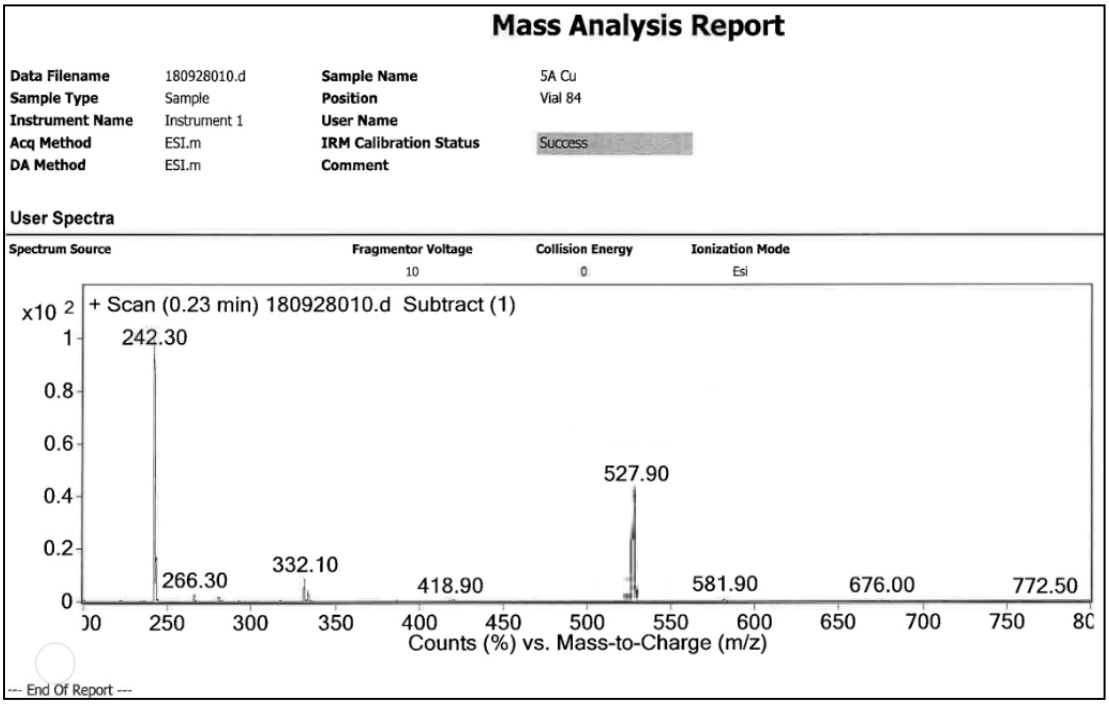

Fig. 5.32b: ESI-mass spectrum of **S4R1**–Cu^{2+} complexes

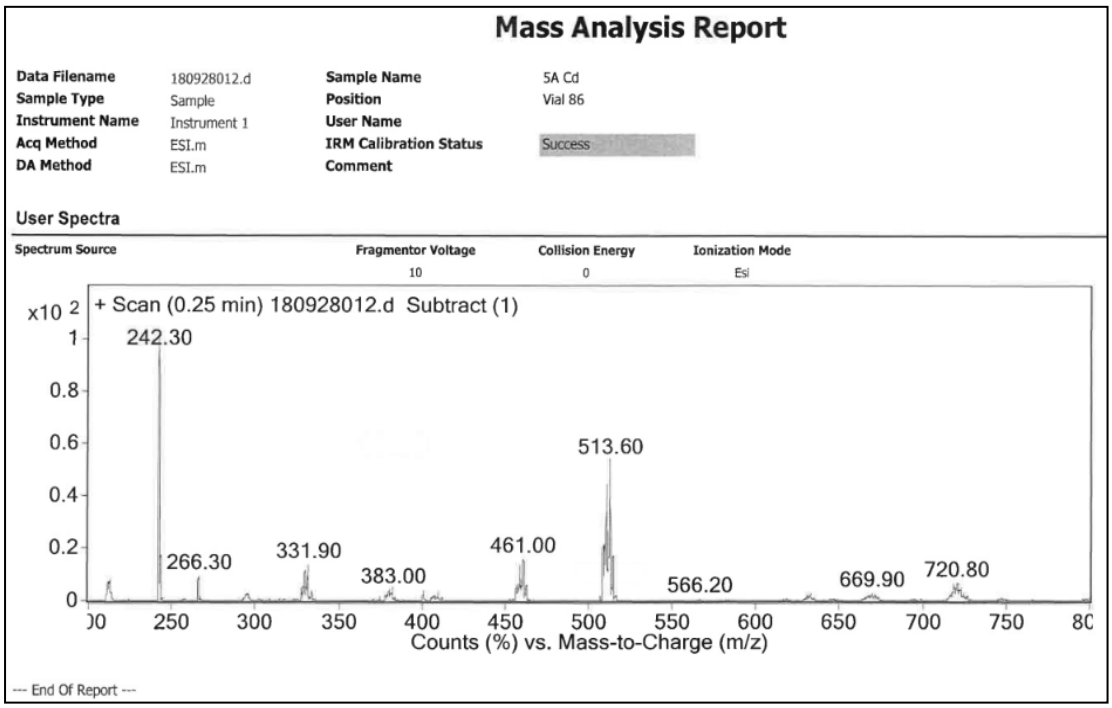

Fig. 5.32c: ESI-mass spectrum of **S4R1**–Cd^{2+} complexes

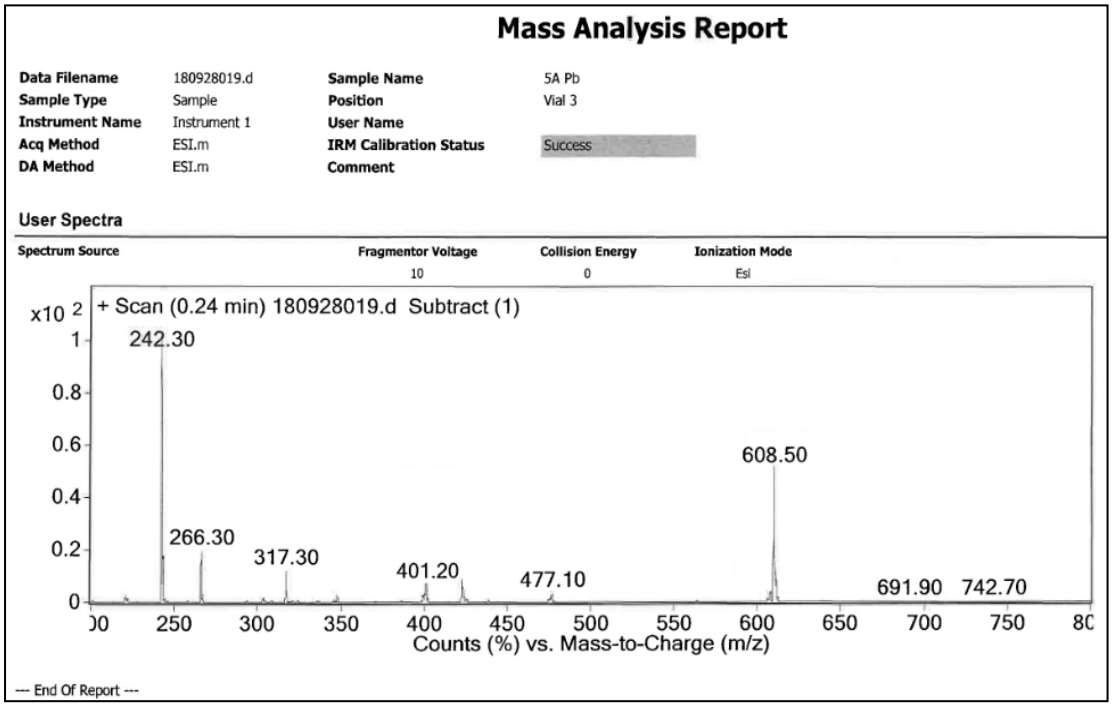

Fig. 5.32d: ESI-mass spectrum of **S4R1**–Pb^{2+} complexes

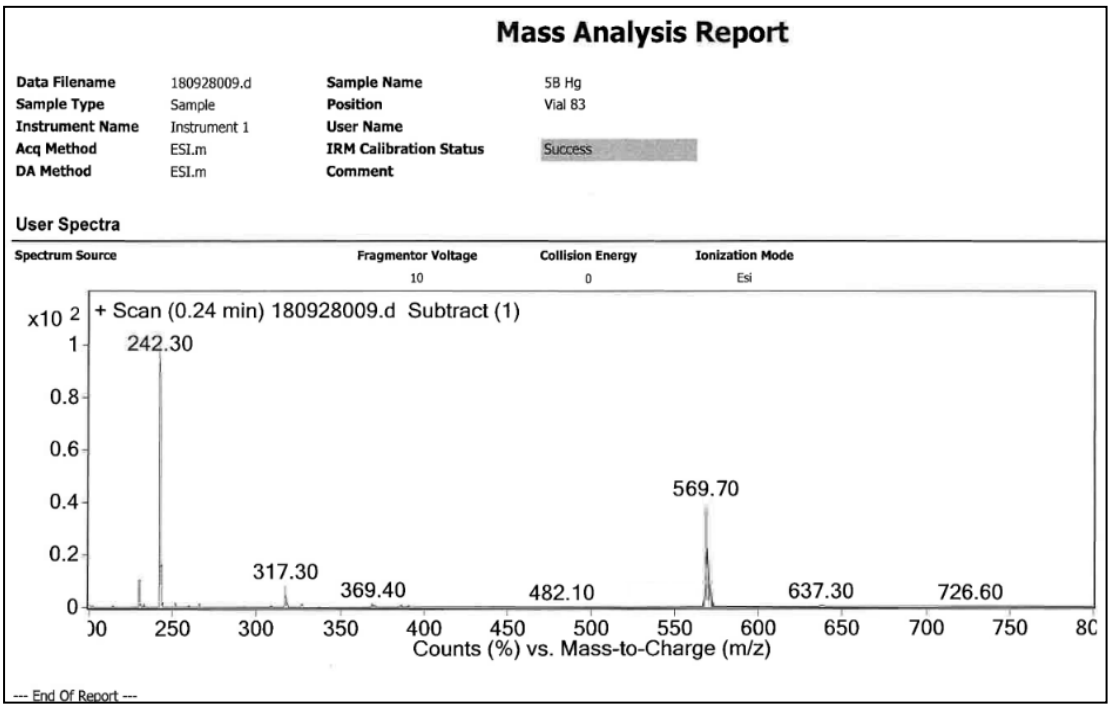

Fig. 5.33a: ESI-mass spectrum of **S4R2**–Hg^{2+} complexes

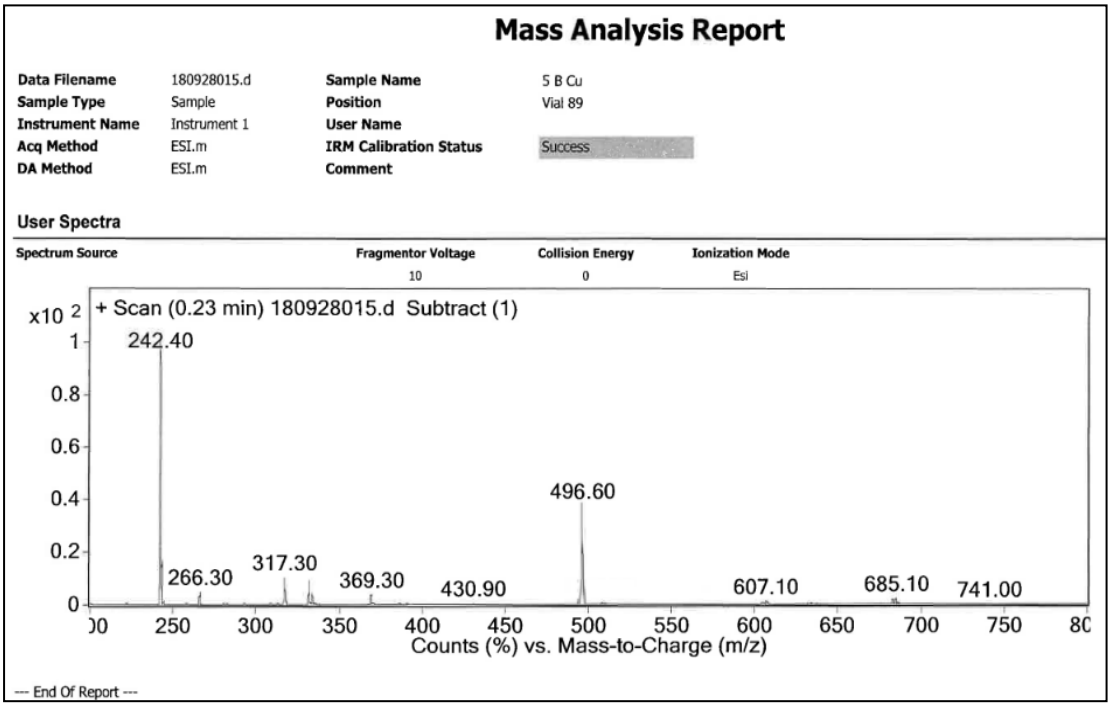

Fig. 5.33b: ESI-mass spectrum of **S4R2**–Cu^{2+} complexes

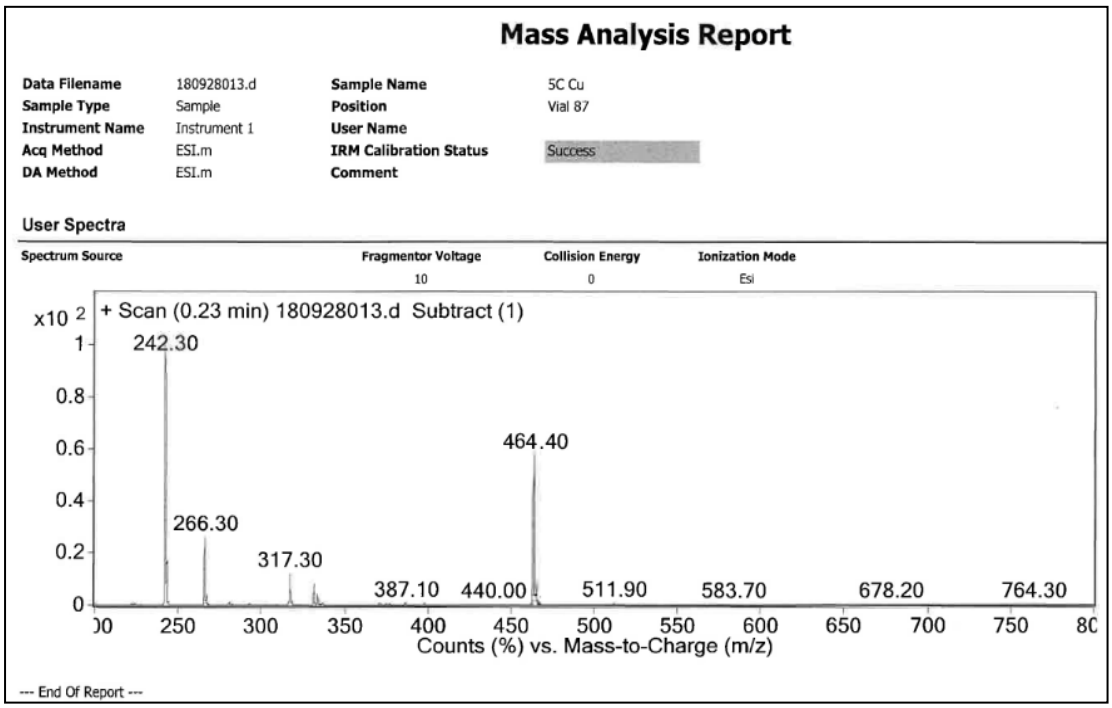

Fig. 5.34a: ESI-mass spectrum of **S4R3**–Cu^{2+} complexes

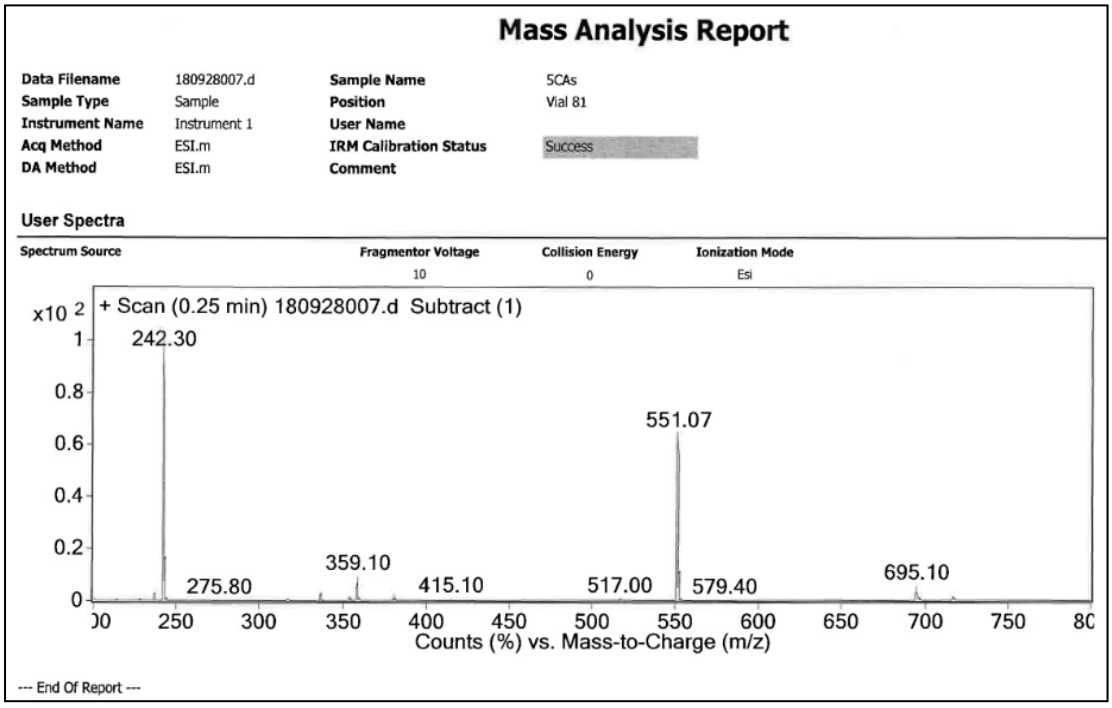

Fig. 5.34b: ESI-mass spectrum of **S4R3**–AsO_2^- complexes

Further, the theoretical DFT calculation results were compared with the practical investigational data; a good correlation was found among them as discoursed in the above DFT section. **Fig. 5.35** represents the binding interaction among **S4R1–S4R3** with different metal ions.

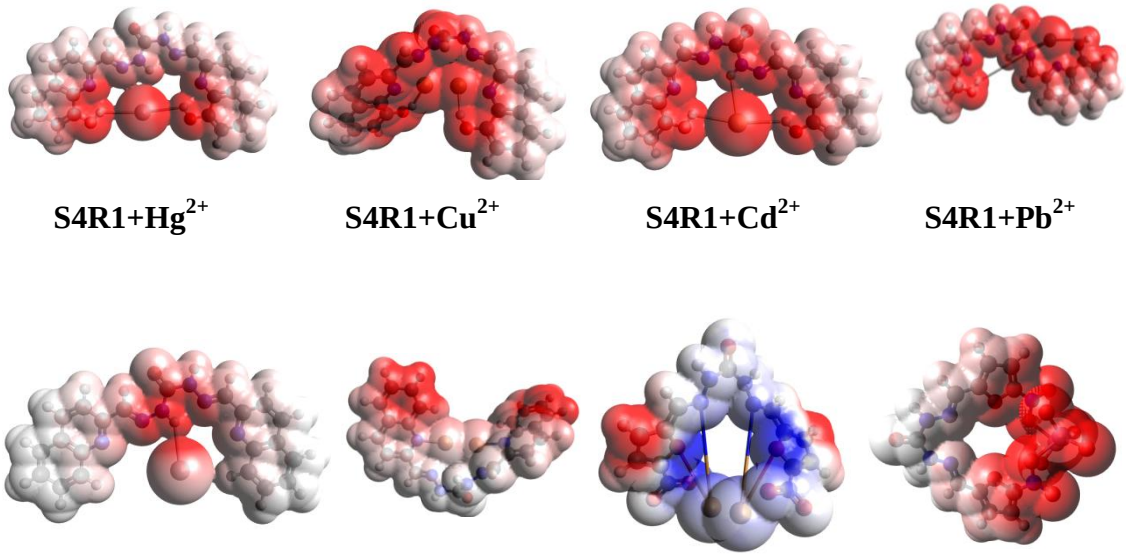

Fig. 5.35: Proposed interaction among **S4R1–SR3** and different metal ions

5.3.6. Test strip application

The chemosensors **S4R1–S4R3** exhibit good color change and sensitivity towards heavy metal ions. Because of this, a practical application using a simple test strip method for the determination of heavy metal ions have demonstrated. The chemosensors **S4R1–S4R3** (1×10^{-3} M) were prepared in DMSO solution and immersed the Whatman filter paper (1cm width, 4 cm height) for about 30 min, then dried the filter paper at room temperature. 2 ppm of Pb^{2+}, Hg^{2+}, Cd^{2+}, Cu^{2+}, and AsO_2^- ions were prepared in the de-ionized water. About 10 µL of each solution was added to the individual test strips (previously dipped and dried) and dried in the air. Upon the addition of heavy metal solution, a good color change was observed as depicted in **Fig. 5.36**. This result confirms the potential application of developed chemosensors **S5R1–S4R3** for the detection of heavy metal ions by the simple naked eye.

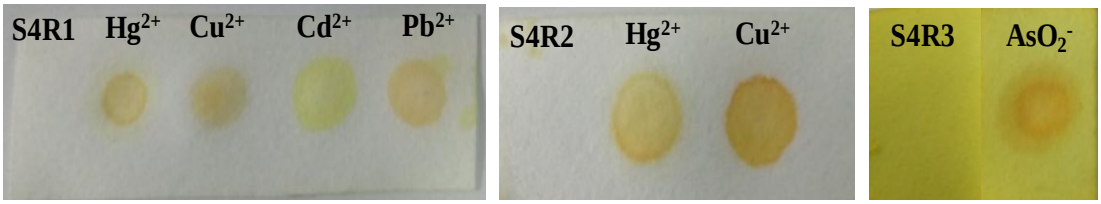

Fig. 5.36: Test strip application of **S4R1–S4R3** for the detection of heavy metal ions

5.4. Conclusions

To conclude, three carbohydrazide based colorimetric sensors **S4R1–S4R3** to sense the Pb^{2+}, Hg^{2+}, Cd^{2+}, Cu^{2+}, and AsO_2^- ions selectively over the other competitive metals have covered in this chapter. Amongst the reported chemosensor, **S4R1** gave multi-color change in the presence of Pb^{2+}, Hg^{2+}, Cd^{2+} and Cu^{2+} ions in water and exhibits minimal detection amount at ppb levels. This multi-ion selectivity was recognized owing to the existence of multiple binding sites in its structure (imine, (–C=N), hydroxy (–OH), and quinoline nitrogen (–C=N)) in comparison with other chemosensors (i.c S4R2 and S4R3). The **S4R1** has a preference in binding with Hg^{2+} ions than other selective metal ions (Cu^{2+}, Cd^{2+}, and Pb^{2+}). The **S4R2** has shown a dual colorimetric signal for Hg^{2+} and Cu^{2+} ions with a good linear range and detection limit at ppb levels. The **S4R3**, in particular, binds with Cu^{2+} and AsO_2^- ions, and it exhibited a detection limit at ppb levels. Strong association constant and good linear range with detection limit at ppb levels signifies the potential applications of the presently developed chemosensors (**S4R1–S4R3**).

In comparison with the reported three chemosensors, **S4R1** sowed superior selectivity for multi-analytes such as Hg^{2+}, Pb^{2+}, Cd^{2+}, and Cu^{2+} ions. Whereas the **S4R2** and **S4R3** did not show any activity towards Cd^{2+} and Pb^{2+} like **S4R1**, this might be due to not have hydroxy (–OH) group in their molecular structure. Further, the experimental results were well coordinated with the calculated theoretical DFT results. Among the reported chemosensors, the **S4R1** has a low detection limit for Hg^{2+} ions than compare to other chemosensors. The naked eye responses, good linear range, and detection limit at ppb levels of reported chemosensors **S4R1–S4R3** for selective metal ions indicates that the quantitative and qualitative application in the field of colorimetric chemosensors.

CHAPTER-6

SIMPLE COLORIMETRIC RESPONSE FOR ARSENATE, ARSENITE, Cu^{2+} AND Hg^{2+} IONS: SYNTHESIS, SPECTRAL RESPONSE and TEST STRIP APPLICATION

CHAPTER-6

6. SIMPLE COLORIMETRIC RESPONSE FOR ARSENATE, ARSENITE, Cu^{2+} AND Hg^{2+} IONS: SYNTHESIS, SPECTRAL RESPONSE AND TEST STRIPS APPLICATION

Abstract

In this chapter, the design, syntheses, and characterization of new diaminomaleonitrile derivatives as a colorimetric chemosensor for Hg^{2+}, Cu^{2+}, AsO_2^- and AsO_4^{2-} ion have included. The colorimetric cation recognition properties, detection mechanism, and test strips application have discussed in detail.

6.1. Introduction

Cations are imperative in the wide range of biological and chemical systems. Different hard work has been put to produce a several chemosensors for the detection of cations species since few decades (Bansod et al. 2017; Chauhan et al. 2017; Das and Sarkar 2016; Ganesabaskaran and Kandasamy 2015; Kundu et al. 2015; SIRAWATCHARIN et al. 2014; Udhayakumari et al. 2014; Yadav and Singh 2016; Z and K 2009; Zhang et al. 2017)(Hu et al. 2015; Kaur et al. 2018; Yin et al. 2018). Molecular recognition is one of the most important areas and is related to ionic (cation/anion) or neutral species in the field of supramolecular chemistry. The ion detection achieved through the selective attraction between the chemosensor molecule (host) and metal ions (guest) via supramolecular interactions results from a chemosensor metal (host-guest) complex. Formally, colorimetric chemosensing method is a capable method allowing qualitative, quantitative application of environmental pollutants and toxic ions, like Hg^{2+}, Cd^{2+}, Pb^{2+}, Cu^{2+}, arsenate, and arsenite, without any advanced instrumentation techniques like, inductively coupled plasma optical emission spectrometry (ICP-OES), inductively coupled plasma mass spectrometry (ICP-MS) and Atomic absorption spectroscopy (AAS) (Michon et al. 2007; Ronkart et al. 2007; Tuzen et al. 2010; Xiong et al. 2010). Colorimetric chemosensors offer numerous advantages than other instrumental methods. Such as, test kit application for on-site detection, quick naked-eye detection, selectivity/simplicity (do not require any pre-treatment of the sample), cost-effective

and they are non-destructive (Fegade et al. 2014; Gattás-Asfura and Leblanc 2003; Hong et al. 2007; Kato et al. 1990; Kim et al. 2012; Küpper and Schultze 1997; Yin et al. 2010), these advantages make an attractive technique among the investigators.

The most serious form of environmental contamination is encountered nowadays by metal pollution in water and soil, which has several adverse effects on living organisms, especially humans and animals. The arsenic and mercury metals are highly toxic relative to the other heavy metals like Cd^{2+}, $Pb^{2+}$and Cr^{3+}. Many reports are available in the literature regarding the toxicity, environmental, and comprehensive public health worry linked with environmental pollution by these heavy metal ions have been addressed in the literature (He et al. 2005; Sarkar 2002; Stevens et al. 1990; Tchounwou et al. 2012).

Arsenic is a metalloid element and can exist in 4 different oxidation states (–3, 0, +3 & +5), the arsenic enters into the environment by the various chemical industries such as pesticide production, metal, and alloy manufacturing, wood treatments and petroleum refining, these arsenic compounds can be found in rock, soil, water and air (Karlsson et al. 2014). Generally, the organic form of arsenic and an inorganic form of arsenic can be found in the water and usually appears as oxyanions (Hughes et al. 2011; Sharma and Sohn 2009; Smedley and Kinniburgh 2002). Generally, arsenic co-occur as arsenite / As^{3+}, arsenate/ As^{5+} in environmental water system, undergoes reciprocal conversion in groundwater, these are highly toxic and can result in several adverse health effects like dermatitis, skin, renal, lung, liver cancers (Choong et al. 2007; Hughes et al. 2011; Sharma and Sohn 2009; Smedley and Kinniburgh 2002). Accordingly, surveillance of arsenic (in the inorganic form) in the environmental water system is significant in high arsenic contamination areas. Similarly, mercury is taken as extremely dangerous, poisonous, and easily it can be changed into a mainly toxic form like CH_3-Hg. Due to the various human activities and later bioaccumulates via the food chain and tend to spread in the environment system widely. Therefore, the selective/sensitive chemosensor for mercury ions is of enormous significance. Hence, the extreme toxicity of arsenic and mercury their quantitative/qualitative monitoring and control of these metals in the environment is essential due to the high toxicity of these metals. The WHO and the US–EPA has set the maximum acceptable amount for arsenic, mercury to be 0.002 ppm, and 0.01 ppm,

respectively, in the drinking water system (Choong et al. 2007). Hence, the early detection of these toxic elements is desirable via colorimetric chemosensing method, numerous synthetic organic chemosensor having various binding moieties are developed in the past but, very few chemosensors are available in the literature for the detection of arsenic (Chauhan et al. 2017; Das and Sarkar 2016; SIRAWATCHARIN et al. 2014; Yadav and Singh 2016). Recently, benzothiazole Schiff's base as a colorimetric chemosensor for arsenic detection in an equal ratio of DMSO–water system and N, S chelate of the benzothiazole derivative was developed (Chauhan et al. 2017), but the detection in 100% aqueous system need to be developed.

With this background, herein the three chemosensors (**S5R1–S5R3**) synthesized using simple Schiff's base condensation reaction between diaminomaleonitrile and three different aldehyde containing good chromospheres resulting suitable binding sites like hydroxy (–OH), imine (–C=N) and quinoline for the quick naked eye response in an aqueous system. The chemosensor **S5R1** shows a multi-color response towards dissimilar metal ions like arsenate/arsenite, Hg^{2+}, and Cu^{2+} ions, **S5R2** exhibits a selective response in the presence of Cu^{2+} ions and the **S5R3** gave selective dual ion response towards Hg^{2+} and Cu^{2+} ions. All the synthesized chemosensors **S5R1–S5R3** exhibited a detection limit at ppb levels.

6.2. Experimental section

6.2.1. Materials and methods

The analytical reagent grade metal nitrate salts, sodium arsenite, sodium arsenate salts, chemicals, and solvents (chromatography grade) are purchased from commercial distributors and utilized as such. The ^{1}H-NMR, ^{13}C NMR spectra of chemosensors **S5R1–S5R3** were recorded on the Varian-NMRS-400MHz spectrometer, and DMSO-d_6 solvent was used. The ^{1}H NMR and ^{13}C NMR chemical shifts are reported on the δ scale (in ppm) relative to tetramethylsilane (TMS, δ 0.00) and DMSO-d_6 (39.50), respectively, as internal reference standards. Using Bio-cote (SMP10) instrument melting point was recorded for the chemosensors. Fourier Transform Infrared (FT-IR) spectra were done using a Bruker Alpha (silicon carbide as IR source) instrument. The LC-MS mass (ESI) spectra of chemosensors S5R1-S5R3 done on Agilent 6410 instrument. All UV-Vis studies were done on

Analytikjena Specord S600 UV–Vis spectrophotometer using a 3.0 mL quartz sample holder having two optical transparent windows with a Path length of 10 mm.

6.2.2. Analytical solutions preparation

Initially, all accurately weighed the required weight of all metal standards in separate and dissolved in deionized water, having a stock concentration of 1.0×10^{-2} M and used for the further adequate low standard solution preparation. The synthesized chemosensors **S5R1-S5R3** were dissolved in dimethyl sulphoxide (DMSO) solvent having a stock concentration of 1.0×10^{-3} M in separate volumetric flasks and further, diluted these chemosensors to 2.0×10^{-5} M using the same solvent. Dilution and metal solution added to the chemosensor solution done using micropipette in the colorimetric and instrumental analysis. All the photographs and absorption spectra were taken immediately at ambient temperature after the mixing of the appropriate volume of metal and chemosensors solution. DMSO solvent is taken as a reference before taking the UV–Vis spectra in the titration and other experiments.

6.2.3. Synthesis of chemosensor S5R1–S5R4

The synthesis procedure of **S5R1–S5R3** has illustrated in the **scheme 6.1**. The synthesis of chemosensor **S5R1:** 2,3-diaminomaleonitrile (0.0601g, 0.56mmol) and 3-Bromo-5-chlorosalisilaldehyde (0.131.1g, 0.56 mmol) were separately dissolved in 10 mL ethanol. Then aldehydehyde solution was added drop-wise with constant stirring to the thiophene-2-carboxylic acid hydrazide solution. To this a catalytic amount of acetic acid was added and the reaction mixture was stirred at room temperature for 3 hours. The progress of reaction was monitored by TLC. After the completion of reaction the reaction mixture was filtered and washed with hot ethanol. Similarly, the **S5R2** and **S5R3** were synthesized as stated above synthetic methodology. The **S5R2** was synthesized by the reaction of 2,3-diaminomaleonitrile (0.0751g, 0.69mmol) and 5-chlorosalisilaldehyde (0.1051g, 0.69mmol). The **S5R3** was synthesized by the reaction of 2,3-diaminomaleonitrile (0.0692g, 0.64mmol) and quinoline-2-carbaldehyde (0.1006g, 0.64mmol). The final obtained desired compounds were characterized by using standard spectroscopic methods as given below.

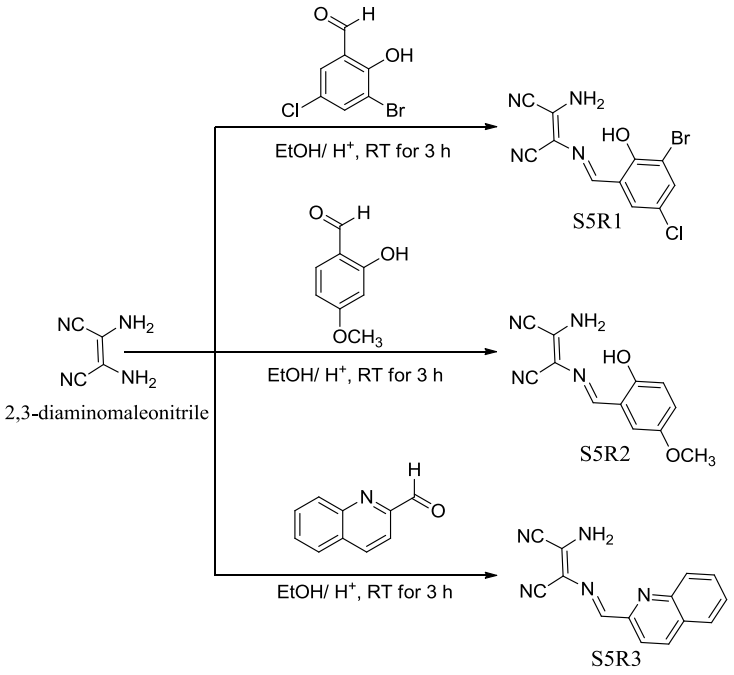

Scheme 6.1: Synthesis of chemosensors **S5R1 - S5R3**

2-amino-3-((E)-(3-bromo-5-chloro-2-hydroxybenzylidene)amino)maleonitrile (S5R1): Yield: 77.8%, **M.P:** 242–243˚C. **FT-IR (ATR, cm^{-1}):** 3414, 3292, 2964, 2243, 2206, 1630, 1592, 1441, 1216, 1019, 853, 705. **^{1}H NMR (400MHz, DMSO-d_6, δ_{ppm}):** 10.927 (s, 1H, aromatic –OH), 8.479 (s, 1H, imine (HC=N), 8.235 (s, 2H, =C–NH_2), 8.093–8.087 (d, 1H, aromatic (–C=CH), J=2.4Hz), 7.769–7.762 (d, 1H, aromatic (–C=CH), J=2.8Hz), **(Fig. 6.2)**. **^{13}C-NMR (100MHz, DMSO-d_6, δ_{ppm}):** 153.7 (HC=N), 153.3 (aromatic –C–OH), 135.0 (aromatic –C–Cl), 129.4 (aromatic –C–Br), 127.9 (=N–C–CN), 124.8 (CN =C–N), 124.2 (CN –C–N H_2), 114.7, 114.2, 112.6 aromatic –C=C–), 102.4 (=C–NH_2), **(Fig. 6.5)**. **LC-MS (ESI) m/z:** Cald. for $C_{11}H_6BrClN_4O$, 325.55 and found, 324.9 (M–1) **(Fig. 6.8)**.

2-amino-3-((E)-(2-hydroxy-4-methoxybenzylidene)amino)maleonitrile (S5R2): Yield: 89.8 %, **M.P:** 247–248˚C. **FT-IR (ATR, cm^{-1}):** 3459, 3331, 2926, 2241, 2203, 1619, 1562, 1496, 1280, 1036, 815, 722 **(Fig. 6.1)**. **^{1}H NMR (400MHz, DMSO-d_6, δ_{ppm})** 9.947(s, 1H, aromatic –OH), 8.544 (s,1H, imine (HC=N)), 7.880 (s, 2H, –C=C–NH_2), 7.582 –7.575 (d, 1H, aromatic (–C=CH), J=4.8Hz), 6.945–6.914 (d,d, 1H, aromatic (–C=CH), J=12.4Hz), 6.850–6.828 (d, 1H, aromatic (–C=CH), J=8.8Hz), 3.721 (s, 3H, aromatic –OCH_3) **(Fig. 6.3)**. **^{13}C-NMR (100MHz, DMSO-d_6, δ_{ppm}):** 153.0 (HC=N), 152.8 (aromatic –C–OH), 152.4 (aromatic –C–OCH_3), 126.5 (=N–C–CN), 121.9 (CN–C–N), 121.2 (CN– C–N H_2), 117.9, 115.1, 114.5, 111.2 (aromatic –

C=C–), 103.9 (=C–NH_2), 56.1 (aromatic –OCH_3) **(Fig. 6.6)**. **LC-MS (ESI) m/z:** Cald. for $C_{12}H_{10}N_4O_2$, 242.23 and found, 241.1 (M–1) **(Fig. 6.9)**.

2-amino-3-((E)-(quinolin-2-ylmethylene)amino)maleonitrile (S5R3): Yield: 92.2 %, **M.P**: 245–246˚C. **FT-IR (ATR, cm^{-1}):** 3304, 2972, 2240, 2200, 1628, 1608, 1558, 1501, 1379, 1217, 946, 828, 751 **(Fig. 6.1)**. **^{1}H NMR (400MHz, DMSO-d_6, δ_{ppm}):** 8.545–8.523 (d, 1H, imine (HC=N), J=8.8Hz), 8.447–8.395 (m, 3H, aromatic (–C=CH), 8.290–8.262 (d, 1H, (–C=CH), J=11.2Hz), 8.070–7.978 (m, 2H, (CN–C=C–NH_2), 7.818–7.776 (t, 1H, aromatic (–C=CH), J=16.8Hz), 7.674–7.634 **(**t, 1H, aromatic (–C=CH), J=16.0Hz) **(Fig. 6.4)**. **^{13}C-NMR (100MHz, DMSO-d_6, δ_{ppm}):** 154.9 (HC=N), 154.5 (Quinoline HC=N–), 147.9 (aromatic quinoline ring –C–NC), 137.0 (CN–C–N), 130.7 (CN–C–NH_2), 129.1, 128.8, 128.4 128., 119.5, 114.5, 113.8(aromatic quinoline ring –C=C–), , 102.3(=C–NH_2) **(Fig. 6.7)**. **LC-MS (ESI) m/z:** Cald. for $C_{14}H_9N_5$, 247.25 and found, 245.8 (M–1) **(Fig. 6.10)**.

6.2.4. Characterization data of S5R1-S5R3

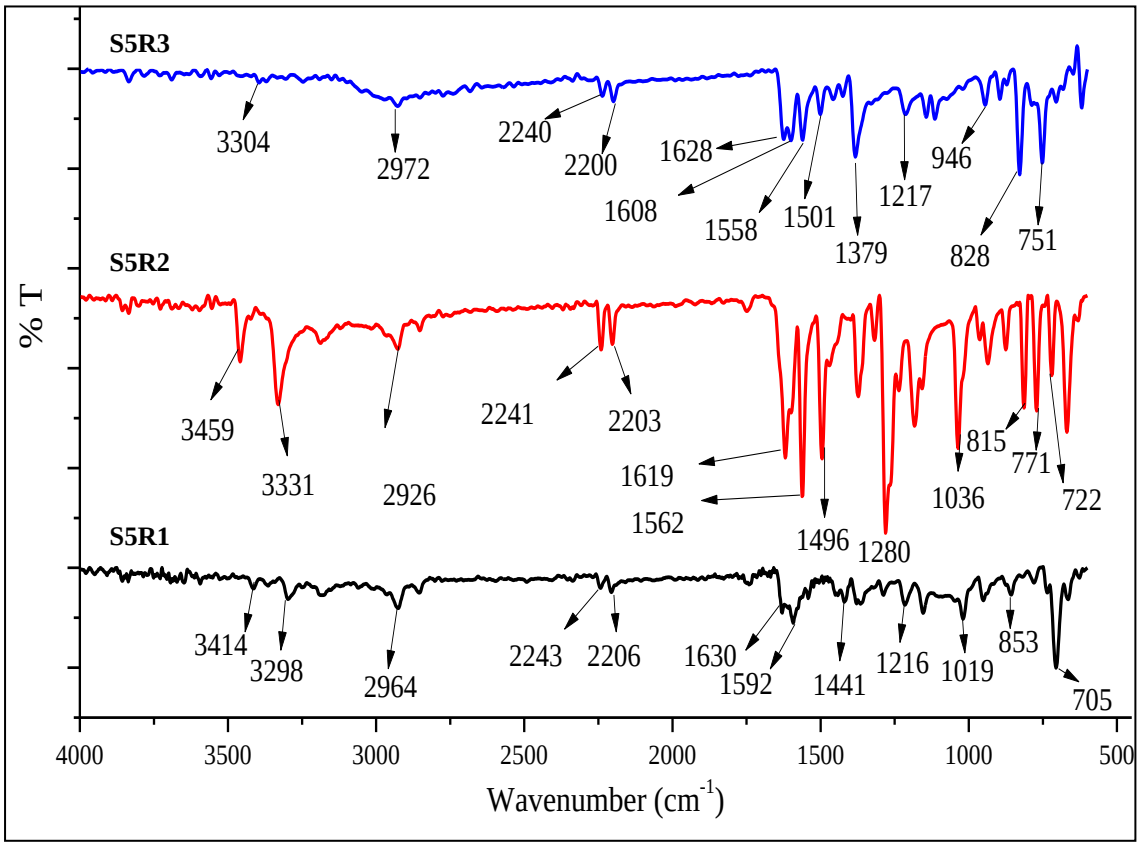

Fig. 6.1: FT-IR Spectra of chemosensor **S5R1-S5R3**

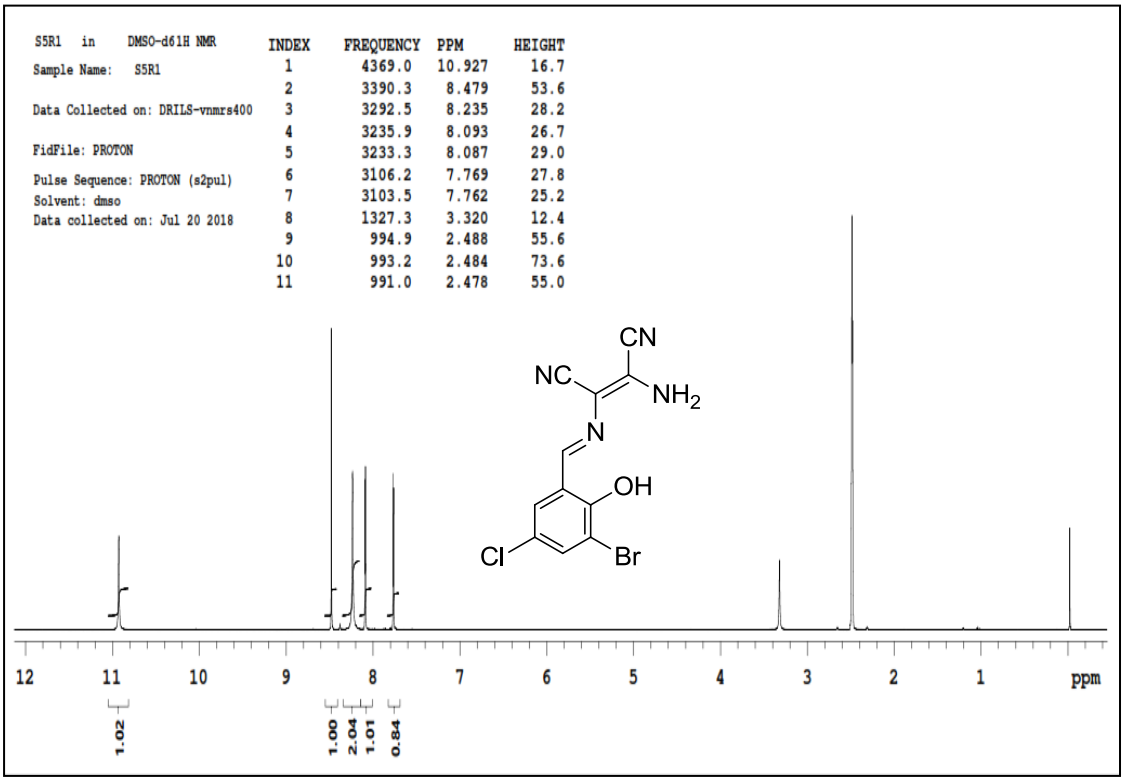

Fig. 6.2: ^{1}H NMR spectrum of chemosensor **S5R1**

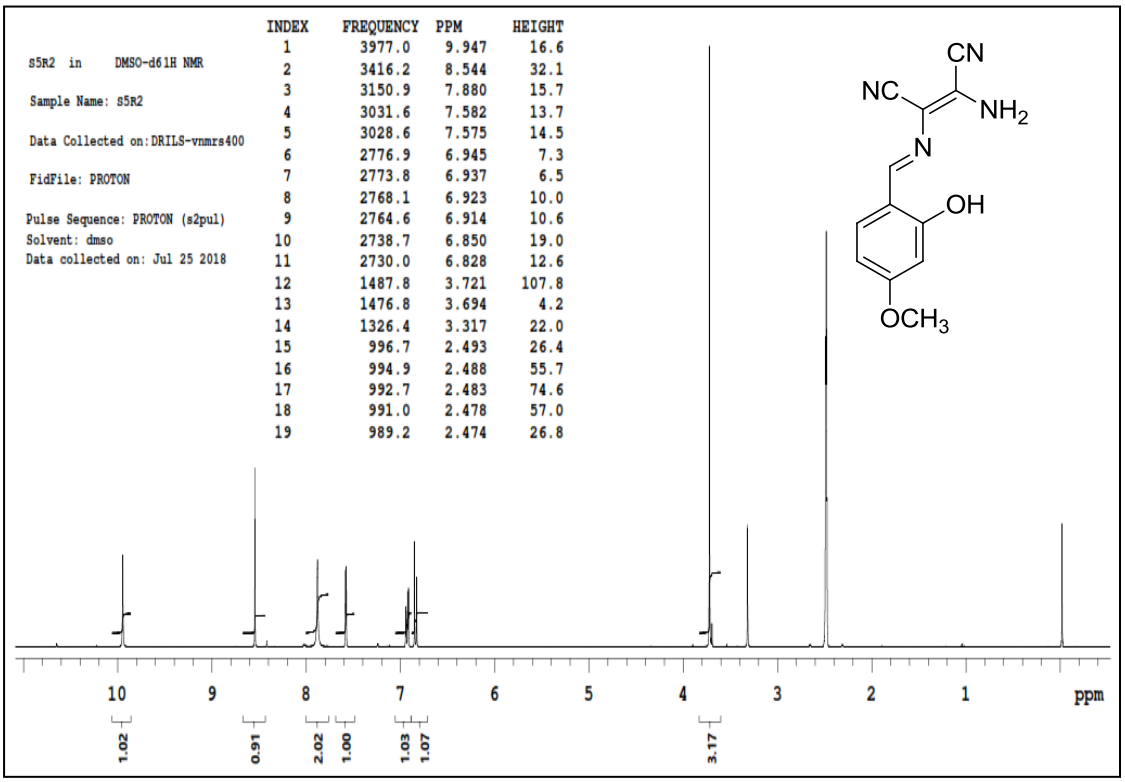

Fig. 6.3: ^{1}H NMR of spectrum chemosensor **S5R2**

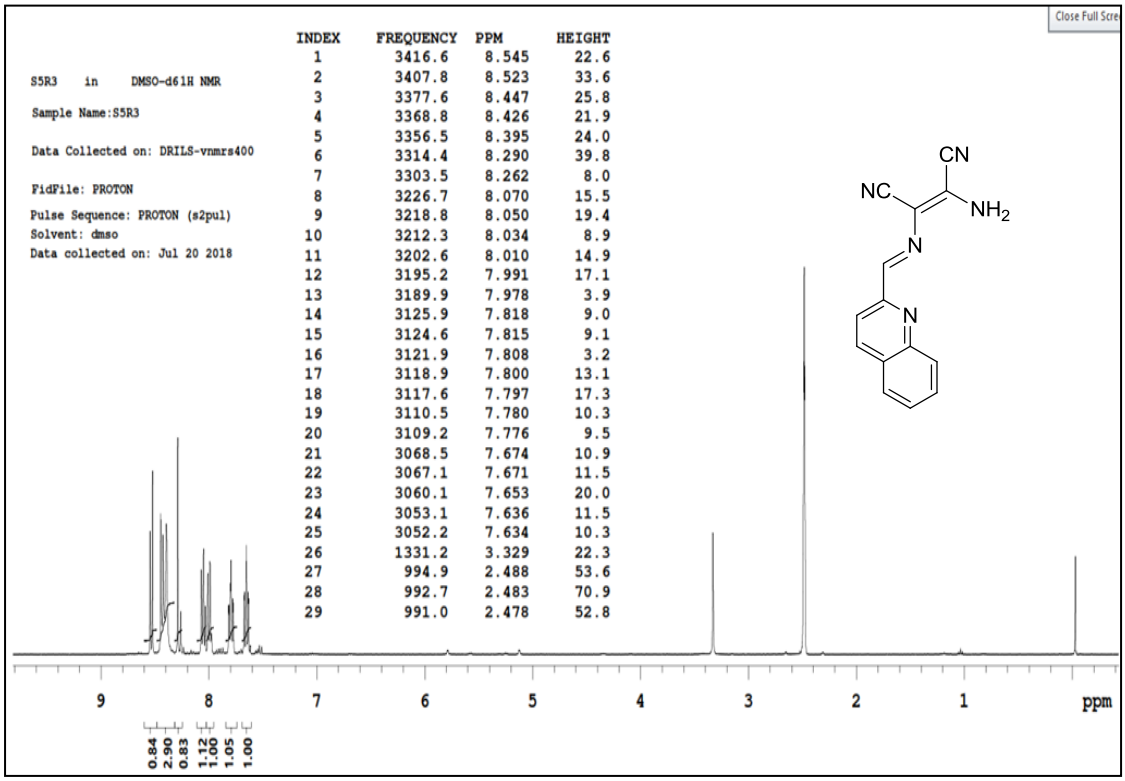

Fig. 6.4: ^{1}H NMR spectrum of chemosensor **S5R3**

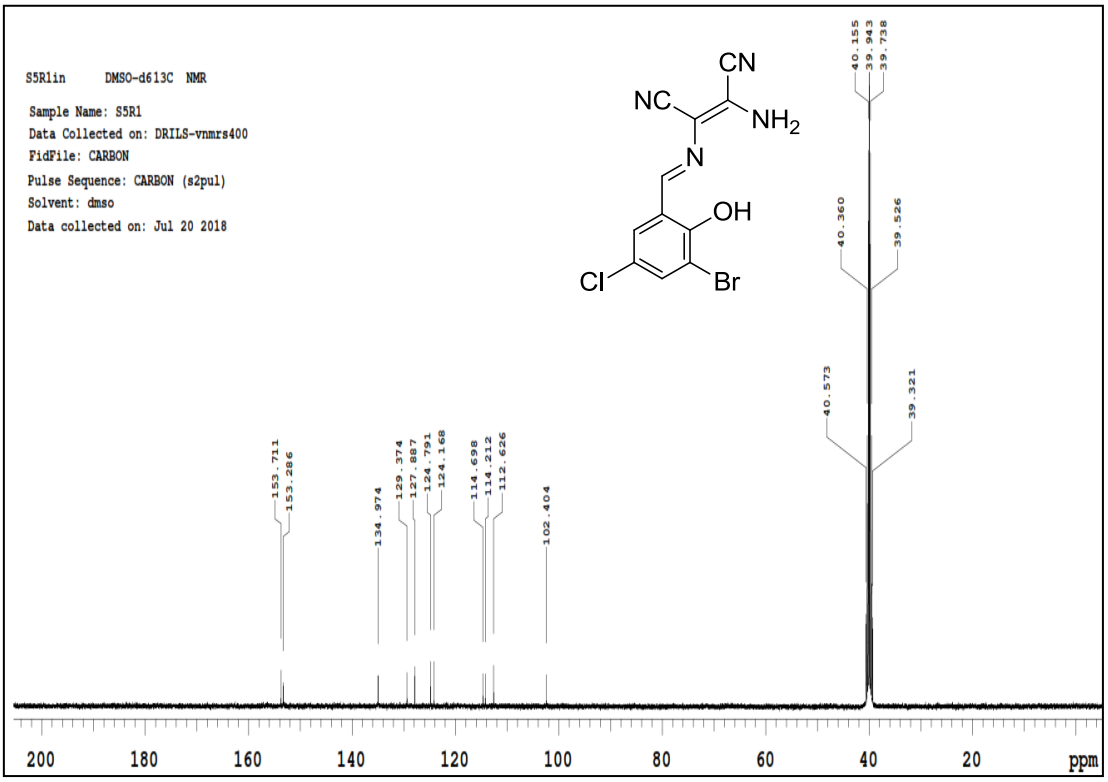

Fig. 6.5: ^{13}C NMR spectrum of chemosensor **S5R1**

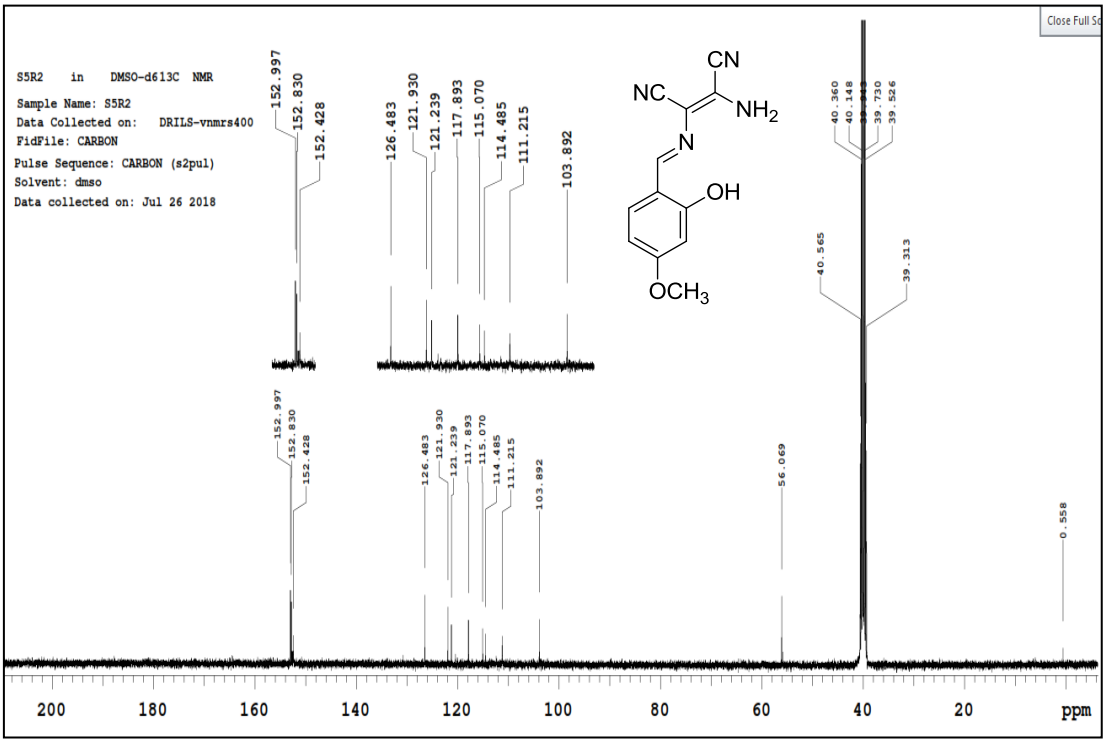

Fig. 6.6: ^{13}C NMR spectrum of chemosensor **S5R2**

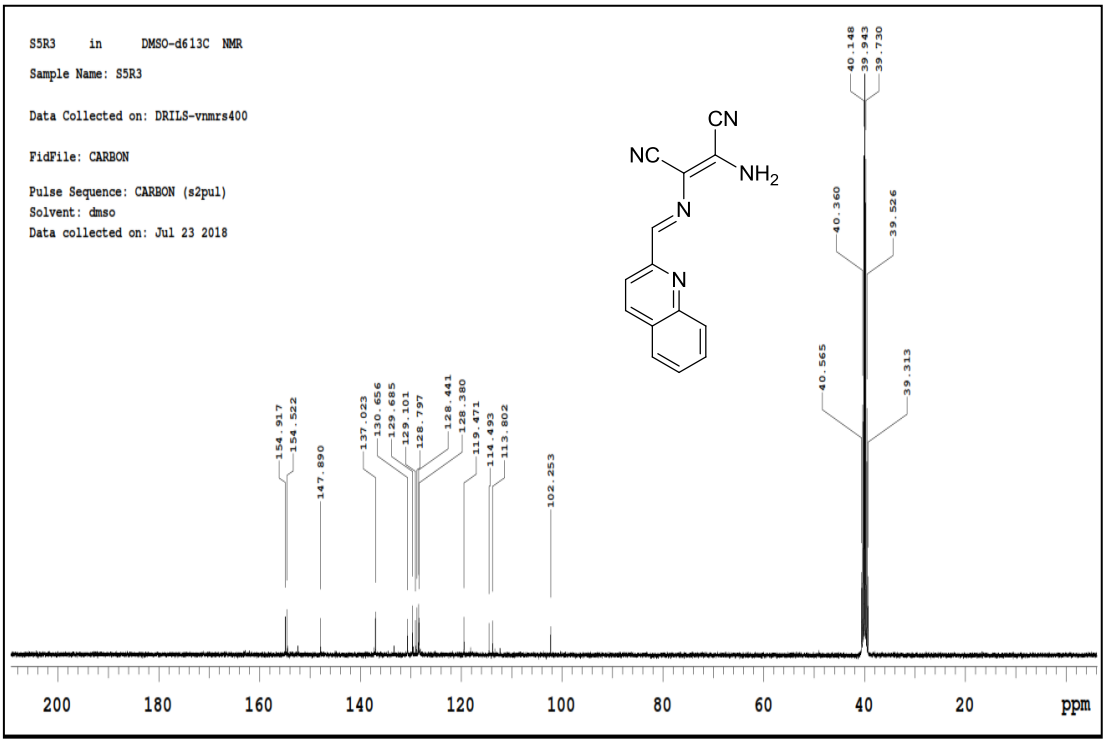

Fig. 6.7: ^{13}C NMR spectrum of chemosensor **S5R3**

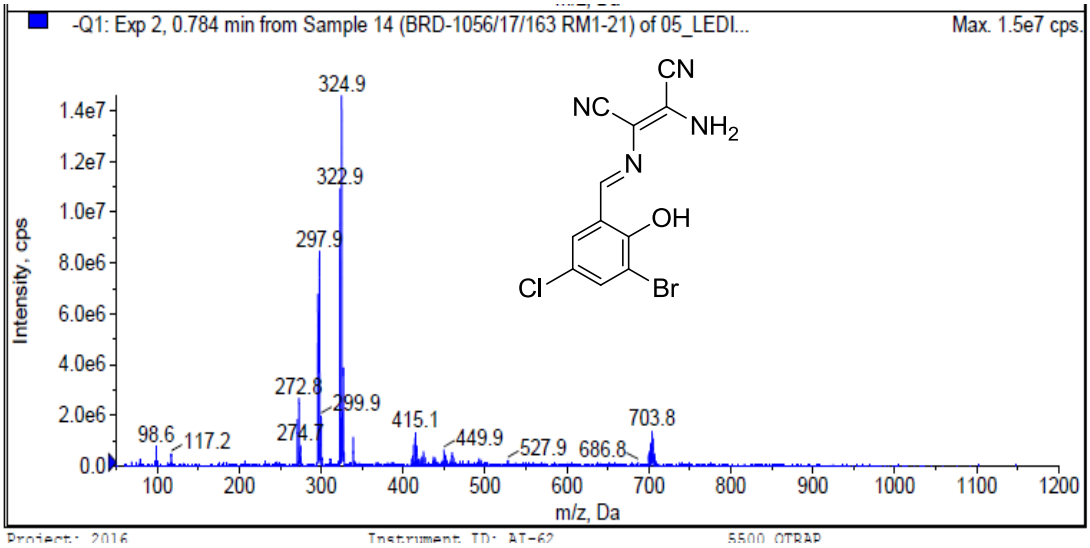

Fig. 6.8: LC-Mass (ESI, M–1) spectrum of chemosensor **S5R1**

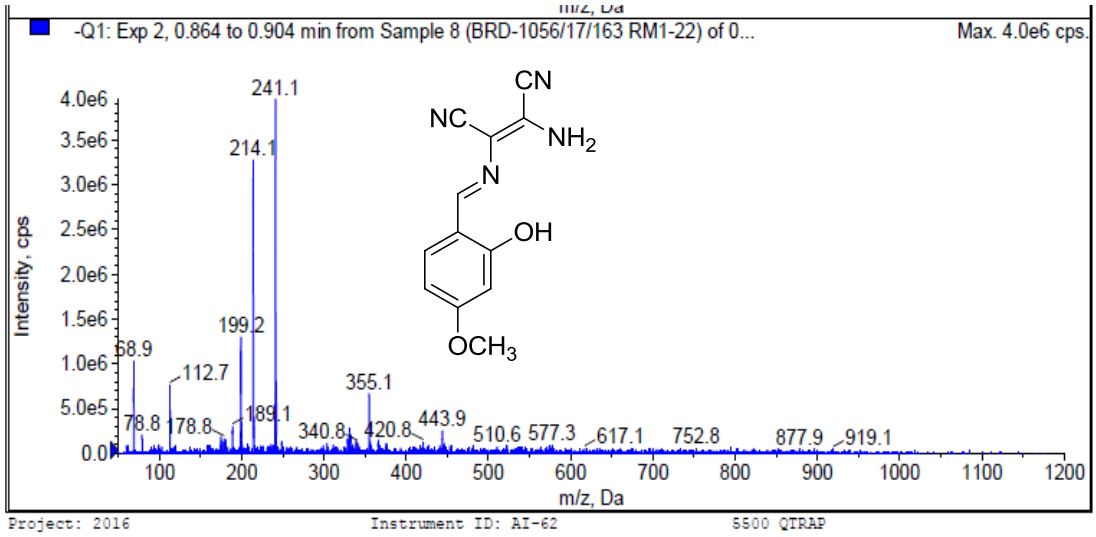

Fig. 6.9: LC-Mass (ESI, M–1) mass spectrum of chemosensor **S5R2**

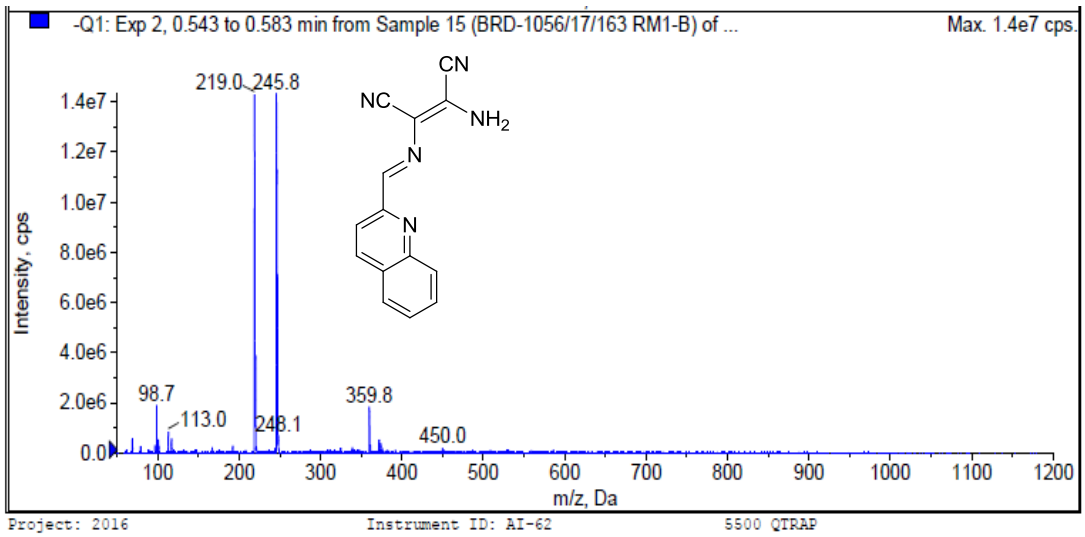

Fig. 6.10: LC-Mass (ESI, M–1) mass spectrum of chemosensor **S5R3**

6.3. Results and discussion

6.3.1 Naked-eye detection studies

The naked-eye detection studies were conducted to chemosensors **S5R1–S5R3** for the finding of a variety of ions such as Hg^{2+}, Cu^{2+}, AsO_2^-, AsO_4^{2-}, Ni^{2+}, Co^{2+}, Cr^{3+}, Al^{3+}, Zn^{2+}, Fe^{2+}, Cd^{2+}, Mn^{2+}, Mg^{2+}, Pb^{2+}, Ca^{2+}, Na^+, and K^+ ions. The 2.0 mL of chemosensor **S5R1** (4.0×10^{-5} M) exhibits selective multi-color response with the addition of 1.0 equivalence of Hg^{2+}, Cu^{2+}, AsO_2^- and AsO_4^{2-} ions (from pale pink to colorless for Hg^{2+}, pale orange for Cu^{2+}, orange-red for AsO_2^- and AsO_4^{2-} ions) (**Fig. 6.11**). Whereas, **S5R1** did not give any color response with the other ions tested at a higher concentration (i.c. of 3.0 equivalences) **(Fig. 6.11)**. In similarly the other two chemosensors **S5R2, S5R3** was investigated, the chemosensor **S5R2** exhibits selective color response with the Cu^{2+} ions (pale yellow to orange), and the **S5R3** selectivity exhibits the dual-color response from colorless to yellow for Hg^{2+}, pink color for Cu^{2+} ions **(Fig. 6.11)**. This selective colorimetric response indicates that the chemosensors **S5R1–S5R3** selectivity towards, Hg^{2+}, Cu^{2+}, AsO_2^-, AsO_4^{2-} ions over the other tested ions.

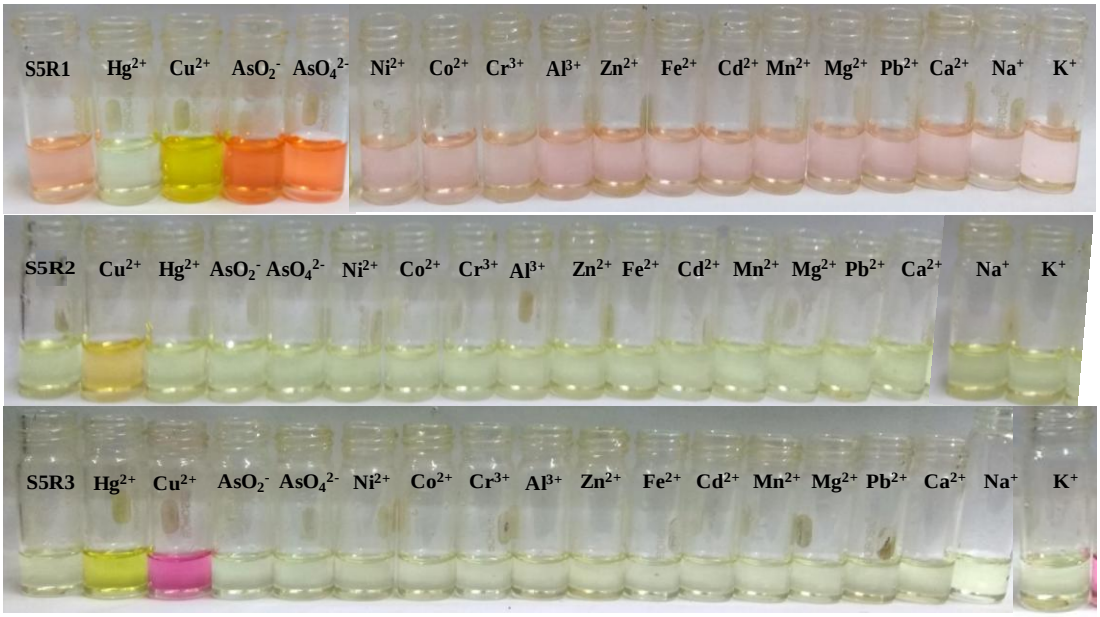

Fig. 6.11: The colorimetric response of chemosensors **S5R1–S5R3** (4.0×10^{-5} M) with the addition of 1.0 equivalence of Hg^{2+}, Cu^{2+} ions and 3.0 equivalence of other ions

6.3.2 Recognition of ions by UV–Visible studies

To confirm the selectivity of chemosensors **S5R1–S5R3** towards Hg^{2+}, Cu^{2+}, AsO_2^-, AsO_4^{2-} ions, further, UV–Visible experimental studied have been conducted. With the addition of 3.0 equivalences of Ni^{2+}, Co^{2+}, Cr^{3+}, Al^{3+}, Zn^{2+}, Fe^{2+}, Cd^{2+}, Mn^{2+}, Mg^{2+}, Pb^{2+}, Ca^{2+}, Na^+, and K^+ ions to the chemosensor **S5R1** did not generate any significant absorption changes whereas, significant absorption change was observed with the inclusion of 1.0 equivalence of Cu^{2+}, Hg^{2+}, AsO_2^-, AsO_4^{2-} ions to the chemosensor **S5R1 (Fig. 6.12a).** These significant changes indicate the multi-selectivity of chemosensor **S5R1** towards active ions. Similarly, the chemosensor **S5R2** exhibits a considerable absorption response in the UV–Vis spectrum with the addition of Cu^{2+} ions (1.0 equivalence). There was no considerable absorption response with the addition of other interfering ions (3.0 equivalences), except Cu^{2+} ions **(Fig. 6.12b)**. A similar comparative and selectivity test for the chemosensor **S5R3** with the addition of 3.0 equivalences of AsO_2^-, AsO_4^{2-}, Ni^{2+}, Co^{2+}, Cr^{3+}, Al^{3+}, Zn^{2+}, Fe^{2+}, Cd^{2+}, Mn^{2+}, Mg^{2+}, Pb^{2+}, Ca^{2+}, Na^+, and K^+ ions, no remarkable change was observed in the absorption of the **S5R3**. **S5R3** exhibits selectively good absorption changes with the inclusion of 1.0 equivalence of Cu^{2+}, Hg^{2+}ions **(Fig. 6.12c)**.

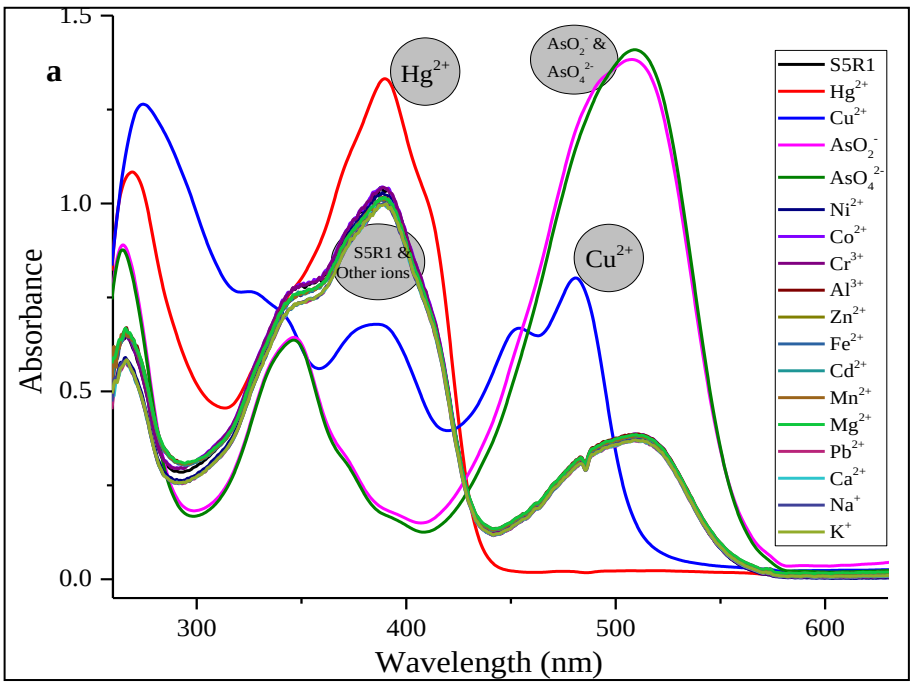

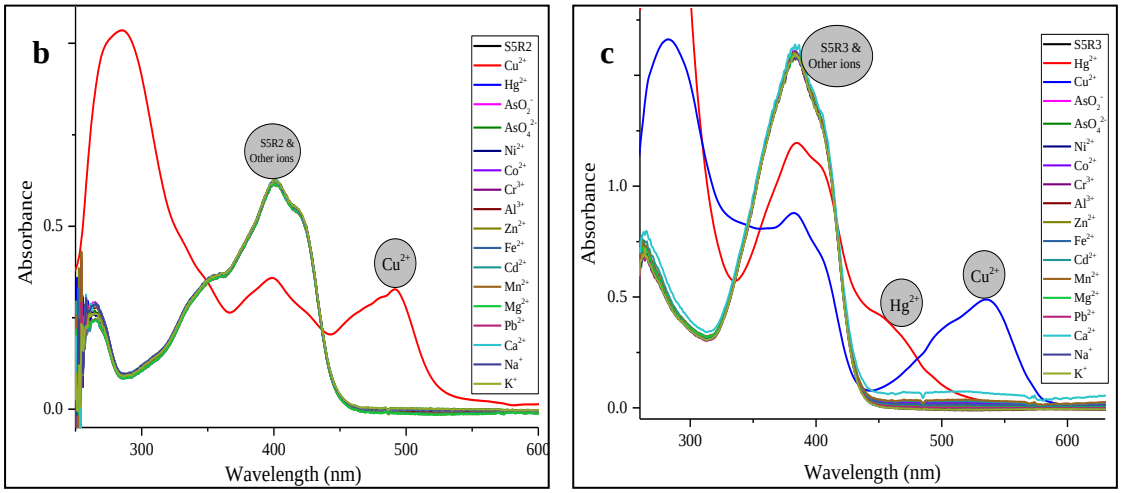

Fig. 6.12: Absorption response of chemosensor **S5R1–S5R3** (4.0×10^{-5} M in DMSO) with the addition of 3.0 equivalence of various ions and 1.0 equivalence of Hg^{2+}, Cu^{2+}, AsO_2^-, AsO_4^{2-} ions in de-ionized water, **a). S5R1** and other ions, **b). S5R2** and other ions, **c). S5R3** and other ions

6.3.3 UV–Visible titration experiments

The chemosensors **S5R1–S5R3** are selectively binding to the Hg^{2+}, Cu^{2+}, AsO_2^-, AsO_4^{2-} ions have been confirmed by colorimetric and UV–Vis comparative studies. With this knowledge, further, established binding properties (association constant, stoichiometry interaction) and the detection limit for the chemosensors **S5R1–S5R3** with the active ions using the UV–Vis titration experiments.

The free chemosensor **S5R1** (4.0×10^{-5} M in DMSO) exhibit two characteristic absorption band at 390 nm, 510 nm, and allocated to π–π* and n–π* transition in its molecule. The band at 510 nm was decreased upon the gradual addition of Hg^{2+} ions (0.0–1.5 equivalence) in the absorption spectra **(Fig. 6.13a)**. This change indicates the formation of the chemosensor metal complex; the absorption decreased due to metal to ligand charge transfer phenomenon. Similar titrations were done with the gradual addition of other active ions (Cu^{2+}, AsO_2^- & AsO_4^{2-}) to the chemosensor **S5R1**. A blue shift (from 510 nm to 480 nm) was observed with the quantitative incremental addition (0.0–2.2 equivalences) of Cu^{2+} ions to the **S5R1**. The new band appeared at 480 nm and increased quantitatively in the UV–Vis spectrum **(Fig. 6.13b)**. In the **S5R1**–Cu^{2+} titration spectrum shows a clear isosbestic point at 424 nm, this indicates the changeover state in chemosensor and chemosensor-

metal complex. The blue shift in the absorption spectra due to metal to ligand charge transfers like **S5R1**–Hg^{2+} interaction and is accountable for the naked-eye response (from pink to orange color) of the chemosensor **S5R1**. The UV–Vis peak at 390 nm decreased, and peak at 510 nm increased gradually with the incremental addition (0.0 to 1.6 equivalences) of AsO_2^-, AsO_4^{2-} ions to the chemosensor **S5R1 (Fig. 6.13c-d)**. A clear isosbestic point was found at 429 nm in both the titration graphs of **S5R1**–AsO_2^- and **S5R1**–AsO_4^{2-}. The absorption enhance at 510 nm may due to charge transfer from chemosensor to AsO_2^- / AsO_4^{2-} ions; this decreases the energy gap between HOMO & LUMO and accountable for the redshift in the absorption spectrum.

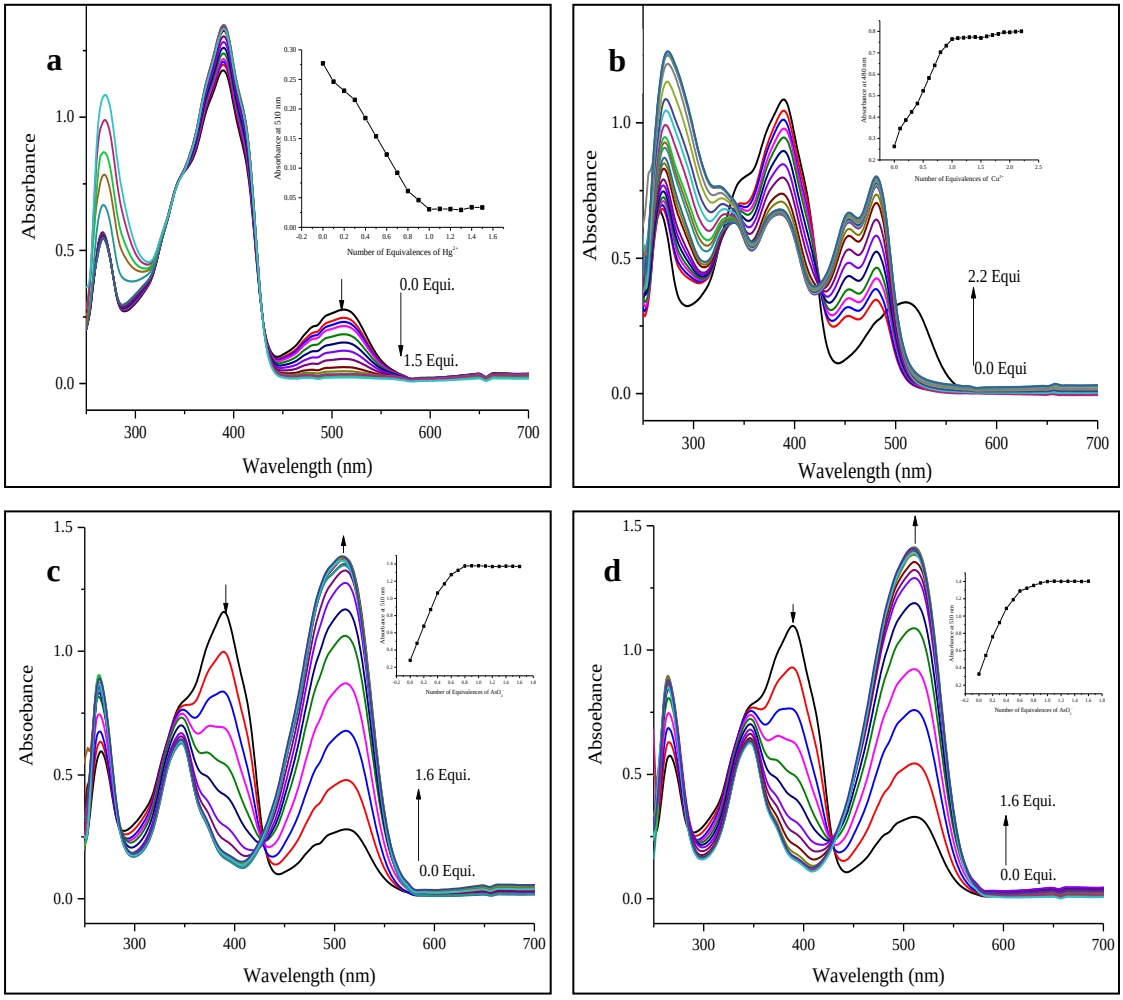

Fig. 6.13: Absorption changes of chemosensor **S5R1** (4.0×10^{-5} M in DMSO) with the quantitative addition of Hg^{2+}, Cu^{2+}, AsO_2^-, AsO_4^{2-} ions, insert plot shows absorbance changes at a particular wavelength with various concentration of ions. **a). S5R1**–Hg^{2+}, **b). S5R1**–Cu^{2+}, **c). S5R1–**AsO_2^-, **d). S5R1–**AsO_4^{2-}

The **S5R2** exhibits an un-separated peak at 400-420 nm in the non-attendance of Cu^{2+}, which is attributed to the π–π* and n–π* transition in its molecular structure of **S5R2**. With the quantitative titration (0.0 to 1.6 equivalences) of Cu^{2+} ions to the **S5R2**, a new absorption band was observed at 492 nm and increased gradually **(Fig. 6.14)**. The red-shift by 92 nm increment is owing to the formation of the chemosensor-metal complex via ligand to metal charge transfer, which is accountable for the naked-eye response of **S5R2** (pale yellow to orange color). The charge transfer may be due to chemosensor interact with metal ion through hydroxyl (─OH), imine (–C=N), and free amino groups present in the chemosensor **S5R2** molecule, these groups act as suitable binding sites for the metal ion.

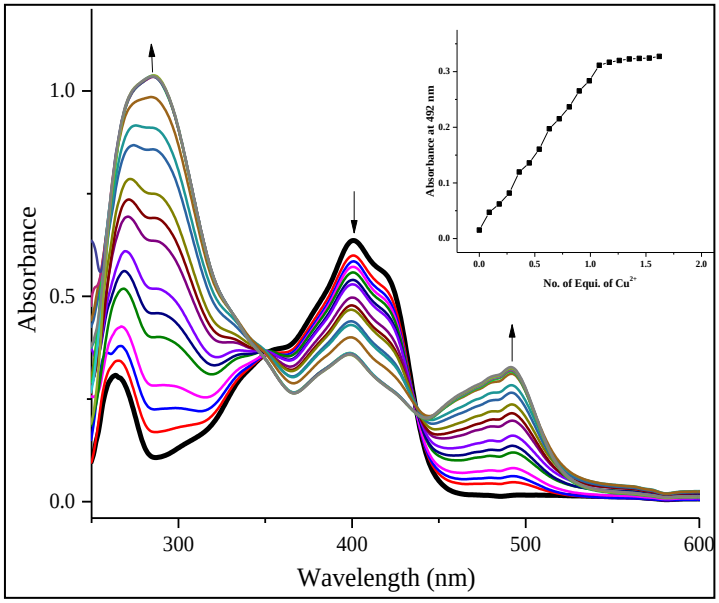

Fig. 6.14: Absorption changes of chemosensor **S5R2** (4.0×10^{-5} M in DMSO) with the quantitative inclusion of Cu^{2+} ions (0.0 to 1.6 equivalences) and the insert plot shows absorbance changes at 492 nm with various concentration of Cu^{2+} ions

The chemosensor **S5R3** has quinoline moiety in its molecular structure, and the free chemosensor **S5R3** (4.0×10^{-5} M in DMSO) exhibits a major absorption band at 383 nm is due to the π–π* transition. Whereas, by the quantitative inclusion of Cu^{2+} and Hg^{2+} ions (0.0 to 1.5 equivalences) to the chemosensor **S5R3**, exhibits a red-shift by 153 nm and 63 nm increment in the absorption spectrum respectively **(Fig. 6.15a-b)**. The newly appeared bands at 450 nm (**S5R3**–Hg^{2+}) and 535 nm (**S5R3–**Cu^{2+}) in titration spectra were increased by the further incremental addition of Hg^{2+}, Cu^{2+} ions to the **S5R3**.

The isosbestic points at 335 nm, 417 nm in **S5R3**–Hg^{2+} and 345 nm, 433 nm in **S5R3**–Cu^{2+} titration graphs represent the transition state between chemosensor **S5R3** and metal ions. The red-shift may be due to the formation of complex trough ligand to metal charge transfer via quinoline imine nitrogen, imine nitrogen, and amino group present in the **S5R3** molecular structure.

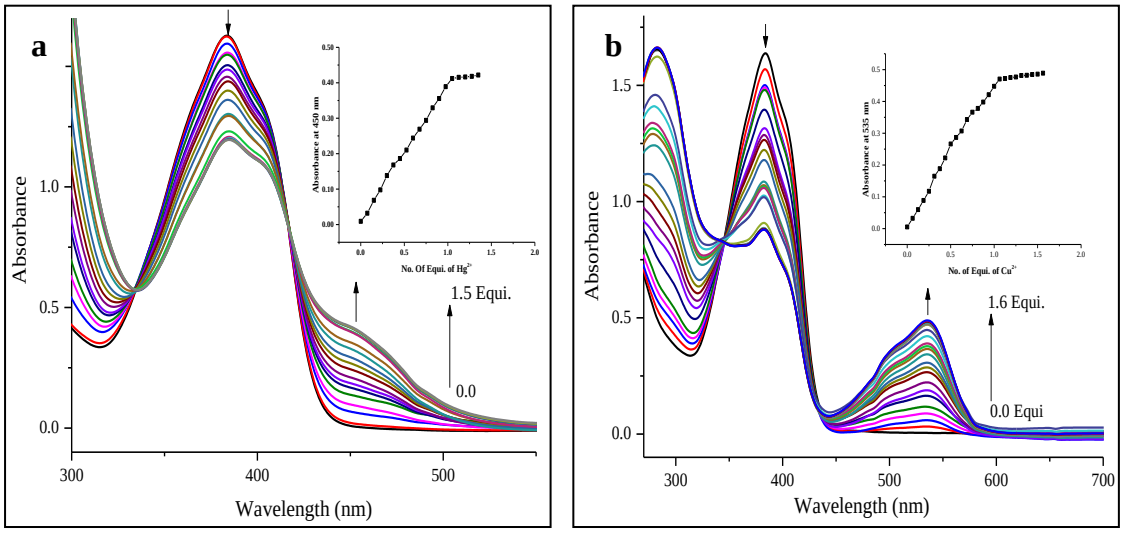

Fig. 6.15: Absorption changes of chemosensor **S5R3** (4.0×10^{-5} M in DMSO) with the quantitative inclusion of Hg^{2+}, Cu^{2+} ions (0.0 to 1.5 equivalences), insert plot shows absorbance changes at a particular wavelength with various concentration of ions. **a). S5R3** with Hg^{2+}, **b). S5R3** with Cu^{2+}

6.3.4 Investigation of binding properties and detection limit (DL)

The association constant (K), the stoichiometric binding ratio of the chemosensor, ions, and the detection limit was determined by using UV–Vis experiments. From the UV-Vis titration studies, B-H plots (Momidi et al. 2017) were drown **(Fig. 6.16)**, the linear fitting of the plot $(1/A–A_0)$ vs. 1/[M] shows the 1:1 binding stoichiometry of chemosensors and ions. It was observed that a good linear fitting between absorption changes and concentration of ions with an R^2 of more than 0.99, which suggests the 1:1 binding ratio of all chemosensors and ions. The calculated association constant values for chemosensors and ions were depicted in **table 6.1**. Further, the UV–Vis minimal detection amount for the ions Hg^{2+}, Cu^{2+}, AsO_2^- and AsO_4^{2-} was determined via a calibration curve **(Fig. 6.17).** The calibration curves drown between the absorbance of the chemosensor complex at selected wavelengths versus the concentration of ions, and it exhibits a good correlation of R^2

is >0.99. The minimum recognition amount calculated using formula was mentioned by the (International Conference on Harmonization (ICH) guidelines(Ich 2005). All the calculated detection values for the Hg^{2+}, Cu^{2+}, AsO_2^- and AsO_4^{2-} ions were represented in **table 6.1**.

Table 6.1: Linear range, formation constant and the detection limit for the Hg^{2+}, Cu^{2+}, AsO_2^- and AsO_4^{2-} ions

Sensor	Analyte	Wavelength(nm)	K (M^{-1})	Range (µM)	DL (ppb)
S5R1	Hg^{2+}	510	5.8×10^4	0.0 – 40	24.0
	Cu^{2+}	480	3.3×10^4	0.0 – 40	121.0
	AsO_2^-	510	2.3×10^4	0.0 – 28	8.0
	AsO_4^{2-}	510	2.5×10^4	0.0 – 24	13.0
S5R2	Cu^{2+}	492	4.0×10^3	0.0 – 43	65.0
S5R3	Hg^{2+}	450	9.2×10^3	0.0 – 39	276.0
	Cu^{2+}	535	2.5×10^3	0.0 – 42	16.0

K- Formation Constant, DL-Detection Limit.

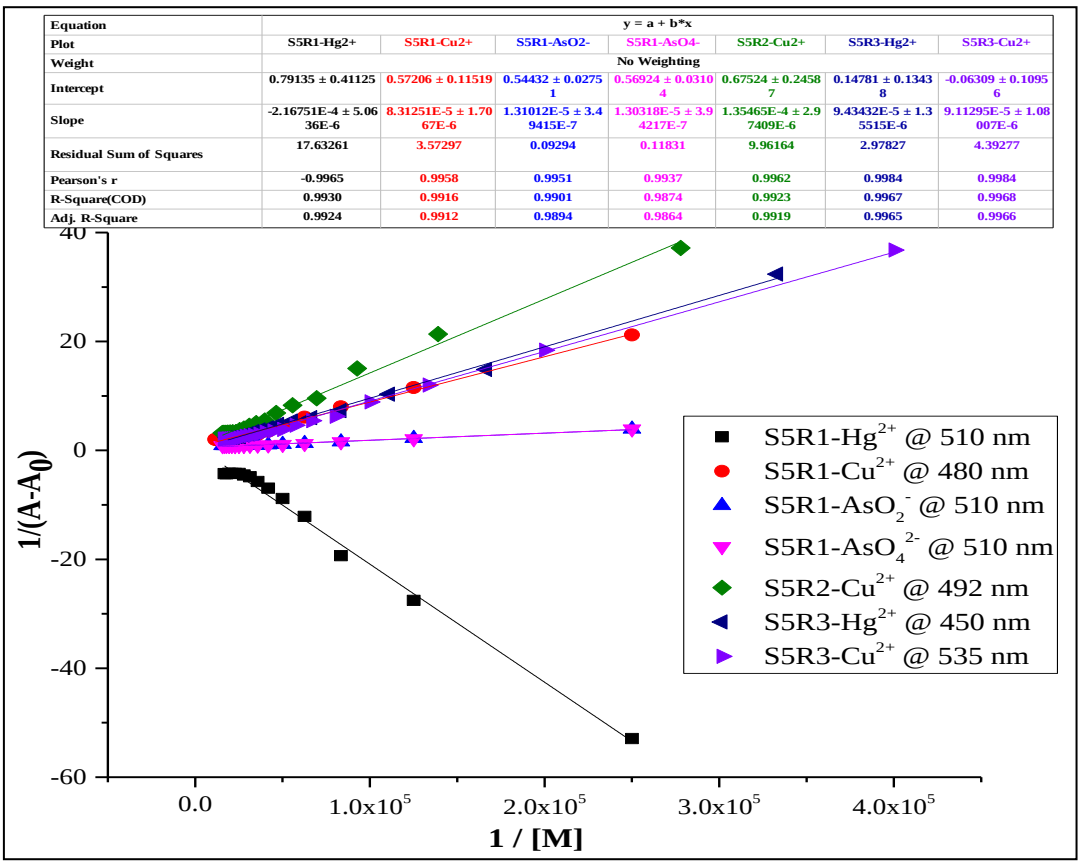

Fig. 6.16: Benesi-Hildebrand plot of chemosensor **S5R1–S5R3** (4.0×10^{-5} in DMSO) in the attendance of Cu^{2+}, Hg^{2+}, AsO_2^- and AsO_4^{2-} ions

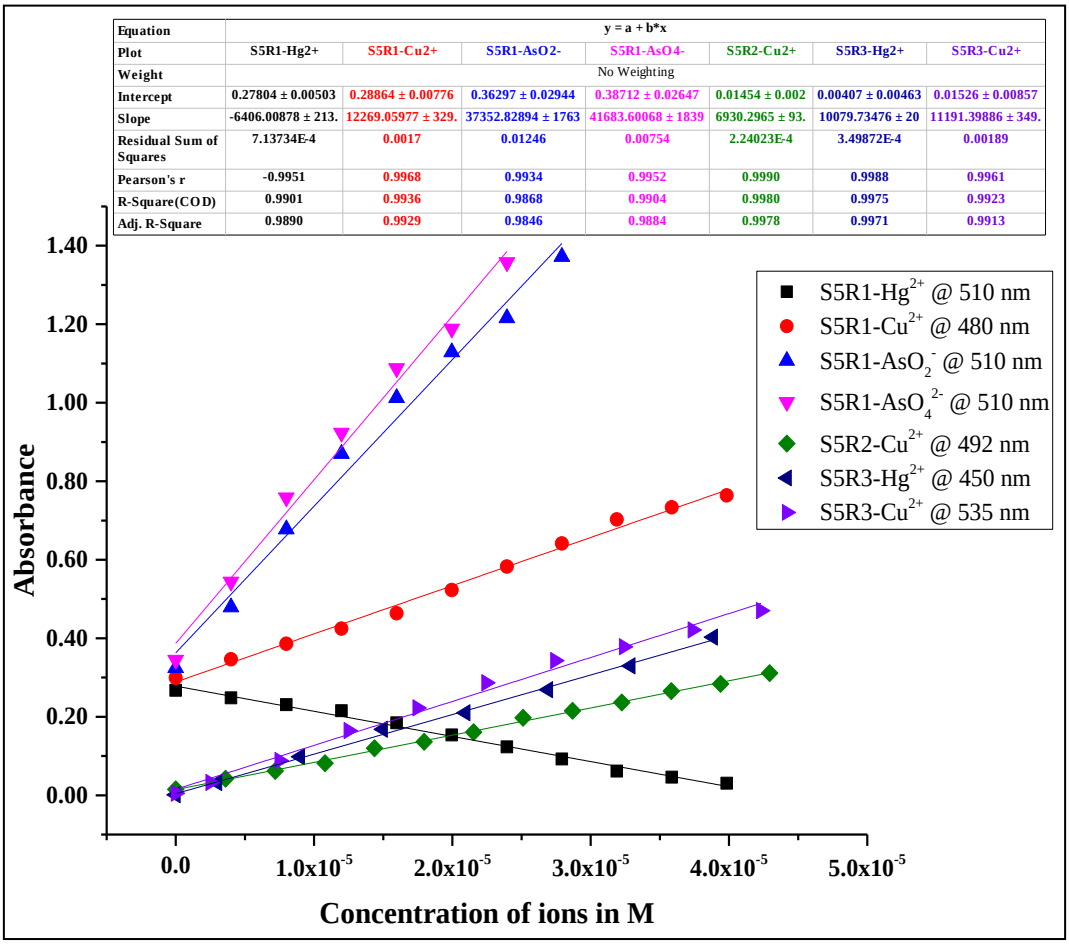

Fig. 6.17: Linear calibration plot of absorbance of complex (**S5R1–S5R3**+M) versus concentration of Hg^{2+}, Cu^{2+}, AsO_2^- and AsO_4^{2-} ions

6.3.5 Investigation of binding interaction by FT-IR and Mass analysis

The UV–Vis spectrum results suggest that the chemosensor **S5R1** interacts with the Hg^{2+}, Cu^{2+}, AsO_2^- and AsO_4^{2-} ions by the distinguished color changes. Likewise, the chemosensor **S5R2** selectively binds with Cu^{2+}, and chemosensor **S5R3** selectively senses the Hg^{2+}, Cu^{2+} ions. Further, to supports the selective binding between chemosensors **S5R1-S5R3** and active ions, it was confirmed by the FT-IR, mass results.

When compared the FT-IR spectrum of **S5R1** with that of complex spectra of **S5R1**–Hg^{2+}, **S5R1**–Cu^{2+}, and **S5R1**–AsO_2^-, it was identified that some noticeable changes in the vibration frequency's of some functional groups such as amine (–NH_2), hydroxy (–OH), imine (–C=N) and –C–O **(Fig. 6.18)**. Similar changes were found when compared to the FT-IR spectrum of **S5R2** with that of **S5R2**–Cu^{2+} complex

spectrum, as shown in **Fig. 6.19**. Whereas, some noticeable changes were identified when compared with that of bare chemosensor **S5R3** in the FT-IR spectra of **S5R3**–Hg^{2+}, **S5R3**–Cu^{2+} **(Fig. 6.20)**. The imine (–C=N) frequency was almost decreased after complexation with that of metal ions. Similarly, the small variation was observed in the stretching frequency of the C–N bond. It indicates that the chemosensor **S5R3** binds with that of metal ions via imine and nitrogen of the quinoline ring. From the FT-IR analysis of the complex of chemosensor **S5R1–S5R3**, It was found that the imine group majorly involving in the binding for all the chemosensors with that of active ions. Additionally, the hydroxy (–OH) group played a significant role in the binding of different metal ions in the case of chemosensor **S5R1**. The free amino group in the chemosensors **S5R1–S5R3** also actively involved in the binding of metal ions.

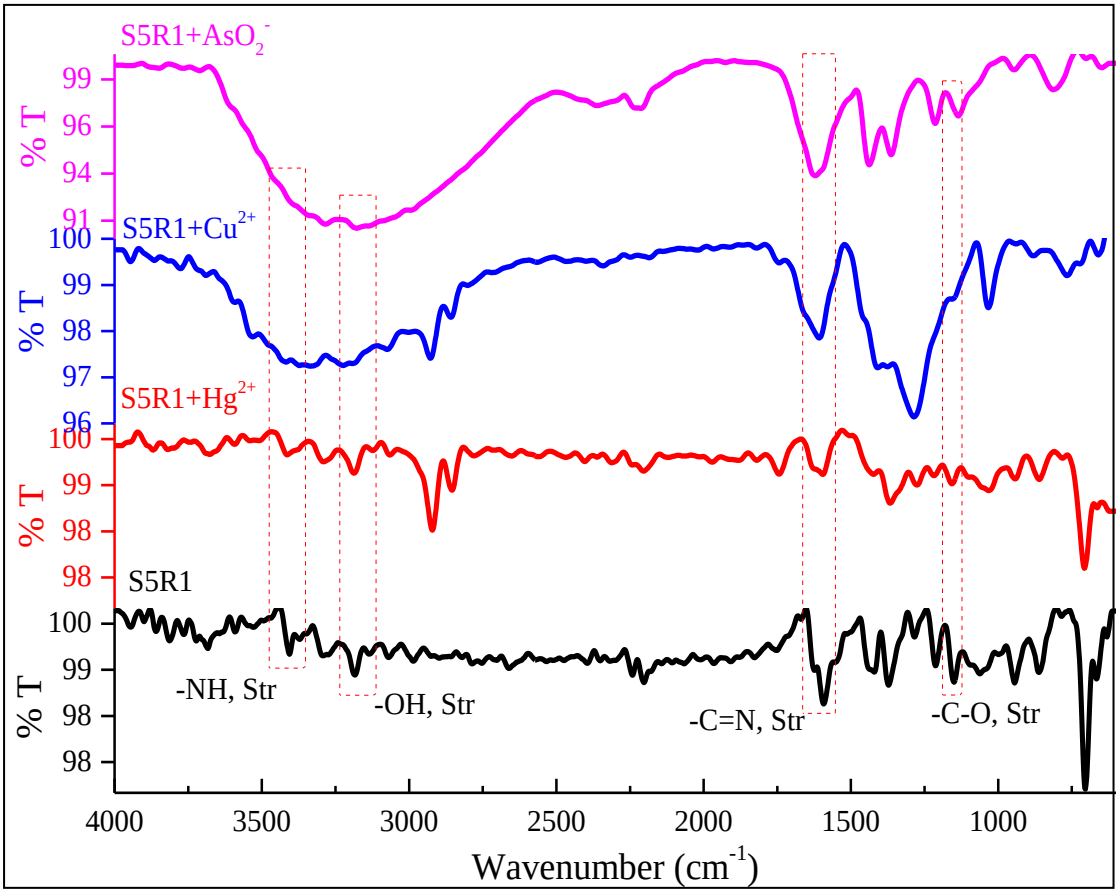

Fig. 6.18: FT-IR spectra of chemosensor **S5R1**–Hg^{2+}, **S5R1**–Cu^{2+} and **S5R1**–AsO_2^- Complex

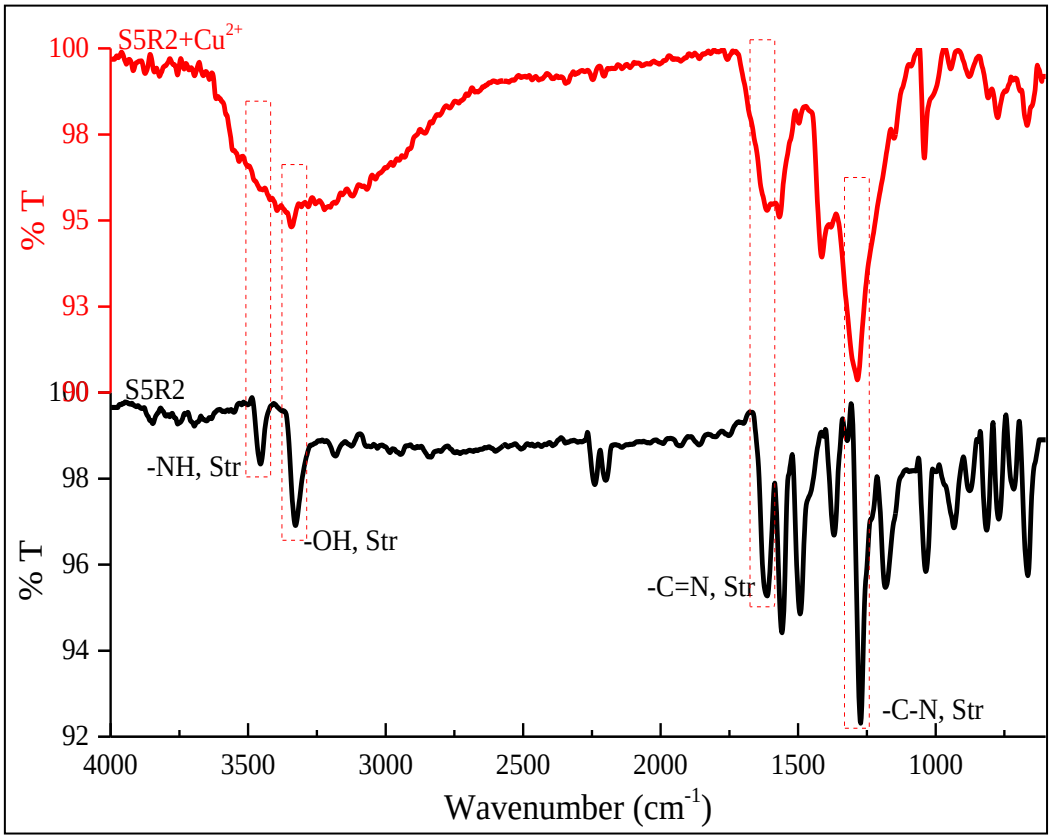

Fig. 6.19: FT-IR spectra of chemosensor **S5R2**–Cu^{2+} complex

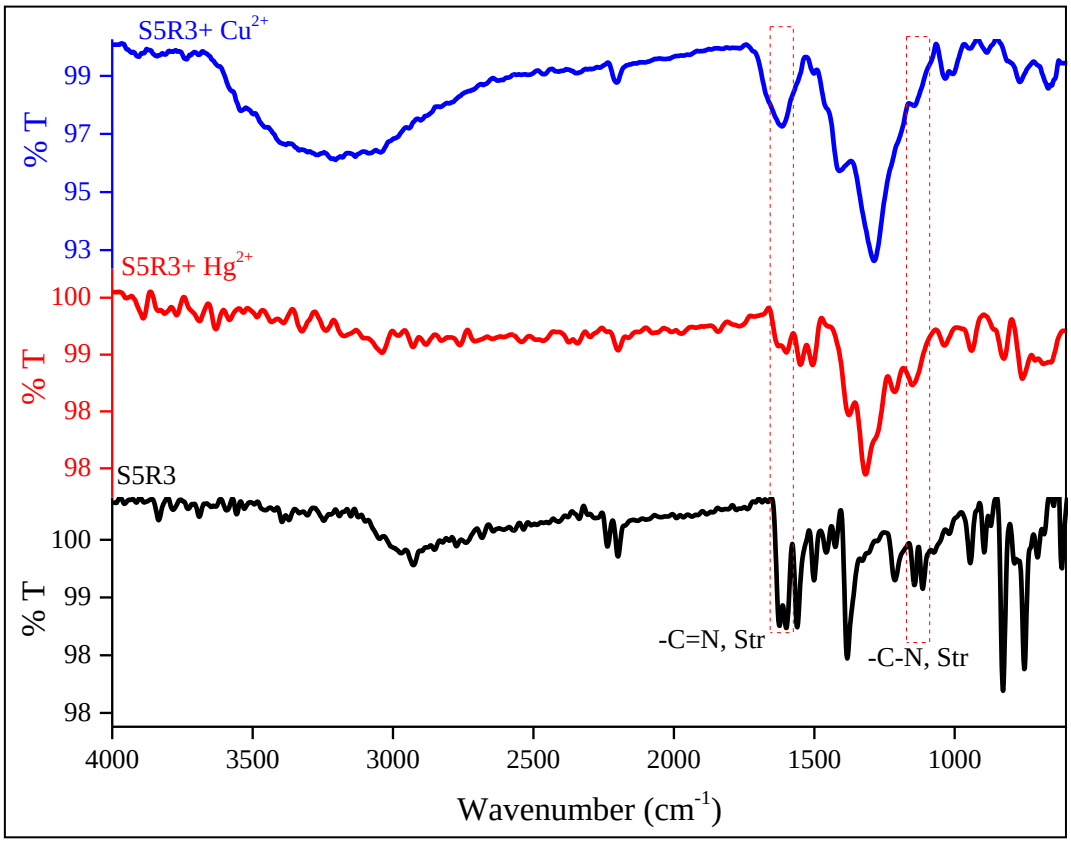

Fig. 6.20: FT-IR spectra of chemosensor **S5R3**–Hg^{2+} and **S5R3**–Cu^{2+} Complex

From the B-H plot results, it was observed that the 1:1 binding ratio of chemosensor and metal ions. Further, it was confirmed by the ESI-mass results of chemosensor complexes **(Fig. 6.21-6.23)**. A prominent mass peaks at m/z = 545.00, 390.10, 431.00 are corresponds to [**S5R1**–Hg^{2+} H_2O], [**S5R1**–Cu^{2+}] and [**S5R1**–AsO_2^-] respectively in the ES-mass spectrum **(Fig. 6.21a-c)**. Similarly the m/z peak at 324.80 for [**S5R2**–Cu^{2+} H_2O] **(Fig. 6.22)**, 466.60 for [**S5R3**–Hg^{2+} H_2O] and 329.90 corresponds to [**S5R3**–Cu^{2+} H_2O] **(Fig. 6.23a-b)** respectively. This mass result confirms the formation of a 1:1 ratio of chemosensor and metal ions complex.

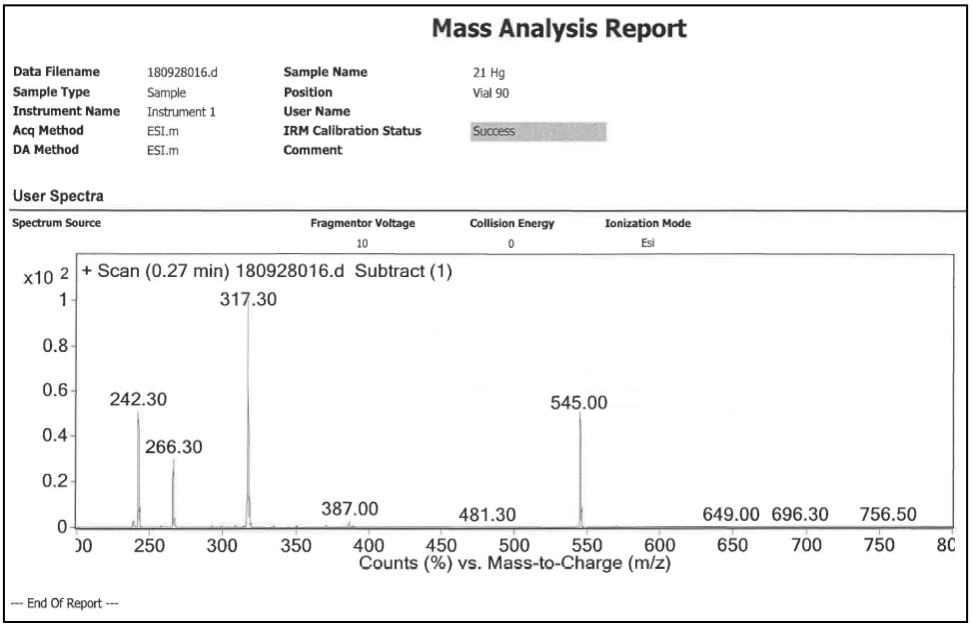

Fig. 6.21a: Mass spectrum of chemosensor **S5R1**–Hg^{2+} complex

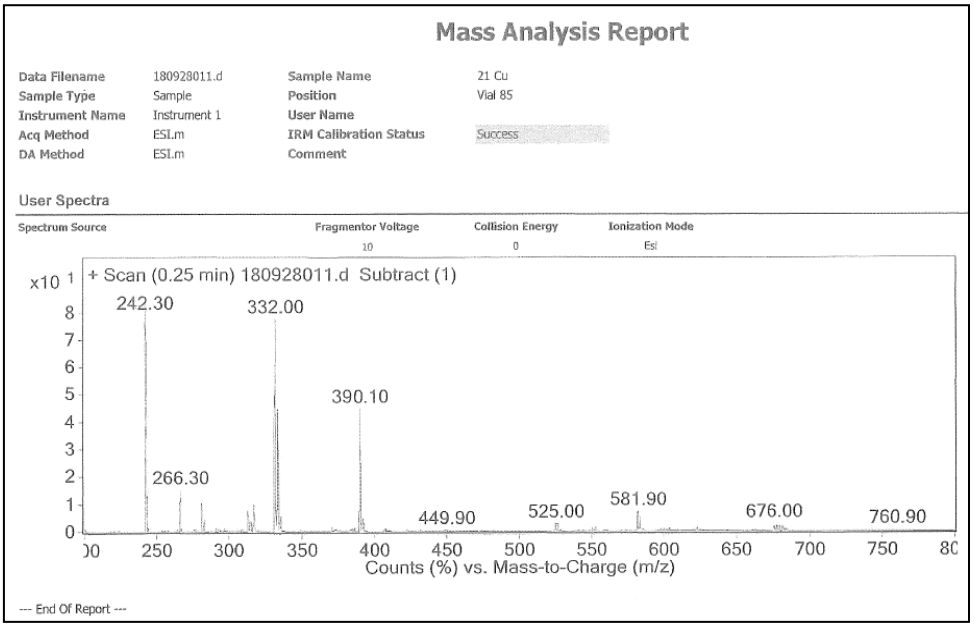

Fig. 6.21b: Mass spectrum of chemosensor **S5R1**–Cu^{2+} complex

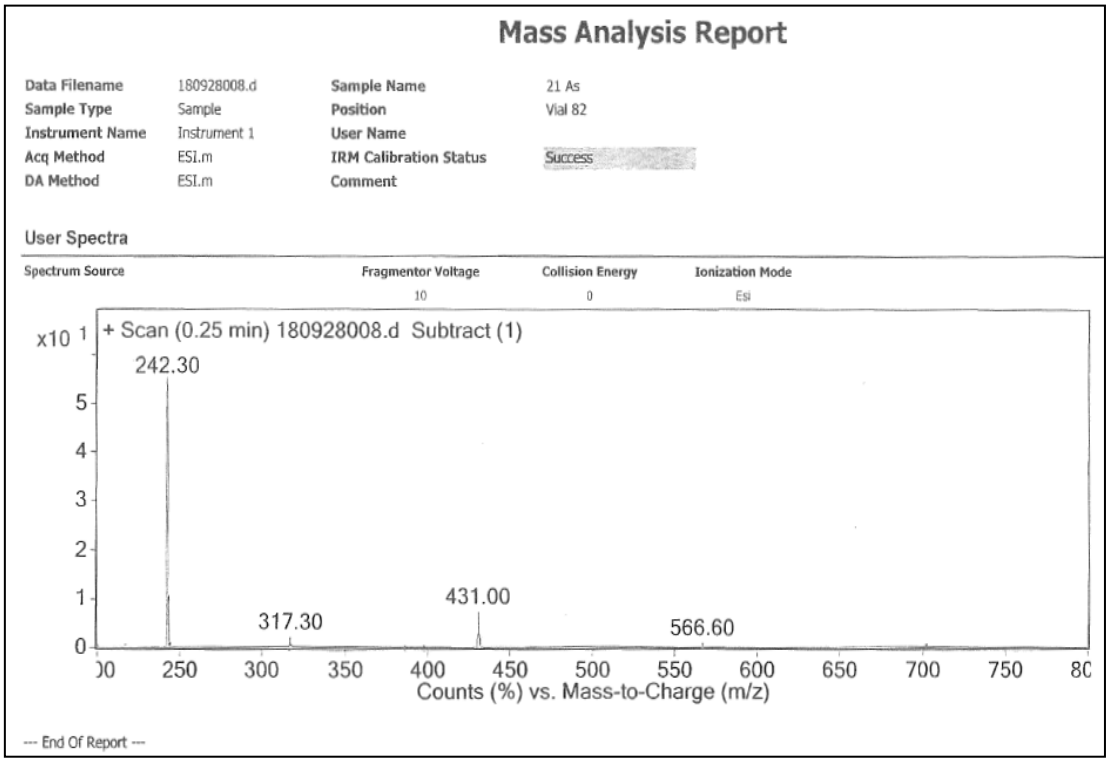

Fig. 6.21c: Mass spectrum of chemosensor **S5R1**–AsO_2^- complex

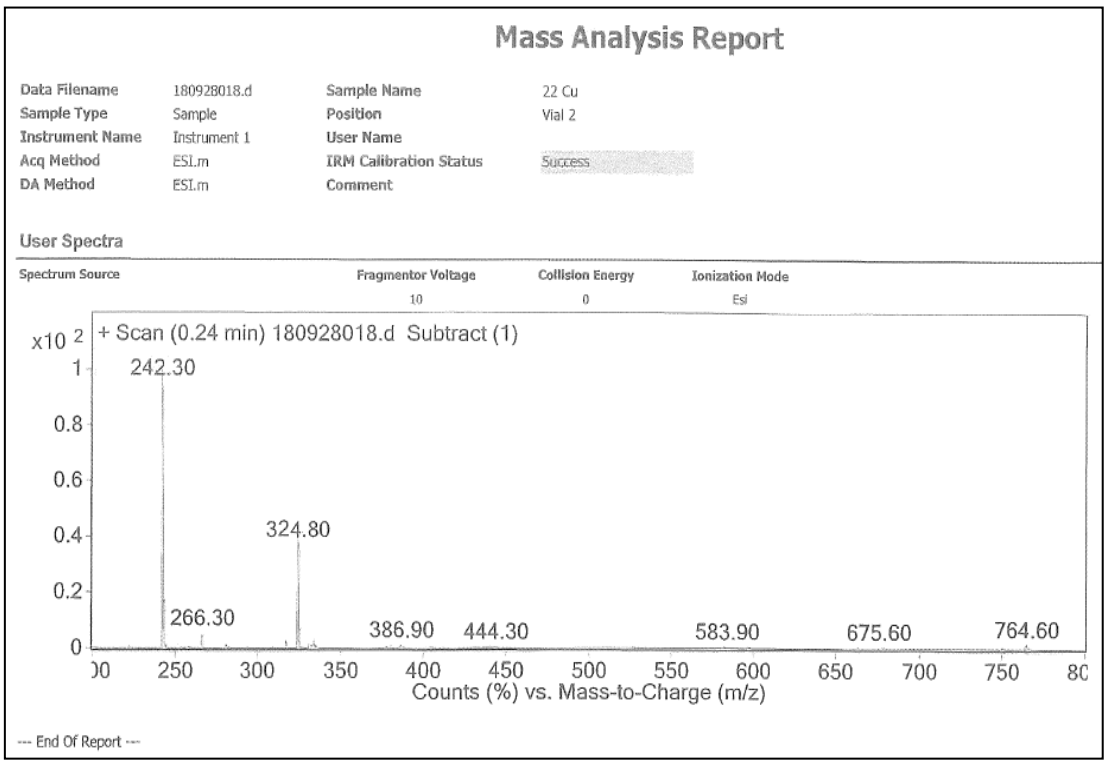

Fig. 6.22: Mass spectrum of chemosensor **S5R2**–Cu^{2+} complex

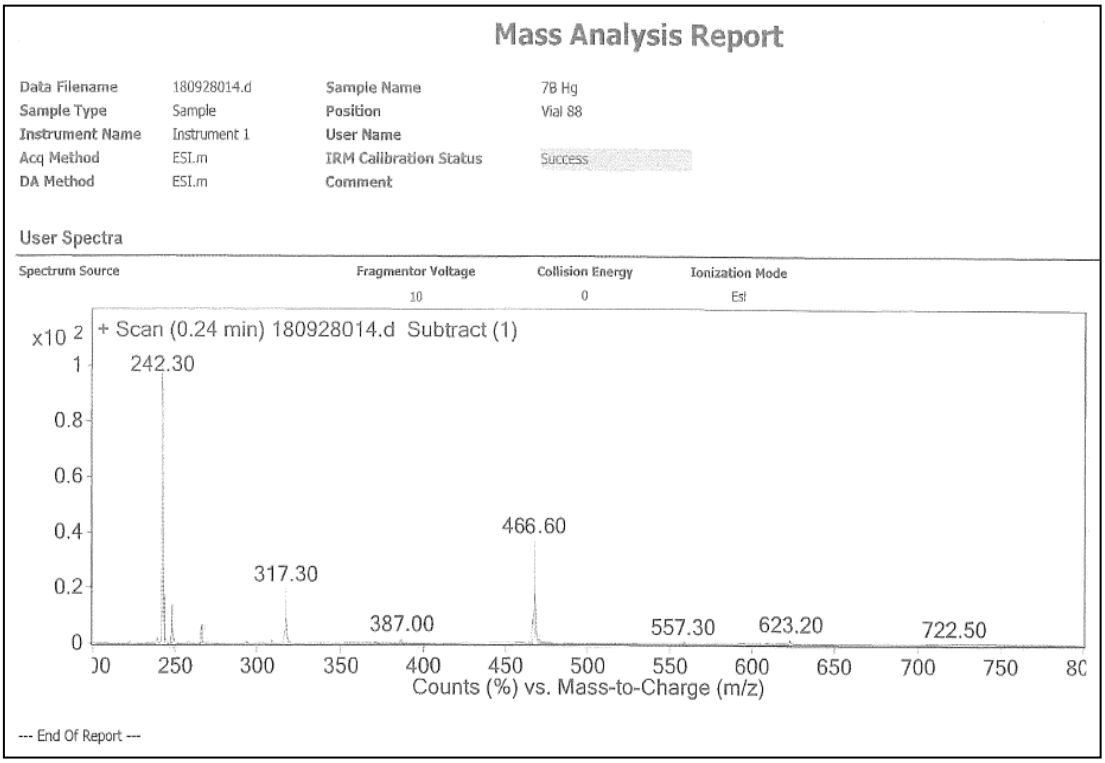

Fig. 6.23a: Mass spectrum of chemosensor **S5R3**–Hg^{2+} complex

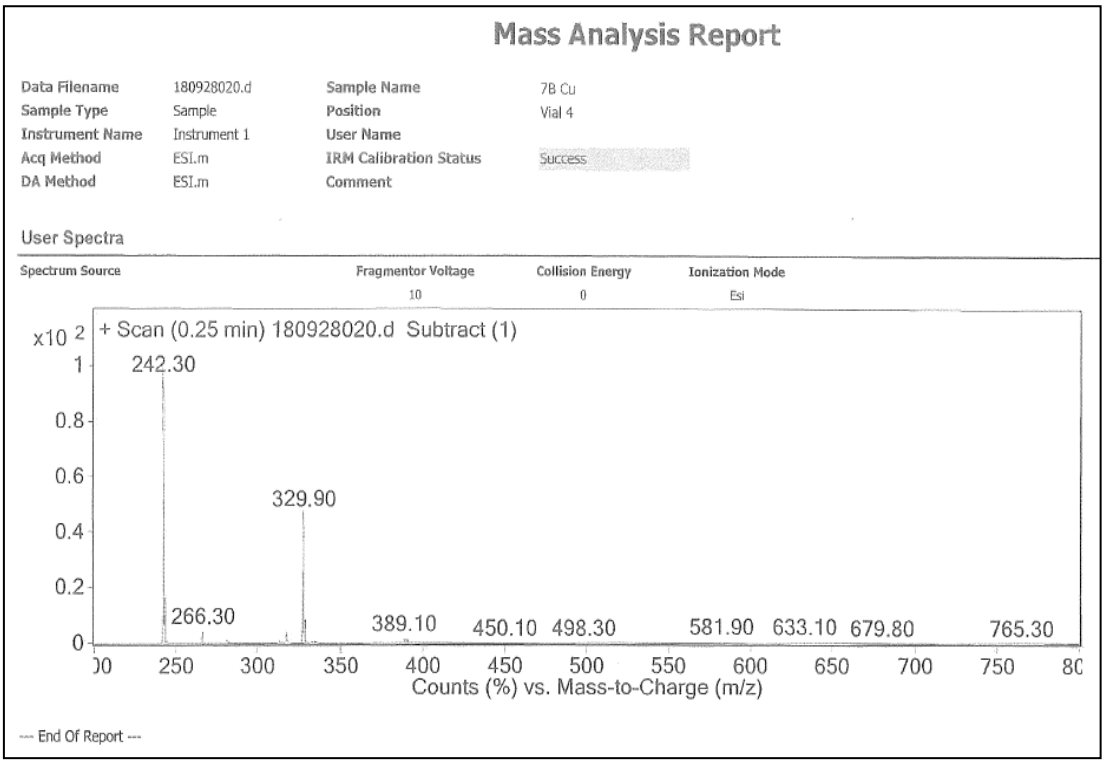

Fig. 6.23b: Mass spectrum of chemosensor **S5R3**–Cu^{2+} complex

Based on the obtained results from FT-IR, UV-Vis, Mass analysis, the proposed binding interaction between chemosensor **S5R1–S5R3** and their metal ions is represented in **Fig. 6.24**.

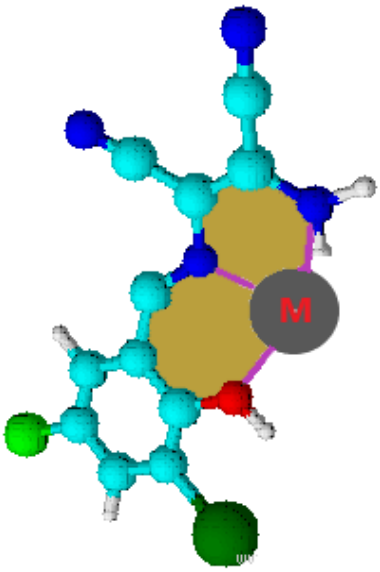

S5R1–Hg^{2+}, **S5R1**–Cu^{2+} and **S5R1**–arsenate/arsenite

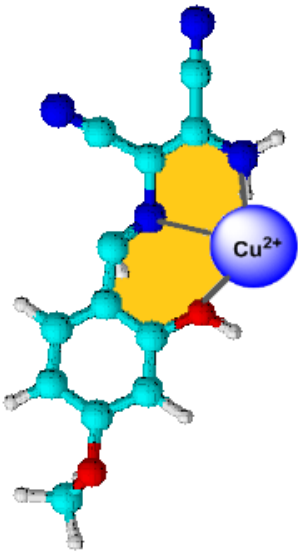

S5R2–Cu^{2+}

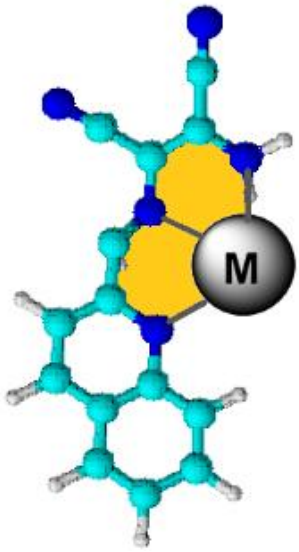

S5R3–Hg^{2+} and **S5R3–**Cu^{2+}

Fig. 6.24: Proposed interaction among **S5R1–S5R3** and different metal ions

6.3.6 Test strip application

The chemosensor S5R1 exhibits good color and sensitivity towards arsenite ions. A practical application has demonstrated for the qualitative and quantitative determination of arsenite using a simple test strip method. The chemosensor **S5R1** (1×10^{-3} M) was prepared in DMSO solution and immersed the Whatman filter paper (1cm width, 4 cm height) for about 30 min, then dried the filter paper at room temperature. A series of arsenite solution (10^{-4}, 10^{-5} and 10^{-6} M), was prepared in the de-ionized water. About 10 μL of each concentration of arsenite was added to the individual test strips (previously dipped in chemosensor **S5R1** and dried) and dried in the air. Upon addition of arsenite solution, a good color change from pale yellow to orange color was observed; the orange color intensity increased with the addition of increased concentration of arsenite ((10^{-4}, 10^{-5} and 10^{-6} M) which is depicted in the **Fig. 6.25**. This result confirms the potential application of developed chemosensor **S5R1** for the detection of arsenite by the simple naked eye.

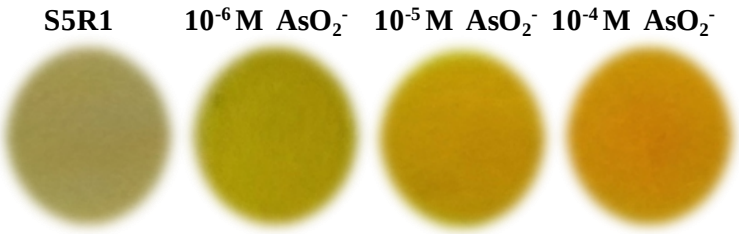

Fig. 6.25: Test strip application of S**5R1** for the detection of arsenite

6.4. Conclusions

In this chapter, three diaminomaleonitrile derivatives from simple Schiff's base condensation reaction have reported. All the chemosensors acted as a colorimetric chemosensor for the detection of Hg^{2+}, Cu^{2+}, AsO_2^- and AsO_4^{2-} ions. The UV–Vis competitive experiments confirm that the high selectivity and sensitivity of chemosensors **S5R1–S5R3** in the presence of other competitive ions. The chemosensor **S5R1** displayed the multi-ion selectivity, this was due to the presence of good binding sites and having good chromophores, compare to the **S5R2–S5R3** chemosensor. The chemosensor **S5R2** displayed good selectivity towards Cu^{2+} ions, whereas the **S5R3** displayed rapid color change with high selectivity towards Hg^{2+}, Cu^{2+} ions is due to quinoline moiety in its molecular structure. The titration

experiments of **S5R1–S5R3** with the ions suggest the quantitative relation between response, the concentration of ions, and the binding affinity ($>10^3$ M^{-1}) indicates good stability of the complex. All the chemosensors displayed sensitivity at ppb level towards active ions. The chemosensor **S5R1** exhibits a sensitivity of 8.0 ppb for the arsenite, which is less than the EPA, WHO stated limit. The good binding content, selectivity, lower detection limit, good linearity as stated range, demonstrate the application of developed chemosensors **S5R1–S5R3**, for the qualitative and quantitative applications of Hg^{2+}, Cu^{2+}, AsO_2^- and AsO_4^{2-} ions. The multi ions selectivity of **S5R1** (Hg^{2+}, Cu^{2+}, AsO_2^-, AsO_4^{2-}) and **S5R3** Hg^{2+}, Cu^{2+}) has more significance, in rapid detection of these ions by the naked eye and UV–Vis method. The binding interaction was confirmed by the FT-IR and mass analysis of complexes.

CHAPTER-7

SUMMARY AND CONCLUSIONS

CHAPTER-7

7. SUMMARY AND CONCLUSIONS

This chapter briefly explains the summary and conclusions drawn from the present research work.

7.1. Summary of the present work

Among the wide range of cations, the detection of heavy metal ions has gained significant attention because of its high toxicity and environmental pollution. However, beyond its acceptable limits is highly health concern as it can be a cause of many diseases. Owing to this, the detection of heavy metal is significant in the environment. More specifically, it will be more advantageous if one chemosensor can detect the presence of more than one heavy metal ions by colorimetrically. Based on the literature reports, it has been aimed at to design and synthesis of new chemosensors that can detect the heavy metal ions colorimetrically over other comparative analytes in the organic media and also in aqueous media.

Considering the significant detection of heavy metal ions in the field of the chemosensor research area, it has been decided to develop new chemosensors for the colorimetric detection of heavy metal ions (Hg^{2+}, Cu^{2+}, Cd^{2+}, Pb^{2+}, AsO_2^- and AsO_4^{2-} ions. The overall research work is summarized below.

- Five variety series of chemosensors based on Schiff's base reaction using various backbones such as thiocarbohydrazide, pyrene-1-carboxaldehyde, thiophene-2-carboxylic acid hydrazide, carbohydrazide, and diaminomaleonitrile have been designed and synthesized for the colorimetric detection of heavy metal ions. These chemosensors utilized for the real-life application to determine the heavy metal ions.
- All the synthesized chemosensors have been characterized using different standard spectroscopic techniques like FT–IR, ^{1}H–NMR, ^{13}C–NMR, and LC–mass (ESI–MS). Three-dimensional structures of selected chemosensors have been determined using Single Crystal X-Ray diffraction (SCXRD) studies.
- The qualitative and quantitative analysis of heavy metal ions with the developed chemosensors has been carried out using UV–Vis spectroscopic studies. The

binding constant (k) for the chemosensors-metal ion complex has been calculated using the Benesi–Hildebrand equation.

- For all the five series of chemosensors, the detection/qualification limits have been calculated using the signal to noise ration formula given by the ICH guidelines (Q2R1) from the UV–Vis titration data.
- The binding mechanisms have been proposed based on UV–Vis titration, and then some have been supported by FT–IR, ^{1}H–NMR, and LC–mass. Further, some series of chemosensors were supported by the theoretical density functional theory (DFT) studies.
- The selectivity and sensitivity of all chemosensors in the presence of various interfering analytes have been demonstrated by colorimetric and UV–Vis spectroscopic studies.
- The chemosensors **S2R1, S3R3, S3R4 S4R1-S4R3**, and **S5R1**, have been used for the demonstration of different practical applications. Further, the **S4R1–S4R3** and **S5R1** successfully used for test strips application for the qualitative/quantitative determination of heavy metal ions.
- The detection limit and application of developed chemosensors (**S1R1–S1R3, S2R2–S2R3, S3R1–S3R4, S4R1–S4R3** and **S5R1–S5R3**) were summarized and compared with the previous literature reports as given in **table 7.1**.

Table-7.1: Summary and comparison of the present developed chemosensors detection limit and applications with the literature reports

Detection method	**Detection limit**	**Application**	**Reference**
Cu^{2+}			
UV-Vis	--	No	(Duan et al. 2012)
Fluorescent & UV-Vis	--	No	(Yu et al. 2013)
UV-Vis	2.14×10^{-7} M	Yes	(Xiong et al. 2016)
Fluorescent	2.73 μM	Yes	(Wang and Wu 2013a)
Fluorescent & UV-Vis	4.83×10^{-7} M	No	(Sun et al. 2015)
Fluorescent	4×10^{-8} M	Yes	(Sarkar et al. 2013)
UV-Vis	5.24×10^{-7}M	No	(Liu et al. 2015)
Fluorescent	--	No	(Shi et al. 2013)
UV-Vis	0.3 μM	No	(Huang et al. 2009)
Fluorescent	0.25 μM	No	(Wang et al. 2011a)
UV-Vis	0.9 μM	No	(You et al. 2015a)
UV-Vis	1.2 μM	No	(Sheng et al. 2008)
UV-Vis	0.37 μM	Yes	(Kim et al. 2015)
Fluorescent	0.2 μM	No	(Ye et al. 2014)
UV-Vis	0.26 μM	No	(Kao et al. 2014)
UV-Vis	2.1 μM	No	(Jo et al. 2015)
UV-Vis	13 ppb	No	S1R1
UV-Vis	57 ppb	No	S1R2
UV-Vis	76 ppb	No	S1R3
UV-Vis	178 ppb	Yes	S3R3
UV-Vis	**11 ppb**	**Yes**	**S4R1**
UV-Vis	13 ppb	Yes	S4R2
UV-Vis	20 ppb	Yes	S4R3
UV-Vis	121 ppb	Yes	S5R1
UV-Vis	65 ppb	Yes	S5R2
UV-Vis	16 ppb	No	S5R3

Cd^{2+}			
Fluorescent	10^{-7} M	No	(Goswami et al. 2013)
Fluorescent	6.47×10^{-7} M	No	(Samanta et al. 2016)
Fluorescent	--	No	(Prodi et al. 2001)
Fluorescent	--	No	(Choi et al. 2001)
Fluorescent	1×10^{-6} M	--	(Bronson et al. 2005)
Fluorescent	--	Yes	(Peng et al. 2007)
Fluorescent	1×10^{-9} M	No	(Cockrell et al. 2008)
Fluorescent	--	Yes	(Yang et al. 2011)
Fluorescent	--	No	(Zhou et al. 2008)
Fluorescent	1×10^{-7} M	No	(Lu et al. 2007)
Fluorescent	--	No	(Gunnlaugsson et al. 2004)
UV–Vis	1.03×10^{-6} M	No	(Arabahmadi et al. 2014)
	4.00×10^{-7} M		
	3.82×10^{-7} M		
UV–Vis	22 ppb	No	S1R1
UV–Vis	22 ppb	Yes	S3R4
UV–Vis	**2 ppb**	**Yes**	**S4R1**
Hg^{2+}			
UV–Vis	2.4×10^{-6} M	No	(Huo et al. 2016)
	3.13×10^{-6} M		
	2.74×10^{-6} M		
	1.96×10^{-6} M		
	3.13×10^{-6} M		
UV–Vis & Fluorescent	25.6 nM	No	(Park et al. 2015)
UV–Vis & Fluorescent	7.91×10^{-7} M	No	(Fang et al. 2015)
Fluorescent	1.0×10^{-5} M	No	(Mahapatra et al. 2012)
UV–Vis	0.41 μM	No	(Chang et al. 2018)
	0.071 μM		
Fluorescent	0.143 nM	No	(Joshi et al. 2017)
Fluorescent	1 nM	No	(Jiao et al. 2017)

UV–Vis & Fluorescent	2.7×10^{-8} M	Yes	(Wang et al. 2014)
UV–Vis	140 ppb	No	S1R1
UV–Vis & Fluorescent	78 & 54 ppb	Yes	S2R1
UV–Vis	**2 ppb**	**Yes**	**S4R1**
UV–Vis	**2 ppb**	**Yes**	**S4R2**
UV–Vis	24 ppb	No	S5R1
UV–Vis	276 ppb	No	S5R3
Pb^{2+}			
Fluorometric	8 nM	Yes	(Ghorai et al. 2016)
UV–Vis	2.3×10^{-7} M	Yes	(Guang et al. 2018)
UV–Vis & Fluorescent	5.44 μM	Yes	(Wang et al. 2018)
UV–Vis & Fluorescent	75 nM	Yes	(Ghosh et al. 2018)
UV–Vis	32 ppb	No	S1R1
UV–Vis	**14 ppb**	**Yes**	**S4R1**
As^{3+}/As^{5+}			
UV–Vis	7.2 ppb/ 6.7ppb	No	(Chauhan et al. 2017)
Fluorescent	10 ppb	Yes	(Saha et al. 2017)
UV–Vis / Fluorescent	66 nM (AsO_2^-)	No	(Yadav and Singh 2016)
Fluorescent	4.1ppb(AsO_3^{3-})	Yes	(Lohar et al. 2014)
UV–Vis	213 ppb	Yes	S4R3
UV–Vis	**8 ppb/13 ppb**	**Yes**	**S5R1**

7.2. Conclusions

Based on the obtained experimental results, the following important conclusions have been derived.

- A five different series of colorimetric chemosensors have been designed, synthesized, and characterized using standard spectroscopic techniques like FT–IR, ^{1}H-NMR, ^{13}C–NMR and LC–mass (ESI-MS). Few chemosensor structures were determined using Single Crystal X-Ray diffraction (SCXRD) studies.
- Chemosensors **S1R1–S1R3**, have developed using thiocarbohydrazide as a backbone for the selective detection of Hg^{2+}, Cu^{2+}, Pb^{2+} and Cd^{2+} ions over other tested cations.
- The **S1R1** has shown response towards metal ions viz., Hg^{2+}, Cu^{2+}, Cd^{2+}, and Pb^{2+} in an aqueous medium with ppb detection limits. The multi-metal ion detection is due to the presence of the more active binding site in its molecular structure (hydroxyquinoline) than the other chemosensors (**S1R2–S1R3**).
- The **S1R1** and **S1R3** shown colorimetric response towards Cu^{2+} ions with ppb detection limits of 57 & 76 ppb, respectively, which is lower than the WHO/US–EPA/ USP stated value (1.3 ppm).
- The chemosensors **S1R1–S1R3** exhibited a good binding consent range of 10^3 to 10^5 M^{-1} with a 1:1 binding stoichiometric ratio with that of metal ions.
- The correlation study (absorption (A_0/A) versus ionic radii /electronegativity), results reveals that, the high affinity of chemosensors **S1R1–S1R3** towards Hg^{2+}, Cu^{2+}, Pb^{2+}, and Cd^{2+} than other tested cations.
- The chemosensor **S1R1** is versatile in its function binding Hg^{2+}, Cu^{2+}, Cd^{2+}, and Pb^{2+} ions with a distinct colorimetric response in an aqueous medium compared to chemosensors **S1R2, S1R3**, and the multi-metal ion sensing activity of **S1R1** gains significance in the field of colorimetric chemosensors for heavy metal ions detection.
- The chemosensors **S1R1–S1R3** have shown a good linear range from 0 to 10^{-6} M.
- Among the reported chemosensors in the second series (i.e., **S2R1–S2R3**), the chemosensor **S2R1** shown selectivity and sensitivity towards Hg^{2+} ions by producing a noticeable naked-eye color change.

- The colorimetric, UV–Vis, and fluoresce studies confirmed the selectivity of chemosensor **S2R1** with the Hg^{2+} ions and in the attendance of other competitive tested metal ions.
- The Hg^{2+}-induced hydrolysis of the **S2R1** detection mechanism was confirmed through optical (UV–Vis/ Fluoresce), spectroscopy (FT–IR, Mass, and ^{1}H–NMR), and theoretical DFT study results.
- The chemosensor **S2R1** was accomplished for the detection of 78 ppb (UV–Vis) and 54 ppb (Fluoresce) of $\mathbf{Hg^{2+}}$ ions in the water medium.
- The **S2R2** and **S2R3** did not show any activity towards other tested cations and $\mathbf{Hg^{2+}}$ ions; this may be a lack of suitable binding sites in their molecular structure like **S2R1.**
- The **S2R1** has more acidic compared to that of **S2R2,** and **S2R3** may be due to this the **S2R1** undergone hydrolysis with the Hg^{2+} ions**.** The real-time analysis results suggest that the **S2R1** could produce accurate and linear results for routine applications.
- Among the 3rd series chemosensors (i.e., **S3R1-S3R4**); the **S3R3, S3R4** exhibit the qualitative and quantitative determination of $\mathbf{Cu^{2+}}$ and $\mathbf{Cd^{2+}}$ ions in an aqueous medium through a remarkable color change from colorless to yellow color which can be easily identified by naked-eye.
- The **S3R1** and **S3R2** did not show any activity towards $\mathbf{Cu^{2+}}$ and $\mathbf{Cd^{2+}}$ ions and other tested cations due to lack of suitable heteroatom in the thiophene ring-like **S3R3** and **S3R4**.
- The real-time applications and analytical method validated results of **S3R3, S3R4** demonstrate that the proposed analytical method would produce precise, accurate, and linear results for the determination of $\mathbf{Cu^{2+}}$ and $\mathbf{Cd^{2+}}$ ions in environmental water samples.
- The chemosensors **S3R3** and **S3R4** have the advantage over the other published methods in terms of method validation and selectivity in the presence of other competitive cations and anions.
- The carbohydrazide based colorimetric chemosensors **S4R1–S4R3** (i.e., 4th series) displayed selective for Hg^{2+}, Cu^{2+}, Pb^{2+}, Cd^{2+}, and AsO_2^- ions in the presence of other competitive metals.

- The chemosensor **S4R1** gave multi-color responses in the presence of Hg^{2+}, Cu^{2+}, Cd^{2+}, and Pb^{2+} in water media. This multi selectivity was recognized owing to the existence of multiple binding sites in its structure (i.e., imine, hydroxy, and quinoline nitrogen) in comparison with other chemosensors (**S4R2–S4R3**).
- The **S4R1** exhibits high preference in binding with Hg^{2+} ions than other selective metal ions (Cu^{2+}, Cd^{2+}, and Pb^{2+}) and it was confirmed by colorimetric and UV–Vis studies.
- The **S4R2** exhibits a dual colorimetric signal for Hg^{2+} and Cu^{2+} ions. The **S4R3** specifically binds Cu^{2+} and AsO_2^- ions with remarkable naked-eye color change.
- The good association constant values were observed for the chemosensors **S4R1–S4R3** with that of metal ions.
- The **S4R2** and **S4R3** did not show any activity towards Cd^{2+} and Pb^{2+} like **S4R1**; this might be due to not have a hydroxy (–OH) group in quinoline ring.
- Among the 4^{th} series of chemosensors (i.e., **S4R1–S4R3**), the **S4R1** has a low detection limit for Hg^{2+} ions (2 ppb) than comparing to other chemosensors.
- A good linear range and detection limit at ppb were found for the chemosensors **S4R1–S4R3**. It indicates that the quantitative and qualitative applications in the field of colorimetric chemosensors.
- The experimental results of **S4R1–S4R3** were well coordinated with that of calculated theoretical DFT results.
- The chemosensors **S5R1–S5R3** (i.e., 5^{th} series) were designed from diaminomaleonitrile derivatives, using simple Schiff's base condensation reaction.
- The UV–Vis competitive experiments have confirmed the high selectivity and sensitivity of chemosensors **S5R1–S5R3** in the presence of other competitive ions.
- The chemosensor **S5R1** displayed the multi-ion selectivity (Hg^{2+}, Cu^{2+}, AsO_2^- and AsO_4^{2-} ions), this was due to the presence of good binding sites and having good chromophores, compare to the **S5R2–S5R3**.
- The chemosensor **S5R2** displayed good selectivity for Cu^{2+} ions, whereas the **S5R3** displayed rapid color change with high selectivity towards Hg^{2+}, Cu^{2+} ions is due to quinoline moiety in its molecular structure and failed to sense the AsO_2^- and AsO_4^{2-} ions due to lack of hydroxy (–OH) group in its molecular structure like **S5R1**.

- The titration experiments of **S5R1–S5R3** with the active ions, suggests the quantitative relation between response versus concentration of ions and the binding affinity (>10^3 M^{-1}) indicates good stability of the complex.
- The chemosensors **S5R1–S5R3** displayed sensitivity at ppb level towards active ions. The **S5R1** accomplished the sensitivity of 8.0 ppb for the arsenite, which is less than the EPA/WHO stated limits (10.0 ppb).
- The good binding content, selectivity, lower detection limit, good linearity as stated range, demonstrate the developed chemosensors **S5R1–S5R3** for the qualitative and quantitative applications of Hg^{2+}, Cu^{2+}, AsO_2^- and AsO_4^{2-} ions.
- Successfully demonstrated the practical application of **S5R1** by test strips application method.
- The multi ions selectivity of **S5R1** (Hg^{2+}, Cu^{2+}, AsO_2^-, AsO_4^{2-}) and **S5R3** (Hg^{2+}, Cu^{2+}) has more significance, in rapid detection of these ions by the naked eye and UV–Vis method.

7.3. Future work

7.3.1. Heavy metal ions detection and application

The development of colorimetric chemosensors for the detection of cations is one of the promising areas in the field of supramolecular chemistry. The majority of the sensors have been developed for the detection of cations such as Cu^{2+}, Ni^{2+}, Zn^{2+}, Fe^{2+}, Fe^{3+}, and Co^{2+}. However, there are very few chemosensors that have been designed for the selective detection of heavy metal ions in an aqueous media. The selective detection of Hg^{2+}, Pb^{2+}, Cd^{2+}, and Cr^{3+} ions at the ppm detection limit is a difficult task due to their chemical and physical properties. Throughout the last few years, various researchers established heavy metals detection using colorimetric and fluoresce sensors. The majority of these chemosensors have only quantitative applications and very few reports available with the qualitative applications.

Hence, looking at the difficulty of heavy metal detection, some simple suitable functionalized molecules have decided to synthesized, with this hope that these chemosensors will act as potent heavy metal ion detectors. Further, the synthesized sensors will be applying for the quantitative and qualitative applications in an aqueous media. Further, the naked eye detection would utilize to develop simple and low-cost detection methods by using smartphone and test strips applications. This method would be enabled to field monitoring of toxic heavy metal ions.

REERENCES

REFERENCES

Anand, T., and Sahoo, S. K. (2019). "Cost-effective approach to detect Cu(II) and Hg(II) by integrating a smartphone with the colorimetric response from a NBD-benzimidazole based dyad." *Phys. Chem. Chem. Phys.*, 21(22), 11839–11845.

Arabahmadi, R., Orojloo, M., and Amani, S. (2014). "Azo Schiff bases as colorimetric and fluorescent sensors for recognition of F^-, Cd^{2+} and Hg^{2+} ions." *Anal. Methods*, 6(18), 7384–7393.

Aragay, G., Pons, J., and Merkoçi, A. (2011). "Recent trends in macro-, micro-, and nanomaterial-based tools and strategies for heavy-metal detection." *Chem. Rev.*

Azadbakht, R., Almasi, T., Keypour, H., and Rezaeivala, M. (2013). "A new asymmetric Schiff base system as fluorescent chemosensor for Al^{3+} ion." *Inorg. Chem. Commun.*, 33, 63–67.

Bansod, B. K., Kumar, T., Thakur, R., Rana, S., and Singh, I. (2017). "A review on various electrochemical techniques for heavy metal ions detection with different sensing platforms." *Biosens. Bioelectron.*, Elsevier B.V.

Beer, P. D., and Gale, P. A. (2001). "Anion recognition and sensing: The state of the art and future perspectives." *Angew. Chemie - Int. Ed.*

Bhalla, V., Roopa, Kumar, M., Sharma, P. R., and Kaur, T. (2013). "Hg^{2+} induced hydrolysis of pentaquinone based Schiff base: A new chemodosimeter for Hg2+ ions in mixed aqueous media." *Dalt. Trans.*, 42(42), 15063–15068.

Bronson, R. T., Michaelis, D. J., Lamb, R. D., Husseini, G. A., Farnsworth, P. B., Linford, M. R., Izatt, R. M., Bradshaw, J. S., and Savage, P. B. (2005). "Efficient immobilization of a cadmium chemosensor in a thin film: Generation of a cadmium sensor prototype." *Org. Lett.*, 7(6), 1105–1108.

Brown, D. R. (2001). "Copper and prion disease." *Brain Res. Bull.*, 165–173.

Burdette, S. C., and Lippard, S. J. (2001). "ICCC34 - Golden edition of coordination chemistry reviews. Coordination chemistry for the neurosciences." *Coord. Chem. Rev.*

Burdette, S. C., and Lippard, S. J. (2003). "Meeting of the minds:

Metalloneurochemistry." *Proc. Natl. Acad. Sci. U. S. A.*, 100(7), 3605–3610.

Chaney, R. L. (1991). "The Heavy Elements: Chemistry, Environmental Impact, and Health Effects." *J. Environ. Qual.*, 20(4), 876.

Chang, L. L., Gao, Q., Liu, S., Hu, C. C., Zhou, W. J., and Zheng, M. M. (2018). "Selective and differential detection of Hg^{2+} and Cu^{2+} with use of a single rhodamine hydrazone-type probe in the absence and presence of UV irradiation." *Dye. Pigment.*, 153, 117–124.

Chapter, U. S. P. (2016). "232> Elemental Impurities-Limits." *Pharmacopeial Forum*.

Chauhan, K., Singh, P., Kumari, B., and Singhal, R. K. (2017). "Synthesis of new benzothiazole Schiff base as selective and sensitive colorimetric sensor for arsenic on-site detection at ppb level." *Anal. Methods*, 9(11), 1779–1785.

Chen, Y., Zhu, C., Yang, Z., Li, J., Jiao, Y., He, W., Chen, J., and Guo, Z. (2012). "A new 'turn-on' chemodosimeter for Hg^{2+}: ICT fluorophore formation via Hg^{2+}-induced carbaldehyde recovery from 1,3-dithiane." *Chem. Commun.*, 48(42), 5094–5096.

Choi, M., Mihyang, K., Lee, K. D., Han, K. N., Yoon, I. A., Chung, H. J., and Yoon, J. (2001). "A new reverse PET chemosensor and its chelatoselective aromatic cadmiation." *Org. Lett.*, 3(22), 3455–3457.

Choi, Y. W., You, G. R., Lee, M. M., Kim, J., Jung, K.-D., and Kim, C. (2014). "Highly selective recognition of mercury ions through the naked-eye" *Inorg. Chem. Commun.*, 46, 43–46.

Choong, T. S. Y., Chuah, T. G., Robiah, Y., Gregory Koay, F. L., and Azni, I. (2007). "Arsenic toxicity, health hazards and removal techniques from water: an overview." *Desalination*, 217(1–3), 139–166.

Cockrell, G. M., Zhang, G., VanDerveer, D. G., Thummel, R. P., and Hancock, R. D. (2008). "Enhanced metal ion selectivity of 2,9-di-(pyrid-2-yl)-1,10-phenanthroline and its use as a fluorescent sensor for cadmium(II)." *J. Am. Chem. Soc.*, 130(4), 1420–1430.

Das, J., and Sarkar, P. (2016). "A new dipstick colorimetric sensor for detection of

arsenate in drinking water." *Environ. Sci. Water Res. Technol.*, 2(4), 693–704.

Das, P., Ghosh, A., Bhatt, H., and Das, A. (2012). "A highly selective and dual responsive test paper sensor of Hg^{2+}/Cr^{3+} for naked eye detection in neutral water." *RSC Adv.*, 2(9), 3714–3721.

Duan, Y. L., Shi, Y. G., Chen, J. H., Wu, X. H., Wang, G. K., Zhou, Y., and Zhang, J. F. (2012). "1,8-Naphthyridine modified rhodamine B derivative and Cu^{2+} complex: Colorimetric sensing of thiols in aqueous media." *Tetrahedron Lett.*, 53(48), 6544–6547.

Dutta, M., and Das, D. (2012). "Recent developments in fluorescent sensors for trace-level determination of toxic-metal ions." *TrAC - Trends Anal. Chem.*

Edition, F. (2011). "Guidelines for drinking-water quality." *WHO Chron.*, 38(4), 104–108.

El-Shwiniy, W. H., and Zordok, W. A. (2018). "Synthesis, spectral, DFT modeling, cytotoxicity and microbial studies of novel Zr(IV), Ce(IV) and U(VI) piroxicam complexes." *Spectrochim. Acta - Part A Mol. Biomol. Spectrosc.*, 199, 290–300.

Emerit, J., Edeas, M., and Bricaire, F. (2004). "Neurodegenerative diseases and oxidative stress." *Biomed. Pharmacother.*

Ermakova, E., Michalak, J., Meyer, M., Arslanov, V., Tsivadze, A., Guilard, R., and Bessmertnykh-Lemeune, A. (2013). "Colorimetric Hg^{2+} sensing in water: From molecules toward low-cost solid devices." *Org. Lett.*, 15(3), 662–665.

Fang, Y., Zhou, Y., Li, J. Y., Rui, Q. Q., and Yao, C. (2015). "Naphthalimide-Rhodamine based chemosensors for colorimetric and fluorescent sensing Hg^{2+} through different signaling mechanisms in corresponding solvent systems." *Sensors Actuators, B Chem.*, 215, 350–359.

Fegade, U., Saini, A., Sahoo, S. K., Singh, N., Bendre, R., and Kuwar, A. (2014). "2,2′-(Hydrazine-1,2-diylidenedimethylylidene)bis(6-isopropyl-3-methylphenol) based selective dual-channel chemosensor for Cu2+in semi-aqueous media." *RSC Adv.*, 4(75), 39639–39644.

Frisch, M. J., Trucks, G. W., Schlegel, H. B., Scuseria, G. E., Robb, M. A.,

Cheeseman, J. R., Scalmani, G., Barone, V., Mennucci, B., Petersson, G. A., and others. (2009). “Gaussian 09, revision A. 1.” *Gaussian Inc. Wallingford CT*, 27, 34.

Ganesabaskaran, S., and Kandasamy, K. (2015). “Chemosensors for Hg Ions: A Review of Literature.” *Biosens. J.*, s4(2), 1–9.

Gattás-Asfura, K. M., and Leblanc, R. M. (2003). “Peptide-coated CdS quantum dots for the optical detection of copper (II) and silver (I).” *Chem. Commun.*, (21), 2684–2685.

Ghorai, A., Mondal, J., Saha, R., Bhattacharya, S., and Patra, G. K. (2016). “A highly sensitive reversible fluorescent-colorimetric azino bis-Schiff base sensor for rapid detection of Pb^{2+} in aqueous media.” *Anal. Methods*, 8(9), 2032–2040.

Ghosh, A., Das, S., Kundu, S., Maiti, P. K., and Sahoo, P. (2018). “Rapid estimation of lead in lipsticks.” *Sensors Actuators, B Chem.*, 266, 80–85.

Goswami, S., Aich, K., Das, S., Das, A. K., Manna, A., and Halder, S. (2013). “A highly selective and sensitive probe for colorimetric and fluorogenic detection of Cd^{2+} in aqueous media.” *Analyst*, 138(6), 1903.

Graham, N. (1999). “Guidelines for Drinking-Water Quality, 2nd edition, Addendum to Volume 1 – Recommendations, World Health Organisation, Geneva, 1998, 36 pages.” *Urban Water*, 1(2), 183.

Guang, Y. S., Ren, X., Zhao, S., Yan, Q. Z., Zhao, G., and Xu, Y. H. (2018). “A novel 4-phenyl amino thiourea derivative designed for real-time ratiometric–colorimetric detection of toxic Pb^{2+}.” *J. Environ. Sci. Heal. - Part A Toxic/Hazardous Subst. Environ. Eng.*, 53(6), 555–560.

Guideline, I. C. H. H. T. (2005). “Validation of analytical procedures: text and methodology Q2 (R1).” *Int. Conf. Harmon. Geneva, Switz.*, 11–12.

Gunnlaugsson, T., Clive Lee, T., and Parkesh, R. (2004). “Highly selective fluorescent chemosensors for cadmium in water.” *Tetrahedron*, 60(49), 11239–11249.

Hahn, S. H., Tanner, M. S., Danke, D. M., and Gahl, W. A. (1995). “Normal metallothionein synthesis in fibroblasts obtained from children with indian childhood cirrhosis or copper-associated childhood cirrhosis.” *Biochem. Mol. Med.*, 54(2), 142–

145.

Hammud, H. H., Shazly, S. El, Sonji, G., Sonji, N., and Bouhadir, K. H. (2015). "Thiophene aldehyde-diamino uracil Schiff base: A novel fluorescent probe for detection and quantification of cupric, silver and ferric ions." *Spectrochim. Acta - Part A Mol. Biomol. Spectrosc.*, 150, 94–103.

Hanwell, M. D., Curtis, D. E., Lonie, D. C., Vandermeerschd, T., Zurek, E., and Hutchison, G. R. (2012). "Avogadro: An advanced semantic chemical editor, visualization, and analysis platform." *J. Cheminform.*, 4(8), 7.

Hariharan, P. C., and Pople, J. A. (1973). "The influence of polarization functions on molecular orbital hydrogenation energies." *Theor. Chim. Acta*, 28(3), 213–222.

Häussermann, U., Dolg, M., Stoll, H., Preuss, H., Schwerdtfeger, P., and Pitzer, R. M. (1993). "Accuracy of energy-adjusted quasirelativistic ab initio pseudopotentials all-electron and pseudopotential benchmark calculations for Hg, HgH and their cations." *Mol. Phys.*, 78(5), 1211–1224.

He, Z. L., Yang, X. E., and Stoffella, P. J. (2005). "Trace elements in agroecosystems and impacts on the environment." *J. Trace Elem. Med. Biol.*

Hehre, W. J., Ditchfield, K., and Pople, J. A. (1972). "Self-consistent molecular orbital methods. XII. Further extensions of gaussian-type basis sets for use in molecular orbital studies of organic molecules." *J. Chem. Phys.*, 56(5), 2257–2261.

Hong, S., Kang, T., Moon, J., Oh, S., and Yi, J. (2007). "Surface plasmon resonance analysis of aqueous copper ions with amino-terminated self-assembled monolayers." *Colloids Surfaces A Physicochem. Eng. Asp.*, 292(2–3), 264–270.

Hu, S., Song, J., Zhao, F., Meng, X., and Wu, G. (2015). "Highly sensitive and selective colorimetric naked-eye detection of Cu^{2+} in aqueous medium using a hydrazone chemosensor." *Sensors Actuators, B Chem.*, 215, 241–248.

Huang, J., Xu, Y., and Qian, X. (2009). "A colorimetric sensor for Cu^{2+} in aqueous solution based on metal ion-induced deprotonation: Deprotonation/protonation mediated by Cu^{2+} -ligand interactions." *Dalt. Trans.*, (10), 1761–1766.

Hughes, M. F., Beck, B. D., Chen, Y., Lewis, A. S., and Thomas, D. J. (2011).

"Arsenic exposure and toxicology: A historical perspective." *Toxicol. Sci.*, 123(2), 305–332.

Huo, Y., Wang, S., Lu, T., Pan, C., Lu, Y., Yang, X., Hu, D., and Hu, S. (2016). "Highly selective and sensitive colorimetric chemosensors for Hg^{2+} based on novel diaminomaleonitrile derivatives." *RSC Adv.*, 6(7), 5503–5511.

Jeon, C. H., Park, C. S., Lee, C. S., and Ha, T. H. (2018). "Simple immobilization of mercury ion chemosensors to solid substrate." *J. Ind. Eng. Chem.*, 57, 370–376.

Jeong, U., and Kim, Y. (2015). "Colorimetric detection of heavy metal ions using aminosilane." *J. Ind. Eng. Chem.*, 31, 393–396.

Jesus, R. M. De, Silva, L. O. B., Castro, J. T., Azevedo Neto, A. D. De, Jesus, R. M. De, and Ferreira, S. L. C. (2013). "Determination of mercury in phosphate fertilizers by cold vapor atomic absorption spectrometry." *Talanta*, 106, 293–297.

Jiang, J., Gou, C., Luo, J., Yi, C., and Liu, X. (2012). "A novel highly selective colorimetric sensor for Ni(II) ion using coumarin derivatives." *Inorg. Chem. Commun.*, 15, 12–15.

Jiang, X. H., Wang, B. D., Yang, Z. Y., Liu, Y. C., Li, T. R., and Liu, Z. C. (2011). "8-Hydroxyquinoline-5-carbaldehyde Schiff-base as a highly selective and sensitive Al^{3+} sensor in weak acid aqueous medium." *Inorg. Chem. Commun.*, 14(8), 1224–1227.

Jiao, Y., Zhou, L., He, H., Yin, J., and Duan, C. (2017). "A new fluorescent chemosensor for recognition of Hg^{2+} ions based on a coumarin derivative." *Talanta*, 162(September 2016), 403–407.

Jo, H. Y., Park, G. J., Na, Y. J., Choi, Y. W., You, G. R., and Kim, C. (2014). "Sequential colorimetric recognition of Cu^{2+} and CN^{-} by asymmetric coumarin-conjugated naphthol groups in aqueous solution." *Dye. Pigment.*, 109, 127–134.

Jo, T. G., Na, Y. J., Lee, J. J., Lee, M. M., Lee, S. Y., and Kim, C. (2015). "A diaminomaleonitrile based selective colorimetric chemosensor for copper(ii) and fluoride ions." *New J. Chem.*, 39(4), 2580–2587.

Joshi, S., Kumari, S., Sarmah, A., Pant, D. D., and Sakhuja, R. (2017). "Detection of

Hg2+ions in aqueous medium using an indole-based fluorescent probe: Experimental and theoretical investigations." *J. Mol. Liq.*, 248, 668–677.

Kao, S. L., Lin, W. Y., Venkatesan, P., and Wu, S. P. (2014). "Colorimetric detection of Cu(II): Cu(II)-induced deprotonation of NH responsible for color change." *Sensors Actuators, B Chem.*, 204, 688–693.

Karlsson, H. L., Toprak, M. S., and Fadeel, B. (2014). "Toxicity of Metal and Metal Oxide Nanoparticles." *Handb. Toxicol. Met. Fourth Ed.*, 75–112.

Kato, T., Nakamura, S., and Morita, M. (1990). "Determination of nickel, copper, zinc, silver, cadmium and lead in seawater by isotope dilution inductively coupled plasma mass spectrometry." *Anal. Sci.*, 6(4), 623–626.

Kaur, B., Kaur, N., and Kumar, S. (2018). "Colorimetric metal ion sensors – A comprehensive review of the years 2011–2016." *Coord. Chem. Rev.*, Elsevier B.V.

Kaur, K., Saini, R., Kumar, A., Luxami, V., Kaur, N., Singh, P., and Kumar, S. (2012). "Chemodosimeters: An approach for detection and estimation of biologically and medically relevant metal ions, anions and thiols." *Coord. Chem. Rev.*

Kim, H. N., Ren, W. X., Kim, J. S., and Yoon, J. (2012). "Fluorescent and colorimetric sensors for detection of lead, cadmium, and mercury ions." *Chem. Soc. Rev.*

Kim, J. H., Kim, H. J., Bae, C. W., Park, J. W., Lee, J. H., and Kim, J. S. (2010). "Hg^{2+}-Induced hydrolysis-based selective fluorescent chemodosimeter." *Arkivoc*, 2010(7), 170–178.

Kim, Y. S., Park, G. J., Lee, S. A., and Kim, C. (2015). "A colorimetric chemosensor for the sequential detection of copper ion and amino acids (cysteine and histidine) in aqueous solution." *RSC Adv.*, 5(39), 31179–31188.

Kumar, P., Kim, K. H., Bansal, V., Lazarides, T., and Kumar, N. (2017). "Progress in the sensing techniques for heavy metal ions using nanomaterials." *J. Ind. Eng. Chem.*, 54, 30–43.

Kundu, A., Hariharan, P. S., Prabakaran, K., and Anthony, S. P. (2015). "Synthesis of new colori/fluorimetric chemosensor for selective sensing of biologically important

Fe^{3+}, Cu^{2+} and Zn^{2+} metal ions." *Spectrochim. Acta - Part A Mol. Biomol. Spectrosc.*, 151, 426–431.

Küpper, M., and Schultze, J. W. (1997). "A new copper ion selective microelectrode for electrochemical applications." *J. Electroanal. Chem.*, 427(1–2), 129–135.

Labbé, R. F., Vreman, H. J., and Stevenson, D. K. (1999). "Zinc protoporphyrin: a metabolite with a mission." *Clin. Chem.*, 45(12), 2060–2072.

Lauwerys, R. R., Bernard, A. M., Roels, H. A., and Buchet, J. P. (1994). "Cadmium: Exposure markers as predictors of nephrotoxic effects." *Clin. Chem.*, 1391–1394.

Lee, C., Yang, W., and Parr, R. (1988). "Development of the Colle- Salvetti correlation energy formula into a functional of the electron density." *Phys Rev B*, 37(2), 785–789.

Lee, H., Lee, H. S., Reibenspies, J. H., and Hancock, R. D. (2012). "Mechanism of 'turn-on' fluorescent sensors for mercury(II) in solution and its implications for ligand design." *Inorg. Chem.*, 51(20), 10904–10915.

Lee, S. Y., Bok, K. H., and Kim, C. (2017). "A fluorescence 'turn-on' chemosensor for Hg^{2+} and Ag^{+} based on NBD (7-nitrobenzo-2-oxa-1,3-diazolyl)." *RSC Adv.*, 7(1), 290–299.

Li, C. Y., Xu, F., Li, Y. F., Zhou, K., and Zhou, Y. (2012a). "A fluorescent chemosensor for Hg2+based on naphthalimide derivative by fluorescence enhancement in aqueous solution." *Anal. Chim. Acta*, 717, 122–126.

Li, K., and Xue, D. (2006). "Estimation of electronegativity values of elements in different valence states." *J. Phys. Chem. A*, 110(39), 11332–11337.

Li, M., Lu, H.-Y., Liu, R.-L., Chen, J.-D., and Chen, C.-F. (2012). "Turn-On Fluorescent Sensor for Selective Detection of Zn^{2+}, Cd^{2+}, and Hg^{2+} in Water." *J. Org. Chem.*, 77(7), 3670–3673.

Li, Z., Xiang, Y., and Tong, A. (2008). "Ratiometric chemosensor for fluorescent determination of Zn^{2+} in aqueous ethanol." *Anal. Chim. Acta*, 619(1), 75–80.

Lin, Q., Fu, Y. P., Chen, P., Wei, T. B., and Zhang, Y. M. (2013). "Colorimetric chemosensors designed to provide high sensitivity for Hg^{2+} in aqueous solutions."

Dye. Pigment., 96(1), 1–6.

Lin, W., Yuan, L., Tan, W., Feng, J., and Long, L. (2009). "Construction of fluorescent probes via protection/deprotection of functional groups: A ratiometric fluorescent probe for Cu^{2+}." *Chem. - A Eur. J.*, 15(4), 1030–1035.

Liu, Q., Fei, Q., Fei, Y., Fan, Q., Shan, H., Feng, G., and Huan, Y. (2015). "A novel colorimetric probe derived from isonicotic acid hydrazide for copper(II) determination based on internal charge transfer (ICT)." *Spectrochim. Acta - Part A Mol. Biomol. Spectrosc.*, 151, 785–789.

Liu, W., Xu, L., Sheng, R., Wang, P., Li, H., and Wu, S. (2007). "A water-soluble 'switching on' fluorescent chemosensor of selectivity to Cd^{2+}." *Org. Lett.*, 9(19), 3829–3832.

Lohar, S., Pal, S., Sen, B., Mukherjee, M., Banerjee, S., and Chattopadhyay, P. (2014). "Selective and sensitive turn-on chemosensor for arsenite ion at the ppb level in aqueous media applicable in cell staining." *Anal. Chem.*, 86(22), 11357–11361.

Lu, C., Xu, Z., Cui, J., Zhang, R., and Qian, X. (2007). "Ratiometric and highly selective fluorescent sensor for cadmium under physiological pH range: A new strategy to discriminate cadmium from zinc." *J. Org. Chem.*, 72(9), 3554–3557.

Ma, L. J., Yan, Y., Chen, L., Cao, W., Li, H., Yang, L., and Wu, Y. (2012). "A fluorescence reagent for the highly selective recognition and separation of lead ion (II) from aqueous solutions." *Anal. Chim. Acta*, 751, 135–139.

Mahapatra, A. K., Roy, J., Manna, S. K., Kundu, S., Sahoo, P., Mukhopadhyay, S. K., and Banik, A. (2012). "Hg^{2+}-selective 'turn-on' fluorescent chemodosimeter derived from glycine and living cell imaging." *J. Photochem. Photobiol. A Chem.*, 240, 26–32.

Malm, O. (1998). "Gold mining as a source of mercury exposure in the Brazilian Amazon." *Environ. Res.*, 77(2), 73–78.

Manandhar, E., and Wallace, K. J. (2012). "Host-guest chemistry of pyrene-based molecular receptors." *Inorganica Chim. Acta*, 381(1), 15–43.

Marbella, L., Serli-Mitasev, B., and Basu, P. (2009). "Development of a fluorescent

Pb2+ sensor." *Angew. Chemie - Int. Ed.*, 48(22), 3996–3998.

Michon, J., Deluchat, V., Shukry, R. Al, Dagot, C., and Bollinger, J. C. (2007). "Optimization of a GFAAS method for determination of total inorganic arsenic in drinking water." *Talanta*, 71(1), 479–485.

Momidi, B. K., Tekuri, V., and Trivedi, D. R. (2017). "Multi-signaling thiocarbohydrazide based colorimetric sensors for the selective recognition of heavy metal ions in an aqueous medium." *Spectrochim. Acta - Part A Mol. Biomol. Spectrosc.*, 180, 175–182.

Nair, R. R., Raju, M., Patel, N. P., Raval, I. H., Suresh, E., Haldar, S., and Chatterjee, P. B. (2015). "Naked eye instant reversible sensing of Cu^{2+} and its in situ imaging in live brine shrimp Artemia." *Analyst*, 140(16), 5464–5468.

Narayanaswamy, N., and Govindaraju, T. (2012). "Aldazine-based colorimetric sensors for Cu 2+ and Fe 3+." *Sensors Actuators, B Chem.*, 161(1), 304–310.

Noël, M., Christensen, J. R., Spence, J., and Robbins, C. T. (2015). "Using laser ablation inductively coupled plasma mass spectrometry (LA-ICP-MS) to characterize copper, zinc and mercury along grizzly bear hair providing estimate of diet." *Sci. Total Environ.*, 529, 1–9.

Nordberg, G. F. (1992). "Cadmium in the human environment: toxicity and carcinogenicity." *IARC Sci. Publ.*, 118, 1–470.

Park, J., In, B., and Lee, K.-H. (2015). "Highly selective colorimetric and fluorescent detection for Hg^{2+} in aqueous solutions using a dipeptide-based chemosensor." *RSC Adv.*, 5(69), 56356–56361.

Patil, S. R., Nandre, J. P., Patil, P. A., Sahoo, S. K., Devi, M., Pradeep, C. P., Fabiao, Y., Chen, L., Redshaw, C., and Patil, U. D. (2015). "A uracil nitroso amine based colorimetric sensor for the detection of Cu^{2+} ions from aqueous environment and its practical applications." *RSC Adv.*, 5(28), 21464–21470.

Pearson, R. G. (1963). "Hard and Soft Acids and Bases." *J. Am. Chem. Soc.*, 85(22), 3533–3539.

Peng, X., Du, J., Fan, J., Wang, J., Wu, Y., Zhao, J., Sun, S., and Xu, T. (2007). "A

Selective Fluorescent Sensor for Imaging Cd^{2+} in Living Cells." *J. Am. Chem. Soc.*, 129(6), 1500–1501.

Peterson, K. A. (2003). "Systematically convergent basis sets with relativistic pseudopotentials. I. Correlation consistent basis sets for the post-d group 13-15 elements." *J. Chem. Phys.*, 119(21), 11099–11112.

Prodi, L., Montalti, M., Zaccheroni, N., Bradshaw, J. S., Izatt, R. M., and Savage, P. B. (2001). "Characterization of 5-chloro-8-methoxyquinoline appended diaza-18-crown-6 as a chemosensor for cadmium." *Tetrahedron Lett.*, 42(16), 2941–2944.

Quang, D. T., and Kim, J. S. (2010). "Fluoro- and chromogenic chemodosimeters for heavy metal ion detection in solution and biospecimens." *Chem. Rev.*, 110(10), 6280–6301.

Que, E. L., Domaille, D. W., and Chang, C. J. (2008). "Metals in neurobiology: Probing their chemistry and biology with molecular imaging." *Chem. Rev.*, 108 (5), 1517-1549.

Renzoni, A., Zino, F., and Franchi, E. (1998). "Mercury levels along the food chain and risk for exposed populations." *Environ. Res.*, 77(2), 68–72.

Ronkart, S. N., Laurent, V., Carbonnelle, P., Mabon, N., Copin, A., and Barthélemy, J. P. (2007). "Speciation of five arsenic species (arsenite, arsenate, MMAAV, DMAAV and AsBet) in different kind of water by HPLC-ICP-MS." *Chemosphere*, 66(4), 738–745.

Rout, K., Manna, A. K., Sahu, M., and Patra, G. K. (2019). "A guanidine based bis Schiff base chemosensor for colorimetric detection of Hg(II) and fluorescent detection of Zn(II) ions." *Inorganica Chim. Acta*, 486(October 2018), 733–741.

Saha, J., Roy, A. D., Dey, D., Nath, J., Bhattacharjee, D., and Hussain, S. A. (2017). "Development of arsenic(V) sensor based on Fluorescence Resonance Energy Transfer." *Sensors Actuators, B Chem.*, 241, 1014–1023.

Sahoo, S. K., Sharma, D., Moirangthem, A., Kuba, A., Thomas, R., Kumar, R., Kuwar, A., Choi, H. J., and Basu, A. (2016). "Pyridoxal derived chemosensor for chromogenic sensing of Cu2+and fluorogenic sensing of Fe^{3+} in semi-aqueous

medium.” *J. Lumin.*, 172, 297–303.

Samanta, S., Datta, B. K., Boral, M., Nandan, A., and Das, G. (2016). “A multi-responsive turn-on flurogenic probe to sense Zn^{2+}, Cd^{2+} and Pb^{2+}: Left-right-center emission signal swing.” *Analyst*, 141(14), 4388–4393.

Santra, M., Ryu, D., Chatterjee, A., Ko, S. K., Shin, I., and Ahn, K. H. (2009). “A chemodosimeter approach to fluorescent sensing and imaging of inorganic and methylmercury species.” *Chem. Commun.*, 0(16), 2115–2117.

Sarkar, B. (2002). *Heavy Metals In The Environment*. *Heavy Met. Environ., CRC Press.*

Sarkar, S., Roy, S., Sikdar, A., Saha, R. N., and Panja, S. S. (2013). “A pyrene-based simple but highly selective fluorescence sensor for Cu^{2+} ions via a static excimer mechanism.” *Analyst*, 138(23), 7119.

Selvaganapathi, P., Thirumaran, S., and Ciattini, S. (2017). “Synthesis, spectral, crystal structures, Hirshfeld surface analysis and DFT studies on phenylmercury(II) dithiocarbamate complexes and their utility for the preparation of mercury sulfide nanoparticles.” *J. Mol. Struct.*, 1148, 547–556.

Shannon, R. D. (1976). “Revised effective ionic radii and systematic studies of interatomic distances in halides and chalcogenides.” *Acta Crystallogr. Sect. A Cryst. physics, diffraction, Theor. Gen. Crystallogr.*, 32(5), 751–767.

Sharma, V. K., and Sohn, M. (2009). “Aquatic arsenic: Toxicity, speciation, transformations, and remediation.” *Environ. Int.*, 35(4), 743–759.

Sheng, R., Wang, P., Gao, Y., Wu, Y., Liu, W., Ma, J., Li, H., and Wu, S. (2008). “Colorimetric Test Kit for Cu^{2+} Detection.” *Org. Lett.*, 10(21), 5015–5018.

Shi, Z., Tang, X., Zhou, X., Cheng, J., Han, Q., Zhou, J. A., Wang, B., Yang, Y., Liu, W., and Bai, D. (2013). “A highly selective fluorescence ‘turn-on’ probe for Cu(II) based on reaction and its imaging in living cells.” *Inorg. Chem.*, 52(21), 12668–12673.

Singhal, D., Gupta, N., and Singh, A. K. (2015). “Chromogenic ‘naked eye’ and fluorogenic ‘turn on’ sensor for mercury metal ion using thiophene-based Schiff

base." *RSC Adv.*, 5(81), 65731–65738.

Sirawatcharin, S., Saithongdee, A., Chaicham, A., Tomapatanaget, B., Imyim, A., and Praphairaksit, N. (2014). "Naked-eye and Colorimetric Detection of Arsenic(III) Using Difluoroboron-curcumin in Aqueous and Resin Bead Support Systems." *Anal. Sci.*, 30(12), 1129–1134.

Smedley, P. L., and Kinniburgh, D. G. (2002). "A review on the sources, behavior and distribution of arsenic in natural waters." *Appl. Geochemistry*, 17(5), 517–568.

Song, K. C., Kim, J. S., Park, S. M., Chung, K. C., Ahn, S., and Chang, S. K. (2006). "Fluorogenic Hg^{2+}-selective chemodosimeter derived from 8-hydroxyquinoline." *Org. Lett.*, 8(16), 3413–3416.

Srivastava, P., Ali, R., Razi, S. S., Shahid, M., Patnaik, S., and Misra, A. (2013). "A simple blue fluorescent probe to detect Hg^{2+} in semiaqueous environment by intramolecular charge transfer mechanism." *Tetrahedron Lett.*, 54(28), 3688–3693.

Srivastava, P., Razi, S. S., Ali, R., Gupta, R. C., Yadav, S. S., Narayan, G., and Misra, A. (2014). "Selective naked-eye detection of Hg^{2+} through an efficient turn-on photoinduced electron transfer fluorescent probe and its real applications." *Anal. Chem.*, 86(17), 8693–8699.

Srivastava, P., Shahid, M., and Misra, A. (2011). "Protein assisted fluorescence enhancement of a dansyl containing fluorescent reagent: Detection of Hg^{+} ion in aqueous medium." *Org. Biomol. Chem.*, 9(14), 5051–5055.

Steed, J. W., and Atwood, J. L. (2010). *Supramolecular chemistry*. *John Wiley Sons*.

Stevens, A. A., Moore, L. A., Slocum, C. J., Smith, B. L., Seeger, D. R., and Ireland, J. C. (1990). "Chemistry, environmental impact and health effects." *Water chlorination*, 579–604.

Sun, Z., Li, H., Guo, D., Liu, Y., Tian, Z., and Yan, S. (2015). "A novel piperazine-bis(rhodamine-B)-based chemosensor for highly sensitive and selective naked-eye detection of Cu^{2+} and its application as an INHIBIT logic device." *J. Lumin.*, 167, 156–162.

Suresh, P., Azath, I. A., and Pitchumani, K. (2010). "Naked-eye detection of Fe^{3+} and

Ru^{3+} in water: Colorimetric and ratiometric sensor based on per-6-amino-β-cyclodextrin/p-nitrophenol." *Sensors Actuators, B Chem.*, 146(1), 273–277.

Tang, X. L., Peng, X. H., Dou, W., Mao, J., Zheng, J. R., Qin, W. W., Liu, W. S., Chang, J., and Yao, X. J. (2008). "Design of a semirigid molecule as a selective fluorescent chemosensor for recognition of Cd(II)." *Org. Lett.*, 10(17), 3653–3656.

Tang, Y., Sun, J., and Yin, B. (2016). "A dual-response fluorescent probe for Zn^{2+} and Al^{3+} detection in aqueous media: pH-dependent selectivity and practical application." *Anal. Chim. Acta*, 942, 104–111.

Tchounwou, P. B., Ayensu, W. K., Ninashvili, N., and Sutton, D. (2003). "Environmental exposure to mercury and its toxicopathologic implications for public health." *Environ. Toxicol.*,18 (3), 149-175

Tchounwou, P. B., Yedjou, C. G., Patlolla, A. K., and Sutton, D. J. (2012). "Heavy Metal Toxicity and the Environment." *Springer*, 133–164.

Tharmaraj, V., and Pitchumani, K. (2012). "An acyclic, dansyl based colorimetric and fluorescent chemosensor for Hg(II) via twisted intramolecular charge transfer (TICT)." *Anal. Chim. Acta*, 751, 171–175.

Tomasi, J., and Persico, M. (1994). "Molecular Interactions in Solution: An Overview of Methods Based on Continuous Distributions of the Solvent." *Chem. Rev.*, 94(7), 2027–2094.

Tuzen, M., Saygi, K. O., Karaman, I., and Soylak, M. (2010). "Selective speciation and determination of inorganic arsenic in water, food and biological samples." *Food Chem. Toxicol.*, 48(1), 41–46.

Udhayakumari, D., Suganya, S., Velmathi, S., and MubarakAli, D. (2014). "Naked eye sensing of toxic metal ions in aqueous medium using thiophene-based ligands and its application in living cells." *J. Mol. Recognit.*, 27(3), 151–159.

United States Environmental Protection Agency. (2013). "Drinking water contaminants - Standards and regulations."

Vinod Kumar, V., and Anthony, S. P. (2014). "Silver nanoparticles based selective colorimetric sensor for Cd^{2+}, Hg^{2+} and Pb^{2+} ions: Tuning sensitivity and selectivity

using co-stabilizing agents." *Sensors Actuators, B Chem.*, 191, 31–36.

Waggoner, D. J., Bartnikas, T. B., and Gitlin, J. D. (1999). "The role of copper in neurodegenerative disease." *Neurobiol. Dis.*

Wang, D., Shiraishi, Y., and Hirai, T. (2011a). "A BODIPY-based fluorescent chemodosimeter for Cu(II) driven by an oxidative dehydrogenation mechanism." *Chem. Commun.*, 47(9), 2673–2675.

Wang, F., Nandhakumar, R., Moon, J. H., Kim, K. M., Lee, J. Y., and Yoon, J. (2011b). "Ratiometric fluorescent chemosensor for silver ion at physiological pH." *Inorg. Chem.*, 50(6), 2240–2245.

Wang, H. F., and Wu, S. P. (2013a). "A pyrene-based highly selective turn-on fluorescent sensor for copper(II) ions and its application in living cell imaging." *Sensors Actuators, B Chem.*, 181, 743–748.

Wang, H. F., and Wu, S. P. (2013b). "Highly selective fluorescent sensors for mercury(II) ions and their applications in living cell imaging." *Tetrahedron*, 69(8), 1965–1969.

Wang, M., Yan, F. Y., Zou, Y., Yang, N., Chen, L., and Chen, L. G. (2014). "A rhodamine derivative as selective fluorescent and colorimetric chemosensor for mercury (II) in buffer solution, test strips and living cells." *Spectrochim. Acta - Part A Mol. Biomol. Spectrosc.*, 123, 216–223.

Wang, Y. T., Hu, S., Zhang, Y., Gong, H., Sun, R., Mao, W., Wang, D. H., and Chen, Y. (2018). "A colorimetric Pb^{2+} chemosensor: Rapid naked-eye detection, high selectivity, theoretical insights, and applications." *J. Photochem. Photobiol. A Chem.*, 355, 101–108.

Wang, Z., Zhang, D., and Zhu, D. (2005). "A sensitive and selective 'turn on' fluorescent chemosensor for Hg(II) ion based on a new pyrene-thymine dyad." *Anal. Chim. Acta*, 549(1–2), 10–13.

Wu, G., Shi, B., Hu, B., Zhang, Y., Lin, Q., Yao, H., and Wei, T. (2014). "A rational designed dual-channel chemosensor for mercury ions based on hydrolysis of Schiff base." *Chinese J. Chem.*, 32(7), 637–644.

Wu, Y.-S., Li, C.-Y., Li, Y.-F., Li, D., and Li, Z. (2016). “Development of a simple pyrene-based ratiometric fluorescent chemosensor for copper ion in living cells.” *Sensors Actuators B Chem.*, 222, 1226–1232.

Xie, Z., Wang, K., Zhang, C., Yang, Z., Chen, Y., Guo, Z., Lu, G. Y., and He, W. (2011). “A fluorometric/colorimetric dual-channel Hg^{2+} sensor derived from a 4-amino-7-nitro-benzoxadiazole (ANBD) fluorophore.” *New J. Chem.*, 35(3), 607–613.

Xiong, C., Qin, Y., and Hu, B. (2010). “On-line separation/preconcentration of V(IV)/V(V) in environmental water samples with CTAB-modified alkyl silica microcolumn and their determination by inductively coupled plasma-optical emission spectrometry.” *J. Hazard. Mater.*, 178(1–3), 164–170.

Xiong, J. J., Huang, P. C., Zhang, C. Y., and Wu, F. Y. (2016). “Colorimetric detection of Cu^{2+} in aqueous solution and on the test kit by 4-aminoantipyrine derivatives.” *Sensors Actuators, B Chem.*, 226, 30–36.

Yadav, N., and Singh, A. K. (2016). “Dual anion colorimetric and fluorometric sensing of arsenite and cyanide ions.” *RSC Adv.*, 6(102), 100136–100144.

Yadav, U. N., Pant, P., Sahoo, S. K., and Shankarling, G. S. (2014). “A novel colorimetric and fluorogenic chemosensor for selective detection of Cu^{2+} ions in mixed aqueous media.” *RSC Adv.*, 4(80), 42647–42653.

Yan, Y., Ding, G., and Xu, H. (2015). “A selective and sensitive ‘naked-eye’ rhodamine-based ‘turn-on’ sensor for recognition of Hg^{2+} ion in aqueous solution.” *J. Ind. Eng. Chem.*, 25, 73–77.

Yang, Y., Cheng, T., Zhu, W., Xu, Y., and Qian, X. (2011). “Highly selective and sensitive near-infrared fluorescent sensors for cadmium in aqueous solution.” *Org. Lett.*, 13(2), 264–267.

Ye, J. H., Xu, J., Chen, H., Bai, Y., Zhang, W., and He, W. (2014). “A colorimetric and highly sensitive and selective chemodosimeter for Cu^{2+} and its application in live cell imaging.” *Tetrahedron Lett.*, 55(45), 6269–6273.

Yin, B. C., Zuo, P., Huo, H., Zhong, X., and Ye, B. C. (2010). “DNAzyme self-assembled gold nanoparticles for determination of metal ions using fluorescence

anisotropy assay." *Anal. Biochem.*, 401(1), 47–52.

Yin, J., Bing, Q., Wang, L., and Wang, G. (2018). "Ultrasensitive and highly selective detection of Cu^{2+} ions based on a new carbazole-Schiff." *Spectrochim. Acta - Part A Mol. Biomol. Spectrosc.*, 189, 495–501.

You, G. R., Park, G. J., Lee, J. J., and Kim, C. (2015a). "A colorimetric sensor for the sequential detection of Cu^{2+} and CN- in fully aqueous media: Practical performance of Cu^{2+}." *Dalt. Trans.*, 44(19), 9120–9129.

You, L., Zha, D., and Anslyn, E. V. (2015b). "Recent Advances in Supramolecular Analytical Chemistry Using Optical Sensing." *Chem. Rev.*, 115(15), 7840–7892.

Yu, M., Yuan, R., Shi, C., Zhou, W., Wei, L., and Li, Z. (2013). "1,8-Naphthyridine and 8-hydroxyquinoline modified Rhodamine B derivatives: 'turn-on' fluorescent and colorimetric sensors for Al^{3+} and Cu^{2+}." *Dye. Pigment.*, 99(3), 887–894.

Z, J. F., and K, J. S. (2009). "Small-molecule Fluorescent Chemosensors for Hg^{2+} ion." *Anal. Chem.*, 25(November), 1271–1281.

Zhang, L. N., Liu, A. L., Liu, Y. X., Shen, J. X., Du, C. X., and Hou, H. W. (2015). "A luminescent europium metal-organic framework with free phenanthroline sites for highly selective and sensitive sensing of Cu^{2+} in aqueous solution." *Inorg. Chem. Commun.*, 56, 137–140.

Zhang, S., Wu, X., Niu, Q., Guo, Z., Li, T., and Liu, H. (2017). "Highly Selective and Sensitive Colorimetric and Fluorescent Chemosensor for Rapid Detection of Ag^{+}, Cu^{2+} and Hg^{2+} Based on a Simple Schiff Base." *J. Fluoresc.*, 27(2), 729–737.

Zhou, Y., Xiao, Y., and Qian, X. (2008). "A highly selective Cd^{2+} sensor of naphthyridine: fluorescent enhancement and red-shift by the synergistic action of forming binuclear complex." *Tetrahedron Lett.*, 49(21), 3380–3384.

http://en.wikipedia.org/wiki/Ionic_radius

https://www.epa.gov/dwstandardsregulations

LIST OF PUBLICATIONS

LIST OF PUBLICATIONS

Papers Published/Communicated in International Journals

1. **Tekuri, V**., Momidi, B. K., and Trivedi, D. R. (2017). "Multi-signaling thiocarbohydrazide based colorimetric sensors for the selective recognition of heavy metal ions in an aqueous medium." Spectrochim. Acta Part A Mol. Biomol. Spectrosc. 180, 175–182.

2. **Tekuri, V**., and Trivedi, D. R. (2017). "A new colorimetric chemosensors for Cu^{2+} and Cd^{2+} ions detection: Application in environmental water samples and analytical method validation." Anal. Chim. Acta, 972, 81–93.

3. **Tekuri, V.,** Sahoo, S. K., and Trivedi, D. R. (2019). 'Hg^{2+} induced hydrolysis of thiazole amine based Schiff base: Colorimetric and fluorogenic chemodosimeter for Hg^{2+} ions in an aqueous medium'. Spectrochim. Acta - Part A Mol. Biomol. Spectrosc., 218, 19–26.

4. **Venkatadri Tekuri,** Makesh Mohan and Darshak R Trivedi. "Smart colorimetric response for the heavy metal detection: Synthesis, spectral response and DFT studies." **(Manuscript communicated to *Chemistry Select*).**

5. **Venkatadri Tekuri** and Darshak R Trivedi." Simple colorimetric response for arsenate, arsenite, Cu^{2+} and Hg^{2+} ions: Synthesis, spectral response and test strip application." **(Manuscript communicated to *Sensors Actuators, B Chemical*).**

Papers presented in international conferences

1. **Venkatadri Tekuri**, Bharath Kumar Momidi & **Dr. Darshak R. Trivedi**. "A simple thiazole amine based colorimetric chemosensor for the selective and sensitive mercury ion detection in an aqueous medium" paper presented in "International conference on Science and Technology: Future Challenges and Solutions, 7th Annual Conference of Indian JSPS Alumni Association" August 08-09, (2016), Mysore University, Mysore.
2. **Venkatadri Tekuri** & Dr. Darshak R. Trivedi. "6-(thiophen-2-yl) picolinaldehyde based colorimetric chemosensor for the selective detection of mercury ions in an aqueous medium "International conference on Crystal ball vision on science & engineering for societal upliftment, 8th Annual Conference of Indian JSPS Alumni Association" August 07-08, (2017), NIO-Goa.

CURRICULUM VITAE

PERSONAL INFORMATION

Name	**Venkatadri Tekuri**
Address	2-35 Upparapalli, Vangimalla, Veeraballi (M), Kadapa (Dist), A.P (State), India-516268
Telephone	+91 8123750756, +91 8073769795
E-mail	chemistryno1@gmail.com
Nationality	Indian (Hindu)
Place and Date of Birth	Upparapalli, Kadapa, India. June, 4th 1988.
Passport	M2223773 released on 11/09/2014 and Expiry date 10-/09/2024 (Republic of India)

RESEARCH EXPERIENCE

- Dates (From-To): June 2015–Oct 2019
- Position held: **Ph.D. Research Scholar**
- Name and type of the organization: National Institute of Technology Karnataka, Surathkal, India-575025. https://www.nitk.ac.in
- Main activities and responsibilities:
  - Design, synthesis, and characterization of new colorimetric chemosensors for the detection of heavy metal ions.
  - Investigation of sensing properties by colorimetric, UV-Vis, and fluorescence spectroscopy.
  - Investigation of binding mechanism by different spectroscopic techniques like FT-IR, UV-Vis, NMR and mass.
  - Study of qualitative and quantitative analytical applications for the determination of heavy metal ions in different environmental samples.
  - Developing the test strips application for the real-time analysis of heavy metal ions.

TEACHING EXPERIENCES

- Dates (From-To): June 2015–Oct 2019
- Position held: **Research Scholar**
- Name and type of the organization: Department of chemistry, National Institute of Technology Karnataka, Surathkal, India-575025.

- Main activities and responsibilities

- Mentored four students to accomplish their master's research thesis
- Managed undergraduate (B. Tech.) students in Chemistry laboratory courses.
- Assisted students in conducting general chemistry experiments
- Managed master's (M. Sc.) students in analytical, inorganic chemistry laboratory courses.
- Taught them in operation of analytical instruments and educated them on the handling of different instruments, like colorimetric, UV–Vis and FT-IR spectroscopic techniques, etc.

INDUSTRIAL WORK EXPERIENCE

Cipla Ltd & CDYMAX Bangalore
From Jan-2011 to May-2013
Possition: Staff Quality

Bio-gen Extracts Pvt. Ltd. Bangalore
From Dec-2013 to July-2015
Possition: Senior Officer QA

Dr. Reddy's Laboratories Pvt. Ltd Hyderabad India.
From Dec-2013 to July 2015
Possition: Research Associate Analytical R&D

Main activities and responsibilities

- Initiation and monitoring of stability studies for API and intermediates as per the ICH guidelines
- Analytical method validation performing by HPLC and GC techniques and routine analysis.
- Preparation of Analytical method validation protocols reports & review.
- Analytical method transfer to the quality department.
- Qualification of working, reference standards, and maintenance.
- Preparation and review of SOP's, specifications, and method of analysis.
- Validation of analytical methods as per ICH, FDA Guidelines, Pharmacopoeias (USP, Ph.Eur/B.P, IP).
- Monitoring of GMP and GLP with the laboratory, conducting internal quality audits.
- Preparation and Review of all Quality documents.
- Initiation and monitoring of change controls and incidents/deviations.

EDUCATION AND TRAINING

• Dates (From-To)	June-2015 – October- 2019
• Name of the institute	National Institute of Technology Karnataka, Surathkal, India-575025
• Title of qualification awarded	**Ph.D. in Chemistry** under the supervision of **Dr. Darshak R Trivedi.** Curriculum in Chemical Science: Supramolecular chemistry. Thesis in "***Design, synthesis, and characterization of colorimetric chemosensors for the detection of heavy metal ions.***"
• Dates (From-To)	June-2008 – April-2010
• Name of the university	Sri Venkateswara University Tirupati, A.P India.
• Title of qualification awarded	M.Sc. in Medicinal Chemistry. Percentage of marks obtained: 66.0 %
• Principal subjects covered	Organic Synthesis, Inorganic chemistry, physical chemistry, Advanced Spectroscopy, Heterocyclic chemistry, General chemistry, Chromatography and medicinal chemistry
• Dates (From-To)	June-2005 – April-2008
• Name of the university	Sri Venkateswara University Tirupati, A.P India.
• Title of qualification awarded	B.Sc. in Chemistry, Botany and Zoology. Percentage of marks obtained: 80.1 % (*Distinction)*
• Principal subjects covered	Bachelor's level Chemistry, Botany and Zoology.

TECHNICAL SKILLS AND COMPETENCES

With specific kinds of analytical instruments and computers, etc.	• High-Performance Liquid Chromatography (HPLC) Make: Agilent and Shimadzu. (Software's: Empower-3, Chemstation and EZ-Chrom Elite). • Gas Chromatography (GC), Make: Agilent. (Software's: Empower-3, Chemstation and EZ-Chrom Elite). • Powder X-ray diffractometer, Make: Rigaku

(Miniflex-II).

- Single crystal X-ray diffractometer, Make: Bruker (Software Apex-2 and Apex-3)
- UV–Vis spectrophotometer, Make: Analytik Jena (Software: Win ASPECT)
- FT–IR Spectrophotometer, Make: Perkin Elmer & Bruker
- K.F Autotitrater, Make: Methrom.
- Computer DTP and application
- Windows Microsoft office
- Technical software: ChemDraw, Origin, Mercury and MestReNova for NMR.

PUBLICATIONS

[1]. Momidi, B. K., **Tekuri, V.**, and Trivedi, D. R. (2016). "Selective detection of mercury ions using benzothiazole based colorimetric chemosensor." *Inorg. Chem. Commun.*, 74, 1–5.

[2]. Momidi, B. K., **Tekuri, V.**, and Trivedi, D. R. (2017). "Multi-signaling thiocarbohydrazide based colorimetric sensors for the selective recognition of heavy metal ions in an aqueous medium." *Spectrochim. Acta - Part A Mol. Biomol. Spectrosc.*, 180, 175–182.

[3]. Nechipadappu, S. K., **Tekuri, V**., and Trivedi, D. R. (2017). "Pharmaceutical Co-Crystal of Flufenamic Acid: Synthesis and Characterization of Two Novel Drug-Drug Co-Crystal." *J. Pharm. Sci.*, 106(5), 1384–1390

[4]. **Tekuri, V.**, and Trivedi, D. R. (2017). "A new colorimetric chemosensors for Cu^{2+} and Cd^{2+} ions detection: Application in environmental water samples and analytical method validation." *Anal. Chim. Acta*, 972, 81–93.

[5]. TG, A. K., **Tekuri, V**., Mohan, M., and Trivedi, D. R. (2019). "Selective colorimetric chemosensor for the detection of Hg^{2+} and arsenite ions using Isatin based Schiff's bases; DFT Studies and Applications in test strips." *Sensors Actuators, B Chem.*, 271–280.

[6]. **Tekuri, V.,** Sahoo, S. K., & Trivedi, D. R. (2019). "Hg^{2+} induced hydrolysis of thiazole amine based Schiff base: Colorimetric and fluorogenic chemodosimeter for Hg^{2+} ions in an aqueous medium." *Spectrochim. Acta. Part A: Mol. and Biomol. Spectrosc*. 218, 19-26

[7]. **Venkatadri Tekuri,** Makesh Mohan and Darshak R Trivedi. "Smart colorimetric response for the heavy metal detection: Synthesis, spectral response and DFT studies." The manuscript was communicated to the *Chemistry Select.*

[8]. **Venkatadri Tekuri** and Darshak R Trivedi." Simple colorimetric response for arsenate, arsenite, Cu^{2+} and Hg^{2+} ions: Synthesis, spectral response and test strip application". Manuscript was communicated to the *Sensors Actuators, B Chemical*.

INTERNATIONAL CONFERENCES

[1]. **Venkatadri Tekuri**, Bharath Kumar Momidi & Dr. Darshak R. Trivedi. "A simple thiazole amine based colorimetric chemosensor for the selective and sensitive mercury ion detection in an aqueous medium" paper presented in "International conference on Science and Technology: Future Challenges and Solutions, 7th Annual Conference of Indian JSPS Alumni Association" August 08-09, (2016), Mysore University, Mysore.

[2]. **Venkatadri Tekuri** & Dr. Darshak R. Trivedi. "6-(thiophen-2-yl)picolinaldehyde based colorimetric chemosensor for the selective detection of mercury ions in an aqueous medium "International conference on Crystal ball vision on science & engineering for societal upliftment, 8th Annual Conference of Indian JSPS Alumni Association" August 07-08, (2017), NIO-Goa.

[3]. Srikala P., **Venkatadri Tekuri** and Dr. Darshak R. Trivedi. Photophysical and electroanalytical response of organic receptors: anion and cation binding studies. "International conference on Crystal ball vision on science & engineering for societal upliftment, 8th Annual Conference of Indian JSPS Alumni Association" August 07-08, (2017), CSIR-NIO-Goa.

[4]. Darshak R Trivedi, Akshay Krishna TG &**Venkatadri Tekuri**. "Selective naked eye detection of mercury and arsenic using isatin based colorimetric chemo-sensors: Test strips application and DFT study. "International conference on advancement in science and

	technology 9th Annual Conference of Indian JSPS Alumni Association" Sep-03-04, (2018), Visva Bharathi University, Santiniketan, India.

GRANTS AND AWARDS

April 2003	School first in 10^{th} standard (Z.P. High School Upparapalli).
April 2008	College first and town first in B.Sc. (B.Z.C) (Y.V.N.R Degree College Rayachoti).
April 2010	Class second in M.Sc. Medicinal chemistry.
July 2015 to July 2017	Junior Research fellowship from NITK, Surathkal, India.
July 2017 to October 2019	Senior Research fellowship from NITK, Surathkal, India.

PERSONAL SKILLS AND COMPETENCES

Languages	Telugu (mother tongue) English (Good skills in reading, writing and verbal). Hindi (Good skills in reading, writing and verbal). Kannada (Good skill in verbal).
Organizational skills	▪ Good skills in teamwork and coordination of the various research projects. ▪ Good teaching skills developed during the Lab duties and mentoring activities

REFERENCES

[1]. Dr. Darshak R. Trivedi,
Associate Professor,
Department of Chemistry,
National Institute of Technology
Karnataka, Surathkal
Mangalore, Karnataka-575 025, India.
Ph: +91 9481271272.
Email: darshak_rtrivedi@yahoo.co.in

[2]. Dr. Adka Nityananda Shetty,
Professor,
Department of Chemistry,
National Institute of Technology
Karnataka, Surathkal
Mangalore, Karnataka-575 025, India.
Ph: +91 9448779922.
Email: nityanand@nitk.ac.in

[3]. Mr. S. Ramanjaneyulu,
Asst. Manager A R&D,
Dr. Reddy's Laboratories Ltd. Hyderabad, India.
Ph: +91 8008665552.
E-mail: sramanjaneyulu8@gmail.com